Université Libre de Bruxelles
Faculté des Sciences Appliquées

Semi-microscopic and microscopic three-body models of nuclei and hypernuclei

Thèse présentée en vue
de l'obtention du grade de
Docteur en Sciences de l'Ingénieur

Marc Theeten

Juin 2009

Je tiens tout d'abord à remercier vivement les professeurs Daniel Baye et Pierre Descouvemont, mes directeurs de thèse. C'est grâce à leur aide, leur soutien, leurs conseils que j'ai pu réaliser ce travail. J'ai bénéficié constamment de leur expérience et de leur enseignement. Je leur suis extrêmement reconnaissant pour toute leur attention, leur patience et leur grande disponibilité.

Je remercie également les professeurs Y. Fujiwara et Y. Suzuki du Japon, avec qui nous avons collaboré dans ce projet. Ils m'ont permis de valider et de tester mes résultats numériques pour les modèles semi-microscopiques. Ils nous ont aussi indiqué la méthode de calcul des potentiels RGM effectifs indépendants de l'énergie.

Je remercie aussi les membres du service de Physique Nucléaire Théorique et Physique Mathématique (PNTPM) de l'ULB. Je pense avant tout aux deux chefs successifs de PNTPM, les professeurs Christiane Leclercq-Willain et Pierre Descouvemont. Je remercie ensuite mes jeunes collègues, Gérald Goldstein, Pierre Capel, Jean-Marc Sparenberg et Rachid Kamouni, avec qui j'ai passé de bons moments et qui m'ont tous bien encouragé. Je salue également les nouveaux doctorants: Alix Damman, Thomas Druet et Edna Carolina Pinalla, en leur souhaitant bonne chance dans leur travaux. Je n'oublierais pas non plus les nombreux visiteurs et post-docs de passage dans le service, en particulier Veerle Hellemans et Rajdeep Chatterjee.

Mes remerciements s'adressent aussi collectivement à tous les autres doctorants et chercheurs que j'ai rencontrés et qui m'ont encouragé, en particulier Claire Noël, Laura Lopez Honorez et Geoffrey Compère. Michaël Hurtgen m'a également beaucoup aidé pour ma rédaction en anglais.

Je remercie ma famille, mes parents et mes frères de m'avoir soutenu et encouragé dans mon parcours.

Je remercie enfin les organismes qui ont financé ce travail. Je remercie d'abord Christiane Leclercq-Willain et Pierre Descouvemont pour les contrats de recherche IISN. Je remercie aussi le service d'Automatique de la faculté des Sciences Appliquées et Michel Kinnaert pour le mandat de chargé d'exercices en analyse complexe. Je remercie pour terminer la faculté des Sciences pour le mandat d'assistant en physique générale.

Contents

Chapter 1

Introduction

1.1 Cluster structures

The internal structure of the atomic nuclei clearly plays a role in many phenomena, such as nuclear collisions and radioactivity. The most striking processes are nuclear reactions, which occur when nuclei collide. In a nuclear reaction, for example, a nucleus can break up into fragments, and/or exchange some nucleons (or even fuse) with another nucleus. This shows that nuclei are highly dynamical systems. The radioactivity, in excited or unstable nuclei, also reveals dynamical properties of the nuclear states. In particular, certain excited nuclei can decay by spontaneously emitting nuclear particles (such as an α-particle, or other clusters of nucleons).

The energy of these phenomena, as well as their mechanisms, which are rather complex, depend on the dymanics of the nucleons, in each nucleus. In general, the binding energy and the strong correlations between nucleons essentially determine the nuclear structure. All observable nuclear properties must be deduced from this structure. Nuclear models are then developed in order to understand the structure of the nuclei and the nuclear processes, such as the nuclear reactions.

In particular, many nuclear states and many reaction mechanisms are well described assuming simple stable cluster structures [1–5] in nuclei. That is, in certain circumstances, the nucleons tend to form clusters (i.e., stable compact subunits, e.g. α-particles) in the nucleus, in order to reduce their uncorrelated motions. The fundamental condition is that each cluster (e.g. an α-particle) must be energetically advantageous, in terms of stability and binding energy per nucleon. A reliable criterion to identify a cluster structure is that the binding energies between the clusters in the nucleus must be weak, in comparison with the substantial binding energies inside the clusters.

In this work, we will consider the specific case of three-cluster structures. Such structures occur in nuclei, such as ^{6}He, ^{9}Be, ^{12}C, and in many other nuclear systems. They allow us to describe these nuclei and their properties, essentially by three-body models. Let us now briefly present these nuclei, and their respective internal three-body structures.

1.2 Three-cluster structures

The binding energy is very important in the nuclear structure. In particular, it can be useful to consider the nucleon separation energies. These experimental data are given in Table 1.1 for relevant helium, beryllium and carbone isotopes. The neutron separation energy S_n is defined as the energy needed to remove a neutron. Similarly, the proton separation energy S_p is the energy to remove a proton.

Among the nuclei that exhibit a clear three-body structure, there are the halo nuclei [2, 6, 7], such as ^{6}He and ^{11}Li. These are β-unstable neutron-rich nuclei that have exotic properties: in particular, their matter radii are significantly larger than in all other light nuclei. For instance, the matter radius of ^{6}He is 2.48 ± 0.03 fm, while the corresponding radius for ^{4}He is 1.57 ± 0.04 fm [8, 9]. (These radii are derived from interaction cross section mesurements.) Hence the halo nuclei (e.g. ^{6}He and ^{11}Li) display a particularly extended matter density. This is actually due to two valence neutrons that are very weakly bound to the nucleus. As a result, there is a significant probability of finding these neutrons very far from the core of the nucleus. For this reason, these two neutrons are said to form a "halo" surrounding the core of the nucleus. Such halo nuclei are well described by a three-body model, with a compact nuclear core and two valence neutrons. In the case of ^{6}He, the weak binding energy between the two valence neutrons and the core is $S_{2n} = 0.98$ MeV. That corresponds to the two-neutron separation energy, i.e., the energy needed to remove two neutrons. This value is the addition of the neutron separation energies S_n of ^{6}He and ^{5}He in Table 1.1.

The three-body structure of ^{6}He is thus an α-particle plus two valence neutrons, forming the halo. It is interesting to note that such a halo system is typically a Borromean binding [6, 7], i.e., a weakly bound three-body system in which none of the corresponding two-body subsystems are bound. Indeed, $\alpha + n + n$ is bound in ^{6}He, but $\alpha + n$ is unbound (because ^{5}He is unstable and spontaneously emits a neutron, as seen in Table 1.1). The dineutron $(n + n)$ is also not bound. In other words, the halo structure, involving two weakly bound neutrons, is remarkably fragile. If one of the halo neutrons is

	S_n	S_p	Q_α	
^{4}He	20.58	19.81		stable
^{5}He	-0.89 ± 0.05	21.83 ± 0.12	0.89 ± 0.05	unstable ($\alpha + n$)
^{6}He	1.87 ± 0.05	26.52 ± 0.95		unstable (β^-)
^{8}Be	18.90	17.26	0.092	unstable ($\alpha + \alpha$)
^{9}Be	1.67	16.89	-2.47 ± 0.05	stable
^{12}C	18.72	15.96	-7.37	stable

Table 1.1: Experimental values of S_n, S_p, and Q_α (in MeV) for the ^{4,5,6}He, ^{8,9}Be and ^{12}C nuclei [14–16]

removed, the other neutron will also be removed at the same time, since ^{5}He, unlike ^{6}He, is an unbound ($S_n < 0$) system.

Another illustrative example of three-cluster nucleus is ^{12}C in the first 0^+ excited state. This resonant state of ^{12}C is situated slightly above the threshold for fragmentation into three α-particles. Hence the ^{12}C nucleus, in this state, is basically a three-body system, made up of three α-particles. This state plays a crucial role in nuclear astrophysics because it enables the so-called *triple-α process* in stars, in which three α-particles combine to form ^{12}C [4, 10, 11]. This is a two-step reaction. First, two α-particles collide ($\alpha + \alpha \rightarrow {}^8$Be) to form ^{8}Be. Note that the ^{8}Be nucleus is unstable (it spontaneously decays back into two α-particles, as seen in Table 1.1). Nevertheless before decaying ($\tau_{1/2} = 0.968 \times 10^{-16}$ s), this ^{8}Be nucleus, in stars, can capture a third α-particle to form ^{12}C in the 0^+ resonant state ($^8\text{Be} + \alpha \rightarrow {}^{12}\text{C}^*$). This 3α resonance of ^{12}C is called the *Hoyle state*, because it was first predicted by Hoyle in 1953 [12, 13] before being experimentally discovered. The existence of this resonance in ^{12}C strongly enhances the cross section of the triple-α process. It is decisive in accounting for the observed abundance of ^{12}C in the universe, via the nucleosynthesis.

Another example of three-cluster nucleus is ^{9}Be. In Table 1.1, we see that the neutron separation energy of ^{9}Be is especially weak, in comparison with the other stable nuclei. This suggests that ^{9}Be can be viewed as a ^{8}Be system plus a valence neutron. However, ^{8}Be has clearly an $\alpha + \alpha$ cluster structure (since it decays into two α-particles). Hence the ^{9}Be nucleus can be reasonably described as an $\alpha + \alpha + n$ structure.

We have seen the examples of ^{6}He, ^{9}Be, and ^{12}C, which have $\alpha+n+n$, $\alpha+\alpha+n$, and 3α structures, respectively. We will study these cluster structures. However, we will also explore some interesting variants, namely the hypernuclei ${}^{6}_{\Lambda\Lambda}$He and ${}^{9}_{\Lambda}$Be. The hypernuclei are unstable systems very similar to atomic nuclei, except that they contain some exotic baryons (e.g. the Λ baryon) instead of some nucleons. The ${}^{6}_{\Lambda\Lambda}$He and ${}^{9}_{\Lambda}$Be will be studied as $\alpha+\Lambda+\Lambda$ and $\alpha+\alpha+\Lambda$ systems, respectively [17–19].

Moreover, it is interesting to mention that our examples of ^{6}He, ^{9}Be, and ^{12}C are Borromean structures, since the three-body systems ($\alpha+n+n$, $\alpha+\alpha+n$, and 3α) are bound, but the corresponding two-body subsystems are not (i.e. $\alpha+n$ (^{5}He), $\alpha+\alpha$ (^{8}Be), as well as $n+n$ (the dineutron) are unbound).

1.3 Three-body models

Three-body models are useful to describe the three-cluster systems (such as ^{6}He, ^{9}Be, ^{12}C, ${}^{6}_{\Lambda\Lambda}$He and ${}^{9}_{\Lambda}$Be). However, physically speaking, they are just approximations. They have their shortcomings: they assume the nuclei to be three-particle systems. These particles in the nuclei are typically nuclear clusters. Developing three-cluster models, all dynamical effects must be included in the interactions between the clusters. In particular, the Pauli exclusion principle is highly fundamental in the nuclear structure: it has important effects, which cannot be ignored, when the clusters overlap. The aim of the present work is precisely to take into account the Pauli principle in the three-body models [20–23].

Indeed, the clusters are composite particles, made of nucleons. The nucleons are fermions, and in their mutual interactions, they must satisfy the Pauli principle. In the simple three-body approximations, the effects of the Pauli principle must be simulated in the cluster-cluster potentials. In this thesis, we will study and improve the Pauli treatment in the models by considering *non-local potentials*[1] between the clusters.

1.4 Microscopic and macroscopic models

We will study e.g. ^{6}He, ^{9}Be and ^{12}C, described as a $\alpha+n+n$, $\alpha+\alpha+n$ and 3α systems, respectively. Notice the predominance of the α-particle

[1] A potential is *nonlocal* if it is represented by an integral operator in the Schrödinger equation. Such an interaction potential requires the precise knowledge of the wave function in the whole physical space. This nonlocality is an essential consequence of the Pauli principle. It arises from the formal permutations of nucleons between the clusters.

in the cluster structures. This is due to its high internal stability. The binding energy per nucleon of the α-particle is indeed larger than in all other neighbouring light nuclei [3, 4]. Moreover the first excited state of the α-particle resides very high, at 20.21 MeV.

Of course, in the models, the internal structure of the α-particles must be taken into account, because of the Pauli principle. (The α-particles are composed of two protons and two neutrons.) Hence the most realistic models, for the cluster structures, are the so-called *microscopic models*, which consider explicitly all the nucleons, in order to respect the Pauli principle exactly. The microscopic models describe the cluster systems with a fully antisymmetrised wave function, involving all nucleon coordinates. This is a complicated detailed approach, starting from the nucleon-nucleon interactions. This, of course, involves many laborious calculations, because of the formal antisymmetrisation. Therefore, in practice, the microscopic cluster models are limited to light nuclei, because they require extremely long technical calculations.

Hence there is a need for easier models, especially the *macroscopic models* (or "*non-microscopic models*"), which consider the clusters as pointlike particles, interacting via effective potentials. In other words, the clusters are treated as stuctureless particles, in order to drastically simplify the calculations. The nuclear models are then reduced to a simple three-body problem, in the case of a three-cluster system. However, this approach requires to choose effective cluster-cluster potentials.

1.5 Semi-microcopic models

In the above examples, namely ^{6}He, ^{9}Be and ^{12}C (described as $\alpha + n + n$, $\alpha + \alpha + n$, and 3α system, respectively), the three-body macroscopic models require effective $\alpha\alpha$, αn and nn potentials. These potentials are rather well known [24–26], at least to describe cluster-cluster elastic phase shifts (i.e., $\alpha + \alpha$, $\alpha + n$, or $n + n$ phase shifts).

Unfortunately, the simplest effective $\alpha\alpha$ and αn potentials are not able to reproduce accurately the experimental energies of ^{6}He, ^{9}Be and ^{12}C, without readjustment [20, 27]. This motivates the use of more realistic potentials (especially improving the Pauli treatment).

To this end, Fujiwara and co-worker have suggested a more satisfactory approach [17, 28], which is to use the so-called *non-local RGM cluster-cluster potentials* (with an ad hoc prescription) in three-body models. We call this approach the *semi-microscopic model*, because it is a natural, plausible three-

body approximation of a microscopic cluster model. These $\alpha\alpha$ and αn potentials are sophisticated potentials that take into account the composite structure of the α-clusters and incorporate all the effects of the Pauli principle. The aim of this approach is to judiciously simulate the effects of the Pauli principle in the cluster-cluster potentials. The cluster-cluster potentials are nonlocal because of the antisymmetrisation principle between nucleons in interacting clusters. Indeed the Pauli principle is known to drastically affect the relative motions between two overlapping clusters. In the present work, we will first test this semi-microscopic three-body model, and discover that it can be deficient in some respects. After identifying these deficiences, we will then improve the semi-microscopic model, by calculating other (more appropriate) effective potentials. We will thus develop another semi-microscopic model. In this study, we will compare macroscopic, semi-microscopic, and fully microscopic models, in order to evaluate the quality of the Pauli treatments in each model.

1.6 Outline

This work is structured as follows. In Chapter 2, we review the cluster-cluster interaction potentials, coming from well-known two-cluster studies. In particular, we discuss the RGM, which is a microscopic cluster model, which can generate effective cluster-cluster potentials. We also consider the simpler approximate potentials, inspired from the RGM. In Chapter 3, we give the used technique to solve the three-body Schrödinger equation, namely the hyperspherical method, with the Lagrange meshes. In particular, we generalise this technique to the case of the integro-differential equations occurring in the semi-microscopic models. In Chapter 4, we present the three-cluster microscopic model. In Chapter 5, we present and compare the non-microscopic, semi-microscopic, and microscopic cluster models. In Chapter 6, we apply the models to two hypernuclei: ${}^{6}_{\Lambda\Lambda}$He and ${}^{9}_{\Lambda}$Be. In Chapter 7, we apply the first semi-microscopic model to ^{6}He, ^{9}Be and ^{12}C. We compare the semi-microscopic and microscopic models. In Chapter 8, we apply the second semi-microscopic model, in comparison with the first model. This will improve the results significantly. In Chapter 9 we draw a general conclusion.

Chapter 2

Effective potentials between clusters

2.1 Potentials in cluster models

The "macroscopic" models, which treat the clusters as pointlike particles, are approaches that require effective potentials between the clusters. The first step in developing such models is thus the choice of the potentials able to represent the cluster-cluster interactions.

There are, however, several approaches to determine an effective potential between two clusters. The simplest potentials are purely phenomenological [24, 25]. Such potentials are just approximations. They must simply fit some relevant empirical data (such as energy levels and cluster-cluster scattering phase shifts). Their purpose is to lead to easy calculations in practical applications, when clusters are treated as point particles. This typically gives several variants of rudimentary potentials, which are more or less satisfactory. Another, more fundamental, approach consists in deriving the inter-cluster potentials from microscopic models [1, 2, 29]. In that case, the internal structure of the clusters is taken into account and the potentials are deduced from the nucleon-nucleon interactions. However, because of the Pauli principle and the exchanges of nucleons between the clusters, those potentials may have complicated forms. In particular, the inter-cluster potentials are nonlocal.

In quantum mechanics, a potential $\hat{V}$ is said to be *nonlocal* if it is defined by an integral operator which acts on the wave function, i.e.,

$$(\hat{V}\psi)(\boldsymbol{r}) = \int V(\boldsymbol{r}, \boldsymbol{r}')\, \psi(\boldsymbol{r}')\, d\boldsymbol{r}', \tag{2.1}$$

with a kernel $V(\boldsymbol{r},\boldsymbol{r}') \not\propto \delta(\boldsymbol{r}-\boldsymbol{r}')$, where the variable $\boldsymbol{r}$ denotes the relative coordinate between the two interacting particles, and $\psi(\boldsymbol{r})$ denotes the wave function. Otherwise, when $V(\boldsymbol{r},\boldsymbol{r}') \propto \delta(\boldsymbol{r}-\boldsymbol{r}')$, the potential is *local*[1], like a simple classical potential.

In this chapter, we first review in Section 2.2 a two-cluster microscopic model: the resonating-group method. One deduces from it effective nonlocal potentials, representing the interactions between clusters. Then in Section 2.3 we consider some alternative potentials: they are simpler local potentials, based on more phenomenological approaches.

2.2 Two-cluster Resonating-group method

2.2.1 RGM wave function

The resonating-group method (RGM)[1, 2, 29–31] is a well-known microscopic model, which explicitly involves all the nucleons and takes the Pauli antisymmetrisation into account. It was invented by Wheeler in 1937 [5, 32]. It is a variational method which assumes a cluster structure of the wave function. We consider here the case of a system of two clusters, our aim being essentially to derive effective potentials between the clusters.

Consider a system of A nucleons divided into two clusters of A_1 and A_2 nucleons ($A_1 + A_2 = A$) respectively. The RGM describes this system by a wave function defined as

$$\psi = \mathcal{A}(\phi_1\phi_2\, g(\boldsymbol{r})), \tag{2.2}$$

where ϕ_1 and ϕ_2 are the internal wave functions of the clusters, $g(\boldsymbol{r})$ is a function that describes the relative motion between the clusters, and $\mathcal{A}$ is an operator that ensures the complete antisymmetrisation with respect to all the nucleons. The vector $\boldsymbol{r}$ represents the relative coordinate between the centres of mass of the clusters. It depends on the coordinates $\boldsymbol{r}_j$ ($j = 1, ..., A$) of the nucleons: it is defined as

$$\boldsymbol{r} = \frac{1}{A_1}\sum_{j=1}^{A_1}\boldsymbol{r}_j - \frac{1}{A_2}\sum_{j=A_1+1}^{A_1+A_2}\boldsymbol{r}_j. \tag{2.3}$$

[1]Since with a $\delta(\boldsymbol{r}-\boldsymbol{r}')$ factor in the kernel, the wave function will not be integrated but just evaluated at $\boldsymbol{r}' = \boldsymbol{r}$.

This definition corresponds to a configuration in which nucleons $j = 1, ..., A_1$ form the first cluster, and nucleons $j = A_1 + 1, ..., A_1 + A_2$ compose the second cluster. The wave functions ϕ_1 and ϕ_2 represent the internal structure of the clusters. They are defined according to this partition: ϕ_1 which describes the nucleons in the first cluster depends on nucleon coordinates $j = 1, ..., A_1$, while ϕ_2, describing the second cluster, depends on nucleon coordinates $j = A_1 + 1, ..., A_1 + A_2$. These wave functions are translation invariant. Moreover, they are assumed to be square integrable and antisymmetric with respect to the nucleons.

The wave function ψ (2.2) is antisymmetric, according to the Pauli principle. Its antisymmetrisation with respect to all the nucleon coordinates is performed by the operator $\mathcal{A}$. This operator is called the *antisymmetriser*: it is a projector ($\mathcal{A}^2 = \mathcal{A}$) which can be written as

$$\mathcal{A} = \frac{1}{A!} \sum_P (-)^P P, \tag{2.4}$$

where P represents an operator of permutation of the nucleon coordinates and $(-)^P$ symbolises the sign of the permutation. The sum runs over all the $A!$ possible permutations of the coordinates of the nucleons ($j = 1, ..., A$). The value of the coefficient $(-)^P$ is ± 1 according to whether the permutation P is even or odd.

The antisymmetrisation of ψ (2.2) plays a fundamental role. The clusters are physically affected by the Pauli principle. The antisymmetriser exchanges nucleons between the clusters (it sums all the possibilities of interchanging nucleon coordinates). Hence it is not possible to discern specifically which nucleons are in which cluster. Inside a nucleus, the clusters must be interpreted as collective correlations between nucleons, in which all the nucleons of the nucleus take part. The nucleons are indeed indiscernible by virtue of the antisymmetrisation.

Nevertheless, there is one very specific context in which the clusters tend to behave like distinct particles [31]. This occurs asymptotically (but only asymptotically) when the clusters tend to be so far apart that they are not overlapping (i.e., for $|\boldsymbol{r}| \to \infty$):

$$\psi \underset{r\to\infty}{\sim} \frac{A_1! A_2!}{A!} \phi_1 \phi_2 \left(g(\boldsymbol{r}) + (-1)^{A_1} \delta_{A_1 A_2} \delta_{Z_1 Z_2} \, g(-\boldsymbol{r}) \right), \tag{2.5}$$

where Z_i is the proton number in cluster i. This asymptotic form follows from the fact that the functions ϕ_1 and ϕ_2 are square integrable and antisymmetric. The physical interpretation of the wave function in this asymptotic regime is clear. The two clusters then represent two separated nuclei, and the function

$g(\boldsymbol{r})$ describes their relative motion. Hence the wave function ψ can be used to study a collision between two nuclei. Note that if the nuclei are identical ($A_1 = A_2$ and $Z_1 = Z_2$)[2], the boson or fermion nature of the nuclei appears in the relative motion wave function (2.5), as an effect of the antisymmetriser. This is the only condition imposed asymptotically by the Pauli principle between two nuclei. Otherwise, when the clusters do overlap the wave function must be fully antisymmetric, with respect to all nucleons.

In the RGM, the internal wave functions of the clusters ϕ_1 and ϕ_2 are usually approximated in a harmonic-oscillator model [1, 2, 29–31]. They are antisymmetric and translation invariant. For example, in the particular case of an α-cluster (made up of two protons and two neutrons) in its ground state, the internal wave function is

$$\phi_1 = \exp\left(-\frac{1}{2b^2}\sum_{j=1}^{4}|\boldsymbol{r}_j - \boldsymbol{R}|^2\right)\chi_1, \tag{2.6}$$

where $\boldsymbol{r}_j$ ($j = 1, ..., 4$) are the nucleon coordinates,

$$\boldsymbol{R} = \frac{1}{4}\sum_{j=1}^{4}\boldsymbol{r}_j \tag{2.7}$$

is the centre-of-mass coordinate of the α-cluster, b is a parameter, and χ_1 denotes a spinor. The spinor contains the spin and isospin coordinates of the nucleons. It also ensures the antisymmetry of ϕ_1, according to the Pauli principle.

2.2.2 RGM equation

Let us consider the Hamiltonian h_A of the A-nucleon system,

$$h_A = \sum_{i=1}^{A} t_i - T_{\text{c.m.}} + \sum_{i>j=1}^{A} v_{ij}, \tag{2.8}$$

where t_i denotes the kinetic energy of nucleon i, $T_{\text{c.m.}}$ is the kinetic energy of the centre of mass, and v_{ij} is an effective nucleon-nucleon potential. This Hamiltonian is defined in the centre-of-mass reference frame.

[2]For simplicity, in equation (2.5), if $A_1 = A_2$ and $Z_1 = Z_2$, both (identical) nuclei are assumed to be in the same state (i.e., ϕ_1 and ϕ_2 are identical).

In the RGM [1, 2, 29–31], one seeks the solutions of the Schrödinger equation

$$h_A\psi = E_A\psi, \tag{2.9}$$

where E_A is the energy of the system. Assuming a two-cluster structure of the system, the wave function is approximated by the function defined in equation (2.2).

From here, it is convenient to denote by τ_i the set of all internal degrees of freedom of cluster i. This notation symbolises the variables of the wave function ϕ_i. Thus τ_i represents the set of relative coordinates of the nucleons in cluster i. Equation (2.2) is rewritten by displaying the variables as

$$\psi(\tau_1, \tau_2, \boldsymbol{r}) = \mathcal{A}\left(\phi_1(\tau_1)\,\phi_2(\tau_2)\,g(\boldsymbol{r})\right). \tag{2.10}$$

The RGM consists in substituting ψ (2.10) into the Schrödinger equation (2.9). An equation for the relative motion $g(\boldsymbol{r})$ is determined by multiplying both sides of the Schrödinger equation by $\phi_1^*(\tau_1)\phi_2^*(\tau_2)$ and by integrating over the internal variables τ_i of the clusters, i.e. all the variables except the vector $\boldsymbol{r}$. Equation (2.9) becomes

$$\mathcal{H}_{\mathcal{A}}g = E_A\,\mathcal{N}g, \tag{2.11}$$

with

$$\mathcal{N}g = \iint \phi_1^*(\tau_1)\phi_2^*(\tau_2)\,\psi(\tau_1, \tau_2, \boldsymbol{r})\,d\tau_1\,d\tau_2, \tag{2.12}$$

$$= \iint \phi_1^*(\tau_1)\phi_2^*(\tau_2)\mathcal{A}\left(\phi_1(\tau_1)\phi_2(\tau_2)g(\boldsymbol{r})\right)\,d\tau_1\,d\tau_2, \tag{2.13}$$

and

$$\mathcal{H}_{\mathcal{A}}g = \iint \phi_1^*(\tau_1)\phi_2^*(\tau_2)\,h_A\,\psi(\tau_1, \tau_2, \boldsymbol{r})\,d\tau_1\,d\tau_2, \tag{2.14}$$

$$= \iint \phi_1^*(\tau_1)\phi_2^*(\tau_2)\,h_A\,\mathcal{A}\left(\phi_1(\tau_1)\phi_2(\tau_2)g(\boldsymbol{r})\right)\,d\tau_1\,d\tau_2. \tag{2.15}$$

The symbols $\mathcal{N}$ and $\mathcal{H}_{\mathcal{A}}$ represent integral (or integro-differential) operators acting on the function $g(\boldsymbol{r})$. These operators are a consequence of the antisymmetriser $\mathcal{A}$. They can also be written

$$\mathcal{N}g = \int N(\boldsymbol{r}, \boldsymbol{r}')\,g(\boldsymbol{r}')\,d\boldsymbol{r}', \tag{2.16}$$

$$\mathcal{H}_{\mathcal{A}}g = \int H_A(\boldsymbol{r}, \boldsymbol{r}')\,g(\boldsymbol{r}')\,d\boldsymbol{r}', \tag{2.17}$$

with kernels, which can be formally represented as matrix elements [2]:

$$N(\boldsymbol{r},\boldsymbol{r}') = \langle\phi_1(\tau_1)\phi_2(\tau_2)\,\delta(\boldsymbol{r}''-\boldsymbol{r})|\,\mathcal{A}\,|\phi_1(\tau_1)\phi_2(\tau_2)\,\delta(\boldsymbol{r}''-\boldsymbol{r}')\rangle\,, \quad (2.18)$$

$$H_A(\boldsymbol{r},\boldsymbol{r}') = \langle\phi_1(\tau_1)\phi_2(\tau_2)\,\delta(\boldsymbol{r}''-\boldsymbol{r})|\,h_A\mathcal{A}\,|\phi_1(\tau_1)\phi_2(\tau_2)\,\delta(\boldsymbol{r}''-\boldsymbol{r}')\rangle\,, \quad (2.19)$$

where, in such matrix elements, $\boldsymbol{r}''$ denotes the relative coordinate (2.3) between the clusters, while $\boldsymbol{r}'$ and $\boldsymbol{r}$ are then treated as parameters.

2.2.3 Inter-cluster relative-motion energy

In equation (2.11), E_A is the total energy of the system, which includes the internal energies of the clusters. The function $g(\boldsymbol{r})$ describes the relative motion of the clusters. Hence it is desirable to remove from the equation the contributions of the internal energies of the clusters, in order to obtain an equation depending only on the relative-motion energy [25, 29].

Assuming that ϕ_1 and ϕ_2 are the exact wave functions of the clusters, the internal energies, E_1 and E_2, are given by Schrödinger equations

$$h_{A_1}\phi_1 = E_1\phi_1, \quad (2.20)$$

$$h_{A_2}\phi_2 = E_2\phi_2, \quad (2.21)$$

where h_{A_1} and h_{A_2} are Hamiltonians defined as h_A (2.8), for A_1 and A_2 nucleons, respectively. The internal Hamiltonians h_{A_1} and h_{A_2} are, of course, included in the Hamiltonian h_A of the system ($A = A_1 + A_2$):

$$h_A = h_{A_1} + h_{A_2} + h_{12}, \quad (2.22)$$

where h_{12} then contains the relative motion between the clusters.

Because h_{A_1} and h_{A_2} are Hermitian operators, we have

$$\langle\phi_1\phi_2\delta(\boldsymbol{r}''-\boldsymbol{r})|\,h_{A_i}\mathcal{A}\,|\psi\rangle = E_i\,\langle\phi_1\phi_2\delta(\boldsymbol{r}''-\boldsymbol{r})|\,\mathcal{A}\,|\psi\rangle\,, \qquad i=1,2. \quad (2.23)$$

A relative-motion operator $\mathcal{H}$ can therefore be defined as

$$\mathcal{H} = \mathcal{H}_{\mathcal{A}} - (E_1+E_2)\mathcal{N}. \quad (2.24)$$

The kernel of that operator is then given by

$$H(\boldsymbol{r},\boldsymbol{r}') = \langle\phi_1(\tau_1)\phi_2(\tau_2)\delta(\boldsymbol{r}''-\boldsymbol{r})|\,h_{12}\mathcal{A}\,|\phi_1(\tau_1)\phi_2(\tau_2)\delta(\boldsymbol{r}''-\boldsymbol{r}')\rangle\,, \quad (2.25)$$

and

$$\mathcal{H}g = \int H(\boldsymbol{r},\boldsymbol{r}')\,g(\boldsymbol{r}')\,d\boldsymbol{r}'. \quad (2.26)$$

Equation (2.11) can be written as

$$\mathcal{H}g = \varepsilon\,\mathcal{N}g, \tag{2.27}$$

where

$$\varepsilon = E_A - E_1 - E_2 \tag{2.28}$$

is the energy of the inter-cluster relative motion.

In practice, however, the kernels of $\mathcal{H}$ and $\mathcal{N}$ are evaluated by approximating the internal waves functions ϕ_1 and ϕ_2 in a harmonic-oscillator shell model (see, e.g., equation (2.6)). Such an approximation corresponds to a variational calculation. In this case, the internal energies may be estimated as

$$E_i = \frac{\langle\phi_i|h_{A_i}|\phi_i\rangle}{\langle\phi_i|\phi_i\rangle}. \tag{2.29}$$

2.2.4 Effective two-body Schrödinger equation

We discuss here briefly the RGM equation (2.27). The operators $\mathcal{N}$ and $\mathcal{H}$ have a particular structure: their kernels contain a local term plus a short-range nonlocal term [2, 29].

By renormalising the functions, the kernel $N(\boldsymbol{r},\boldsymbol{r}')$ can be written[3] as

$$N(\boldsymbol{r},\boldsymbol{r}') = \delta(\boldsymbol{r}-\boldsymbol{r}') - K_N(\boldsymbol{r},\boldsymbol{r}'), \tag{2.30}$$

where $K_N(\boldsymbol{r},\boldsymbol{r}')$ is a bounded and short-range function. The local term is a simple $\delta(\boldsymbol{r}-\boldsymbol{r}')$ (which means that $g(\boldsymbol{r})$ (2.16) is left unchanged by this term). This structure follows from definition (2.18), which indicates that $N(\boldsymbol{r},\boldsymbol{r}')$ is a matrix element of the antisymmetriser $\mathcal{A}$. The δ function in (2.30) results from the permutation terms of the expansion (2.4) of $\mathcal{A}$ that involve no exchange of nucleons between the two clusters, that is, the permutations that do not modify the relative coordinate[4] (2.3). The function $K_N(\boldsymbol{r},\boldsymbol{r}')$

[3]The normalisation consists in having a coefficient equal to 1 for the $\delta(\boldsymbol{r}-\boldsymbol{r}')$ term in (2.30). However, if both clusters are identical, the situation is subtle: equation (2.30) to be valid requires that the boson (fermion) symmetry (see, e.g., equation (2.5)) is adequately taken into account by defining $g(\boldsymbol{r})$ as an even (odd) function [2].

[4]However, in the case of two identical clusters, a change of sign ($\boldsymbol{r} \to -\boldsymbol{r}$) of (2.3) counts as a 'non-modification' of the relative coordinate (this is indeed a trivial permutation of the identical clusters, which does not exchange any nucleon between the clusters). This contributes to the δ term in (2.30), considering the parity symmetry of $g(\boldsymbol{r})$ [2, 29].

comes from all the other terms of $\mathcal{A}$, which exchange nucleons between the clusters and thus modify (2.3). This function is bounded and short-range because the internal functions ϕ_i are themselves bounded and short-range.

With the same normalisation, the kernel $H(\boldsymbol{r}, \boldsymbol{r}')$ can be written in the form

$$H(\boldsymbol{r}, \boldsymbol{r}') = \delta(\boldsymbol{r} - \boldsymbol{r}') \left(-\frac{\hbar^2}{2\mu} \Delta + V_D(\boldsymbol{r}) \right) + K_H(\boldsymbol{r}, \boldsymbol{r}'), \tag{2.31}$$

where

$$\mu = \frac{A_1 A_2}{A_1 + A_2} m_N \tag{2.32}$$

is the reduced mass of the two clusters, with m_N denoting the nuclear mass unit, defined as the average mass of a nucleon, Δ is the Laplacian operator and $V_D(\boldsymbol{r})$ and $K_H(\boldsymbol{r}, \boldsymbol{r}')$ are two functions. Here again, the terms with the δ function result from the permutations of the antisymmetriser $\mathcal{A}$ that do not make any exchanges of nucleons between the clusters, whereas $K_H(\boldsymbol{r}, \boldsymbol{r}')$ results from the exchanges of nucleons between clusters[5]. The function $K_H(\boldsymbol{r}, \boldsymbol{r}')$ is bounded and short-range.

Defining a function $K(\varepsilon, \boldsymbol{r}, \boldsymbol{r}')$ by

$$K(\varepsilon, \boldsymbol{r}, \boldsymbol{r}') = K_H(\boldsymbol{r}, \boldsymbol{r}') + \varepsilon \, K_N(\boldsymbol{r}, \boldsymbol{r}'), \tag{2.33}$$

the RGM equation (2.27) can be written

$$\left(-\frac{\hbar^2}{2\mu} \Delta + V_D(\boldsymbol{r}) \right) g(\boldsymbol{r}) + \int K(\varepsilon, \boldsymbol{r}, \boldsymbol{r}') \, g(\boldsymbol{r}') \, d\boldsymbol{r}' = \varepsilon \, g(\boldsymbol{r}). \tag{2.34}$$

Formally, this equation resembles a Schrödinger equation for the relative motion of the clusters. The term $-(\hbar^2/2\mu)\Delta$ represents the kinetic energy of the relative motion. In the right-hand side, there is the total relative-motion energy ε. Hence the $V_D(\boldsymbol{r})$ term and the integral may be interpreted as representing the potential energy and, therefore, the effective interaction between the clusters.

Thus, interpreting (2.34) as a Schrödinger equation, an effective potential between the clusters may be defined. This effective potential is nonlocal and depends on the value of the energy ε. It contains a local term $V_D(\boldsymbol{r})$, which is

[5]Notice that if the nucleon-nucleon potential v_{ij} (2.8) includes exchange operators, then those exchange operators also induce exchanges of nucleons between clusters, besides the antisymmetrisation.

generally termed the direct potential, and a nonlocal term determined by the kernel $K(\varepsilon, \boldsymbol{r}, \boldsymbol{r}')$. This potential is deduced from the RGM: it is the result of the nucleon-nucleon interactions and incorporates the effects of the Pauli principle. The nonlocal term is a consequence of the exchanges of nucleons between the clusters. The energy dependence of $K(\varepsilon, \boldsymbol{r}, \boldsymbol{r}')$ is an effect of the Pauli antisymmetrisation.

2.2.5 Pauli Forbidden states

Among the solutions of the RGM equation (2.27) [or (2.34)], the functions $g_0(\boldsymbol{r})$ for which

$$\mathcal{N} g_0 = 0 \tag{2.35}$$

are to be excluded, because they are physically irrelevant. Indeed, condition (2.35) implies that the corresponding antisymmetrised wave function vanish identically,

$$\mathcal{A}\left(\phi_1\phi_2\, g_0(\boldsymbol{r})\right) = 0. \tag{2.36}$$

Hence

$$\mathcal{H} g_0 = 0. \tag{2.37}$$

Such functions $g_0(\boldsymbol{r})$ are clearly unphysical: they are eliminated by the antisymmetriser $\mathcal{A}$ and are called *Pauli forbidden states* of the relative motion of two clusters [2, 29, 33]. They are also known as *spurious* or *redundant states* because they can be added with an arbitrary coefficient to a physical state $g(\boldsymbol{r})$, since they vanish after antisymmetrisation,

$$\psi = \mathcal{A}\left(\phi_1\phi_2\left(g(\boldsymbol{r}) + c\, g_0(\boldsymbol{r})\right)\right) = \mathcal{A}\left(\phi_1\phi_2\, g(\boldsymbol{r})\right), \tag{2.38}$$

c being any number. Because of properties (2.35) and (2.37), the (unphysical) functions $g_0(\boldsymbol{r})$ satisfy the RGM equation (2.27) [(2.34)] whatever the energy ε. Therefore, any solution $g(\boldsymbol{r})$ of the RGM equation may contain some Pauli forbidden states as components.

The physical solutions $g(\boldsymbol{r})$ are defined as having no component in the (unphysical) space of the Pauli forbidden states, i.e., the physical functions $g(\boldsymbol{r})$ are defined with the orthogonality condition

$$\int g(\boldsymbol{r}) g_0^*(\boldsymbol{r})\, d\boldsymbol{r} = 0, \tag{2.39}$$

for all Pauli forbidden states $g_0(\boldsymbol{r})$ (2.35).

Note that definition (2.35) of the forbidden states $g_0(\boldsymbol{r})$ is equivalent to the condition

$$\int K_N(\boldsymbol{r},\boldsymbol{r}')\, g_0(\boldsymbol{r})\, d\boldsymbol{r} = g_0(\boldsymbol{r}). \tag{2.40}$$

Forbidden states exist and are well known [2, 29, 34] in the particular cases where both clusters are described in harmonic-oscillator shell models with a same frequency. They are then given by harmonic-oscillator eigenfunctions associated with the reduced mass μ (2.32) and with the oscillator frequency.

2.2.6 Partial wave of orbital angular momentum

Up to this point, we have considered the RGM equation for the wave ψ (2.2). However, in practice, the wave function is usually expanded into partial waves with a given angular momentum.

For simplicity, we first assume that the clusters have no spin (like e.g. α-clusters). The more general case of clusters with explicit spin will be discussed in section 2.2.8.

For a given partial wave, the relative-motion function $g(\boldsymbol{r})$ can be written

$$g(\boldsymbol{r}) = \frac{u_l(r)}{r}\, Y_l^m(\Omega), \tag{2.41}$$

where l is the orbital angular momentum of the relative motion, with m its projection, r and Ω denote the norm and the direction of the vector $\boldsymbol{r}$, respectively, $Y_l^m(\Omega)$ is a spherical harmonic and $u_l(r)$ a radial function. If the system is rotation-invariant, the kernels of the operators $\mathcal{N}$ and $\mathcal{H}$ can be expanded as

$$N(\boldsymbol{r},\boldsymbol{r}') = (rr')^{-1} \sum_{lm} Y_l^{m*}(\Omega')\, Y_l^m(\Omega)\, N_l(r,r'), \tag{2.42}$$

$$H(\boldsymbol{r},\boldsymbol{r}') = (rr')^{-1} \sum_{lm} Y_l^{m*}(\Omega')\, Y_l^m(\Omega)\, H_l(r,r'), \tag{2.43}$$

defining radial kernels $N_l(r,r')$ and $H_l(r,r')$. The RGM equation (2.27) can be written for the partial wave as

$$\mathcal{H}_l u_l = \varepsilon\, \mathcal{N}_l u_l, \tag{2.44}$$

where $\mathcal{N}_l$ and $\mathcal{H}_l$ are operators defined by

$$\mathcal{N}_l u_l = \int N_l(r,r')\, u_l(r')\, dr', \tag{2.45}$$

$$\mathcal{H}_l u_l = \int H_l(r,r')\, u_l(r')\, dr'. \tag{2.46}$$

Similarly, the nonlocal kernel $K(\varepsilon, \boldsymbol{r}, \boldsymbol{r}')$ can be expanded as

$$K(\varepsilon, \boldsymbol{r}, \boldsymbol{r}') = (rr')^{-1} \sum_{lm} Y_l^{m*}(\Omega')\, Y_l^m(\Omega)\, k_l(\varepsilon, r, r'). \tag{2.47}$$

Therefore, the effective Schrödinger equation (2.34) can be written for the radial function $u_l(r)$ as

$$\left[-\frac{\hbar^2}{2\mu}\left(\frac{d^2}{dr^2} - \frac{l(l+1)}{r^2}\right) + V_D(r)\right] u_l(r) + \int_0^\infty k_l(\varepsilon, r, r') u_l(r') dr' = \varepsilon\, u_l(r). \tag{2.48}$$

In that case (without spin), the direct potential $V_D(r)$ is usually central and does not depend on l.

2.2.7 Renormalisation into another effective two-body Schrödinger equation

We have seen in section 2.2.4 that an effective nonlocal potential between the clusters may be determined from the RGM equation (2.34). However, the so-defined potential has some drawbacks [35]. This nonlocal potential $K(\varepsilon, \boldsymbol{r}, \boldsymbol{r}')$ depends explicitly on the energy ε, which may be considered as a disadvantage. Furthermore, two functions $g(\boldsymbol{r})$ and $g'(\boldsymbol{r})$ which satisfy the equation for two distinct energies ε and ε',

$$\mathcal{H} g = \varepsilon \mathcal{N} g, \tag{2.49}$$
$$\mathcal{H} g' = \varepsilon' \mathcal{N} g', \tag{2.50}$$

obey the condition

$$\langle g | \mathcal{N} | g' \rangle = \delta(\varepsilon - \varepsilon'), \tag{2.51}$$

where the functions are assumed to be suitably normalised (and to represent states for continuous energies). This relation corresponds to the orthogonality of the RGM wave functions ψ (2.2). Indeed, from definition (2.13) of $\mathcal{N}$, equation (2.51) can be written as

$$\langle \mathcal{A}\,(\phi_1 \phi_2\, g) \,| \mathcal{A}\,(\phi_1 \phi_2\, g') \rangle = \delta(\varepsilon - \varepsilon'). \tag{2.52}$$

Nevertheless, the relation (2.51) between $g(\boldsymbol{r})$ and $g'(\boldsymbol{r})$ is not a direct orthogonality of two functions: the orthogonality requires the presence of the operator $\mathcal{N}$. Therefore, the function $g(\boldsymbol{r})$ does not behave like an usual

probability amplitude. This may be regarded as another disadvantage in the interpretation of equation (2.34) as an effective Schrödinger equation.

Thus, equation (2.34) has some drawbacks with respect to a true two-body Schrödinger equation: the nonlocal potential in the Hamiltonian depends on the energy ε, and $g(\boldsymbol{r})$ cannot be interpreted as a direct probability amplitude (inasmuch as it obeys a special orthogonality rule). This situation may, however, be corrected [1, 2, 25, 29, 31, 35, 36]. It is indeed possible to modify the RGM equation in order to write an effective Schrödinger equation, with an energy-independent potential and a function that behaves like a wave function. To this end, we must introduce the eigenstates (and the eigenvalues) of the operator $\mathcal{N}$.

The operator $\mathcal{N}$ is Hermitian. It commutes with the orbital angular momentum of the relative motion of the clusters (as you may see from the rotation-invariance (2.42)). Therefore $\mathcal{N}$ has a basis of common eigenstates with the orbital angular momentum:

$$\mathcal{N}\varphi_{nlm} = \mu_{nl}\varphi_{nlm}, \tag{2.53}$$

where n, l and m represent the node number, the angular momentum and the projection of the angular momentum, respectively. The eigenstates φ_{nlm} form a complete set in the space of the wave functions. The eigenvalues μ_{nl} are positive and admit an accumulation point at the value 1 [2, 30, 34], i.e.,

$$0 \leq \mu_{nl}, \quad \text{and} \quad \lim_{n\to\infty} \mu_{nl} = 1 \tag{2.54}$$

(with the normalisation adopted in equation (2.30)). The Pauli forbidden states (2.35) are by definition the eigenstates belonging to $\mu_{nl} = 0$.

The operator can be written as

$$\mathcal{N} = \sum_{nlm} \mu_{nl} \left|\varphi_{nlm}\right\rangle \left\langle\varphi_{nlm}\right| . \tag{2.55}$$

One defines the square root of the operator by

$$\mathcal{N}^{1/2} = \sum_{nlm} \mu_{nl}^{1/2} \left|\varphi_{nlm}\right\rangle \left\langle\varphi_{nlm}\right| , \tag{2.56}$$

and its inverse,

$$\mathcal{N}^{-1/2} = \sum_{\substack{nlm \\ \mu_{nl}\neq 0}} \mu_{nl}^{-1/2} \left|\varphi_{nlm}\right\rangle \left\langle\varphi_{nlm}\right| , \tag{2.57}$$

with the restriction $\mu_{nl} \neq 0$. The inversion is thus limited to the subspace of the physical states:

$$\mathcal{N}^{-1/2}\mathcal{N}^{1/2} = \mathcal{I}, \tag{2.58}$$

where $\mathcal{I}$ is a projector that excludes the Pauli forbidden states ($\mu_{nl} = 0$),

$$\mathcal{I} = \sum_{\substack{nlm \\ \mu_{nl}\neq 0}} |\varphi_{nlm}\rangle \langle\varphi_{nlm}| . \tag{2.59}$$

This projector $\mathcal{I}$ behaves like the identity operator in the subspace of the physical states (2.39).

The operators $\mathcal{N}^{1/2}$ and $\mathcal{N}^{-1/2}$ allow a reformulation of the RGM equation. The idea is to define an auxiliary function $\widetilde{g}(\boldsymbol{r})$ from $g(\boldsymbol{r})$ [2, 25, 29, 31, 35] as

$$\widetilde{g} = \mathcal{N}^{1/2} g, \tag{2.60}$$

and an operator $\widetilde{\mathcal{H}}$ as

$$\widetilde{\mathcal{H}} = \mathcal{N}^{-1/2}\mathcal{H}\mathcal{N}^{-1/2}. \tag{2.61}$$

The RGM equation (2.27) can be rewritten

$$\widetilde{\mathcal{H}}\widetilde{g} = \varepsilon\widetilde{g}. \tag{2.62}$$

This form of the RGM equation is interesting because it has the structure of a regular Schrödinger equation. Indeed, the operator $\widetilde{\mathcal{H}}$ is Hermitian. It has therefore the properties of an effective Hamiltonian for the relative motion of the clusters. Equation (2.62), which states that the energy ε is an eigenvalue of this Hamiltonian, may thus be regarded as an effective Schrödinger equation. This approach requires however to consider the modified function $\widetilde{g}$ instead of g. It is a reinterpretation of the wave function of the relative motion of the clusters. Its advantage is that it does not possess the drawbacks of g mentioned above. Indeed, the modified functions obey the usual orthogonality relation,

$$\langle \widetilde{g}|\widetilde{g}'\rangle = \delta(\varepsilon - \varepsilon'), \tag{2.63}$$

where $\widetilde{g}'$ corresponds to the energy ε'.

Equation (2.63) follows from the hermiticity of $\widetilde{\mathcal{H}}$, but it can also be established from equation (2.52) because, following definition (2.60), there is the direct equivalence

$$\langle \widetilde{g}|\widetilde{g}'\rangle = \langle g|\,\mathcal{N}\,|g'\rangle = \langle \mathcal{A}\,(\phi_1\phi_2\,g)\,|\mathcal{A}\,(\phi_1\phi_2\,g')\rangle\,. \tag{2.64}$$

This nice property encourages the interpretation of $\widetilde{g}$ as an effective relative-motion wave function, in the sense that $\widetilde{g}$ yields the same probability amplitudes as the original microscopic wave function.

Moreover, the function $\widetilde{g}(\boldsymbol{r})$ has the same asymptotic behavior as $g(\boldsymbol{r})$:

$$\widetilde{g}(\boldsymbol{r}) \underset{r\to\infty}{\sim} g(\boldsymbol{r}) \tag{2.65}$$

(because the operator $\mathcal{N}^{1/2}$ differs from the identity by short-range (nonlocal) terms). Therefore the function $\widetilde{g}(\boldsymbol{r})$ may be used directly, instead of $g(\boldsymbol{r})$, in scattering calculations. We also notice that by definition, because of operator $N^{1/2}$, the function $\widetilde{g}(\boldsymbol{r})$ is orthogonal to the Pauli forbidden states.

The Hamiltonian $\widetilde{\mathcal{H}}$ can be represented by a kernel $\widetilde{H}(\boldsymbol{r},\boldsymbol{r}')$,

$$\widetilde{\mathcal{H}}\widetilde{g} \;=\; \int \widetilde{H}(\boldsymbol{r},\boldsymbol{r}')\,\widetilde{g}(\boldsymbol{r}')\,d\boldsymbol{r}'. \tag{2.66}$$

This kernel has the following structure:

$$\widetilde{H}(\boldsymbol{r},\boldsymbol{r}') = \delta(\boldsymbol{r}-\boldsymbol{r}')\left(-\frac{\hbar^2}{2\mu}\Delta + V_D(\boldsymbol{r})\right) + \widetilde{K}(\boldsymbol{r},\boldsymbol{r}'), \tag{2.67}$$

where $\widetilde{K}(\boldsymbol{r},\boldsymbol{r}')$ is a short-range nonlocal term. The form of the kernel $\widetilde{H}(\boldsymbol{r},\boldsymbol{r}')$ is rather similar to $H(\boldsymbol{r},\boldsymbol{r}')$ (2.31). The local terms of both kernels are identical.

Equation (2.67) allows us to rewrite equation (2.62):

$$\left(-\frac{\hbar^2}{2\mu}\Delta + V_D(\boldsymbol{r})\right)\widetilde{g}(\boldsymbol{r}) + \int \widetilde{K}(\boldsymbol{r},\boldsymbol{r}')\,\widetilde{g}(\boldsymbol{r}')\,d\boldsymbol{r}' = \varepsilon\,\widetilde{g}(\boldsymbol{r}). \tag{2.68}$$

This equation is equivalent to the RGM equation (2.34), as long as the relation (2.60) between $\widetilde{g}(\boldsymbol{r})$ and $g(\boldsymbol{r})$ is taken into account. This formulation with $\widetilde{g}(\boldsymbol{r})$ is interesting because it introduces a nonlocal potential that does not depend on the energy ε. Indeed, the kernel $\widetilde{K}(\boldsymbol{r}',\boldsymbol{r})$, unlike $K(\varepsilon,\boldsymbol{r},\boldsymbol{r}')$ in (2.34), is independent of the energy.

Of course, equation (2.68) can also be written for partial waves as

$$\left[-\frac{\hbar^2}{2\mu}\left(\frac{d^2}{dr^2} - \frac{l(l+1)}{r^2}\right) + V_D(r)\right]\widetilde{u}_l(r) + \int_0^\infty \widetilde{k}_l(r,r')\,\widetilde{u}_l(r')\,dr' = \varepsilon\,\widetilde{u}_l(r), \tag{2.69}$$

with $\widetilde{u}_l(r)$ defined by

$$\widetilde{g}(\boldsymbol{r}) = \frac{\widetilde{u}_l(r)}{r}\, Y_l^m(\Omega), \tag{2.70}$$

and the kernel $\widetilde{k}_l(r,r')$ defined by

$$\widetilde{K}(\boldsymbol{r},\boldsymbol{r}') = (rr')^{-1} \sum_{lm} Y_l^{m*}(\Omega')\, Y_l^m(\Omega)\, \widetilde{k}_l(r,r'). \tag{2.71}$$

These relations assume, for simplicity, the absence of spin but can be generalised without difficulty in the cases with spin.

2.2.8 Spin of the clusters

So far, we have not considered any spin effect. If the clusters have non-zero spins (and if the interactions include spin-dependent terms), then the wave functions must be modified. For a given partial wave, the wave function (2.2) becomes

$$\psi_{lS}^{JM} = \mathcal{A}\left(\Big[[\phi_1 \otimes \phi_2]^S \otimes Y_l(\Omega) \Big]^{JM}\ r^{-1}\, u_{lS}^J(r) \right), \tag{2.72}$$

where J denotes the total angular momentum, M its projection, and S the total spin. The total angular momentum J is the result of the coupling of the spin S with the orbital angular momentum l. This change of wave function, however, does not affect the principle of the RGM. Following the same lines as previously, one can derive a RGM equation for the function $u_{lS}^J(r)$. The operator $\mathcal{N}_l$ (2.42) and $\mathcal{H}_l$ (2.43) must be suitably modified: they become dependent on quantum numbers S and J. RGM equation (2.44) becomes

$$\mathcal{H}_{lS}^J\, u_{lS}^J = \varepsilon\, \mathcal{N}_{lS}^J\, u_{lS}^J, \tag{2.73}$$

with generalised operators $\mathcal{N}_{lS}^J$ and $\mathcal{H}_{lS}^J$, taking into account the spin.

Of course, a function

$$\widetilde{u}_{lS}^J \;=\; \left(\mathcal{N}_{lS}^J\right)^{1/2} u_{lS}^J, \tag{2.74}$$

and a modified Hamiltonian

$$\widetilde{\mathcal{H}}_{lS}^J \;=\; \left(\mathcal{N}_{lS}^J\right)^{-1/2} \mathcal{H}_{lS}^J \left(\mathcal{N}_{lS}^J\right)^{-1/2}, \tag{2.75}$$

may be defined in order to write

$$\widetilde{\mathcal{H}}_{lS}^J\, \widetilde{u}_{lS}^J = \varepsilon\, \widetilde{u}_{lS}^J. \tag{2.76}$$

Equations (2.73) and (2.76) may also be formally written as effective Schrödinger equations with nonlocal potentials depending on l, S and J. Such equations are direct generalisations of (2.48) and (2.69).

In what follows, for simplicity, when we consider the RGM, we mainly refer to equations (2.34) with $g(\boldsymbol{r})$ and (2.68) with $\widetilde{g}(\boldsymbol{r})$. Of course, this does not exclude the spin and all conclusions can be directly extended to the spin.

2.3 Effective interactions between clusters

2.3.1 Nonlocal RGM potentials

We have seen that the RGM equation may be interpreted as defining effective cluster-cluster potentials. Such potentials are the result of the nucleon-nucleon interactions and contain the effects of the Pauli antisymmetrisation. They are determined by identifying the equation that describes the inter-cluster relative motion with a two-body Schrödinger equation. However, for a given system, the RGM offers two possible choices of effective potentials according to the formulation of the RGM equation that one adopts.

The first possibility is to consider $g(\boldsymbol{r})$ as the wave function of the relative motion of the clusters. This function is defined from the total wave function ψ (2.2). The asymptotic behaviour (2.5) of ψ supports the interpretation of $g(\boldsymbol{r})$ as the relative-motion wave function. (One also imposes by definition that $g(\boldsymbol{r})$ has no component in the space of the Pauli forbidden states, which vanish after antisymmetrisation (2.36).)

Equation (2.34), satisfied by $g(\boldsymbol{r})$, determines the nonlocal potential V,

$$(Vg)(\boldsymbol{r}) = V_D(\boldsymbol{r})\, g(\boldsymbol{r}) + \int K(\varepsilon, \boldsymbol{r}, \boldsymbol{r}')\, g(\boldsymbol{r}')\, d\boldsymbol{r}'. \tag{2.77}$$

This potential represents the effective interaction between the clusters. Its nonlocal part, defined by the kernel $K(\varepsilon, \boldsymbol{r}, \boldsymbol{r}')$, depends on the energy ε of the relative motion. The potential has also a local term, the direct potential $V_D(\boldsymbol{r})$.

The formulation with $\widetilde{g}(\boldsymbol{r})$ of the RGM equation offers an alternative to define an effective potential between the clusters. Indeed, equation (2.68), satisfied by $\widetilde{g}(\boldsymbol{r})$, can also be identified with a two-body Schrödinger equation describing the inter-cluster relative motion. The function $\widetilde{g}(\boldsymbol{r})$ is then regarded as an effective wave function. This approach is supported by the properties of $\widetilde{g}(\boldsymbol{r})$.

The function $\widetilde{g}(\boldsymbol{r})$ is defined by equation (2.60). It has the same asymptotic behaviour (2.65) as $g(\boldsymbol{r})$, and therefore gives the same results in the scattering calculations. It obeys the usual orthogonality relation (2.63) of

the wave functions. Moreover the scalar product (2.64) of the functions $\widetilde{g}(\boldsymbol{r})$ is equal to the scalar product of the original microscopic wave functions. In addition, the function $\widetilde{g}(\boldsymbol{r})$ is orthogonal to the Pauli forbidden states.

The Schrödinger equation (2.68) allows the definition of another effective potential $\widetilde{V}$ between the clusters,

$$(\widetilde{V}\,\widetilde{g})(\boldsymbol{r}) = V_D(\boldsymbol{r})\,\widetilde{g}(\boldsymbol{r}) + \int \widetilde{K}(\boldsymbol{r},\boldsymbol{r}')\,\widetilde{g}(\boldsymbol{r}')\,d\boldsymbol{r}'. \tag{2.78}$$

This potential $\widetilde{V}$, unlike V, is independent of the energy. Its local part is given by the direct potential $V_D(\boldsymbol{r})$.

The explicit expressions of the RGM potentials (2.77) for the α+n and α+α systems are written in Appendix C. The calculations of the corresponding energy-independent potentials (2.78) are given in Appendix E.

Both potentials, V and $\widetilde{V}$, are different through their nonlocal terms. Nevertheless, they are equivalent from the experimental point of view, in particular with respect to the scattering data. The wave functions $g(\boldsymbol{r})$ and $\widetilde{g}(\boldsymbol{r})$ have indeed exactly the same asymptotic form. Hence, as long as only the asymptotic regime of the wave functions is concerned, the potentials V and $\widetilde{V}$ give the same results independently. Otherwise, if the physical observables involve the behaviour of the wave functions at short distances, then the relation between $g(\boldsymbol{r})$ and $\widetilde{g}(\boldsymbol{r})$ has to be taken into account. In that case, it may also be useful to refer to the original microscopic wave function ψ.

2.3.2 Local potentials

The nonlocal potentials lead to integro-differential Schrödinger equations. The nonlocality may require very long calculations. Therefore, from a practical point of view, it is more convenient to replace, if possible, the effective potentials by simplified local potentials. The local potentials are indeed much easier to handle.

By local potentials, we mean potentials for which the Schrödinger equation can be written as an equation without any integral operator. The local potentials, in that sense, may depend on the angular momentum (although such a dependence should be expressed from projectors on partial waves, and thus corresponds to a certain form of nonlocality). Such potentials can nevertheless be considered as local if, for each partial wave, they act as simple local terms, in the equations.

The approaches with local potentials are approximations which simplify the description of cluster systems. These potentials are determined in order to reproduce experimental scattering properties of colliding nuclei (corresponding to the clusters). They are phenomenological potentials whose validity is limited to certain energies. They may be derived directly from the experimental data. They may also be inspired from insights obtained from the RGM.

Orthogonality Condition Model

The direct potential $V_D(\boldsymbol{r})$ (2.34) is a local potential which can be extracted from the RGM. It has the structure of a double-folding potential [2, 35, 37].

The use of the direct potential $V_D(\boldsymbol{r})$ alone in a Schrödinger equation does not give satisfactory results. It means that the nonlocality of the RGM is absolutely not negligible.

However, Saito introduced an approximation [29, 33] that simplifies the RGM from local potentials of folding type, like $V_D(\boldsymbol{r})$. This simplification is called the Orthogonality Condition Model (OCM). The idea is to consider that the essential effect of the nonlocality in the RGM is the exclusion of the Pauli forbidden states. One then assumes that this effect is predominant and that the nonlocal terms can be simulated by requiring the relative motion wave function to be orthogonal to the forbidden states. The OCM consists in using a simplified (local) potential and in solving the Schrödinger equation under the constraint that the wave function be orthogonal to the Pauli forbidden states [6].

The choice of the direct potential $V_D(\boldsymbol{r})$ as local potential in the OCM may be a reasonable approximation, for example, in the case of the elastic scattering of two α-particles. Otherwise, it turns out that the effective local potential to be used in the OCM depends strongly on the considered systems. Hence in general, the potential may be quite different from $V_D(\boldsymbol{r})$ and determined phenomenologically [29, 38, 39].

However, the Schrödinger equation in the OCM is still nonlocal, because it necessarily involves a projector that excludes the Pauli forbidden states. Nevertheless, the OCM has inspired approximate local potentials that do not require any projector in the Schrödinger equation. These are the deep potentials, described in the next paragraphs.

[6] Equation (2.39) states the orthogonality condition.

Deep local potential

The idea of the OCM is that the Pauli principle excludes certain states of the relative motion of the clusters. The wave functions are then constrained to be orthogonal to the Pauli forbidden states. The practical result is that the wave functions will have nodes in the region where the clusters overlap.

These effects of the Pauli principle can be taken into account in a purely local model [25]. To this end, one creates simple deep local potentials (with, e.g., Gaussian-like shapes). The Pauli forbidden states in the RGM are given by eigenstates of harmonic oscillator. The very deep potentials may be similar, at least near their bottom, to a harmonic oscillator well. Hence the idea that the lowest bound states generated by these potentials may approximate the Pauli forbidden states. One thus develops deep enough local potentials so that they give rise to bound states that can play the role of forbidden states. Those bound states are considered as being unphysical. They are situated at very negative energies, below the relevant energies of the physical states.

Such deep local potentials enables one to easily fulfill the orthogonality condition. One just solves a local Schrödinger equation, by simply discarding the bound states corresponding to the forbidden states. All other solutions given by the potential are interpreted as being physical. These physical solutions (e.g., the scattering states) are then automatically orthogonal to the unphysical bound states. Hence they have, qualitatively, the same node structure as in the OCM.

The deep potentials are fitted to scattering data. They have the advantage to be purely local and to consider the exclusion effects of the Pauli principle. For this purpose, they are judiciously elaborated with unphysical bound states playing the role of the Pauli forbidden states.

Shallow local potential

The shallow local potentials are another possibility for representing the cluster-cluster interactions. Such potentials are very simple. A shallow potential means that this potential, unlike a deep potential, does not generate any unphysical bound states simulating the Pauli forbidden states. In other words, all states generated by a shallow potential are to be considered as physical states.

The shallow potentials are thus local potentials, neglecting the internal structure of the clusters. They are developed phenomenologically in non-microscopic approaches. They include a short-range repulsive core [24] in

order to simulate approximately the effects of the Pauli principle. They may depend on the angular momentum but they are local for each partial wave. Their parameters are fitted to reproduce scattering data.

From the point of view of the experimental phase shifts, shallow and deep potentials give equivalent results. However, the wave functions of both approaches are in general quite different. In particular, they have not the same number of nodes, because the shallow potentials do not take into account the Pauli forbidden states.

Supersymmetry between deep and shallow potentials

The supersymmetric transformations [40, 41] allow us to convert any deep potential into a shallow potential. It is a technique that modifies a potential by suppressing the ground bound state, but reproducing exactly all the rest of the energy spectrum and the scattering phase shifts.

This technique can be applied to a deep potential in order to remove the unphysical bound states, which simulate the Pauli forbidden states. If the potential supports several unphysical bound states, the removal of these states can be done in several steps. Specifically, the unphysical bound states are the ground states of certain partial waves. The potential is transformed separately for each partial wave in which there are forbidden states. At each step of the transformation, you have a new potential and you eliminate the ground state in the considered partial wave. The forbidden bound states are thus removed one after the other.

Let us consider a deep potential $V_{ls}^{j}(r)$ for a given partial wave in which there is a forbidden state (l, s and j denoting the orbital angular momentum, the spin and the total angular momentum of this wave, respectively). The ground state supported by $V_{ls}^{j}(r)$ is a forbidden state. It corresponds to a mathematical solution $u_{ls}^{j(0)}(r)$ of the Schrödinger equation:

$$\left(-\frac{\hbar^2}{2\mu}\left(\frac{d^2}{dr^2}-\frac{l(l+1)}{r^2}\right)+V_{ls}^{j}(r)\right)u_{ls}^{j(0)}(r)=\varepsilon^{(0)}\,u_{ls}^{j(0)}(r), \tag{2.79}$$

where $\varepsilon^{(0)}$ is the ground-state eigenvalue. Note that $\varepsilon^{(0)}$ is an unphysical energy, since it corresponds to a forbidden state.

The supersymmetric transformation modifies $V_{ls}^{j}(r)$ in order to remove $\varepsilon^{(0)}$ from the bound spectrum associated with the potential. It defines a new potential $\widetilde{V}_{ls}^{j}(r)$ as

$$\widetilde{V}_{ls}^{j}(r)=V_{ls}^{j}(r)-\frac{\hbar^2}{\mu}\frac{d^2}{dr^2}\ln\int_0^r[u_{ls}^{j(0)}(r')]^2dr'. \tag{2.80}$$

The potentials $\widetilde{V}_{ls}^{j}(r)$ and $V_{ls}^{j}(r)$ generate exactly the same energy spectrum, apart from the unphysical ground level $\varepsilon^{(0)}$, which is suppressed in the transformation.

The wave functions obtained with $\widetilde{V}_{ls}^{j}(r)$ are connected to those obtained with $V_{ls}^{j}(r)$ through

$$\widetilde{u}_{ls}^{j}(r) = u_{ls}^{j}(r) - u_{ls}^{j(0)}(r)\frac{\int_0^r u_{ls}^{j}(r')\, u_{ls}^{j(0)}(r')dr'}{\int_0^r [u_{ls}^{j(0)}(r')]^2 dr'}, \tag{2.81}$$

where $u_{ls}^{j}(r)$ and $\widetilde{u}_{ls}^{j}(r)$ are the real solutions of the Schrödinger equations corresponding to a same energy ε,

$$\left(-\frac{\hbar^2}{2\mu}\left(\frac{d^2}{dr^2} - \frac{l(l+1)}{r^2}\right) + V_{ls}^{j}(r)\right) u_{ls}^{j}(r) = \varepsilon\, u_{ls}^{j}(r), \tag{2.82}$$

$$\left(-\frac{\hbar^2}{2\mu}\left(\frac{d^2}{dr^2} - \frac{l(l+1)}{r^2}\right) + \widetilde{V}_{ls}^{j}(r)\right) \widetilde{u}_{ls}^{j}(r) = \varepsilon\, \widetilde{u}_{ls}^{j}(r). \tag{2.83}$$

Relation (2.81) clearly indicates that the forbidden state has been removed from the bound spectrum because if $u_{ls}^{j}(r) = u_{ls}^{j(0)}(r)$ then $\widetilde{u}_{ls}^{j}(r) = 0$. It also shows that $\widetilde{u}_{ls}^{j}$ and u_{ls}^{j} have the same asymptotic behaviour since the difference $\widetilde{u}_{ls}^{j}(r) - u_{ls}^{j}(r)$ vanishes for $r \to \infty$. Hence the potential $\widetilde{V}_{ls}^{j}(r)$ provides the same phase shifts as $V_{ls}^{j}(r)$.

The potential $\widetilde{V}_{ls}^{j}(r)$ includes a repulsive term in r^{-2}, which can be regarded as approximately simulating the Pauli principle related to the suppressed forbidden state.

The supersymmetric transformation can be applied in each partial wave, until all the Pauli forbidden states are removed. This method allows us to obtain a 'phase-equivalent' shallow potential from any deep potential. The shallow potential depends on the angular momenta. It gives the same phase shifts and the same energy levels for the physical states as the original deep potential. However, the wave functions generated by both potentials are quite different. The wave functions of the shallow potential does not indeed have the nodes corresponding to the Pauli forbidden states.

Chapter 3

Hyperspherical harmonics method for three-body models

3.1 Introduction

Three-body systems allow us to model nuclei that have a pronounced three-cluster structure. In these approches, the clusters are treated as pointlike particles, which interact through effective potentials.

In the present work, we will solve the three-body Schrödinger equations by the hyperspherical harmonics method [19, 27]. This method uses hyperspherical coordinates to represent the relative positions of three particles. It is a variational method in which the wave functions are expanded in a set of basis functions, called *hyperspherical harmonics*.

This chapter presents the hyperspherical formalism and its application in solving the three-body Schrödinger equation. It starts with definitions of Jacobi coordinates, which allow the hyperspherical coordinates to be defined. Next it defines the hyperspherical harmonics, and introduces their properties. After these definitions, the chapter considers the application of the hyperspherical harmonics to the three-body problem. The cases of local and nonlocal cluster-cluster potentials are treated. The Schrödinger equation is converted into equivalent equations in hyperspherical coordinates. These equations are solved by a variational approximation, called the *Lagrange-mesh* method. The chapter continues by presenting this technique. This finally leads to a discretisation of the equations into an equivalent algebraic eigenvalue problem, which can be numerically solved.

3.2 Jacobi coordinates

3.2.1 Definition of Jacobi coordinates

Let us consider a system of three particles labelled 1, 2 and 3, with mass numbers A_1, A_2 and A_3 (in nuclear mass unit m_N), and space coordinates $\boldsymbol{r}_1$, $\boldsymbol{r}_2$ and $\boldsymbol{r}_3$, respectively.

We introduce the centre-of-mass coordinate,

$$\boldsymbol{R} = \frac{A_1\boldsymbol{r}_1 + A_2\boldsymbol{r}_2 + A_3\boldsymbol{r}_3}{A_1 + A_2 + A_3}, \tag{3.1}$$

and three normalised sets of Jacobi coordinates $(\boldsymbol{x}_k, \boldsymbol{y}_k)$ (with $k = 1, 2, 3$) to represent the relative positions of the particles. These coordinates are defined as

$$\boldsymbol{x}_k = \sqrt{\mu_{ij}}\,(\boldsymbol{r}_i - \boldsymbol{r}_j)\,, \tag{3.2}$$

$$\boldsymbol{y}_k = \sqrt{\mu_{(ij)k}}\left(\boldsymbol{r}_k - \frac{A_i\boldsymbol{r}_i + A_j\boldsymbol{r}_j}{A_i + A_j}\right), \tag{3.3}$$

where

$$\mu_{ij} = \frac{A_iA_j}{A_i + A_j}, \tag{3.4}$$

$$\mu_{(ij)k} = \frac{(A_i + A_j)\,A_k}{A_i + A_j + A_k} \tag{3.5}$$

are reduced masses, and (i, j, k) is a cyclic permutation of $(1, 2, 3)$. The variable $\boldsymbol{x}_k$ is proportional to the distance between particles i and j, while $\boldsymbol{y}_k$ is proportional to the relative coordinate of particle k with respect to the centre of mass of the subsystem formed by i and j.

3.2.2 Change of Jacobi coordinates

The Jacobi coordinates $(\boldsymbol{x}_k, \boldsymbol{y}_k)$ are defined for a given index k. As this index can take the values $k = 1, 2$ or 3, there are three possible sets $(\boldsymbol{x}_k, \boldsymbol{y}_k)$ defined by equations (3.2) and (3.3). These sets of Jacobi coordinates are not independent. They are related by linear combinations. Let $i \neq k$. The relation between $(\boldsymbol{x}_k, \boldsymbol{y}_k)$ and $(\boldsymbol{x}_i, \boldsymbol{y}_i)$ is given [42] by

$$\boldsymbol{x}_k = -\cos\varphi_{ki}\,\boldsymbol{x}_i + \sin\varphi_{ki}\,\boldsymbol{y}_i, \tag{3.6}$$

$$\boldsymbol{y}_k = -\sin\varphi_{ki}\,\boldsymbol{x}_i - \cos\varphi_{ki}\,\boldsymbol{y}_i, \tag{3.7}$$

where

$$\varphi_{ki} = (-1)^P \arctan \sqrt{\frac{AA_j}{A_i A_k}}, \tag{3.8}$$

with the total mass number $A = A_1 + A_2 + A_3$, j such that (k, i, j) forms a permutation of $(1, 2, 3)$, and P being even (resp. odd) if this permutation is even (resp. odd).

The change from one set of Jacobi coordinates $(\boldsymbol{x}_i, \boldsymbol{y}_i)$ to another $(\boldsymbol{x}_k, \boldsymbol{y}_k)$ is quite useful in practice. When we consider the interaction potential between a given pair of particles, it is usually more convenient to use the set $(\boldsymbol{x}_k, \boldsymbol{y}_k)$ in which $\boldsymbol{x}_k$ is directly proportional to the distance between the two interacting particles.

3.3 Hyperspherical coordinates

3.3.1 Definition of hyperspherical coordinates

The Jacobi coordinates $\boldsymbol{x}_k$ and $\boldsymbol{y}_k$ can be transformed into an equivalent system of hyperspherical coordinates [7, 42]. These coordinates are defined from the norms and directions of $\boldsymbol{x}_k$ and $\boldsymbol{y}_k$. The vector $\boldsymbol{x}_k$ is represented by its norm x_k and its direction $\Omega_{x_k} = (\theta_{x_k}, \varphi_{x_k})$, where θ_{x_k} and φ_{x_k} denote two angles that identify the direction. Similarly, $\boldsymbol{y}_k$ is represented by its norm y_k and its direction $\Omega_{y_k} = (\theta_{y_k}, \varphi_{y_k})$.

From the norms x_k and y_k, a hyperradius ρ and an angle α_k are defined as

$$\rho = \sqrt{x_k^2 + y_k^2}, \tag{3.9}$$

$$\alpha_k = \arctan \frac{y_k}{x_k}. \tag{3.10}$$

With these definitions, x_k and y_k are given by

$$x_k = \rho \cos \alpha_k, \tag{3.11}$$

$$y_k = \rho \sin \alpha_k. \tag{3.12}$$

The value of ρ is independent of index k. It is identical for the three sets of Jacobi coordinates ($k = 1, 2, 3$):

$$\rho^2 = x_1^2 + y_1^2 = x_2^2 + y_2^2 = x_3^2 + y_3^2. \tag{3.13}$$

It can also be written using the coordinates $\boldsymbol{r}_i$ of the particles and the centre-of-mass coordinate $\boldsymbol{R}$:

$$\rho^2 = \sum_{i=1}^{3} A_i |\boldsymbol{r}_i - \boldsymbol{R}|^2 \tag{3.14}$$

$$= \frac{1}{A} \sum_{j<i=1}^{3} A_i A_j |\boldsymbol{r}_i - \boldsymbol{r}_j|^2. \tag{3.15}$$

Equation (3.14) shows us that ρ^2 corresponds to the moment of inertia of the system, with respect to the centre of mass.

The angle α_k (3.10) depends on index k, which means that its value is specific to the considered set of Jacobi coordinates. This value is bounded:

$$0 \leq \alpha_k \leq \frac{\pi}{2}. \tag{3.16}$$

The hyperspherical coordinates are composed of ρ, α_k and the directions Ω_{x_k} and Ω_{y_k}. It is convenient to use a notation Ω_{5k} that represents the angular coordinates collectively,

$$\Omega_{5k} = (\alpha_k, \Omega_{x_k}, \Omega_{y_k}), \tag{3.17}$$

$$= (\alpha_k, \theta_{x_k}, \varphi_{x_k}, \theta_{y_k}, \varphi_{y_k}). \tag{3.18}$$

The hyperradius ρ and the five angular coordinates Ω_{5k} are equivalent to the Jacobi vectors $\boldsymbol{x}_k$ and $\boldsymbol{y}_k$.

3.3.2 Kinetic energy in hyperspherical coordinates

In Jacobi coordinates, the centre-of-mass motion easily separates,

$$\frac{1}{A_1}\Delta_{\boldsymbol{r}_1} + \frac{1}{A_2}\Delta_{\boldsymbol{r}_2} + \frac{1}{A_3}\Delta_{\boldsymbol{r}_3} = \frac{1}{A}\Delta_{\boldsymbol{R}} + \Delta_{\boldsymbol{x}_k} + \Delta_{\boldsymbol{y}_k}. \tag{3.19}$$

The symbol $\Delta_{\boldsymbol{r}}$ represents the Laplacian operator for the variable $\boldsymbol{r}$. The kinetic-energy operator of the relative motion is thus given by

$$T = -\frac{\hbar^2}{2m_N}\left(\Delta_{\boldsymbol{x}_k} + \Delta_{\boldsymbol{y}_k}\right), \tag{3.20}$$

where m_N is the mass unit. The sum of Laplacians can be written in hyperspherical coordinates (ρ, Ω_{5k}):

$$\Delta_{\boldsymbol{x}_k} + \Delta_{\boldsymbol{y}_k} = \frac{\partial^2}{\partial\rho^2} + \frac{5}{\rho}\frac{\partial}{\partial\rho} - \frac{1}{\rho^2}\mathrm{K}^2(\Omega_{5k}), \tag{3.21}$$

where $\mathrm{K}^2(\Omega_{5k})$ is a differential operator [42] in the angular coordinates Ω_{5k},

$$\mathrm{K}^2(\Omega_{5k}) = -\frac{\partial^2}{\partial\alpha_k^2} - 4\cot(2\alpha_k)\frac{\partial}{\partial\alpha_k} + \frac{L_x^2}{\cos^2\alpha_k} + \frac{L_y^2}{\sin^2\alpha_k}, \tag{3.22}$$

L_x^2 and L_y^2 denoting the orbital angular momentum operators corresponding to the coordinates $\boldsymbol{x}_k$ and $\boldsymbol{y}_k$,

$$\boldsymbol{L_x} = -i\boldsymbol{x}_k \times \boldsymbol{\nabla}_{\boldsymbol{x}_k}, \qquad \Delta_{\boldsymbol{x}_k} = \frac{1}{x_k}\frac{\partial^2}{\partial x_k^2}\, x_k - \frac{L_x^2}{x_k^2}, \tag{3.23}$$

$$\boldsymbol{L_y} = -i\boldsymbol{y}_k \times \boldsymbol{\nabla}_{\boldsymbol{y}_k}, \qquad \Delta_{\boldsymbol{y}_k} = \frac{1}{y_k}\frac{\partial^2}{\partial y_k^2}\, y_k - \frac{L_y^2}{y_k^2}. \tag{3.24}$$

3.4 Hyperspherical harmonics

3.4.1 Definition of hyperspherical harmonics

The *hypersherical harmonics* [7, 42] are the eigenfunctions of the operator $\mathrm{K}^2(\Omega_{5k})$. They are functions of the angular variables $\Omega_{5k} = (\alpha_k, \Omega_{x_k}, \Omega_{y_k})$. As the dependence of $\mathrm{K}^2(\Omega_{5k})$ (3.22) on the directions Ω_{x_k} and Ω_{y_k} is exclusively through the operators L_x^2 and L_y^2, the hyperspherical harmonics $\mathcal{Y}^{m_x m_y}_{K l_x l_y}(\Omega_{5k})$ are defined from the following separation of variables:

$$\mathcal{Y}^{m_x m_y}_{K l_x l_y}(\Omega_{5k}) = \phi(\alpha_k)\; Y^{m_x}_{l_x}(\Omega_{x_k})\, Y^{m_y}_{l_y}(\Omega_{y_k}), \tag{3.25}$$

where $\phi(\alpha_k)$ is a function of the angle α_k and $Y^m_l(\Omega)$ denotes a spherical harmonic. Hence the hyperspherical harmonics are also eigenstates of L_x^2 and L_y^2,

$$L_x^2\, \mathcal{Y}^{m_x m_y}_{K l_x l_y}(\Omega_{5k}) = l_x(l_x+1)\, \mathcal{Y}^{m_x m_y}_{K l_x l_y}(\Omega_{5k}) \tag{3.26}$$

$$L_y^2\, \mathcal{Y}^{m_x m_y}_{K l_x l_y}(\Omega_{5k}) = l_y(l_y+1)\, \mathcal{Y}^{m_x m_y}_{K l_x l_y}(\Omega_{5k}), \tag{3.27}$$

where l_x and l_y are the orbital angular momentum associated with the relative coordinates $\boldsymbol{x}_k$ and $\boldsymbol{y}_k$. The symbols m_x and m_y represent the projection quantum numbers corresponding to l_x and l_y, respectively.

Using equations (3.22) and (3.25), the eigenvalue equation for $\phi(\alpha_k)$ is found to be

$$-\frac{d^2\phi}{d\alpha_k^2} - 4\cot(2\alpha_k)\frac{d\phi}{d\alpha_k} + \left(\frac{l_x(l_x+1)}{\cos^2\alpha_k} + \frac{l_y(l_y+1)}{\sin^2\alpha_k}\right)\phi = \lambda\phi \tag{3.28}$$

where λ is the eigenvalue. The solutions which are finite at $\alpha_k = 0$ and $\alpha_k = \pi/2$ [43] are

$$\phi(\alpha_k) = N(\cos\alpha_k)^{l_x}(\sin\alpha_k)^{l_y} P_n^{l_y+\frac{1}{2}, l_x+\frac{1}{2}}(\cos 2\alpha_k), \tag{3.29}$$

where N is a normalisation constant and $P_n^{a,b}(x)$ is a Jacobi polynomial of degree n [44]. The corresponding eigenvalues are

$$\lambda = (2n + l_x + l_y)(2n + l_x + l_y + 4), \tag{3.30}$$

where n must be zero or a positive integer: $n = 0, 1, 2, ...$

It is useful to introduce a quantity K defined as

$$K = 2n + l_x + l_y. \tag{3.31}$$

The hypersperical harmonics $\mathcal{Y}^{m_x m_y}_{K l_x l_y}(\Omega_{5k})$ are then defined as

$$\mathcal{Y}^{m_x m_y}_{K l_x l_y}(\Omega_{5k}) = N_K^{l_x l_y} (\cos\alpha_k)^{l_x} (\sin\alpha_k)^{l_y} P_n^{l_y+\frac{1}{2}, l_x+\frac{1}{2}}(\cos 2\alpha_k) \\ Y^{m_x}_{l_x}(\Omega_{x_k})\, Y^{m_y}_{l_y}(\Omega_{y_k}), \tag{3.32}$$

with the normalisation coefficient

$$N_K^{l_x l_y} = \sqrt{\frac{2\,(K+2)\,n!\,(n + l_x + l_y + 1)!}{\Gamma(n + l_x + 3/2)\,\Gamma(n + l_y + 3/2)}}. \tag{3.33}$$

They are eigenfunctions of $\mathrm{K}^2(\Omega_{5k})$, with eigenvalues $K(K+4)$,

$$\mathrm{K}^2(\Omega_{5k})\, \mathcal{Y}^{m_x m_y}_{K l_x l_y}(\Omega_{5k}) = K(K+4)\, \mathcal{Y}^{m_x m_y}_{K l_x l_y}(\Omega_{5k}). \tag{3.34}$$

The integer K is called the *hypermomentum* [7] because the operator $\mathrm{K}^2(\Omega_{5k})$ may be interpreted, following equation (3.21), as a generalisation of the concept of angular momentum to three-body systems in hyperspherical coordinates. The hypermomentum K is a quantum number such that $K \geq l_x + l_y$ and $K - l_x - l_y = 2n$, with n integer. It is a good quantum number in the special case of a system of three non-interacting particles.

The harmonics $\mathcal{Y}^{m_x m_y}_{K l_x l_y}(\Omega_{5k})$ are orthogonal:

$$\int \mathcal{Y}^{m'_x m'_y *}_{K' l'_x l'_y}(\Omega_{5k})\, \mathcal{Y}^{m_x m_y}_{K l_x l_y}(\Omega_{5k})\, d\Omega_{5k} = \delta_{KK'}\, \delta_{l_x l'_x}\, \delta_{l_y l'_y}\, \delta_{m_x m'_x}\, \delta_{m_y m'_y}, \tag{3.35}$$

where the element $d\Omega_{5k}$ is defined as

$$d\Omega_{5k} = \sin^2\alpha_k \cos^2\alpha_k\, d\alpha_k\, d\Omega_{x_k}\, d\Omega_{y_k}, \tag{3.36}$$

with α_k varying from 0 to $\pi/2$, and the directions Ω_{x_k} and Ω_{x_k} covering unit spheres.

3.4.2 Angular Momentum coupling

The hyperspherical harmonics $\mathcal{Y}^{m_x m_y}_{K l_x l_y}(\Omega_{5k})$ (3.32) read

$$\mathcal{Y}^{m_x m_y}_{K l_x l_y}(\Omega_{5k}) = \phi^{l_x l_y}_K(\alpha_k)\, Y^{m_x}_{l_x}(\Omega_{x_k})\, Y^{m_y}_{l_y}(\Omega_{y_k}), \tag{3.37}$$

with

$$\phi^{l_x l_y}_K(\alpha_k) = N^{l_x l_y}_K(\cos\alpha_k)^{l_x}(\sin\alpha_k)^{l_y}\, P^{l_y+\frac{1}{2},l_x+\frac{1}{2}}_n(\cos 2\alpha_k). \tag{3.38}$$

They are eigenfunctions of $\mathrm{K}^2(\Omega_{5k})$, L^2_x and L^2_y, but they are not eigenfunctions of the total angular momentum. This can be easily corrected. Hyperspherical harmonics $\mathcal{Y}^{M_L}_{K l_x l_y L}(\Omega_{5k})$ are then defined [7] by coupling l_x and l_y,

$$\mathcal{Y}^{M_L}_{K l_x l_y L}(\Omega_{5k}) = \phi^{l_x l_y}_K(\alpha_k)\, \left[Y_{l_x}(\Omega_{x_k}) \otimes Y_{l_y}(\Omega_{y_k})\right]^{L M_L}, \tag{3.39}$$

where L is the total orbital angular momentum and M_L its projection. They are connected to the $\mathcal{Y}^{m_x m_y}_{K l_x l_y}(\Omega_{5k})$ through the linear combinations:

$$\mathcal{Y}^{M_L}_{K l_x l_y L}(\Omega_{5k}) = \sum_{m_x m_y} (l_x l_y m_x m_y | L M_L)\, \mathcal{Y}^{m_x m_y}_{K l_x l_y}(\Omega_{5k}), \tag{3.40}$$

where $(l_x l_y m_x m_y | L M_L)$ stands for a Clebsch-Gordan coefficient.

In general, we must also take the spin into account. The spin states are represented by spinors $\chi^{S M_S}$, where S denotes the total spin and M_S its projection. The harmonics $\mathcal{Y}^{M_L}_{K l_x l_y L}(\Omega_{5k})$ and the spinors $\chi^{S M_S}$ are then coupled. Hyperspherical harmonics $\mathcal{Y}^{JM}_{\gamma K}(\Omega_{5k})$ [7, 45] with a given total angular momentum J are defined as

$$\begin{aligned} \mathcal{Y}^{JM}_{\gamma K}(\Omega_{5k}) &= \left[\mathcal{Y}_{K l_x l_y L}(\Omega_{5k}) \otimes \chi^S\right]^{JM} && (3.41)\\ &= \phi^{l_x l_y}_K(\alpha_k)\, \left[\left[Y_{l_x}(\Omega_{x_k}) \otimes Y_{l_y}(\Omega_{y_k})\right]^L \otimes \chi^S\right]^{JM}, && (3.42) \end{aligned}$$

where γ is a collective index which stands for $\{l_x l_y L S\}$, and M denotes the projection quantum number associated with J. These functions can also be written

$$\mathcal{Y}^{JM}_{\gamma K}(\Omega_{5k}) = \sum_{M_L M_S} (L S M_L M_S | J M)\; \mathcal{Y}^{M_L}_{K l_x l_y L}(\Omega_{5k})\; \chi^{S M_S}, \tag{3.43}$$

with Clebsch-Gordan coefficients. The total angular momentum J is the result of the coupling of the angular momentum L with the spin S.

3.4.3 Properties of the hyperspherical harmonics

The main properties of $\mathcal{Y}^{m_x m_y}_{K l_x l_y}(\Omega_{5k})$ are preserved by $\mathcal{Y}^{JM}_{\gamma K}(\Omega_{5k})$. The hyperspherical harmonics are eigenfunctions of $\mathrm{K}^2(\Omega_{5k})$, with the eigenvalues $K(K+4)$ (3.34), i.e.,

$$\mathrm{K}^2(\Omega_{5k})\,\mathcal{Y}^{JM}_{\gamma K}(\Omega_{5k}) = K(K+4)\,\mathcal{Y}^{JM}_{\gamma K}(\Omega_{5k}). \tag{3.44}$$

They are also eigenfunctions of total angular momentum J, with projection M, and of various underlying angular momenta represented by γ (i.e., l_x, l_y, L and S). They are normalised and form an orthogonal set (3.35),

$$\int \mathcal{Y}^{J'M'\dagger}_{\gamma' K'}(\Omega_{5k})\,\mathcal{Y}^{JM}_{\gamma K}(\Omega_{5k})\,d\Omega_{5k} = \delta_{\gamma\gamma'}\,\delta_{KK'}\,\delta_{JJ'}\,\delta_{M'M}, \tag{3.45}$$

where the dagger † indicates the complex conjugation and the transposition of the spinors.

In addition, $\mathcal{Y}^{JM}_{\gamma K}(\Omega_{5k})$ are functions with a definite parity. The parity operator Π transforms the functions by reversing the orientation of all vectors corresponding to space coordinates. It reverses the directions Ω_{x_k} and Ω_{y_k} but does not modify the angle α_k. The parity of the spherical harmonics is well known [46, 47]:

$$\Pi Y^{m_x}_{l_x}(\Omega_{x_k}) = (-1)^{l_x}\,Y^{m_x}_{l_x}(\Omega_{x_k}), \tag{3.46}$$

$$\Pi Y^{m_y}_{l_y}(\Omega_{y_k}) = (-1)^{l_y}\,Y^{m_y}_{l_y}(\Omega_{y_k}). \tag{3.47}$$

Therefore, following equation (3.37) or (3.42), the parity of the hyperspherical harmonics is given by the product of $(-1)^{l_x}$ and $(-1)^{l_y}$. The hypermomentum K is related to l_x and l_y by definition (3.31). Hence

$$(-1)^{l_x+l_y} = (-1)^K, \tag{3.48}$$

and

$$\Pi\mathcal{Y}^{JM}_{\gamma K}(\Omega_{5k}) = (-1)^K\,\mathcal{Y}^{JM}_{\gamma K}(\Omega_{5k}). \tag{3.49}$$

Thus the quantum number K gives the parity of the harmonics.

3.4.4 Raynal-Revai coefficients

The hypersherical harmonics depend on the angles Ω_{5k}. The index k refers to the Jacobi coordinates $(\boldsymbol{x}_k, \boldsymbol{y}_k)$ on which these angles are based. There are

three possible sets of coordinates for $k = 1, 2$ or 3. In practical calculations, it is convenient to change the value of k in order to systematically use the most appropriate coordinates Ω_{5k}.

The change from one set of coordinates to another is given in Jacobi coordinates by equations (3.6) and (3.7). The corresponding change in terms of hypersherical harmonics can be made via the Raynal-Revai coefficients. The hyperspherical harmonics of two different sets of coordinates are related by a linear combination:

$$\mathcal{Y}^{M_L}_{Kl_xl_yL}(\Omega_{5k}) = \sum_{l'_xl'_y} \langle i, l'_xl'_y|k, l_xl_y\rangle_{KL}\ \mathcal{Y}^{M_L}_{Kl'_xl'_yL}(\Omega_{5i}), \tag{3.50}$$

where $\langle i, l'_xl'_y|k, l_xl_y\rangle_{KL}$ denotes a Raynal-Revai coefficient [42]. This transformation conserves the quantum numbers K, L and M_L. The Raynal-Revai coefficients are defined as by

$$\langle i, l'_xl'_y|k, l_xl_y\rangle_{KL} = \int \mathcal{Y}^{M_L}_{Kl_xl_yL}(\Omega_{5k})\, \mathcal{Y}^{M_L*}_{Kl'_xl'_yL}(\Omega_{5i})\, d\Omega_{5i}, \tag{3.51}$$

where Ω_{5k} depends on Ω_{5i} (following equations (3.6) and (3.7)). They can be calculated by using a formula given in Appendix A.

The number of hyperspherical harmonics involved in the relation (3.50) is finite: l'_x and l'_y, as well as l_x and l_y, must be compatible with K and L, i.e.,

$$K = 2n' + l'_x + l'_y = 2n + l_x + l_y, \tag{3.52}$$

$$|l'_x - l'_y| \le L \le l'_x + l'_y, \tag{3.53}$$

$$|l_x - l_y| \le L \le l_x + l_y, \tag{3.54}$$

where n' and n are non-negative integers. The sum (3.50) runs over all l'_x and l'_y values obeying these conditions.

Of course, relation (3.50) with the Raynal-Revai coefficients also holds for the hyperspherical harmonics of total angular momentum, i.e.,

$$\mathcal{Y}^{JM}_{\gamma K}(\Omega_{5k}) = \sum_{l'_xl'_y} \langle i, l'_xl'_y|k, l_xl_y\rangle_{KL}\ \mathcal{Y}^{JM}_{\gamma' K}(\Omega_{5i}), \tag{3.55}$$

where γ' stands for $\{l'_xl'_yLS\}$ and γ for $\{l_xl_yLS\}$.

3.5 Three-body Schrödinger equation in the hyperspherical formalism

3.5.1 Three-body Hamiltonian

In a three-body model, the clusters are treated as pointlike particles. We assume that the interactions between the clusters can be represented by effective cluster-cluster potentials. Under these assumptions, the Hamiltonian describing a three-cluster system is

$$H = \sum_{i=1}^{3} T_i + \sum_{i>j=1}^{3} V_{ij}, \tag{3.56}$$

where T_i is the kinetic energy of cluster i and V_{ij} is the effective interaction potential between clusters i and j.

The simplest effective potentials V_{ij} are local. However, in our models, the considered potentials V_{ij} can be nonlocal (see Chapter 2). Those nonlocal potentials are derived from microscopic models. They allow us to take account of the Pauli principle.

The Hamiltonian (3.56) includes the kinetic energy of the centre of mass of the system. Because we are interested in the study of the relative motion of the clusters (not in the overall centre-of-mass translation), we separate the motion of the centre of mass. We introduce the kinetic energy T of the relative motion:

$$T = \sum_{i=1}^{3} T_i - T_{\text{c.m.}}, \tag{3.57}$$

where $T_{\text{c.m.}}$ is the centre-of-mass kinetic energy. The Hamiltonian, in the centre-of-mass frame, is then defined as

$$H = T + \sum_{i>j=1}^{3} V_{ij}, \tag{3.58}$$

so that this Hamiltonian describes the relative motion of the clusters.

3.5.2 Wave functions in the hyperspherical harmonic basis

The wave functions $\Psi^{JM\pi}$ describing the three-body system are the solutions of the Schrödinger equation

$$H\Psi^{JM\pi} = E\Psi^{JM\pi}, \tag{3.59}$$

where E is the energy of the system. Using the Hamiltonian (3.58), the Schrödinger equation reads

$$\left(T + \sum_{i>j=1}^{3} V_{ij}\right) \Psi^{JM\pi} = E\Psi^{JM\pi}. \tag{3.60}$$

The wave functions $\Psi^{JM\pi}$ are eigenstates with quantum numbers J, M and π, which are the total angular momentum, the projection of this angular momentum and the parity, respectively.

We solve equation (3.60) by using the hyperspherical harmonics [7, 19, 27]. The relative positions of the clusters are described in hyperspherical coordinates (ρ, Ω_{5q}); and the wave functions are expanded in the hyperspherical harmonic basis as

$$\Psi^{JM\pi} = \frac{1}{\rho^{5/2}} \sum_{\gamma K} \chi^{J\pi}_{\gamma K}(\rho)\, \mathcal{Y}^{JM}_{\gamma K}(\Omega_{5q}), \tag{3.61}$$

where the coefficients $\chi^{J\pi}_{\gamma K}(\rho)$ depends on the hyperradius. The functions $\chi^{J\pi}_{\gamma K}(\rho)$ do not depend on the quantum number M, because the Hamiltonian is rotation invariant. Of course, the values of the angular momenta $\gamma = \{l_x l_y LS\}$ must be compatible with the total angular momentum J. The parity π conditions the parity of K, and the l_x, l_y values in γ, since according to equations (3.48) and (3.49), the parity of the system is

$$\pi = \pi_1\pi_2\pi_3(-1)^K = \pi_1\pi_2\pi_3(-1)^{l_x+l_y}, \tag{3.62}$$

where π_i denotes the intrinsic parity of cluster i. The parity of K is thus imposed in the summation (3.61). Definition (3.31) also imposes $K \geq l_x + l_y$ on each γK value.

The factor $\rho^{-5/2}$ in expansion (3.61) leads to judicious simplifications, in the equations with the functions $\chi^{J\pi}_{\gamma K}(\rho)$. For example, it will cancel out the first derivative with respect to ρ in the kinetic-energy operator T, which is given by equations (3.20) and (3.21). It also allows us to write the square norm of the wave function as

$$\left\langle \Psi^{JM\pi} \,\middle|\, \Psi^{JM\pi} \right\rangle = \sum_{\gamma K} \int_0^{+\infty} \left|\chi^{J\pi}_{\gamma K}(\rho)\right|^2 d\rho. \tag{3.63}$$

Indeed, the hypervolume element for the integrals in hyperspherical coordinates is

$$d\boldsymbol{x}_k\, d\boldsymbol{y}_k = \rho^5 d\rho\, d\Omega_{5k}, \tag{3.64}$$

where $\boldsymbol{x}_k$ and $\boldsymbol{y}_k$ are the Jacobi coordinates and $d\Omega_{5k}$ is defined by equation (3.36). The factors $\rho^{-5/2}$ of the functions (3.61) cancel out the coefficient ρ^5 of the element (3.64).

3.5.3 Local potentials in the hyperspherical formalism

With expansion (3.61) of $\Psi^{JM\pi}$, the Schrödinger equation (3.60) can be transformed into a system of equations in the variable ρ [19, 27]. The coefficients of those equations are matrix elements of the potentials V_{ij} in the basis of the hyperspherical harmonics. We first consider the simple case of local potentials.

A local potential V_{ij} is defined as a function depending on the distance between the interacting particles. This distance may be written in hyperspherical coordinates. So the local potential is written as

$$V_{ij}\left(|\boldsymbol{r}_i-\boldsymbol{r}_j|\right)=V_{ij}\left(\frac{x_k}{\sqrt{\mu_{ij}}}\right)=V_{ij}\left(\frac{\rho\cos\alpha_k}{\sqrt{\mu_{ij}}}\right), \tag{3.65}$$

using definitions (3.2) and (3.11) of the Jacobi and hyperspherical coordinates. The index k corresponds to the label of the third particle, which is not involved in this interaction potential.

From the potential, we define a set of functions which depend on ρ,

$$V^{J\pi\,(ij-q)}_{\gamma'K',\gamma K}(\rho)=\int \mathcal{Y}^{JM\dagger}_{\gamma'K'}(\Omega_{5q})\,V_{ij}\left(\frac{\rho\cos\alpha_k}{\sqrt{\mu_{ij}}}\right)\,\mathcal{Y}^{JM}_{\gamma K}(\Omega_{5q})\,d\Omega_{5q}, \tag{3.66}$$

where index q refers to the hypersperical coordinates used for the expansion (3.61) of the wave function. In the integral, the angle α_k depends on the integration variables Ω_{5q}.

In general, the calculations of the integrals (3.66) are simpler for the particular case $q=k$,

$$V^{J\pi\,(ij-k)}_{\gamma'K',\gamma K}(\rho)=\int \mathcal{Y}^{JM\dagger}_{\gamma'K'}(\Omega_{5k})\,V_{ij}\left(\frac{\rho\cos\alpha_k}{\sqrt{\mu_{ij}}}\right)\,\mathcal{Y}^{JM}_{\gamma K}(\Omega_{5k})\,d\Omega_{5k}, \tag{3.67}$$

because α_k coincides with one integration variable. Otherwise, when $q\neq k$, the dependence of α_k on Ω_{5q} may complicate the calculations (3.66). However, with the Raynal-Revay coefficients [42], any calculation with $q\neq k$ can be reduced to calculations with $q=k$ only. It follows from relation (3.55) that for $q\neq k$,

$$V^{J\pi\,(ij-q)}_{\gamma'K',\gamma K}(\rho)\;=\sum_{l'''_x l'''_y\,l''''_x l''''_y}\langle k,l'''_x l'''_y|q,l_x l_y\rangle_{KL}\,\langle k,l''''_x l''''_y|q,l'_x l'_y\rangle_{K'L'}\,V^{J\pi\,(ij-k)}_{\gamma'''K',\gamma''K}(\rho), \tag{3.68}$$

where indices γ, γ', γ'' and γ''' stand for $\{l_x l_y LS\}$, $\{l'_x l'_y L'S'\}$, $\{l''_x l''_y LS\}$ and $\{l'''_x l'''_y L'S'\}$, respectively. We make use of expansion (3.68) with the Raynal-Revai coefficients to calculate the potential matrix elements. In this way, we just have to evaluate the integrals (3.67) with the hyperspherical harmonics adapted to the potential.

If the potential depends on the orbital angular momentum, the simplification accompanying the integrals (3.67) also lies in the fact that the harmonics $\mathcal{Y}^{JM}_{\gamma K}(\Omega_{5k})$ are then eigenstates of the appropriate orbital angular momentum, which is the quantum number l_x.

We will sum the contributions of the local parts of all the potentials of the three-body Schrödinger equation (3.60) in a single term $V^{J\pi}_{\gamma' K',\gamma K}(\rho)$, defined as

$$V^{J\pi}_{\gamma' K',\gamma K}(\rho) = V^{J\pi\,(12-q)}_{\gamma' K',\gamma K}(\rho) + V^{J\pi\,(13-q)}_{\gamma' K',\gamma K}(\rho) + V^{J\pi\,(23-q)}_{\gamma' K',\gamma K}(\rho). \tag{3.69}$$

3.5.4 Nonlocal potentials in the hyperspherical formalism

Now we consider the case of a nonlocal potential V_{ij}, acting between particles i and j. In this case, the potential is defined by a kernel $W_{ij}(\boldsymbol{r}, \boldsymbol{r}')$. Its action on a wave function $\varphi(\boldsymbol{r})$ is given by

$$(V_{ij}\,\varphi)(\boldsymbol{r}) = \int W_{ij}(\boldsymbol{r}, \boldsymbol{r}')\,\varphi(\boldsymbol{r}')\,d\boldsymbol{r}', \tag{3.70}$$

where $\boldsymbol{r} = \boldsymbol{r}_i - \boldsymbol{r}_j$ denotes the coordinate between the interacting particles. Following definition (3.2) of the Jacobi coordinate $\boldsymbol{x}_k$, the kernel $W_{ij}(\boldsymbol{r}, \boldsymbol{r}')$ can be written

$$W_{ij}(\boldsymbol{r}, \boldsymbol{r}') = W_{ij}\left(\frac{\boldsymbol{x}_k}{\sqrt{\mu_{ij}}}, \frac{\boldsymbol{x}'_k}{\sqrt{\mu_{ij}}}\right). \tag{3.71}$$

Let us consider a partial wave defined as

$$\varphi^{JM\pi}_{\gamma K}(\rho, \Omega_{5q}) = \frac{1}{\rho^{5/2}}\,\chi^{J\pi}_{\gamma K}(\rho)\,\mathcal{Y}^{JM}_{\gamma K}(\Omega_{5q}), \tag{3.72}$$

in hyperspherical coordinates (ρ, Ω_{5q}). Such a partial wave corresponds to a term of the expansion (3.61) of the wave function $\Psi^{JM\pi}$.

According to equation (3.70), the action of the potential on the wave $\varphi_{\gamma K}^{JM\pi}$ is

$$\big(V_{ij}\varphi_{\gamma K}^{JM\pi}\big)(\rho,\Omega_{5q}) = \int W_{ij}(\boldsymbol{r},\boldsymbol{r}')\,\varphi_{\gamma K}^{JM\pi}(\rho',\Omega'_{5q})\,d\boldsymbol{r}', \tag{3.73}$$

and using relation (3.71), this gives

$$\big(V_{ij}\varphi_{\gamma K}^{JM\pi}\big)(\rho,\Omega_{5q}) = \frac{1}{\mu_{ij}^{3/2}}\int W_{ij}\left(\frac{\boldsymbol{x}_k}{\sqrt{\mu_{ij}}},\frac{\boldsymbol{x}'_k}{\sqrt{\mu_{ij}}}\right)\varphi_{\gamma K}^{JM\pi}(\rho',\Omega'_{5q})\,d\boldsymbol{x}'_k, \tag{3.74}$$

where (ρ',Ω'_{5q}) is defined from $\boldsymbol{x}'_k(=\sqrt{\mu_{ij}}\boldsymbol{r}')$ and $\boldsymbol{y}_k$ as

$$\rho' = \sqrt{x_k'^2 + y_k^2}, \quad \Omega'_{5q} = (\alpha'_q,\Omega_{x'_q},\Omega_{y'_q}), \tag{3.75}$$

with Ω'_{5q} corresponding to Jacobi coordinates $(\boldsymbol{x}'_q,\boldsymbol{y}'_q)$,

$$\boldsymbol{x}'_q = -\cos\varphi_{qk}\,\boldsymbol{x}'_k + \sin\varphi_{qk}\,\boldsymbol{y}_k, \tag{3.76}$$
$$\boldsymbol{y}'_q = -\sin\varphi_{qk}\,\boldsymbol{x}'_k - \cos\varphi_{qk}\,\boldsymbol{y}_k, \tag{3.77}$$

where φ_{qk} is given by definition (3.8) if $q \neq k$ (see equations (3.6) and (3.7)), or else $\varphi_{kk} = \pi$. Note that (ρ',Ω'_{5q}) depends on the coordinates (ρ,Ω_{5q}), since $\boldsymbol{y}_k$ depends on (ρ,Ω_{5q}).

We define a set of functions of the hyperradius ρ which represent the action of the nonlocal potential on the partial wave $\varphi_{\gamma K}^{JM\pi}$ in the basis of the hyperspherical harmonics $\mathcal{Y}_{\gamma K}^{JM}(\Omega_{5q})$,

$$W_{\gamma'K',\gamma K}^{J\pi\,(ij-q)}(\rho) = \frac{1}{\mu_{ij}^{3/2}}\int \mathcal{Y}_{\gamma'K'}^{JM\dagger}(\Omega_{5q})\left[\int W_{ij}\left(\frac{\boldsymbol{x}_k}{\sqrt{\mu_{ij}}},\frac{\boldsymbol{x}'_k}{\sqrt{\mu_{ij}}}\right)\varphi_{\gamma K}^{JM\pi}(\rho',\Omega'_{5q})\,d\boldsymbol{x}'_k\right]d\Omega_{5q}. \tag{3.78}$$

With definition (3.72), we rewrite (3.78) as

$$W_{\gamma'K',\gamma K}^{J\pi\,(ij-q)}(\rho) = \frac{1}{\mu_{ij}^{3/2}}\iint\left(\mathcal{Y}_{\gamma'K'}^{JM\dagger}(\Omega_{5q})\,W_{ij}\left(\frac{\boldsymbol{x}_k}{\sqrt{\mu_{ij}}},\frac{\boldsymbol{x}'_k}{\sqrt{\mu_{ij}}}\right)\mathcal{Y}_{\gamma K}^{JM}(\Omega'_{5q})\,d\Omega_{5q}\right)\frac{\chi_{\gamma K}^{J\pi}(\rho')}{\rho'^{5/2}}\,d\boldsymbol{x}'_k. \tag{3.79}$$

In general, the calculations are much simpler when $q = k$, because the hyperspherical coordinates (ρ, Ω_{5q}) then correspond to the Jacobi variables of the potential,

$$W^{J\pi\,(ij-k)}_{\gamma' K',\gamma K}(\rho) = \\ \frac{1}{\mu_{ij}^{3/2}} \iint \left(\mathcal{Y}^{JM\dagger}_{\gamma' K'}(\Omega_{5k})\, W_{ij}\left(\frac{\boldsymbol{x}_k}{\sqrt{\mu_{ij}}}, \frac{\boldsymbol{x}'_k}{\sqrt{\mu_{ij}}} \right) \mathcal{Y}^{JM}_{\gamma K}(\Omega'_{5k})\, d\Omega_{5k} \right) \frac{\chi^{J\pi}_{\gamma K}(\rho')}{\rho'^{5/2}}\, d\boldsymbol{x}'_k. \tag{3.80}$$

Therefore, we make use of the relation (3.55) with the Raynal-Revai coefficients, in order to expand the functions for $q \neq k$ as

$$W^{J\pi\,(ij-q)}_{\gamma' K',\gamma K}(\rho) = \sum_{l'''_x l'''_y\, l'''_x l'''_y} \langle k, l''_x l''_y | q, l_x l_y \rangle_{KL} \, \langle k, l'''_x l'''_y | q, l'_x l'_y \rangle_{K'L'} \, W^{J\pi\,(ij-k)}_{\gamma''' K',\gamma'' K}(\rho), \tag{3.81}$$

where γ, γ', γ'' and γ''' stand for $\{l_x l_y LS\}$, $\{l'_x l'_y L'S'\}$, $\{l''_x l''_y LS\}$ and $\{l'''_x l'''_y L'S'\}$, respectively. For the calculations, we thus reduce the integrals to the simpler case (3.80) with $q = k$.

Also, it is convenient to define a hyperradial kernel $W^{(ij-q)}_{\gamma' K',\gamma K}(\rho, \rho')$ by

$$W^{J\pi\,(ij-q)}_{\gamma' K',\gamma K}(\rho) = \frac{1}{\rho^{5/2}} \int_0^\infty W^{(ij-q)}_{\gamma' K',\gamma K}(\rho, \rho')\; \chi^{J\pi}_{\gamma K}(\rho')\, d\rho', \tag{3.82}$$

which gives the action of the potential on the hyperradial function $\chi^{J\pi}_{\gamma K}(\rho)$.

In the case where the nonlocal potential (3.70) can be expanded in terms of partial waves of relative orbital angular momentum as

$$W_{ij}(\boldsymbol{r}, \boldsymbol{r}') = \sum_{l=0}^{\infty} \sum_{m=-l}^{l} Y_l^{m*}(\Omega_{r'})\, Y_l^m(\Omega_r)\, W^l_{ij}(r, r'), \tag{3.83}$$

the hyperradial kernel, for $q = k$, reduces [19] to

$$W^{(ij-k)}_{\gamma' K',\gamma K}(\rho, \rho') = \\ \frac{\delta_{\gamma\gamma'}}{\mu_{ij}^{3/2} (\rho\rho')^{3/2}} \int_0^{\min(\rho,\rho')} W^{l_x}_{ij}\left(\frac{x}{\sqrt{\mu_{ij}}}, \frac{x'}{\sqrt{\mu_{ij}}} \right) \phi^{l_x l_y}_{K'}(\alpha)\, \phi^{l_x l_y}_{K}(\alpha')\, x\, x'\, y^2\, dy, \tag{3.84}$$

where $x = (\rho^2 - y^2)^{1/2}$, $x' = (\rho'^2 - y^2)^{1/2}$, $\alpha = \arctan(y/x)$, $\alpha' = \arctan(y/x')$, and where the functions $\phi^{l_x l_y}_K(\alpha)$ are defined by equation (3.38).

We will sum the contributions of the nonlocal potentials of the three-body Schrödinger equation (3.60) in a single kernel,

$$W_{\gamma' K',\gamma K}(\rho,\rho') = W^{(12-q)}_{\gamma' K',\gamma K}(\rho,\rho') + W^{(13-q)}_{\gamma' K',\gamma K}(\rho,\rho') + W^{(23-q)}_{\gamma' K',\gamma K}(\rho,\rho'), \quad (3.85)$$

where q is the label of the hyperspherical coordinates (ρ, Ω_{5q}) used for the expansion (3.61) of the wave function $\Psi^{JM\pi}$.

3.5.5 Hyperradial equations

We apply the hyperspherical formalism to the Schrödinger equation. The expansion (3.61) of $\Psi^{JM\pi}$ in hyperspherical harmonics allows us to reduce equation (3.60) to an equivalent set of coupled equations for the hyperradial functions $\chi^{J\pi}_{\gamma K}(\rho)$ [19],

$$\left[-\frac{\hbar^2}{2m_N}\left(\frac{d^2}{d\rho^2} - \frac{(K+3/2)(K+5/2)}{\rho^2}\right) - E\right]\chi^{J\pi}_{\gamma K}(\rho) + \sum_{\gamma' K'} V^{J\pi}_{\gamma K,\gamma' K'}(\rho)\,\chi^{J\pi}_{\gamma' K'}(\rho) + \sum_{\gamma' K'}\int_0^\infty W_{\gamma K,\gamma' K'}(\rho,\rho')\;\chi^{J\pi}_{\gamma' K'}(\rho')\,d\rho' = 0. \quad (3.86)$$

These equations are obtained by using the orthogonality (3.45) of the hyperspherical harmonics. The kinetic-energy terms follow from equations (3.20) and (3.21), giving T in hyperspherical coordinates, and from the property (3.44), giving K. The local and nonlocal potential terms are separated; $V^{J\pi}_{\gamma K,\gamma' K'}(\rho)$ and $W_{\gamma K,\gamma' K'}(\rho,\rho')$ are defined by equations (3.69) and (3.85).

Note that since there is an equation (3.86) for each hyperradial function $\chi^{J\pi}_{\gamma K}(\rho)$, the number of coupled equations is in general infinite.

For the potentials that are bounded, or that do not tend to infinity as fast as $1/\rho^2$ when $\rho \to 0$, the singularity in equation (3.86) arises from the effective centrifugal term, proportional to $(K+3/2)(K+5/2)/\rho^2$. Hence their behaviour near the origin is

$$\chi^{J\pi}_{\gamma K}(\rho) \underset{\rho\to 0}{\sim} \rho^{K+5/2}, \quad (3.87)$$

because the functions $\chi^{J\pi}_{\gamma K}(\rho)$ have to be bounded, and therefore, for $\Psi^{JM\pi}$ (3.61),

$$\rho^{-5/2}\chi^{J\pi}_{\gamma K}(\rho) \underset{\rho\to 0}{\sim} \rho^{K}. \quad (3.88)$$

Also, for a bound state, $\chi^{J\pi}_{\gamma K}(\rho)$ must be square integrable (3.63) and thus asymptotically vanish,

$$\chi^{J\pi}_{\gamma K}(\rho) \underset{\rho\to\infty}{\sim} e^{-k\rho}, \tag{3.89}$$

with $k = \sqrt{2m_N E}/\hbar$.

3.5.6 Truncation of the hyperspherical expansion

The system of equations (3.86) has in principle an infinite number of equations. We solve these equations by a numerical method: we truncate the series (3.61) by imposing a maximum value K_M on the hypermomenta K. The wave function is then approximated as

$$\Psi^{JM\pi} \approx \frac{1}{\rho^{5/2}} \sum_{\gamma,\, K\le K_M} \chi^{J\pi}_{\gamma K}(\rho)\, \mathcal{Y}^{JM}_{\gamma K}(\Omega_{5k}), \tag{3.90}$$

where the sum is limited to a finite number of terms.

The value of K_M is a variational parameter which leads to a finite set of hyperradial equations,

$$\begin{aligned}&\left[-\frac{\hbar^2}{2m_N}\left(\frac{d^2}{d\rho^2} - \frac{(K+3/2)(K+5/2)}{\rho^2}\right) - E\right]\chi^{J\pi}_{\gamma K}(\rho)\\ &+ \sum_{\gamma',K'\le K_M} V^{J\pi}_{\gamma K,\gamma' K'}(\rho)\,\chi^{J\pi}_{\gamma' K'}(\rho) + \sum_{\gamma',K'\le K_M}\int_0^\infty W_{\gamma K,\gamma' K'}(\rho,\rho')\,\chi^{J\pi}_{\gamma' K'}(\rho')\,d\rho' = 0,\end{aligned} \tag{3.91}$$

with the truncation $K \le K_M$. The higher the value of K_M, the more accurate are the solutions of the Schrödinger equation.

3.6 Lagrange-mesh method

3.6.1 General principle of the Lagrange meshes

We solve equations (3.91) by the Lagrange-mesh method [19, 27]. This is an approximate variational method that exploits a Gaussian quadrature [48–52].

The Lagrange functions are defined with a set of N mesh points $u_i \in [0, +\infty[$ with $i = 1, ..., N$. The Lagrange functions $f_i(u)$ are N independent functions that verify at the mesh points u_i the "Lagrange condition":

$$f_i(u_{i'}) = \lambda_i^{-1/2}\delta_{ii'}. \tag{3.92}$$

Each function $f_i(u)$ has thus the property to vanish at all mesh points but one. The constant values λ_i and the mesh points u_i are determined so as to respectively correspond to the weights and the nodes associated with a Gaussian quadrature rule [44], which is a numerical integration method:

$$\int_0^\infty g(u)\,du \approx \sum_{i=1}^{N} \lambda_i\, g(u_i), \tag{3.93}$$

for any (regular enough) integrable function $g(u)$.

The Lagrange-mesh method consists in making use of the quadrature (3.93) and the property (3.92). The wave functions are expanded in the basis of Lagrange functions $f_i(u)$.

The Lagrange condition (3.92) ensures that the basis functions $f_i(u)$ are orthogonal with this Gaussian quadrature. The functions $f_i(u)$ can even be exactly orthonormal:

$$\int_0^\infty f_i(u) f_{i'}(u)\,du = \delta_{ii'}, \tag{3.94}$$

when the Gaussian quadrature is exact for products of Lagrange functions. This is the case, in particular, when the Lagrange functions are constructed from orthogonal polynomials.

The local potentials are represented by diagonal matrices,

$$\int_0^\infty f_i(u) V(u) f_{i'}(u)\,du \approx V(u_i)\,\delta_{ii'}, \tag{3.95}$$

with the Gaussian quadrature. The kinetic-energy terms are given by matrix elements of the operator $-\frac{d^2}{du^2}$. They are evaluated as

$$-\int_0^\infty f_i(u) f''_{i'}(u)\,du \approx -\lambda_i^{1/2} f''_{i'}(u_i), \tag{3.96}$$

where $f''_{i'}(u)$ stands for the second derivative of $f_{i'}(u)$ with respect to u.

In practice, the accuracy of the Lagrange-mesh method turns out to be essentially as good as the accuracy of an exact variational calculation performed with the Lagrange basis $f_i(u)$ [27, 51]. This accuracy remains very good when the method is applied to nonlocal interactions [19, 52].

3.6.2 Lagrange functions

For u varying on $[0, +\infty[$, the Lagrange functions are defined from the Gauss-Laguerre quadrature [27, 52]. They are defined by

$$f_i(u) = (-1)^i u_i^{1/2} \frac{L_N(u)}{u - u_i}\, e^{-u/2}, \tag{3.97}$$

where $L_N(u)$ denotes the Laguerre polynomial of degree N. The mesh points u_i are the roots of the polynomial,

$$L_N(u_i) = 0, \tag{3.98}$$

with $i = 1, ..., N$. Hence $f_i(u)$ is a polynomial of degree $N-1$ multiplied by a decreasing exponential. The weights λ_i of the quadrature are given by [27, 44]

$$\lambda_i = \frac{e^{u_i}}{u_i [L'_N(u_i)]^2}. \tag{3.99}$$

The functions $f_i(u)$ satisfy the Lagrange condition (3.92). The Gaussian quadrature (3.93), using u_i and λ_i, gives exact evaluations of integrals for functions that are products of an exponential e^{-u} and a polynomial of degree $2N-1$, that is,

$$\int_0^\infty e^{-u} P_m(u)\, du = \sum_{i=1}^{N} \lambda_i\, e^{-u_i} P_m(u_i), \tag{3.100}$$

for any polynomial $P_m(u)$ of degree $m \leq 2N-1$. Hence the orthogonality (3.94) is exact for the $f_i(u)$. In the same way, the kinetic-energy terms (3.96), calculated with the Gaussian quadrature, are also exact, with these functions.

3.6.3 Regularisation factor

However, when the Schrödinger equation presents a singularity at the origin of the coordinates (such as a centrifugal barrier or a Coulomb potential) the functions $f_i(u)$ (3.97) are not directly used. Their behaviour near the origin is indeed not appropriate: while the wave functions vanish near the origin, the functions $f_i(u)$ do not. Therefore, in the Lagrange-mesh method, a regularisation factor [27, 49, 50] is introduced, in order to adapt the functions. Regularised functions $\hat{f}_i(u)$ are defined as

$$\hat{f}_i(u) = \left(\frac{u}{u_i}\right)^n f_i(u), \tag{3.101}$$

with an arbitrary power n, to be determined further. The functions $\hat{f}_i(u)$ still satisfy the Lagrange condition (3.92). They vanish at the origin, with a behaviour proportional to u^n.

With these functions $\hat{f}_i(u)$, the potential matrix (3.95) is preserved, i.e.,

$$\int_0^\infty \hat{f}_i(u) V(u) \hat{f}_{i'}(u)\, du \approx V(u_i)\, \delta_{ii'}, \tag{3.102}$$

and the centrifugal terms, in particular, are defined:

$$\int_0^\infty \hat{f}_i(u) \frac{1}{u^2} \hat{f}_{i'}(u)\, du \approx \frac{1}{u_i^2}\, \delta_{ii'}. \tag{3.103}$$

For $n = 1$ and $n = 3/2$, the quadrature (3.103) is even exact, because condition (3.100) is met.

The kinetic-energy matrix at the Gaussian approximation is

$$\hat{T}^G_{ii'} = -\lambda_i^{1/2} \hat{f}''_{i'}(u_i). \tag{3.104}$$

For $\hat{f}_i(u)$ defined by equations (3.101) and (3.97), these terms are [27], for $i = i'$,

$$\hat{T}^G_{ii} = \frac{-12n^2 + 24n - 8 + (4N+2)u_i - u_i^2}{12 u_i^2}, \tag{3.105}$$

and, for $i \neq i'$,

$$\hat{T}^G_{ii'} = (-1)^{i-i'} \frac{u_{i'}^{n-3/2}}{u_i^{n-1/2}} \frac{(2n-1)u_i - (2n-3)u_{i'}}{(u_i - u_{i'})^2}. \tag{3.106}$$

3.6.4 Scale parameter

The mesh points u_i $(i = 1, ..., N)$ are the roots (3.98) of the Laguerre polynomial of degree N. The position of these N mesh points is therefore fixed, for the variable u. In the Lagrange-mesh method, u is however a dummy variable, proportional to a physical variable $\rho = hu$. A scale factor h is indeed introduced in order to optimise the Gaussian quadrature. The physical integration variable is actually ρ, and u is defined by a change of variable, e.g.

$$\int_0^{+\infty} g(\rho)\, d\rho = h \int_0^{+\infty} g(hu)\, du \tag{3.107}$$

$$\approx h \sum_{i=1}^{N} \lambda_i\, g(hu_i) = h \sum_{i=1}^{N} \lambda_i\, g(\rho_i), \tag{3.108}$$

where ρ_i is defined by $\rho_i = hu_i$. The parameter h is aimed to adapt the mesh points ρ_i to the physical size of the problem. This may enable us to reduce the number N of mesh points, and therefore the size of the matrices.

In practice, the parameter h is determined so that the Lagrange-mesh method yields stable accurate results, independently of the precise value of h on a wide plateau [27].

3.6.5 Solving the equations with the Lagrange-mesh method

We solve the hyperradial equations (3.91) by the Lagrange-mesh method [19]. The functions $\chi^{J\pi}_{\gamma K}(\rho)$ are expanded in the basis of Lagrange functions,

$$\chi^{J\pi}_{\gamma K}(\rho) = \frac{1}{\sqrt{h}} \sum_{i=1}^{N} C^{J\pi}_{\gamma K i}\, \hat{f}_i(\rho/h), \tag{3.109}$$

with functions $\hat{f}_i(\rho/h)$ and a scale parameter h.

The power n in the regularisation factor (3.101) of $\hat{f}_i(\rho/h)$ must be able to reproduce the behaviour of $\chi^{J\pi}_{\gamma K}(\rho)$ near the origin, which is proportional to $\rho^{K+5/2}$ (3.87). We take $n = 3/2$ [27]. The basis functions are thus defined as

$$\hat{f}_i(u) = (-1)^i \, \frac{u^{3/2}}{u_i} \, \frac{L_N(u)}{u - u_i} \, e^{-u/2}, \tag{3.110}$$

with $u = \rho/h$. The expansion (3.109) can reproduce the behaviour in $\rho^{K+5/2}$ for small ρ, provided the size N of the basis is larger than $K+1$. This power, $n = 3/2$, gives a kinetic-energy matrix $\hat{T}^G_{ii'}$ (3.106) that is symmetric. Also the matrix (3.103) of the centrifugal term becomes exact for $n = 3/2$,

$$\int_0^\infty \hat{f}_i(u) \frac{1}{u^2} \hat{f}_{i'}(u)\, du = \frac{1}{u_i^2}\, \delta_{ii'}. \tag{3.111}$$

However, the basis functions $\hat{f}_i(u)$ are then only orthonormal with the Gaussian quadrature,

$$\int_0^\infty \hat{f}_i(u) \hat{f}_{i'}(u)\, du \approx \delta_{ii'}, \tag{3.112}$$

but this approximation is reasonable [27] in the eigenvalue problem below.

The expansion (3.109) allows us to reduce the hyperradial equations (3.91) to an algebraic eigenvalue problem. Indeed, when these expansions are inserted in the system of equations, we have then

$$\sum_{\gamma' K' i} \left(H^{J\pi}_{\gamma K i, \gamma' K' i'} - E\, \delta_{\gamma\gamma'}\, \delta_{KK'}\, \delta_{ii'} \right) C^{J\pi}_{\gamma' K' i'} = 0, \tag{3.113}$$

where the matrix $H^{J\pi}_{\gamma Ki,\gamma' K' i'}$ is defined with the Lagrange-mesh method [19] by

$$H^{J\pi}_{\gamma Ki,\gamma' K' i'} = \frac{\hbar^2}{2m_N}\left[\frac{1}{h^2}\hat{T}^G_{ii'} + -\frac{(K+3/2)(K+5/2)}{(hu_i)^2}\,\delta_{ii'}\right]\delta_{\gamma\gamma'}\,\delta_{KK'} + V^{J\pi}_{\gamma K,\gamma' K'}(hu_i)\,\delta_{ii'} \;+\; W^{J\pi}_{\gamma Ki,\gamma' K' i'}. \quad (3.114)$$

The kinetic term $\hat{T}^G_{ii'}$ is given by equations (3.105) and (3.106), with $n = 3/2$. The local potential term $V^{J\pi}_{\gamma K,\gamma' K'}(hu_i)$ is evaluated at the mesh points, according to the quadrature (3.102). The nonlocal potential term $W^{J\pi}_{\gamma Ki,\gamma' K' i'}$ is defined as

$$W^{J\pi}_{\gamma Ki,\gamma' K' i'} = \frac{1}{h}\int_0^\infty d\rho \int_0^\infty d\rho'\, \hat{f}_i(\rho/h)\, W_{\gamma K,\gamma' K'}(\rho,\rho')\, \hat{f}_{i'}(\rho'/h), \quad (3.115)$$

from the kernel $W_{\gamma K,\gamma' K'}(\rho,\rho')$. The calculations of the elements $V^{J\pi}_{\gamma K,\gamma' K'}(hu_i)$ and $W^{J\pi}_{\gamma Ki,\gamma' K' i'}$ is discussed in Appendix B.

Equation (3.113) is an algebraic problem, where the energy E of the three-body system is an eigenvalue of the matrix $H^{J\pi}_{\gamma Ki,\gamma' K' i'}$.

The matrix $H^{J\pi}_{\gamma Ki,\gamma' K' i'}$ is symmetric, because the kernels of the nonlocal potentials are symmetric functions. Moreover this matrix is real, because we consider real potentials.

The eigenvalue problem depends on three parameters: K_M, N and h. The size of the matrix $H^{J\pi}_{\gamma Ki,\gamma' K' i'}$ is determined by K_M and N. The parameter K_M controls the number of γK values, while N is the size of the basis of Lagrange functions (index i runs from 1 to N). The parameter h is a scale factor for the Lagrange mesh. It is aimed to reduce, as much as possible, the value of N in practice.

The energy E and the coefficients $C^{J\pi}_{\gamma Ki}$ of the wave functions are determined by using standard numerical techniques of solving eigenvalue problems, for real symmetric matrix $H^{J\pi}_{\gamma Ki,\gamma' K' i'}$.

To sum up, the three-body Schrödinger equation (3.60), involving nonlocal potentials, is finally reduced to an algebraic eigenvalue problem (3.113). To this end, the wave function is first expanded in the hyperspherical harmonic basis (3.61). Next, by a variational approach, the series expansion is truncated (3.90). The resulting equations (3.91) are then discretized by means of the Lagrange-mesh approximation. The hyperradial functions are expanded in a basis of Lagrange functions (3.109). This leads to the eigenvalue problem (3.113), which can be numerically solved.

Chapter 4

The microscopic three-cluster model in the hyperspherical formalism

4.1 Introduction

The hyperspherical harmonics, defined in the previous chapter, can also be efficiently used in microscopic models. Indeed, Korennov and Descouvemont [53] have developed a microscopic three-cluster model, which is based on the hyperspherical harmonics. This model consists in applying the hyperspherical formalism in the framework of the Generator-Coordinate Method (GCM). The GCM is a variational technique to solve the many-body Schrödinger equation which arises in microscopic cluster models [2, 29–31, 54].

In the present work, we will use the microscopic model of Korennov and Descouvemont for comparisons with non-microscopic models. This chapter gives a brief description of this microscopic model.

4.2 Microscopic three-cluster wave function

4.2.1 Definitions

Consider the Hamiltonian describing a system of A nucleons:

$$h_A = \sum_{i=1}^{A} t_i - T_{\text{c.m.}} + \sum_{i>j=1}^{A} v_{ij}, \tag{4.1}$$

where t_i is the kinetic energy of nucleon i, v_{ij} is an effective nucleon-nucleon potential, and $T_{\text{c.m.}}$ is the kinetic energy of the centre of mass. The wave

function ψ of this system is given by the Schrödinger equation:

$$h_A\psi = E\,\psi, \tag{4.2}$$

where E is the energy of the system.

Here, the system of nucleons is assumed to present a three-cluster structure. In this case, the many-body Schrödinger equation (4.2) can be solved with a variational approach taking into account the cluster structure. The nucleons are distributed into three clusters: we denote by A_1, A_2 and A_3 the numbers of nucleons in the three clusters, respectively. These mass numbers are such that $A_1 + A_2 + A_3 = A$.

The individual spatial coordinates of the nucleons are denoted by $\boldsymbol{r}_i$, with $i = 1, ..., A$. We define three coordinates, $\boldsymbol{R}_1$, $\boldsymbol{R}_2$ and $\boldsymbol{R}_3$, representing the centres of mass of the clusters:

$$\boldsymbol{R}_1 = \frac{1}{A_1}\sum_{i=1}^{A_1}\boldsymbol{r}_i, \qquad \boldsymbol{R}_2 = \frac{1}{A_2}\sum_{i=A_1+1}^{A_1+A_2}\boldsymbol{r}_i, \qquad \boldsymbol{R}_3 = \frac{1}{A_3}\sum_{i=A_1+A_2+1}^{A_1+A_2+A_3}\boldsymbol{r}_i. \tag{4.3}$$

We define Jacobi coordinates, $\boldsymbol{r}_x$ and $\boldsymbol{r}_y$, indicating the relative positions of the clusters:

$$\boldsymbol{r}_x = \boldsymbol{R}_1 - \boldsymbol{R}_2, \tag{4.4}$$

$$\boldsymbol{r}_y = \boldsymbol{R}_3 - \frac{A_1\boldsymbol{R}_1 + A_2\boldsymbol{R}_2}{A_1 + A_2}. \tag{4.5}$$

Of course, these coordinates depend on the coordinates of the nucleons:

$$\boldsymbol{r}_x = \frac{1}{A_1}\sum_{i=1}^{A_1}\boldsymbol{r}_i - \frac{1}{A_2}\sum_{i=A_1+1}^{A_1+A_2}\boldsymbol{r}_i, \tag{4.6}$$

$$\boldsymbol{r}_y = \frac{1}{A_3}\sum_{i=A_1+A_2+1}^{A_1+A_2+A_3}\boldsymbol{r}_i - \frac{1}{A_1+A_2}\sum_{i=1}^{A_1+A_2}\boldsymbol{r}_i. \tag{4.7}$$

We also define the centre of mass of the system:

$$\boldsymbol{R}_{cm} = \frac{A_1\boldsymbol{R}_1 + A_2\boldsymbol{R}_2 + A_3\boldsymbol{R}_3}{A_1 + A_2 + A_3} = \frac{1}{A}\sum_{i=1}^{A}\boldsymbol{r}_i. \tag{4.8}$$

In the microscopic model, the wave function ψ of the system is defined as

$$\psi = \mathcal{A}\,\phi_1\phi_2\phi_3\,g(\boldsymbol{r}_x, \boldsymbol{r}_y), \tag{4.9}$$

where ϕ_1, ϕ_2 and ϕ_3 denote the internal wave functions of the clusters, and $g(\boldsymbol{r}_x, \boldsymbol{r}_y)$ is a function describing the relative motion between the clusters. The wave function respects the Pauli principle: it is fully antisymmetrised with respect to all nucleon coordinates, via the antisymmetriser $\mathcal{A}$ (2.4). Note that this wave function is a simple generalisation of the RGM wave function (2.2) for a three-cluster system. Hence the wave function (4.9) is known as the RGM wave function.

In definition (4.9), of course, the functions ϕ_1, ϕ_2 and ϕ_3, which describe the clusters, must be consistent with the choice of $\boldsymbol{r}_x$ and $\boldsymbol{r}_y$ (which means that ϕ_1 depends on nucleons $i = 1, ..., A_1$, ϕ_2 depends on nucleons $i = A_1 + 1, ..., A_1 + A_2$, and ϕ_3 depends on nucleons $i = A_1 + A_2 + 1, ..., A$). These internal wave functions of the clusters are generally approximated in a translation-invariant harmonic-oscillator shell model. The relative-motion function $g(\boldsymbol{r}_x, \boldsymbol{r}_x)$ is an unknown function, to be determined by solving the Schrödinger equation.

4.2.2 The hyperspherical formalism applied to the RGM wave function

Having introduced the wave function (4.9), we show how the hyperspherical formalism is applied in the microscopic model.

We introduce the reduced masses

$$\mu_{12} = \frac{A_1 A_2}{A_1 + A_2}, \qquad \mu_{(12)3} = \frac{(A_1 + A_2)\, A_3}{A_1 + A_2 + A_3}, \tag{4.10}$$

and renormalise the coordinates:

$$\boldsymbol{x} = \sqrt{\mu_{12}}\ \boldsymbol{r}_x \tag{4.11}$$

$$\boldsymbol{y} = \sqrt{\mu_{(12)3}}\ \boldsymbol{r}_y. \tag{4.12}$$

The hyperspherical coordinates are defined by

$$\rho = \sqrt{x^2 + y^2}, \tag{4.13}$$

$$\alpha = \arctan \frac{y}{x}. \tag{4.14}$$

We use the notation Ω_5, for the 5 angular variables:

$$\Omega_5 = (\alpha, \Omega_x, \Omega_y), \tag{4.15}$$

where Ω_x and Ω_y denote the directions of $\boldsymbol{x}$ and $\boldsymbol{y}$. The hyperspherical coordinates (ρ, Ω_5) are equivalent to the coordinates $\boldsymbol{r}_x$ and $\boldsymbol{r}_y$.

Using these coordinates, the relative-motion function of the wave function (4.9) is expanded in the hyperspherical harmonics:

$$g(\boldsymbol{r}_x, \boldsymbol{r}_y) = \rho^{-5/2} \sum_{K l_x l_y L} \chi^L_{K l_x l_y}(\rho)\, \mathcal{Y}^{M_L}_{K l_x l_y L}(\Omega_5), \tag{4.16}$$

where harmonics $\mathcal{Y}^{M_L}_{K l_x l_y L}(\Omega_5)$ are defined by equation (3.39). This expansion is formally analogous to the expansion (3.61) of the three-body models, but with an essential difference: the hyperspherical coordinates (ρ, Ω_5) here are functions of the coordinates of the nucleons, according to equations (4.6) and (4.7).

Thus, the RGM wave function (4.9) reads

$$\psi = \mathcal{A}\, \phi_1 \phi_2 \phi_3\, \rho^{-5/2} \sum_{K l_x l_y L} \chi^L_{K l_x l_y}(\rho)\, \mathcal{Y}^{M_L}_{K l_x l_y L}(\Omega_5). \tag{4.17}$$

Note that the antisymmetriser $\mathcal{A}$ acts on the whole wave function.

The idea of such a formalism is to replace the unknown function $g(\boldsymbol{r}_x, \boldsymbol{r}_y)$ by an equivalent set of functions $\chi^L_{K l_x l_y}(\rho)$, which depend only on the hyperradius ρ.

So far, the spins of the clusters have not been considered in order to simplify the presentation. We can now take into account the spin. In particular, we shall couple the angular momenta and the spins, in order to define a wave function that is an eigenstate of the total angular momentum.

We define the total spin S as resulting from the coupling of the different spins of the clusters. The wave functions, ϕ_1, ϕ_2 and ϕ_3, include spinors, representing the respective spin states of the clusters (see equation (2.6)). Eigenstates of the total spin S can be defined by

$$\Phi^{S M_S}_{S_{12}} = \Big[\big[\phi_1 \otimes \phi_2\big]^{S_{12}} \otimes \phi_3 \Big]^{S M_S}, \tag{4.18}$$

where M_S is the projection quantum number associated with S; and S_{12} is the result of the coupling of the spins of clusters 1 and 2. The total spin S is the result of the coupling of S_{12} with the spin of cluster 3.

Now, we couple the total orbital angular momentum L of the hyperspherical harmonics $\mathcal{Y}^{M_L}_{K l_x l_y L}(\Omega_5)$ with the total spin S. The wave function (4.17) then becomes

$$\psi^{J M \pi} = \mathcal{A} \sum_{\gamma K} \rho^{-5/2} \chi^{J\pi}_{\gamma K}(\rho) \left[\mathcal{Y}_{K l_x l_y L}(\Omega_5) \otimes \Phi^S_{S_{12}} \right]^{J M}, \tag{4.19}$$

where γ stands for $\{l_x l_y L S_{12} S\}$. This wave function $\psi^{JM\pi}$ has the following good quantum numbers: the total angular momentum J, with its projection M, and the parity π. The wave function is antisymmetrised with respect to all the nucleons. The functions $\Phi_{S_{12}}^{SM_S}$ take into account the internal structure of the clusters. The functions $\chi_{\gamma K}^{J\pi}(\rho)$ and $\mathcal{Y}_{K l_x l_y L}^{M_L}(\Omega_5)$ describe the relative motion between the clusters. These functions $\chi_{\gamma K}^{J\pi}(\rho)$ are analogous to the hyperradial functions of (3.61), but here hyperradius ρ is a function of the coordinates of the nucleons. The parity π of the wave function imposes condition on $\gamma\, K$, according to the selection rule (3.62).

4.3 The generator-coordinate method

4.3.1 GCM basis functions

In the previous section, we have seen the principle of the three-cluster microscopic models in the hyperspherical formalism. However, the form (4.19) of $\psi^{JM\pi}$ is not the most convenient to solve the many-body Schrödinger equation (4.2). In practice, this equation is solved numerically by the Generator-Coordinate Method (GCM) [53, 54].

The GCM is a technique in which the microscopic wave function is expanded into linear combinations of Slater determinants. In this section, we introduce the basis functions of the three-cluster GCM.

The GCM is based on harmonic-oscillator shell models. Let us consider a harmonic-oscillator potential centred at a given point $\boldsymbol{P}_i$. A system of A_i nucleons is represented in the shell model given by this potential by a Slater determinant $\Phi_i^{S_i\nu_i}(\boldsymbol{P}_i)$. Such a wave function represents a cluster located at $\boldsymbol{P}_i$. The wave function $\Phi_i^{S_i\nu_i}(\boldsymbol{P}_i)$ includes a spinor: S_i denotes the spin of the cluster and ν_i the spin projection. The wave function depends on the coordinates of the A_i nucleons, and on $\boldsymbol{P}_i$, which is an independent constant parameter.

The GCM basis functions for a three-cluster model are defined [53, 54] by

$$\Phi_\nu(\boldsymbol{P}_1, \boldsymbol{P}_2, \boldsymbol{P}_3) = \mathcal{A}\, \Phi_1^{S_1\nu_1}(\boldsymbol{P}_1)\, \Phi_2^{S_2\nu_2}(\boldsymbol{P}_2)\, \Phi_3^{S_3\nu_3}(\boldsymbol{P}_3), \tag{4.20}$$

where ν stands for (ν_1, ν_2, ν_3). The parameters $\boldsymbol{P}_1$, $\boldsymbol{P}_2$ and $\boldsymbol{P}_3$ represent the central positions of three clusters, with A_1, A_2 and A_3 nucleons, respectively. These functions are fully antisymmetrised with respect to all the nucleons, via the operator $\mathcal{A}$.

To avoid cumbersome notation, in the following, we drop the explicit mention of the spins S_i, and write more simply the GCM basis function

(4.20) as

$$\Phi_\nu(\boldsymbol{P}_1, \boldsymbol{P}_2, \boldsymbol{P}_3) = \mathcal{A}\, \Phi_1^{\nu_1}(\boldsymbol{P}_1)\, \Phi_2^{\nu_2}(\boldsymbol{P}_2)\, \Phi_3^{\nu_3}(\boldsymbol{P}_3). \tag{4.21}$$

From $\boldsymbol{P}_1$, $\boldsymbol{P}_2$ and $\boldsymbol{P}_3$, one defines two jacobi parameters, $\boldsymbol{R}_x$ and $\boldsymbol{R}_y$, giving the relative positions of the clusters,

$$\boldsymbol{R}_x = \boldsymbol{P}_1 - \boldsymbol{P}_2, \tag{4.22}$$

$$\boldsymbol{R}_y = \boldsymbol{P}_3 - \frac{A_1\boldsymbol{P}_1 + A_2\boldsymbol{P}_2}{A_1 + A_2}. \tag{4.23}$$

The localisation of the centers $\boldsymbol{P}_1$, $\boldsymbol{P}_2$ and $\boldsymbol{P}_3$ is then chosen such that $A_1\boldsymbol{P}_1 + A_2\boldsymbol{P}_2 + A_3\boldsymbol{P}_3 = 0$. With this condition,

$$\boldsymbol{P}_1 = -\frac{A_3}{A}\boldsymbol{R}_y + \frac{A_2}{A_{12}}\boldsymbol{R}_x, \tag{4.24}$$

$$\boldsymbol{P}_2 = -\frac{A_3}{A}\boldsymbol{R}_y - \frac{A_1}{A_{12}}\boldsymbol{R}_x, \tag{4.25}$$

$$\boldsymbol{P}_3 = \frac{A_{12}}{A}\boldsymbol{R}_y, \tag{4.26}$$

where $A_{12} = A_1 + A_2$. The basis functions (4.21) can thus be written

$$\begin{aligned}&\Phi_\nu(\boldsymbol{R}_x, \boldsymbol{R}_y)\\ &= \mathcal{A}\, \Phi_1^{\nu_1}\left(-\frac{A_3}{A}\boldsymbol{R}_y + \frac{A_2}{A_{12}}\boldsymbol{R}_x\right) \Phi_2^{\nu_2}\left(-\frac{A_3}{A}\boldsymbol{R}_y - \frac{A_1}{A_{12}}\boldsymbol{R}_x\right) \Phi_3^{\nu_3}\left(\frac{A_{12}}{A}\boldsymbol{R}_y\right).\end{aligned} \tag{4.27}$$

The parameters $\boldsymbol{R}_x$ and $\boldsymbol{R}_y$, which determine the basis functions, are called *generator coordinates*.

In the basis functions (4.27), the cluster internal functions $\Phi_i^{\nu_i}(\boldsymbol{P}_i)$ are described in a harmonic-oscillator shell model. In practice, it is judicious to choose exactly the same oscillator frequency for all the clusters [30, 53, 54], because the functions (4.27) can then be written as

$$\Phi_\nu(\boldsymbol{R}_x, \boldsymbol{R}_y) = \phi_{cm}\mathcal{A}\phi_1^{\nu_1}\phi_2^{\nu_2}\phi_3^{\nu_3}\, \Gamma\left(\boldsymbol{r}_x - \boldsymbol{R}_x, \frac{b}{\sqrt{\mu_{12}}}\right) \Gamma\left(\boldsymbol{r}_y - \boldsymbol{R}_y, \frac{b}{\sqrt{\mu_{(12)3}}}\right), \tag{4.28}$$

where the centre-of-mass motion is factorised out; $\phi_i^{\nu_i}$ is then a translation-invariant shell-model wave function describing cluster i, and Γ is a Gaussian function defined by

$$\Gamma(\boldsymbol{r}, \beta) = \left(\frac{1}{\pi\beta^2}\right)^{3/4} \exp\left(-\frac{r^2}{2\beta^2}\right). \tag{4.29}$$

The centre-of-mass motion is given by

$$\phi_{cm} = \left(\frac{A}{\pi b^2}\right)^{3/4} \exp\left(-\frac{AR_{cm}^2}{2b^2}\right). \tag{4.30}$$

In equations (4.28) and (4.30), b is the harmonic-oscillator parameter. The variables $\boldsymbol{r}_x$ and $\boldsymbol{r}_y$ are the Jacobi coordinates depending on the nucleons, and defined by equations (4.6) and (4.7).

The GCM consists in expanding the wave function, solution of Schrödinger equation (4.2), in the basis functions $\Phi_\nu(\boldsymbol{R}_x, \boldsymbol{R}_y)$, as

$$\psi = \sum_\nu \int f_\nu(\boldsymbol{R}_x, \boldsymbol{R}_y)\, \Phi_\nu(\boldsymbol{R}_x, \boldsymbol{R}_y)\, d\boldsymbol{R}_x d\boldsymbol{R}_y. \tag{4.31}$$

The advantage of the GCM is that the basis functions are linear combinations of Slater determinants. This property allows systematic calculations of matrix elements of one-body and two-body operators [30, 55].

4.3.2 GCM in the hyperspherical formalism

The so-defined basis functions $\Phi_\nu(\boldsymbol{R}_x, \boldsymbol{R}_y)$ (4.28) depend on two generator coordinates: $\boldsymbol{R}_x$ and $\boldsymbol{R}_y$. Korennov and Descouvemont [53] have applied the hyperspherical formalism to these basis functions, in order to reduce the parameters to a single scalar generator coordinate (namely a generator hyperradius). Their approach is presented here.

In Section 4.2.2, hyperspherical coordinates (ρ, Ω_5) equivalent to $\boldsymbol{r}_x$ and $\boldsymbol{r}_y$ have been defined. Similarly, hyperspherical generator coordinates corresponding to $\boldsymbol{R}_x$ and $\boldsymbol{R}_y$ can be defined. First, the coordinates $\boldsymbol{R}_x$ and $\boldsymbol{R}_y$ are renormalised:

$$\boldsymbol{X} = \sqrt{\mu_{12}}\, \boldsymbol{R}_x \tag{4.32}$$

$$\boldsymbol{Y} = \sqrt{\mu_{(12)3}}\, \boldsymbol{R}_y. \tag{4.33}$$

A generator hyperradius R and a generator angle α_R are then defined:

$$R = \sqrt{X^2 + Y^2}, \tag{4.34}$$

$$\alpha_R = \arctan\frac{Y}{X}. \tag{4.35}$$

The corresponding angular variables are represented by the symbol Ω_{5R}:

$$\Omega_{5R} = (\alpha_R, \Omega_X, \Omega_Y), \tag{4.36}$$

where Ω_X and Ω_Y denote the directions of $\boldsymbol{X}$ and $\boldsymbol{Y}$ respectively. These variables (R, Ω_{5R}) are equivalent to $(\boldsymbol{R}_x, \boldsymbol{R}_y)$.

In the microscopic model, there are thus two distinct hyperspherical systems: there are the coordinates (ρ, Ω_5), equivalent to $\boldsymbol{r}_x$ and $\boldsymbol{r}_y$, and the generator coordinates (R, Ω_{5R}). In order to avoid any confusion, we shall add an index ρ to Ω_5, and thus write $\Omega_{5\rho}$ for Ω_5. Hence the two distinct systems of hyperspherical coordinates are written $(\rho, \Omega_{5\rho})$ and (R, Ω_{5R}).

Note that $(\rho, \Omega_{5\rho})$ depend on the coordinates of the nucleons, while (R, Ω_{5R}) are independent parameters.

Using the coordinates (R, Ω_{5R}), the GCM basis functions (4.28) are expanded in the hyperspherical harmonics as

$$\Phi_\nu(\boldsymbol{R}_x, \boldsymbol{R}_y) = \phi_{cm} \sum_{l_x l_y L M_L K} \mathcal{Y}^{M_L *}_{K l_x l_y L}(\Omega_{5R})\, \Phi^{l_x l_y L M_L}_{\nu K}(R). \tag{4.37}$$

The coefficients $\Phi^{l_x l_y L M_L}_{\nu K}(R)$ are then defined by

$$\Phi^{l_x l_y L M_L}_{\nu K}(R) = \frac{1}{\phi_{cm}} \int \mathcal{Y}^{M_L}_{K l_x l_y L}(\Omega_{5R})\, \Phi_\nu(\boldsymbol{R}_x, \boldsymbol{R}_y)\, d\Omega_{5R}. \tag{4.38}$$

Note that the functions $\Phi^{l_x l_y L M_L}_{\nu K}(R)$ are independent of centre-of-mass motion, since ϕ_{cm} is factorised out in the expansion (4.37).

The functions $\Phi^{l_x l_y L M_L}_{\nu K}(R)$ are determined by using the following expansion:

$$\exp(\boldsymbol{x}\cdot\boldsymbol{X} + \boldsymbol{y}\cdot\boldsymbol{Y}) = \frac{(2\pi)^3}{(\rho R)^2} \sum_{l_x l_y L M_L K} I_{K+2}(\rho R)\, \mathcal{Y}^{M_L *}_{K l_x l_y L}(\Omega_{5R})\, \mathcal{Y}^{M_L}_{K l_x l_y L}(\Omega_{5\rho}), \tag{4.39}$$

where $I_{K+2}(x)$ is a modified Bessel function [44]. This expansion follows from the plane-wave expansion in hyperspherical coordinates [42]:

$$\exp\left[i(\boldsymbol{x}\cdot\boldsymbol{X} + \boldsymbol{y}\cdot\boldsymbol{Y})\right] = \frac{(2\pi)^3}{(\rho R)^2} \sum_{l_x l_y L M_L K} i^K J_{K+2}(\rho R)\, \mathcal{Y}^{M_L *}_{K l_x l_y L}(\Omega_{5R})\, \mathcal{Y}^{M_L}_{K l_x l_y L}(\Omega_{5\rho}), \tag{4.40}$$

where $J_{K+2}(x)$ is a Bessel function. Using (4.28), (4.39) and definition (4.38), the functions $\Phi^{l_x l_y L M_L}_{\nu K}(R)$ reduce to

$$\Phi^{l_x l_y L M_L}_{\nu K}(R) = \mathcal{A}\, \phi_1^{\nu_1} \phi_2^{\nu_2} \phi_3^{\nu_3}\, \mathcal{Y}^{M_L}_{K l_x l_y L}(\Omega_{5\rho})\, G_K(b, \rho, R), \tag{4.41}$$

where

$$G_K(b,\rho,R) = c\left(\frac{b^2}{\rho R}\right)^2 \exp\left(-\frac{\rho^2+R^2}{2b^2}\right) I_{K+2}\left(\frac{\rho R}{b^2}\right), \tag{4.42}$$

with c denoting a constant

$$c = \left(\frac{\mu_{12}\mu_{(12)3}}{\pi^2 b^4}\right)^{3/4} (2\pi)^3 = \left(\frac{A_1A_2A_3}{A}\right)^{3/4}\left(\frac{4\pi}{b^2}\right)^{3/2}. \tag{4.43}$$

Equation (4.41) gives basis functions $\Phi_{\nu K}^{l_x l_y L M_L}(R)$ depending on a single generator coordinate, the hyperradius R. The next step is to couple the total orbital momentum L with the spins, in order to get basis functions that are eigenstates of the total angular momentum J. This is performed by using Clebsch-Gordan coefficients:

$$\Phi_{\gamma K}^{JM\pi}(R) = \sum_{\nu_1\nu_2\nu_3}\sum_{M_L} (S_1S_2\nu_1\nu_2|S_{12}\nu_{12})(S_{12}S_3\nu_{12}\nu_3|SM_S) \\ (LSM_LM_S|JM)\,\Phi_{\nu K}^{l_x l_y L M_L}(R), \tag{4.44}$$

with $\gamma = \{l_x l_y L S_{12} S\}$ (and where $\nu_{12} = \nu_1 + \nu_2$, $M_S = \nu_{12} + \nu_3$). This can also be written

$$\Phi_{\gamma K}^{JM\pi}(R) = \mathcal{A}\left[\mathcal{Y}_{K l_x l_y L}(\Omega_{5\rho}) \otimes \Phi_{S_{12}}^{S}\right]^{JM} G_K(b,\rho,R), \tag{4.45}$$

where $\Phi_{S_{12}}^{SM_S}$ is defined by equation (4.18) from the cluster internal functions $\phi_1^{\nu_1}$, $\phi_2^{\nu_2}$ and $\phi_3^{\nu_3}$.

In the hyperspherical GCM, the wave function $\psi^{JM\pi}$ of the three-cluster system is written as a superposition of the basis functions $\Phi_{\gamma K}^{JM\pi}(R)$ [53], i.e.,

$$\psi^{JM\pi} = \sum_{\gamma K}\int_0^\infty f_{\gamma K}^{J\pi}(R)\,\Phi_{\gamma K}^{JM\pi}(R)\,dR, \tag{4.46}$$

with coefficients $f_{\gamma K}^{J\pi}(R)$ to be determined.

This function $\psi^{JM\pi}$ is formally equivalent to the wave function (4.19) with the hyperradial functions $\chi_{\gamma K}^{J\pi}(\rho)$. The functions are indeed connected to each other through

$$\chi_{\gamma K}^{J\pi}(\rho) = \rho^{5/2}\int_0^\infty f_{\gamma K}^{J\pi}(R)\,G_K(b,\rho,R)\,dR. \tag{4.47}$$

The functions $f^{J\pi}_{\gamma K}(R)$ and the energy E of the system are determined by solving the Hill-Wheeler integral equations [2, 29, 31]:

$$\sum_{\gamma' K'} \int_0^\infty \left(H^{J\pi}_{\gamma K,\gamma' K'}(R,R') - E\, N^{J\pi}_{\gamma K,\gamma' K'}(R,R') \right) f^{J\pi}_{\gamma' K'}(R')\, dR' = 0, \quad (4.48)$$

where

$$H^{J\pi}_{\gamma K,\gamma' K'}(R,R') = \left\langle \Phi^{JM\pi}_{\gamma K}(R) \,\middle|\, h_A \,\middle|\, \Phi^{JM\pi}_{\gamma' K'}(R') \right\rangle, \quad (4.49)$$

$$N^{J\pi}_{\gamma K,\gamma' K'}(R,R') = \left\langle \Phi^{JM\pi}_{\gamma K}(R) \,\middle|\, \Phi^{JM\pi}_{\gamma' K'}(R') \right\rangle, \quad (4.50)$$

with the bracket notation meaning an integration over all the coordinates of the nucleons.

The Hill-Wheeler equations (4.48) are solved numerically. First, the matrix elements (4.49) and (4.50) must be calculated. The main advantage of the GCM is that it involves Slater determinants. Indeed, the basis functions (4.27) can be written as linear combinations of Slater determinants. This greatly facilitates the calculations, because systematic formulae for the calculation of the matrix elements between Slater determinants are available [55]. These formulae are used in calculating the matrix elements (4.49) and (4.50). The elements (4.49) and (4.50) are then reduced to 7-dimensional integrals [53]. In practice, those integrals will be evaluated numerically.

Next, the Hill-Wheeler equations (4.48) must be solved. The advantage of the hyperspherical formalism is that it leads to a single generator coordinate, the hyperradius R. The equations are solved by discretizing the generator coordinate R. The wave function (4.46) is then approximated by a linear combination

$$\psi^{JM\pi} \approx \sum_{\gamma K} \sum_{n=1}^{N} \tilde{f}^{J\pi}_{\gamma K}(R_n)\, \Phi^{JM\pi}_{\gamma K}(R_n), \quad (4.51)$$

with a finite set of N values R_n. The integrals over R are replaced by sums over R_n, and the Hill-Wheeler equations become an algebraic problem. This approximation corresponds to a variational calculation in the finite basis $\Phi^{JM\pi}_{\gamma K}(R_n)$. The algebraic problem is then solved numerically [53].

Chapter 5

The non-microscopic, semi-microscopic, and microscopic three-cluster models

5.1 Introduction

In this chapter, we consider different three-cluster models, in view of applying and comparing them in the next chapters. The first model, which will serve as reference, is the fully antisymmetrised microscopic model, described in the previous chapter. The other models considered here are simple three-body approaches, based on effective cluster-cluster potentials. They are non-microscopic models, which regard the clusters as pointlike particles. From the point of view of the effective potentials, we consider two approaches: we have, on the one hand, the models using local potentials and, on the other hand, the models using the nonlocal RGM potentials. We term the latter – with the RGM potentials – *semi-microscopic models*, and we will determine in next chapters whether or not they can reasonably well approximate the microscopic model.

The chapter starts by describing the models. Next, it briefly gives the spectroscopic values which can serve as points of comparison. After that, it mentions the three-body systems that will be considered in the next chapters. It then describes some potentials that will be common to several applications. These are the effective nucleon-nucleon potentials, used in the microscopic models, and potentials describing the interactions between an α-cluster and a neutron, and between two α-clusters. The question of the Pauli forbidden

states, and their necessary elimination, is treated. Lastly, the question of the energy-dependence of the RGM potentials is mentioned.

5.2 Comparison of three-cluster models

The most elaborate model here is the microscopic model, which takes account of all the coordinates of the nucleons, with fully antisymmetrised wave functions. We consider the three-cluster microscopic model described in Chapter 4. This model is based on a Hamiltonian with effective nucleon-nucleon potentials. The Pauli principle, acting between the nucleons, is fully respected. However, in order to perform the calculations, the internal structure of the clusters is approximated in a harmonic-oscillator model. In spite of this simplification, the microscopic model remains complicated and heavy to handle. Hence the use of the three-cluster microscopic model is in practice limited to light nuclei, because of the laborious computational work, increasing with the number of nucleons.

The non-microscopic models are much simpler. They are easier to use. In these models, the internal structure of the clusters is neglected. The clusters are considered as pointlike particles. The modelling then consists in choosing effective potentials to represent the interactions between the clusters. These potentials are used in the three-body Schrödinger equation (3.60), determining the relative motion of the clusters.

In the simplest approach, the potentials between the clusters are local. We shall call *local models* the non-microscopic models with local potentials. The local potentials are fitted to empirical data, such as scattering phase shifts of the nuclei corresponding to the clusters.

There are however two categories of local potentials (see Section 2.3.2): the deep and shallow potentials. In the shallow potentials, the effects of the Pauli principle between the clusters are just simulated by a repulsive force. In the deep potentials, the simulation of the Pauli principle is improved by taking into account the existence of the Pauli forbidden states. Indeed, the deep potentials generate unphysical bound states that play the role of the Pauli forbidden states. The physical wave functions are then orthogonal to these Pauli forbidden states. The question of the treatment of the forbidden states in three-cluster models will be discussed in Section 5.5.

The *semi-microscopic models* are another version of the cluster models that we analyse and develop in this work. The idea is simple: instead of using purely phenomenological potentials in three-body models, we employ the

nonlocal effective potentials provided by the two-cluster RGM (to represent the inter-cluster potentials). This approach is interesting because these models are then more realistic than the local models. They are also much simpler and faster than the microscopic model, because they are three-body models, assuming pointlike clusters. Moreover, the semi-microscopic models allow us to investigate the fundamental question of the effective cluster-cluster interactions, or in other words, the effective potential between two nuclei. The RGM potentials are deduced from the nucleon-nucleon forces and incorporate the effects of the Pauli principle through their nonlocality.

There are two variants of RGM potentials (see Section 2.3.1): the *energy-dependent* nonlocal potentials and the *energy-independent* nonlocal potentials. The semi-microscopic model that uses the energy-dependent RGM potentials in three-body models has been first developed and worked out by Fujiwara and co-workers [17, 18, 28] (with the Faddeev method). However, we will show that such a model with the energy-dependent RGM potentials turns out to be problematic, especially when applied to the ^{9}Be nucleus [20]. This will motivate the development of the semi-microscopic model using the energy-independent RGM potentials [21–23]. Both energy-dependent and energy-independent potential models will be analysed on specific examples of nuclei and hypernuclei, in the next chapters.

The semi-microscopic models can be regarded as approximations of the microscopic model. The ingedients of the nonlocal RGM potentials are indeed the same (i.e., a nucleon-nucleon potential, and the internal cluster wave functions) as for the microscopic model. Thus, a comparison between the semi-microscopic models and the fully microscopic model is meaningfull and instructive.

In particular, the comparison between the models is interesting considering the Pauli principle. Because the nonlocal RGM potentials come from two-cluster microscopic models (see Chapter 2), they incorporate the effects of the Pauli principle corresponding to two interacting clusters. Hence the semi-microscopic model simulates the Pauli principle between each pair of clusters, but neglects the effects involving the three clusters simultaneously. Thus, the importance of the three-cluster Pauli effects may be estimated by comparing the semi-microscopic models with the fully microscopic model.

In this work, we will compare the local models, the semi-microscopic models, and the microscopic models. The comparison is furthermore facilitated because the models are all based on a common hyperspherical formalism (Chapters 3 and 4).

5.3 Model observables

Solving the respective equations of the models, we obtain the energies and the wave functions of the three-body systems.

The first point of comparison between the models, of course, will be the energy levels E. The zero of energy, $E = 0$, is defined as the three-body dissociation threshold. For bound states, the energy is negative, $E < 0$, and the absolute value $(-E)$ gives the three-body binding energy.

We will also compute the mean-square radius. In the three-body models, the mean-square radius $\langle r^2 \rangle$ is

$$\langle r^2 \rangle \;=\; \left\langle \Psi^{JM\pi} \right| \frac{1}{A} \left(\sum_{j=1}^{3} A_j |\boldsymbol{r}_j - \boldsymbol{R}|^2 + \sum_{j=1}^{3} A_j \, r_{\alpha j}^2 \right) \left| \Psi^{JM\pi} \right\rangle , \quad (5.1)$$

where $\boldsymbol{R}$ is the centre-of-mass coordinate, $\boldsymbol{r}_j$ is the coordinate of cluster j, $\Psi^{JM\pi}$ denotes the wave function; and the size of each cluster is taken into account by $r_{\alpha j}$, which is the intrinsic radius of cluster j.

With the definition (3.14) of the hyperradius ρ, the mean-square radius reduces to

$$\langle r^2 \rangle \;=\; \frac{1}{A} \left\langle \Psi^{JM\pi} \right| \rho^2 \left| \Psi^{JM\pi} \right\rangle + \frac{1}{A} \sum_{j=1}^{3} A_j \, r_{\alpha j}^2 . \quad (5.2)$$

The radius is evaluated with the Lagrange-mesh technique as

$$\langle r^2 \rangle \;\simeq\; \frac{1}{A} \sum_{\gamma K i} (h u_i)^2 |C_{\gamma K i}^{J\pi}|^2 + \frac{1}{A} \sum_{j=1}^{3} A_j \, r_{\alpha j}^2 , \quad (5.3)$$

where $C_{\gamma K i}^{J\pi}$ are the algebraic coefficients (3.113) of the wave function, u_i (with $i = 1, ..., N$) are the mesh points, and h is the scale parameter. The coefficients are normalised as

$$\sum_{\gamma K i} |C_{\gamma K i}^{J\pi}|^2 = 1. \quad (5.4)$$

When we compare the models, the intrinsic radii $r_{\alpha j}$ of the clusters will be defined according to the microscopic model. That is, for an α-cluster, the internal function (2.6), in the harmonic-oscillator shell model, leads to the square radius

$$r_{\alpha j}^2 = \frac{9}{8} b^2 , \quad (5.5)$$

while for a nucleon (when $A_j = 1$), $r_{\alpha j} = 0$, because the nucleons are treated as pointlike particles.

In order to represent the wave functions and to analyse the three-body structure, we will also calculate some probability densities, as functions of the relative distances between the clusters,

$$P^{J\pi}(r_{ij}, r_{k-ij}) = \left(\mu_{ij}\,\mu_{(ij)k}\right)^{1/2}\, x^2 y^2 \int d\Omega_x d\Omega_y\, |\Psi^{JM\pi}(\boldsymbol{x}, \boldsymbol{y})|^2. \qquad (5.6)$$

where $\boldsymbol{x}$ and $\boldsymbol{y}$ are the Jacobi coordinates, r_{ij} and r_{k-ij} are the distances associated with these Jacobi coordinates: r_{ij} is the distance between clusters i and j, and r_{k-ij} is the distance between cluster k and the centre of mass of the subsystem formed by i and j. The probability densities are, of course, normalised:

$$\int_0^\infty \int_0^\infty P(r_{ij}, r_{k-ij})\, dr_{ij}\, dr_{k-ij} = 1. \qquad (5.7)$$

We will also compute other values, such as reduced transition probabilities $B(E2)$ [56], proton or neutron densities (see Appendix F).

5.4 Effective potentials

5.4.1 Three-body systems

In the next chapters, we will consider several physical systems. The first examples will be two hypernuclei: ${}^{\;\;6}_{\Lambda\Lambda}$He and ${}^{\;\;9}_{\Lambda}$Be [19]. These hypernuclei will be studied as three-body $\alpha\Lambda\Lambda$ and $\alpha\alpha\Lambda$ systems, respectively. Such models require $\alpha\alpha$, $\alpha\Lambda$ and $\Lambda\Lambda$ effective potentials. The potentials representing the $\alpha\alpha$ interactions are given in Section 5.4.3. The $\alpha\Lambda$ and $\Lambda\Lambda$ potentials will be given in Chapter 6 with the models of hypernuclei.

The other examples will be atomic nuclei. We will then consider three-body models of ^{6}He, ^{9}Be, and ^{12}C. These nuclei will be described as αnn, $\alpha\alpha n$ and 3α systems, respectively. For those models, we need $\alpha\alpha$, αn and nn potentials. Moreover, for the microscopic models, we need a nucleon-nucleon potential. The different potentials are presented in the next subsections. The results of the models will be discussed in Chapters 7 and 8.

5.4.2 Effective nucleon-nucleon potentials

We first give the effective nucleon-nucleon potentials, used in our models. We consider two different potentials, in order to analyse the sensitivity of

the models with respect to the choice of the interactions. We consider the Minnesota potential (MN) [26] and the Volkov potential (V2) [57]. These potentials are the basic ingredient of the microscopic model and of the RGM potentials.

We write the nucleon-nucleon potential as $v_{ij} = V_{ij}^{NN} + V_{ij}^{C}$, where V_{ij}^{NN} is the nuclear interaction and V_{ij}^{C} is the Coulomb potential.

The nucleon-nucleon potential MN is defined as

$$V_{ij}^{NN} = \left(V_R + \left(\frac{1 + P_{ij}^{\sigma}}{2} \right) V_t + \left(\frac{1 - P_{ij}^{\sigma}}{2} \right) V_s \right) \left(\frac{u}{2} + \left(1 - \frac{u}{2} \right) P_{ij}^{r} \right), \quad (5.8)$$

with

$$\left\{ \begin{array}{rcl} V_R & = & 200 \exp(-1.487\, r^2), \\ V_t & = & -178 \exp(-0.639\, r^2), \\ V_s & = & -91.85 \exp(-0.465\, r^2). \end{array} \right. \quad (5.9)$$

Units, here and in the following, are MeV for the energies, and fm for the lengths. The operator P_{ij}^{r} exchanges the space coordinates, and P_{ij}^{σ} exchanges the spins of the interacting nucleons. The MN potential depends on an exchange parameter u, whose value is typically $u \approx 1$. This potential fits the nucleon-nucleon $^3S_1$ and $^1S_0$ scattering lengths and effective ranges. It also reproduces well the binding energies of the deuteron and the triton.

The nucleon-nucleon potential V2 is simpler, with only the exchange operator P_{ij}^{r}, and is defined as

$$V_{ij}^{NN}(r) \;=\; (V_r + V_a) \left(1 - m + m P_{ij}^{r} \right), \quad (5.10)$$

with

$$\left\{ \begin{array}{rcl} V_r & = & 61.14 \exp\left(-(r/1.01)^2\right), \\ V_a & = & -60.65 \exp\left(-(r/1.8)^2\right), \end{array} \right. \quad (5.11)$$

and the exchange parameter m, whose standard values are usually in the vicinity of $m = 0.6$. This effective nucleon-nucleon potential reproduces reasonably well the binding energies and size of ^{4}He, ^{16}O, and other light p-shell nuclei. However, because of its simplicity, V2 is found to be somewhat too strong in the nucleon-nucleon s-wave: its main drawback is to lead to a bound dineutron.

Of course, when the interacting nucleons are protons, the Coulomb potential must be added to MN (5.8) or V2 (5.10). It reads

$$V_{ij}^{C} = \frac{e^2}{r} \left(\frac{1}{2} - t_{iz} \right) \left(\frac{1}{2} - t_{jz} \right), \quad (5.12)$$

	Effective potentials		Pauli forbidden states
	Local potentials	Nonlocal potentials	in the relative motion
αn	KKNN	RGM-ε, RGM-$\not\varepsilon$	$0s$
$\alpha\alpha$	ABd, BFW	RGM-ε, RGM-$\not\varepsilon$	odd waves, $0s$, $1s$, $0d$

Table 5.1: The various local and nonlocal potentials, used in the models to represent the αn and $\alpha\alpha$ interactions, and the corresponding Pauli forbidden states.

where t_{iz} is the isospin component of nucleon i (with $t_{iz} = -1/2$ for a proton and $t_{iz} = +1/2$ for a neutron) and $e^2 = 1.44$.

Furthermore, in certain cases (treating the αn systems), we also add a spin-orbit force between nucleons [58] defined by

$$V_{ij}^{SO} = -\frac{2S_0}{\hbar^2\kappa^5}\,\exp(-r^2/\kappa^2)\,\boldsymbol{l}_{ij}\cdot\boldsymbol{s}_{ij}, \tag{5.13}$$

where $\boldsymbol{l}_{ij}$ is the relative-motion orbital angular momentum and $\boldsymbol{s}_{ij}$ the total spin of the two interacting nucleons. The spin-orbit force depends on two parameters: a range κ and an amplitude[1] S_0.

5.4.3 Cluster-cluster potentials

In the local and semi-microscopic models, potentials representing αn and $\alpha\alpha$ effective interactions are required. These potentials are listed in Table 5.1. The table also indicates the Pauli forbidden states occuring in the interactions. We describe here the potentials, with their Pauli forbidden states.

In the semi-microscopic models, the αn and $\alpha\alpha$ interactions are represented by the nonlocal RGM potentials. For each interaction, there are, however, two possible potentials that can be extracted from the RGM (See Section 2.3.1): the *energy-dependent* nonlocal potential (RGM-ε) and the *energy-independent* nonlocal potential (RGM-$\not\varepsilon$). These potentials are derived from the nucleon-nucleon interactions (MN (5.8) or V2 (5.10)). The αn and $\alpha\alpha$ RGM-ε potentials are given in Appendix C. The calculations that we perform to obtain the corresponding RGM-$\not\varepsilon$ potentials are given in Appendix E. The question of the energy-dependence of the RGM-ε potentials in the three-body models is treated in Section 5.6.

[1]The amplitude S_0 in (5.13) is defined so that, when considering the αn interaction, there is an existing limit as $\kappa \to 0$ (see Appendix C).

Also, the existence of the Pauli forbidden states (2.36) between the clusters must be taken into account. In the case of the αn interactions, there is one Pauli forbidden state, for $l = 0$ (in the relative motion between the α-particle and the neutron). This Pauli forbidden state is given in the RGM by the $0s$ harmonic-oscillator wave function [34] describing the relative motion. The existence of this *forbidden* state may be interpreted schematically in a shell-model picture, by saying that the Pauli exclusion principle prevents the external neutron n from occupying the $0s$ orbital, because this ground-state orbital is already occupied by the two neutrons inside the α-particle.

In the case of the $\alpha\alpha$ interactions, there are two forbidden states for $l = 0$ (the $0s$ and $1s$ waves in the relative motion between the two α-particles) and one forbidden state for $l = 2$ (the $0d$ wave) [34]. Moreover, all odd l waves are also forbidden, because the α-particles are bosons. The wave functions representing the Pauli forbidden states in the RGM are given by the $0s$, $1s$ and $0d$ harmonic-oscillator functions.

In the semi-microscopic models, the Pauli forbidden states must be projected out from the wave functions. Different techniques of projection are possible. They will be given in the next section.

We also consider the effective local potentials, which are much simpler (and are approximations), and which offer alternatives to represent the αn and $\alpha\alpha$ interactions.

As local αn potentials, we adopt the KKNN potential [59]. This effective local potential reproduces the $\alpha + n$ phase shifts. It depends on the angular momentum, via a parity dependence, and includes a spin-orbit force. This KKNN αn potential reads

$$\begin{aligned} V_{\alpha n}^{\mathrm{KKNN}}(r) = & -96.3\,\exp(-0.36r^2) + 77\,\exp(-0.9r^2) \\ & + (-1)^l \left(34\,\exp(0.2r^2) - 85\,\exp(0.53r^2) + 51\,\exp(2.5r^2)\right) \\ & + 2(\boldsymbol{l}\cdot\boldsymbol{s})\Big[-8.4\,\exp(0.52r^2) \\ & + \left(1 + 0.3(-1)^{l-1}\right)\left(-10\exp(-0.396r^2) + 10\exp(-2.2r^2)\right)\Big], \end{aligned} \tag{5.14}$$

with the energy in MeV and distance in fm, and where $\boldsymbol{l}$ denotes the orbital angular momentum of the αn relative motion, and $\boldsymbol{s}$ the spin of the neutron. This is a deep potential, which generates an unphysical bound state (with $l = 0$) simulating the Pauli forbidden state.

As local $\alpha\alpha$ potential, we consider two variants: the deep BFW potential [25] and the shallow ABd potential [24].

The BFW potential is very simple: this potential reads

$$V_{\alpha\alpha}^{\rm BFW}(r) = -122.6225\exp(-0.22r^2) + 4\times 1.44\frac{\mathrm{erf}(-0.75r^2)}{r}, \qquad (5.15)$$

and reproduces very well the $\alpha+\alpha$ scattering phase shifts. It generates three bound states (two states with $l=0$ and one state with $l=2$). Those bound states are unphysical and play the role of the Pauli forbidden states.

The ABd potential [24] is another $\alpha\alpha$ potential. It is a shallow potential; thus this potential does not take into account the Pauli forbidden states, i.e., the ABd potential generates no bound states. It contains a repulsive force, which may be considered as approximately simulating the repulsion due to the Pauli principle. The potential depends on the orbital angular momentum l, but is local for a given l. The ABd $\alpha\alpha$ potential reads

$$V_{\alpha\alpha}^{\rm ABd}(r) = V_{\alpha\alpha}^{(N)}(r) + 4\times 1.44\frac{\mathrm{erf}(-0.60141r^2)}{r}, \qquad (5.16)$$

with

$$V_{\alpha\alpha}^{(N)}(r) = \begin{cases} 500\exp(-(0.7r)^2) - 130\exp(-(0.475r)^2), & \text{if } l=0, \\ 320\exp(-(0.7r)^2) - 130\exp(-(0.475r)^2), & \text{if } l=2, \\ -130\exp(-(0.475r)^2), & \text{if } l\geq 4. \end{cases} \qquad (5.17)$$

This potential reproduces the $\alpha+\alpha$ phase shifts. Also, the potential is not defined for the odd values of l, because α-particles are bosons.

In the local models, we will have the opportunity to use and compare the ABd and BFW potentials. This will illustrate the influence of the Pauli forbidden states on the wave functions.

5.5 Exclusion of the Pauli forbidden states

The Pauli forbidden states are unphysical. They must be eliminated from the wave functions, except in the models with the shallow potentials, where they do not appear.

In the fully microscopic models, the Pauli forbidden states disappear quite naturally via the antisymmetrisation of the wave function. In the models with deep potentials and in the semi-microscopic models, the Pauli principle is approximately simulated: the Pauli forbidden states exist in those models, but they must be excluded from the three-body wave function, since they would disappear under full antisymmetrisation. Also, this exclusion is actually crucial. Indeed, otherwise, their non-elimination in three-body models gives rise to a strong (unphysical) overbinding of the systems.

Several practical techniques of removal of the Pauli forbidden states in the three-body models exist [45, 60]. We give here the different methods that will be employed.

In the case of a deep local potential, a first possible method consists in using the supersymmetric transformations (2.80). The deep potential is simply transformed into a shallow potential. (The unphysical bound states are removed from the potential, while the phase shifts and the energy spectrum for the physical states remain unchanged.) The shallow potential can be employed, as an effective interaction, in a three-body local model [27].

The other methods consist in orthogonalizing the wave function with respect to the Pauli forbidden states (by means of projectors). In other words, the wave function does not contain the Pauli forbidden states as component. An operator P is defined as the sum of the projectors onto the two-body forbidden states:

$$P = \sum_{i>j=1}^{3} \sum_{n=1}^{N_{ij}} |g_{n,ij}^{FS}\rangle \langle g_{n,ij}^{FS}| \,, \tag{5.18}$$

where N_{ij} is the number of Pauli forbidden states for the relative motion between clusters i and j; and $g_{n,ij}^{FS}$ denote the wave functions of these forbidden states. Note that P is not necessarily a projector although it is a sum of two-body projectors.

In the semi-microscopic models, $g_{n,ij}^{FS}$ are harmonic-oscillator eigenstates [2, 29, 34] according to the RGM potentials[2]. Otherwise, in the local models with a deep potential, the forbidden states $g_{n,ij}^{FS}$ are the wave functions of the unphysical bound states, given by the potential.

The forbidden states are excluded from the wave function by imposing

$$P\,|\Psi^{JM\pi}\rangle = 0, \tag{5.19}$$

where $\Psi^{JM\pi}$ denotes the three-body wave function. Indeed since

$$0 \leq \langle \Psi^{JM\pi}|\, P\,|\Psi^{JM\pi}\rangle \,, \tag{5.20}$$

condition (5.19) is equivalent to

$$\langle \Psi^{JM\pi}|\, P\,|\Psi^{JM\pi}\rangle = 0 \quad \text{i.e.} \quad \langle \Psi^{JM\pi}|g_{n,ij}^{FS}\rangle = 0. \quad \forall n, ij. \tag{5.21}$$

Thus $\Psi^{JM\pi}$ is orthogonal to the Pauli forbidden states.

[2] See, e.g., Sections 5.4.3 or E.2 in Appendix E.

A first simple method to impose condition (5.19) is to add the operator P multiplied by a very large coefficient Λ, as a nonlocal pseudopotential term, to the Hamiltonian H of the system [27,61]. Indeed, in a variational calculation, computing the energy E from this Hamiltonian with the additional term ΛP,

$$E = \langle \Psi^{JM\pi} | \, H + \Lambda P \, | \Psi^{JM\pi} \rangle \, , \quad \Lambda \to \infty, \tag{5.22}$$

will automatically lead to condition (5.19), provided that Λ is sufficiently large and positive. The term ΛP has no effect for the wave functions that satisfy (5.19) but it discriminates all the other wave functions containing forbidden states, since if (5.19) is not met, then the energy E is strongly increased by a term proportional to Λ. Therefore, the minimum values of the energy E are obtained for the wave functions (5.19), which are orthogonal to the Pauli forbidden states. In practice, the constant Λ is chosen as a much larger energy than the characteristic energies of the system (typically $\Lambda \sim 10^6 - 10^9$ MeV whereas $E \sim 1$ MeV). The obtained energies E are insensitive to the choice of Λ when the forbidden states are eliminated.

There is, of course, an alternative method to impose condition (5.19). It consists in diagonalising the matrix that represents the operator P in a variational calculation. The eigenvalues μ_n and eigenvectors $\mathcal{X}_n^{JM\pi}$ of P are computed,

$$P\mathcal{X}_n^{JM\pi} = \mu_n \mathcal{X}_n^{JM\pi}. \tag{5.23}$$

Imposing (5.19) is equivalent to working in the subspace spanned by the eigenvectors $\mathcal{X}_n^{JM\pi}$ belonging to $\mu_n = 0$. In the variational calculation, the wave function $\Psi^{JM\pi}$ is thus defined in this subspace ($\mu_n = 0$) which is orthogonal to the forbidden states: the wave function is expanded in the basis

$$\Psi^{JM\pi} = \sum_{\substack{n \\ \mu_n = 0}} c_n \mathcal{X}_n^{JM\pi}, \tag{5.24}$$

where c_n are coefficients and the summation runs over all states $\mathcal{X}_n^{JM\pi}$ belonging to $\mu_n = 0$. However, in practice, when the calculations are performed numerically, the eigenvalues μ_n are obtained approximately within the numerical precision. The exact condition $\mu_n = 0$ must therefore be replaced by

$$\mu_n < \epsilon, \tag{5.25}$$

where ϵ is arbitrarily close to zero, i.e., ϵ is the threshold under which an eigenvalue may be considered, within the precision of the calculations, as

numerically equivalent to zero. The variational calculation is thus performed with a numerical function defined as

$$\Psi^{JM\pi} = \sum_{\substack{n \\ \mu_n<\epsilon}} c_n \mathcal{X}_\lambda^{JM\pi}, \tag{5.26}$$

with $\mathcal{X}_n^{JM\pi}$ satisfying the condition $\mu_n < \epsilon$.

In practice, this technique is equivalent to the pseudopotential method (5.22). Both methods give the same results numerically [20, 60], provided that ε is taken to be small enough.

Nevertheless, the pseudopotential method (5.22) is simpler to apply in our nonlocal formalism, because it does not need to determine the eigenstates of operator P (5.23).

5.6 Energy-dependent potentials

The models with the nonlocal RGM-ε potentials raises a fundamental question. One of the important aspects of these RGM-ε potentials is that they depend explicitly on the energy ε of the relative motion between the interacting clusters (see Appendix C). Therefore, the use of these potentials in a three-body model requires the two-body energies ε to be determined.

In the two-cluster problems, the energy ε is well defined, and the RGM-ε potentials (2.77) describe correctly the two-cluster systems. However, in the case of a three-cluster system, the energy that is well defined is not ε, but the total energy E of the motion of the three clusters. Indeed, the two-body energy ε is not a constant of motion in a three-body system (because the Hamiltonian of a two-body subsystem does not commute with the three-body Hamiltonian). Hence in the three-body model using the RGM-ε potentials, the values of the two-body energies ε become parameters of the potentials, which must be determined for each pair of clusters.

A plausible approach, suggested by Fujiwara and co-workers [17, 28], is to set these parameters equal to the mean energies of the two-body subsystems,

$$\varepsilon_{ij} = \left\langle \Psi^{JM\pi} \right| T_k + V_{ij}(\varepsilon_{ij}) \left| \Psi^{JM\pi} \right\rangle, \tag{5.27}$$

where $V_{ij}(\varepsilon_{ij})$ is a RGM-ε potential, which depends on the energy ε_{ij}, and T_k is the kinetic energy of the relative motion between clusters i and j (ijk being a cyclic permutation of cluster indices 123). This approach is consistent with the interpretation of the RGM-ε potential as representing the effective interaction between two clusters. The two-body energy ε_{ij} is identified as

the average value of the relative-motion energy of the two interacting clusters. The wave function $\Psi^{JM\pi}$ is the solution of the three-body Schrödinger equation (3.60) with the potential V_{ij}. Since ε_{ij} is a parameter of the RGM-ε potential V_{ij} (and $\Psi^{JM\pi}$ is determined from V_{ij}), a self-consistent resolution of equations (3.60) and (5.27) must be performed. Equations (3.60) and (5.27) are then solved iteratively. The practical calculation of ε_{ij} (5.27) in the hyperspherical formalism is given in Appendix D.

However, we will show [20] that prescription (5.27) is questionable in practice, for example in the case of a three-body model of the ^{9}Be nucleus described as a system with two α clusters and one additional neutron. This critical situation for (5.27) is clearly explicable by analysing the effects of replacing ε by a constant parameter in a RGM-ε potential. This question will be discussed in Chapter 7. This has motivated the development of our semi-microscopic model using the energy-independent RGM-$\not{\varepsilon}$ potentials [21–23].

Chapter 6

Three-body models of the ${}^{6}_{\Lambda\Lambda}$He and ${}^{9}_{\Lambda}$Be hypernuclei

6.1 Introduction

As first physical applications, we consider two hypernuclei, ${}^{6}_{\Lambda\Lambda}$He and ${}^{9}_{\Lambda}$Be. This choice is opportune. It will allow us to test accurately our three-body technique with nonlocal potentials. Indeed there are published results [17,18] of three-body models of ${}^{6}_{\Lambda\Lambda}$He and ${}^{9}_{\Lambda}$Be in a semi-microscopic approach using nonlocal potentials. We will take the same parameters as those models. Comparing the results, this will provide a severe test for our nonlocal calculations [19,20].

In addition, we will also perform new calculations with other potentials, and compute various observables, such as probability densities, radii and reduced transition probabilities. We will compare the nonlocal semi-microscopic models with simple models using local potentials.

This chapter begins by briefly introducing the Λ hyperon. Then, the ${}^{6}_{\Lambda\Lambda}$He and ${}^{9}_{\Lambda}$Be hypernuclei, and their respective three-body models, are defined. Next, the potentials employed in the models are given. Before discussing the physical results, we detail the conditions of the numerical calculations. The results for ${}^{6}_{\Lambda\Lambda}$He and ${}^{9}_{\Lambda}$Be are then discussed and compared.

6.2 The Λ hyperon

The *baryons* [62–64] form a family of particles, which includes the nucleons. They are not elementary particles: the baryons are made up of three quarks. The nucleons are the lightest baryons. Hence they are the constituents of the ordinary nuclear matter. But other baryons exist; those just heavier than the

	Charge	Spin	Isospin	Strangeness	Mass (MeV/c^2)	Mean Life (s)	Quark struct.
p	$+e$	1/2	1/2	0	938.27	stable	uud
n	0	1/2	1/2	0	939.57	885.7	udd
Λ	0	1/2	0	-1	1115.68	2.6×10^{-10}	uds

Table 6.1: Basic properties and quark structure of the nucleons (proton p and neutron n) and the Λ hyperon [64]. The principal decay modes of the Λ are $\Lambda \to p + \pi^-$ (64%) and $\Lambda \to n + \pi^0$ (36%).

The quarks	
Electric charge:	
$-1/3e$	$+2/3e$
d (down)	u (up)
s (strange)	c (charm)
b (bottom)	t (top)

Table 6.2: The six flavors of quarks in the Standard Model of particle physics. They are grouped into 3 generations: each line corresponds to a generation, and each generation of quarks has two members, one with a fractional electric charge $-1/3e$ and another with a charge $+2/3e$.

neutron are called *hyperons*. The hyperons possess a specific property called *strangeness*, which corresponds to a quantum number, that the nucleons do not have (the strangeness of a nucleon is zero). They are unstable and decay, directly or indirectly, into a nucleon plus other particles, such as pions. Such decays proceed by the weak interaction, which is the only interaction able to modify the strangeness quantum number.

The lightest hyperon is the Λ particle. This is the only hyperon that will be considered here. Table 6.1 briefly compares the basic properties of the Λ with respect to the nucleons. The Λ hyperon is electrically neutral, like the neutron. This is a particle with isospin zero, whereas the nucleons, having isospin $\frac{1}{2}$, form an isospin doublet. The Λ differs markedly from the nucleons by its strangeness quantum number -1. The quark structure of the baryons accounts for those differences between the Λ and the nucleons.

The six *flavors* of quarks [63], according to the elementary particle physics, are listed in Table 6.2. The hyperons, by definition, are the baryons formed by u, d, or s quarks, and that contain at least one s quark. The similarities and differences between the Λ and the neutron follow from their

respective quark structure. Indeed, the elementary difference between the neutron (udd) and the Λ (uds) is a d quark that is replaced by a s quark.

The Λ hyperon is a fermion with spin $\frac{1}{2}$, like the nucleons. Its mean life time is 2.6×10^{-10} s, and the main decay channels are $\Lambda \to p + \pi^-$ (64%) and $\Lambda \to n + \pi^0$ (36%). Notice also that the Λ (1115.68 MeV/c^2) is heavier than the neutron (939.57 MeV/c^2).

6.3 The ${}^{6}_{\Lambda\Lambda}$He and ${}^{9}_{\Lambda}$Be hypernuclei

A *hypernucleus* is a many-body system composed of nucleons and one or more hyperons [65–67]. Thus, in other words, a hypernucleus is similar to an atomic nucleus, with a few hyperons among the nucleons. Here, we consider two specific hypernuclei: ${}^{6}_{\Lambda\Lambda}$He and ${}^{9}_{\Lambda}$Be. By definition, the ${}^{6}_{\Lambda\Lambda}$He hypernucleus corresponds to a ^{6}He nucleus in which two neutrons are replaced by two Λ hyperons. Hence the ${}^{6}_{\Lambda\Lambda}$He is a system of two protons, two neutrons and two Λ hyperons. Such a nuclear system, with two Λ hyperons among the nucleons, is usually termed a *double-*Λ *hypernucleus*. The ${}^{9}_{\Lambda}$Be is an example of *single-*Λ *hypernucleus*, i.e., a hypernucleus with only one Λ hyperon. The ${}^{9}_{\Lambda}$Be corresponds to a ^{9}Be nucleus with one Λ instead of one neutron. Thus the ${}^{9}_{\Lambda}$Be is a bound system composed of four protons, four neutrons and one Λ hyperon.

The choice of the hypernuclei as first applications [19] for our models is instructive: it offers an ideal test for our three-body techniques. The hypernuclei correspond to a research field of nuclear physics: both theoretical and experimental studies are available [65–72]. In particular, there are calculations (published in 2004) of three-body models of ${}^{6}_{\Lambda\Lambda}$He and ${}^{9}_{\Lambda}$Be using semi-microscopic nonlocal forces [17, 18]. Those calculations however are performed in the momentum space with the Faddeev method. We can advantageously take the same parameters as those models, in order to make comparable calculations, but in the configuration space and with our hyperspherical method, which we have extended to the case of nonlocal potentials [19]. This allows us to study the hypernuclei but also to test accurately the numerical calculations with the nonlocal forces.

In addition, there is another practical aspect to consider hypernuclei as first applications: the Pauli principle is simpler to apply in those models, because the Λ hyperon is discernible from the nucleons. This brings a simplification in the calculation of the potentials. Indeed, in the hypernuclei, there is no effect of the Pauli principle (no forbidden states, no energy-dependence arising in the potential) in the relative motion between a Λ hyperon and an

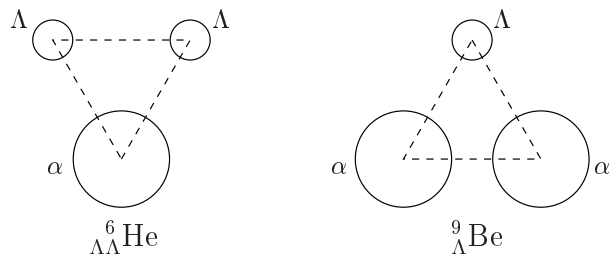

${}^{6}_{\Lambda\Lambda}$He ${}^{9}_{\Lambda}$Be

Figure 6.1: Three-body models of ${}^{6}_{\Lambda\Lambda}$He and ${}^{9}_{\Lambda}$Be

α cluster. Hence the $\alpha\Lambda$ interaction is fundamentally different from the α-neutron interaction. In particular, the $\alpha\Lambda$ potential can form a bound state (namely the ${}^{5}_{\Lambda}$He hypernucleus), while α-neutron cannot form any bound state (^{5}He being particle unstable). Also, in ${}^{6}_{\Lambda\Lambda}$He and ${}^{5}_{\Lambda}$He, the Λ hyperons are in the $0s$ orbital, whereas in ^{6}He and ^{5}He, the valence neutrons must occupy the $0p$ orbital, according to the Pauli principle.

The hypernuclei can be studied by assuming cluster structures [17, 18, 68, 69, 72]. We consider three-body models of the ${}^{6}_{\Lambda\Lambda}$He and ${}^{9}_{\Lambda}$Be [19] (see Figure 6.1). The ${}^{6}_{\Lambda\Lambda}$He hypernucleus is represented by a system with a α-cluster core and two Λ hyperons. Hence this $\alpha\Lambda\Lambda$ model of ${}^{6}_{\Lambda\Lambda}$He requires $\alpha\Lambda$ and $\Lambda\Lambda$ effective interations. These interactions are given in the next section. Considering the $\alpha\Lambda$ interactions, we investigate two variants: we use either a simple local $\alpha\Lambda$ potential or a nonlocal $\alpha\Lambda$ potential taking the internal structure of the α-cluster into account. In the latter case, the model with the nonlocal $\alpha\Lambda$ potential will be essentially equivalent to a three-cluster microscopic model of ${}^{6}_{\Lambda\Lambda}$He.

We also consider the ${}^{9}_{\Lambda}$Be hypernucleus: this hypernucleus is represented in a three-body model as a system with one Λ and two α clusters. This $\alpha\alpha\Lambda$ model for ${}^{9}_{\Lambda}$Be requires the use of an effective $\alpha\alpha$ potential and is therefore not equivalent to a microscopic model. However, if the $\alpha\alpha$ interaction is represented by a RGM potential (see Section 5.4.3) and if the nonlocal $\alpha\Lambda$ potential is employed, then the $\alpha\alpha\Lambda$ model corresponds to a semi-microscopic model of the ${}^{9}_{\Lambda}$Be hypernucleus.

We will determine to what extent the models can account for the experimental data concerning the hypernuclei. Although the study of ${}^{6}_{\Lambda\Lambda}$He remains experimentally extremely difficult, a first measurement of the binding energy of ${}^{6}_{\Lambda\Lambda}$He is available [71]. This measurement is deduced from one single but clear observation of ${}^{6}_{\Lambda\Lambda}$He, in 2001, called the NAGARA event. Of course,

such a result must be treated carefully since it follows from only one event. Nevertheless, the NAGARA event is claimed to be the first observation in which the ${}^{6}_{\Lambda\Lambda}$He is uniquely identifiable, without possible ambiguity[1]. This is a very scarce experimental data concerning ${}^{6}_{\Lambda\Lambda}$He, so far.

The experimental status for the single-Λ hypernuclei, such as ${}^{9}_{\Lambda}$Be, is incomparably more advanced: those hypernuclei are relatively well-known systems and spectroscopic measurements can be made. Indeed, accurate experimental data for the binding energy [74] and the fine structure of excited states of ${}^{9}_{\Lambda}$Be are available [70].

6.4 ΛΛ, αΛ and αα potentials

For the semi-microscopic models of ${}^{6}_{\Lambda\Lambda}$He and ${}^{9}_{\Lambda}$Be, we adopt the same potentials (SB) as defined in Refs. [17, 18]. These effective potentials are derived from baryon-baryon collision matrices generated by a quark model [28, 75]. Units are MeV and fm throughout.

The SB nucleon-Λ potential is defined as

$$V_{ij}^{N\Lambda} = \left(\left(\frac{1+P_{ij}^{\sigma}}{2} \right) V_T + \left(\frac{1-P_{ij}^{\sigma}}{2} \right) V_S \right) \left(\frac{\tilde{u}}{2} + \left(1 - \frac{\tilde{u}}{2} \right) P_{ij}^{r} \right), \qquad (6.1)$$

with

$$\begin{cases} V_T &= 1072 \exp(-13.74\, r^2) - 56.31 f_{N\Lambda} \exp(-0.7517\, r^2) \\ V_S &= 1015 \exp(-5.383\, r^2) - 128 \exp(-0.8908\, r^2), \end{cases} \qquad (6.2)$$

where P_{ij}^{σ} and P_{ij}^{r} are the spin and space exchange operators, respectively. The parameter $f_{N\Lambda} = 1$ corresponds to the bare interaction. This potential is obtained by supersymmetric inversion [76] from the ${}^1S_0$ and ${}^3S_0$ nucleon-Λ phase shifts derived in a quark model of Ref. [75]. The parameter $\tilde{u}$ is usually set to $\tilde{u} = 1$ [17]. The interaction is then taken as zero for odd waves ($P_{ij}^{r} \to -1$) of the nucleon-Λ system.

The SB ΛΛ potential [18] reads

$$V_{ij}^{\Lambda\Lambda} = 658.2 \exp(-5.936\, r^2) - 103.9 f_{\Lambda\Lambda} \exp(-1.176\, r^2), \qquad (6.3)$$

with $f_{\Lambda\Lambda} = 1$ for two bare Λ hyperons. It is obtained by inverting the ${}^1S_0$ phase shift of the quark model. This ΛΛ potential is defined for the even

[1] Since 1966 [73], there have been three previous experimental observations of double-Λ hypernuclei, but those reported events however were not accurate evidences, because they allowed more than one possible interpretation [71] in terms of identification of the species and their binding energy.

$\Lambda\Lambda$ partial waves. For odd partial waves the potential is expected to be different, but there will be no odd waves in our applications, because of the Pauli principle for ${}^{6}_{\Lambda\Lambda}$He (see Section 6.5.1).

The SB $\alpha\Lambda$ potential is generated from the nucleon-Λ interactions by taking into account the internal structure of the α-particle. This is a nonlocal potential: it is obtained by folding the interaction $V_{ij}^{N\Lambda}$ (6.1) with a $(0s)^4$ oscillator density $|\phi_1|^2$ (2.6) representing the α-particle. For a Gaussian term

$$\left(\frac{1 \pm P_{ij}^{\sigma}}{2}\right) \exp(-\kappa\, r^2) \left(\frac{\tilde{u}}{2} + \left(1 - \frac{\tilde{u}}{2}\right) P_{ij}^{r}\right) \tag{6.4}$$

of the nucleon-Λ interaction (6.1), the resulting $\alpha\Lambda$ potential [19] is given by a local term,

$$V_{\alpha\Lambda}^{\rm SB} = X_d \left(\frac{8\nu}{3\kappa + 8\nu}\right)^{3/2} \exp\left(-\frac{8\nu\kappa\, r^2}{3\kappa + 8\nu}\right), \tag{6.5}$$

plus a nonlocal term, the kernel of which reads

$$W_{\alpha\Lambda,\,l}^{\rm SB}(r, r') = 4\pi X_e \left(\frac{128\nu}{75\pi}\right)^{3/2} \times \exp\left(-\frac{4(12\kappa + 17\nu)(r^2 + r'^2)}{75}\right) i_l\left(\frac{32(3\kappa - 2\nu)\, r r'}{75}\right), \tag{6.6}$$

where $\nu = 1/2b^2$, with b denoting the oscillator parameter of the wave function of the α-particle (2.6), $X_d = \tilde{u}/2$, $X_e = (1 - \tilde{u}/2)$ for the $(1 - P_{ij}^{\sigma})$ term and $X_d = 3\tilde{u}/2$, $X_e = 3(1 - \tilde{u}/2)$ for the $(1 + P_{ij}^{\sigma})$ term, and $i_l(x)$ denotes a modified spherical Bessel function (or spherical Hankel function) [44]. The kernel (6.6) is written for a partial wave of angular momentum l of the $\alpha\Lambda$ relative motion (see definition (3.83)).

Thus, from $V_{ij}^{N\Lambda}$ (6.1), an effective $\alpha\Lambda$ potential is calculated, as a sum of local and nonlocal terms (6.5) and (6.6). This potential has nonlocal terms (6.6) because of the exchange operator P_{ij}^{r} in the nucleon-Λ interaction. We employ the nonlocal SB $\alpha\Lambda$ potential in the semi-microscopic models of ${}^{6}_{\Lambda\Lambda}$He and ${}^{9}_{\Lambda}$Be.

In our study, we will compare the nonlocal models with simpler local models. In the local models, for the $\alpha\Lambda$ interaction, we take another potential: the Isle potential [77, 78] which reads

$$V_{\alpha\Lambda}^{\rm Isle} = 450.4 \exp\left(-(r/1.25)^2\right) - 404.9 \exp\left(-(r/1.41)^2\right). \tag{6.7}$$

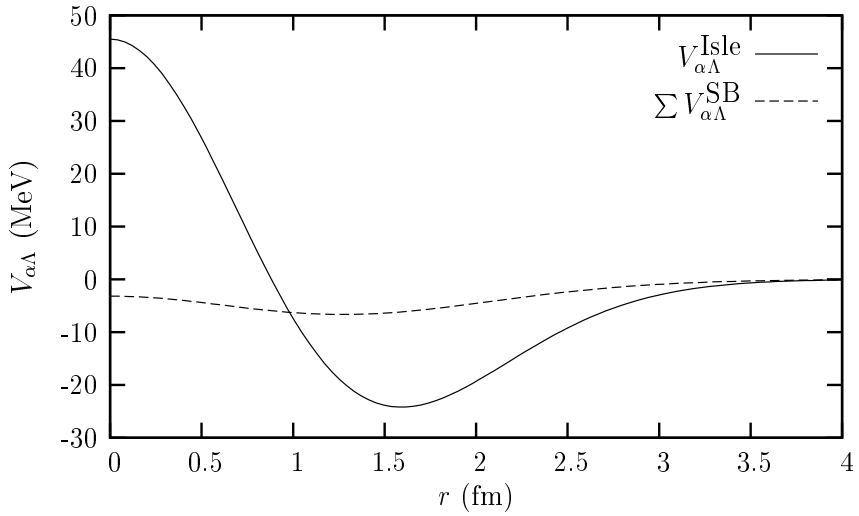

Figure 6.2: The Isle potential ($V_{\alpha\Lambda}^{\rm Isle}$), and the local part of the semi-microscopic SB $\alpha\Lambda$ potential ($\sum V_{\alpha\Lambda}^{\rm SB}$) for comparison.

This is an effective, phenomenological, local $\alpha\Lambda$ potential, with an attractive term and a repulsive core. It admits an $\alpha + \Lambda$ bound state, representing a ${}^{5}_{\Lambda}$He hypernucleus, with the correct binding energy 3.1 MeV. The Isle potential is displayed in Figure 6.2, with the local part of the SB $\alpha\Lambda$ potential (i.e., the sum of terms (6.5)) for comparison. We see that the local terms of the $\alpha\Lambda$ potentials are quite different, which is an essential point in the comparison of the models.

In addition, for the $\alpha\alpha\Lambda$ model of ${}^{9}_{\Lambda}$Be, an effective $\alpha\alpha$ potential is needed. The $\alpha\alpha$ potentials (ABd or BFW in the local models, RGM-ε or RGM-$\not\varepsilon$ in the semi-microscopic models) are described in Section 5.4.3. The RGM and BFW potentials generate Pauli forbidden states that must be eliminated from the wave functions (see Section 5.5). In the case of the deep BFW potential, two techniques of elimination of the bound states are investigated: when the forbidden states are removed using supersymmetric transformations (2.80), the potential is denoted SBFW, and otherwise, when the forbidden bound states are eliminated using the projection technique (5.22) [or (5.26)], the potential is denoted PBFW.

6.5 Results and discussion

6.5.1 Conditions and convergence of calculation

We adopt exactly the same parameters as in Ref. [17]. The calculations are performed with $A_\alpha = 4$ and $A_\Lambda = 1.18826$ as mass numbers of the α-particle and the Λ hyperon, with m_N as mass unit such that $\hbar^2/2m_N = 20.7355$ MeV fm^2. The oscillator parameter of the density of the α-particle is $\nu = 1/2b^2 = 0.257$ fm^{-2}. The effective nucleon-Λ SB potential (6.1) is adjusted with the values $\tilde{u} = 1$ and $f_{N\Lambda} = 0.8923$ [17], so that the nonlocal SB $\alpha\Lambda$ potential yields the right energy of the two-body $\alpha + \Lambda$ bound state (namely the ${}^{5}_{\Lambda}$He hypernucleus). The binding energy of this $\alpha + \Lambda$ system with the nonlocal $\alpha\Lambda$ potential is easily computed with the method of Ref. [52]. With these choices of parameters, the value 3.1202 MeV is obtained, simulating the experimental value 3.12 ± 0.02 MeV of the $\alpha + \Lambda$ binding of ${}^{5}_{\Lambda}$He [74].

For the ${}^{9}_{\Lambda}$Be hypernucleus, in the semi-microscopic models, we use the Minnesota (MN) potential (5.8) as effective nucleon-nucleon force for the $\alpha\alpha$ RGM potentials. The exchange parameter of MN is taken as $u = 0.94687$ [17] in order to reproduce the $\alpha + \alpha$ scattering phase shifts.

In the calculations, we exploit the following symmetry considerations. The ground state of ${}^{6}_{\Lambda\Lambda}$He is a 0^+ state, which implies the equality $L = S$ (where L represents the total orbital angular momentum and S the total spin). Since the potentials that we use are spin-independent, L and S are good quantum numbers in the model. The ground state of ${}^{6}_{\Lambda\Lambda}$He is therefore a $L = S = 0$ state. In the hyperspherical formalism, $L = 0$ implies $l_x = l_y$. Moreover, the Λ hyperons are fermions, hence the wave function must be antisymmetric with respect to the exchange of the Λ particles. If the quantum number l_x denotes the orbital angular momentum of the relative motion between the Λ hyperons, the Pauli antisymmetry imposes $l_x + S$ to be an even value, but since $S = 0$, only the even values of l_x are required, which reduces the size of the hyperspherical basis.

In the case of the ${}^{9}_{\Lambda}$Be, we perform calculations for the $1/2^+$ ground state and the $3/2^+$ or $5/2^+$ excited states of the hypernucleus. Here again, since the potentials are spin-independent, L and S are good quantum numbers. The total spin is the spin $S = 1/2$ of the Λ hyperon (since the α-particles have zero spin). Therefore in our models, the $1/2^+$ ground state corresponds to $L = 0$ and the excited states to $L = 2$. The $3/2^+$ and $5/2^+$ excited states of ${}^{9}_{\Lambda}$Be are thus degenerate in the model. Furthermore, the α-particles are bosons, which leads us to consider only the even values of l_x, provided that l_x

	${}^{6}_{\Lambda\Lambda}$He (0^+)		${}^{9}_{\Lambda}$Be $(1/2^+)$		${}^{9}_{\Lambda}$Be $(3/2^+, 5/2^+)$	
K_M	E	$\sqrt{\langle\rho^2\rangle}$	E	$\sqrt{\langle\rho^2\rangle}$	E	$\sqrt{\langle\rho^2\rangle}$
0	−7.28497	3.40956	1.08723			
2	−7.39194	3.40986	−4.25184	6.12532	−1.0119	6.204
4	−7.76942	3.53180	−6.44122	5.67974	−3.4420	5.553
6	−7.88724	3.53455	−6.86288	5.72831	−3.9261	5.624
8	−7.98036	3.54459	−7.01574	5.78726	−4.0916	5.713
10	−8.03871	3.54086	−7.07490	5.82982	−4.1650	5.787
12	−8.07890	3.53732	−7.08940	5.84651	−4.1853	5.825
14	−8.10536	3.53509	−7.09559	5.85480	−4.1944	5.847
16	−8.12195	3.53340	−7.09822	5.85886	−4.1986	5.862
18	−8.13247	3.53269	−7.09962	5.86101	−4.2008	5.872
20	−8.13909	3.53236	−7.10037	5.86215	−4.2020	5.878
22	−8.14324	3.53232	−7.10071	5.86266	−4.2026	5.881
24	−8.14584	3.53238	−7.10090	5.86296	−4.2029	5.883
26	−8.14748	3.53249	−7.10102	5.86315	−4.2031	5.885
28	−8.14853	3.53262	−7.10108	5.86327		
30	−8.14920	3.53273	−7.10112	5.86335		
32	−8.14963	3.53283	−7.10114	5.86340		
34	−8.14991	3.53291	−7.10115	5.86343		
36	−8.15009	3.53298	−7.10116	5.86346		
38	−8.15021	3.53303	−7.10117	5.86347		
40	−8.15029	3.53307	−7.10117	5.86348		

Table 6.3: Numerical convergence of the energies (in MeV) and r.m.s hyperradius (in fm) with respect to K_M. In these examples, the potentials are the SB potentials for $\alpha\Lambda$ and $\Lambda\Lambda$, and the ABd potential for $\alpha\alpha$.

corresponds to the orbital angular momental of the relative motion between the α-particles. In addition, the considered states have a positive parity. Therefore l_y must be even, since the parity requires $l_x + l_y$ to be even (3.62).

Let us now discuss the numerical convergence of our three-body calculations with the hyperspherical harmonics method. For each K value, all possible l_x, l_y values are included. The number of Lagrange-mesh points for the hyperradial functions (3.109) is $N = 30$ with the scale parameter $h = 0.3$ fm. For the local potentials, integrals (B.4) are performed with a Gauss-Legendre quadrature with 64 points. For the nonlocal potentials, the parameters of the Gaussian quadrature in equation (B.24) are $N_2 = 30$ and

$L=0$		
K_M	$N_{\gamma K}$	$N_{\gamma Ki}$
10	12	360
20	36	1080
30	72	2160
40	121	3630

$L=2$		
K_M	$N_{\gamma K}$	$N_{\gamma Ki}$
10	24	720
20	85	2550
26	140	4200

Table 6.4: Matrix sizes $N_{\gamma Ki}$, for $L=0$ (ground states of ${}^{6}_{\Lambda\Lambda}$He and ${}^{9}_{\Lambda}$Be) and $L=2$ (excited state of ${}^{9}_{\Lambda}$Be), and the corresponding number $N_{\gamma K}$ of γK values in the basis ($N_{\gamma Ki} = N_{\gamma K} \times N$), with respect to K_M.

$h_2 = 0.08$ fm. The integration over y in this equation is performed with a constant step 0.06 fm and extends up to 48 fm.

In order to show in details the convergence of the numerical calculations, we display in Table 6.3 some typical values of the energy and the r.m.s. hyperradius, obtained in differents cases, with increasing values of K_M. Calculations are performed for the ground states of ${}^{6}_{\Lambda\Lambda}$He and ${}^{9}_{\Lambda}$Be ($L=0$) and for the degenerate ($L=2$) excited state, corresponding to $3/2^+$ and $5/2^+$ states of ${}^{9}_{\Lambda}$Be.

The results for ${}^{6}_{\Lambda\Lambda}$He show that an accuracy of 100 keV is obtained for $K_M = 12$, of 10 keV for $K_M = 20$, and of 1 keV for $K_M = 30$. The same accuracies are obtained for the ${}^{9}_{\Lambda}$Be ground state for $K_M = 8$, $K_M = 12$, $K_M = 20$, respectively. Slightly larger values are necessary for the excited state.

The sizes of the numerical matrices (3.114) with respect to K_M are given in Table 6.4. For the ground states ($L=0$) for $K_M = 40$, the number of γK values in the basis is 121 and the matrix size is 3630. For the excited state of ${}^{9}_{\Lambda}$Be ($L=2$), the matrix size is much larger: with the smaller limit $K_M = 26$, the number of γK values is already 140, and the matrix size is 4200.

6.5.2 The ${}^{6}_{\Lambda\Lambda}$He hypernucleus

$\alpha\Lambda\Lambda$ model with the SB potentials

First we make a comparison with a result of Fujiwara et al. [18], obtained with the momentum-space Faddeev method under the same assumptions with the SB potentials. For the ${}^{6}_{\Lambda\Lambda}$He hypernucleus, we obtain the three-body binding energy (see Table 6.3) [19]

$$B({}^{6}_{\Lambda\Lambda}\text{He}) = 8.150 \text{ MeV}. \tag{6.8}$$

	$f_{\Lambda\Lambda}=1$		$f_{\Lambda\Lambda}=0.8$		fitted $f_{\Lambda\Lambda}$		
$V_{\alpha\Lambda}$	E	$\sqrt{\langle r^2\rangle}$	E	$\sqrt{\langle r^2\rangle}$	$f_{\Lambda\Lambda}$	E	$\sqrt{\langle r^2\rangle}$
SB	-8.150	1.820	-7.322	1.879	0.78	-7.248	1.886
Isle	-7.732	1.926	-7.104	1.978	0.85	-7.248	1.965

Table 6.5: Energy (in MeV) and r.m.s matter radius (in fm) of ${}^{6}_{\Lambda\Lambda}$He for the nonlocal SB and local Isle $\alpha\Lambda$ potentials, for different values of the parameter $f_{\Lambda\Lambda}$ in the $\Lambda\Lambda$ potential (6.3).

The corresponding $\Lambda\Lambda$ interaction energy is defined by

$$\Delta B_{\Lambda\Lambda} = B({}^{6}_{\Lambda\Lambda}\mathrm{He}) - 2B({}^{5}_{\Lambda}\mathrm{He}) = 1.910 \text{ MeV}, \tag{6.9}$$

with $B({}^{5}_{\Lambda}\mathrm{He}) = 3.120$ MeV. This is in perfect agreement with the value in Table I of Ref. [18]. The three-body calculation, involving nonlocal potentials, is therefore accurate and correct.

The experimental value is $\Delta B_{\Lambda\Lambda} = 1.01 \pm 0.20$ MeV [71]. It corresponds to an energy $B({}^{6}_{\Lambda\Lambda}\mathrm{He}) = 7.25 \pm 0.20$ MeV. Our binding energy is thus too large by about 0.9 MeV. However, different corrections are not included in the three-body model with the SB potentials. For example, as suggested in Ref. [18], effects such as $\Lambda\Lambda\alpha - \Xi N\alpha$ and $\Lambda\Lambda\alpha - \Sigma\Sigma\alpha$ channel[2] couplings, arising in the baryon-baryon interactions, could account for a part of the discrepancy [18, 79, 80].

Comparison with a simple local model

In order to make a comparison with a simple local model, the energies and radii obtained with the nonlocal SB potential are compared in Table 6.5 with the results obtained with the local $\alpha\Lambda$ Isle potential (6.7). The binding energy with the Isle potential is smaller than with the nonlocal SB potential, i.e., appears to be closer to the experimental value. The r.m.s matter radius of ${}^{6}_{\Lambda\Lambda}$He is calculated as

$$\langle r^2\rangle = \frac{1}{A_\alpha + 2A_\Lambda}\left[\langle\rho^2\rangle + A_\alpha r_\alpha^2\right], \tag{6.10}$$

assuming $r_\alpha = 1.47$ fm for the radius of the α-particle. The r.m.s radius is larger for the local potential as expected for a weaker binding.

[2] Σ and Ξ are other hyperons (with strangeness -2 and -1, respectively); with the nucleons N, the Λ, Σ and Ξ hyperons form a spin-$\frac{1}{2}$ baryon octet [62].

Now we use $f_{\Lambda\Lambda}$ in the $\Lambda\Lambda$ SB interaction (6.3) as a parameter fitted to bring the binding energy within the error bars of the experimental value. This is achieved with $f_{\Lambda\Lambda} = 0.8$ (see Table 6.5). The radii increase since the binding energies decrease but the 0.1 fm difference between the models is essentially maintained. When values of $f_{\Lambda\Lambda}$ are adjusted to reproduce the experimental energy, the radius difference is still 0.08 fm.

The probability density of the ${}^{6}_{\Lambda\Lambda}$He ground state as a function of the $\Lambda\Lambda$ and $\alpha - \Lambda\Lambda$ distances is calculated from the wave function, according to definition (5.7). In Figure 6.3, the probability density obtained in the local model (with the Isle $\alpha\Lambda$ potential) is compared with the one obtained in the nonlocal model (with the SB $\alpha\Lambda$ potential), for the same binding energy ($E = -7.248$ MeV) of ${}^{6}_{\Lambda\Lambda}$He. These probability densities corresponds to $f_{\Lambda\Lambda} = 0.85$ and $f_{\Lambda\Lambda} = 0.78$ for the models with the Isle and SB $\alpha\Lambda$ potentials, respectively. Figure 6.3 shows that the local model and the nonlocal semi-microscopic model yield quite similar probability densities for ${}^{6}_{\Lambda\Lambda}$He. There are however very slight differences: with the nonlocal SB $\alpha\Lambda$ potential, the maximum density (0.16 fm^{-2}) is obtained for a $\Lambda\Lambda$ distance of 2.3 fm and an $\alpha - \Lambda\Lambda$ distance of 1.4 fm, while with the Isle $\alpha\Lambda$ potential, the maximum is lower (0.13 fm^{-2}) and corresponds to a $\Lambda\Lambda$ distance of 2.5 fm and an $\alpha - \Lambda\Lambda$ distance of 1.7 fm. Thus the local model gives similar results to the nonlocal model, but with larger distances between the particles in ${}^{6}_{\Lambda\Lambda}$He.

We have also performed a search for possible excited states of the ${}^{6}_{\Lambda\Lambda}$He. For ${}^{1}P$ and ${}^{1}D$ configurations, we find no indication of such states. When increasing K_M, the energy is negative and decreases but stays significantly above the ${}^{5}_{\Lambda}\mathrm{He} + \Lambda$ separation threshold.

Role of nonlocality and potential energies

In order to see the role of the nonlocal terms in the binding energy of ${}^{6}_{\Lambda\Lambda}$He, we calculate the mean values of the kinetic energy, and the local- and nonlocal-potential energies. These values are given in Table 6.6. The potential energy is separated into several terms: $\langle V_{\Lambda\Lambda}\rangle$ denotes the mean value of the $\Lambda\Lambda$ potential, and $\langle V_{\alpha\Lambda}\rangle$ and $\langle W_{\alpha\Lambda}\rangle$ denote respectively the mean values of the local and nonlocal terms of the $\alpha\Lambda$ potential. There are two $\alpha\Lambda$ interactions in the Hamiltonian of the $\alpha\Lambda\Lambda$ model. The mean potential energies are, of course, identical for both $\alpha\Lambda$ interactions, by symmetry. Hence in Table 6.6, the values $\langle V_{\alpha\Lambda}\rangle$ and $\langle W_{\alpha\Lambda}\rangle$ are multiplied by 2, and therefore correspond to the sum of both $\alpha\Lambda$ interactions. We have $E = \langle T\rangle + \langle V_{\Lambda\Lambda}\rangle + 2\langle V_{\alpha\Lambda}\rangle + 2\langle W_{\alpha\Lambda}\rangle$.

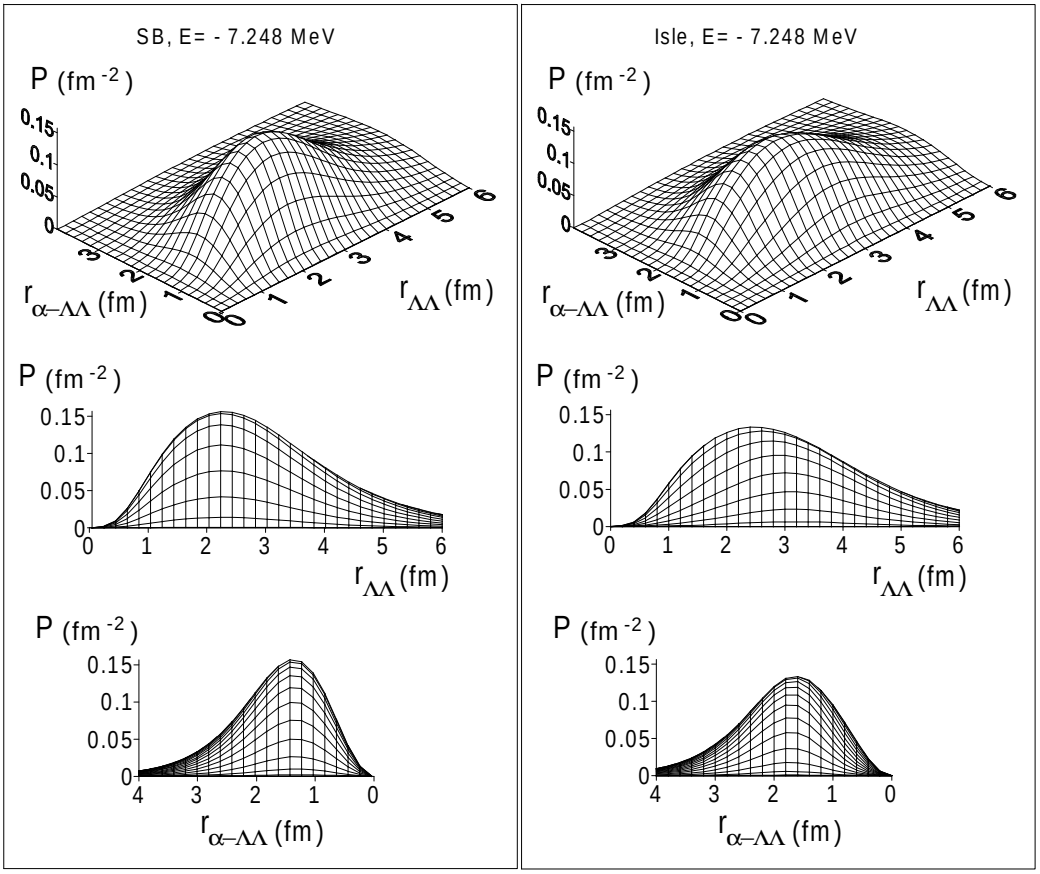

Figure 6.3: Comparison of the probability densities (as functions of the $\Lambda\Lambda$ and $\alpha-\Lambda\Lambda$ Jacobi coordinates) for the ground state of ${}^{6}_{\Lambda\Lambda}$He for the nonlocal SB $\alpha\Lambda$ potential (left) and the local Isle $\alpha\Lambda$ potential (right), when the parameter $f_{\Lambda\Lambda}$ is chosen so that $E = -7.428$ MeV. (3D view, with the corresponding 2D side views along the $r_{\Lambda\Lambda}$ and $r_{\alpha-\Lambda\Lambda}$ axes.)

$V_{\alpha\Lambda}$	$f_{\Lambda\Lambda}$	$\langle T\rangle$	$\langle V_{\Lambda\Lambda}\rangle$	$2\langle V_{\alpha\Lambda}\rangle$	$2\langle W_{\alpha\Lambda}\rangle$	E
SB	1	17.462	−2.421	−11.668	−11.523	−8.150
Isle	1	14.821	−1.926	−20.627	0	−7.732
SB	0.78	15.975	−1.240	−11.082	−10.901	−7.248
Isle	0.85	14.081	−1.240	−20.089	0	−7.248

Table 6.6: Mean contributions $\langle T\rangle$ of the kinetic energy, $\langle V_{\Lambda\Lambda}\rangle$ of the (local) $\Lambda\Lambda$ potential energy, $2\langle V_{\alpha\Lambda}\rangle$ of the local terms of $\alpha\Lambda$ potential energy and $2\langle W_{\alpha\Lambda}\rangle$ of the nonlocal terms of $\alpha\Lambda$ potential energy (in MeV), in the models of ${}^{6}_{\Lambda\Lambda}$He.

In Table 6.6, we see that the ${}^{6}_{\Lambda\Lambda}$He binding is mainly due to the $\alpha\Lambda$ interactions. In the semi-microscopic model (with the SB $\alpha\Lambda$ potential), the nonlocal terms contribute essentially for the half (about -11 MeV) of the total $\alpha\Lambda$ potential energy. This near equality $\langle V_{\alpha\Lambda}\rangle \approx \langle W_{\alpha\Lambda}\rangle$ in magnitude between the local and nonlocal $\alpha\Lambda$ terms may be related to fact that $\tilde{u} = 1$. The question of the influence of the exchange parameter $\tilde{u}$ will be discussed below.

Otherwise, with the Isle potential, $\langle W_{\alpha\Lambda}\rangle = 0$ since the potential is local, but in compensation, the local contribution $2\langle V_{\alpha\Lambda}\rangle$ is about twice as large (about -20 MeV) as with the SB $\alpha\Lambda$ potential. Here, Figure 6.2 displaying the Isle potential and the local term of the SB potential is relevant: it illustrates the difference of the local $\alpha\Lambda$ potential energy between the models.

An interesting comparison in Table 6.6 arises when the models give the same energy ($E = -7.248$ MeV), via different values of $f_{\Lambda\Lambda}$. In this case, we observe that the contribution $\langle V_{\Lambda\Lambda}\rangle$ of the $\Lambda\Lambda$ potential becomes remarkably identical for both models ($\langle V_{\Lambda\Lambda}\rangle = -1.240$ MeV), although the parameter $f_{\Lambda\Lambda}$ of the $\Lambda\Lambda$ potentials (6.3) differs ($f_{\Lambda\Lambda} = 0.78$ and $f_{\Lambda\Lambda} = 0.85$). The kinetic energies $\langle T\rangle$ are however different, as expected from the probability densities of Figure 6.3. The kinetic energy in the nonlocal model (about 16 MeV versus 14 MeV with the Isle potential) is larger by about 2 MeV, but this difference is exactly cancelled out by the total $(2\langle V_{\alpha\Lambda}\rangle + 2\langle W_{\alpha\Lambda}\rangle)$ $\alpha\Lambda$ potential energy, which allows the nonlocal model to give the same ${}^{6}_{\Lambda\Lambda}$He binding energy as with the Isle potential.

In the above comparison, the fundamental difference between the models should not be forgotten. This difference lies in the nature of the $\alpha\Lambda$ interaction potentials. The SB potential takes into account the exchange force of the nucleon-Λ interactions (6.1). Hence the SB $\alpha\Lambda$ potential has a nonlocal term, which plays a decisive role in the binding of ${}^{6}_{\Lambda\Lambda}$He. The phenomenological Isle $\alpha\Lambda$ potential is quite different: it is purely local and contains a repulsive core (see Figure 6.2), but no exchange force.

The exchange parameter $\tilde{u}$

The physical reason for the nonlocality in the SB $\alpha\Lambda$ potential is the exchange force in the nucleon-Λ interactions (6.1). The parameter $\tilde{u}$ allows us to modify the importance of this exchange force. Now we set $f_{\Lambda\Lambda} = 1$ and investigate the sensitivity of the ${}^{6}_{\Lambda\Lambda}$He energy to the exchange parameter $\tilde{u}$.

Figure 6.4 displays the dependence of the energy E on the parameter $\tilde{u}$, in the semi-microscopic model of ${}^{6}_{\Lambda\Lambda}$He. It also displays the corresponding local and nonlocal contributions $2\langle V_{\alpha\Lambda}\rangle$ and $2\langle W_{\alpha\Lambda}\rangle$. We see that the dependence

of the total energy E on $\tilde{u}$ is rather weak, especially in regard to the important modifications of $\langle V_{\alpha\Lambda}\rangle$ and $\langle W_{\alpha\Lambda}\rangle$. The variation of the energy E around the central value $\tilde{u}=1$ ($E=-8.150$ MeV) is $\delta E \approx -0.145\delta\tilde{u}$ for small variations $\delta\tilde{u}$ of the order of 0.1.

The straight lines of $\langle V_{\alpha\Lambda}\rangle$ and $\langle W_{\alpha\Lambda}\rangle$ reflect the $\tilde{u}$-dependence of the $\alpha\Lambda$ potential. Indeed the local and nonlocal terms of the SB $\alpha\Lambda$ potential respectively arise from the local ($\tilde{u}/2$) and exchange ($(1-\tilde{u}/2)P^r_{ij}$) terms of the nucleon-Λ potentials (6.1). Hence the $\alpha\Lambda$ potential depends on the parameter $\tilde{u}$ through the coefficients $X_d \propto \tilde{u}/2$ (for the local terms (6.5)) and $X_e \propto (1-\tilde{u}/2)$ (for the nonlocal terms (6.6)). This accounts for the straight-line behaviour of $\langle V_{\alpha\Lambda}\rangle$ and $\langle W_{\alpha\Lambda}\rangle$ in Figure 6.4.

The crossing of the lines ($\langle V_{\alpha\Lambda}\rangle = \langle W_{\alpha\Lambda}\rangle$) occurs near $\tilde{u}=1$, i.e., when the local ($\tilde{u}/2$) and exchange ($1-\tilde{u}/2$) terms have an equal weight in the nucleon-Λ potential (6.1). The numerical values (E, $2\langle V_{\alpha\Lambda}\rangle$, $2\langle W_{\alpha\Lambda}\rangle$) for $\tilde{u}=1$ are those given above in Table 6.6.

We note that when $\tilde{u}$ increases, the binding of ${}^{6}_{\Lambda\Lambda}$He increases. Thus in the SB $\alpha\Lambda$ potential, the local terms appear to have a more binding effect than the nonlocal (exchange) terms.

6.5.3 The ${}^{9}_{\Lambda}$Be hypernucleus

$\alpha\alpha\Lambda$ model with various potentials

We now consider the ${}^{9}_{\Lambda}$Be hypernucleus, which is described in an $\alpha\alpha\Lambda$ model. We test several local (ABd, SBFW, PBFW) and nonlocal (RGM-ε and RGM-$\not\varepsilon$) $\alpha\alpha$ potentials. The local models are purely phenomenological. The ABd and SBFW are shallow potentials, while PBFW is a deep $\alpha\alpha$ potential, which requires the elimination of the forbidden states. The semi-microscopic models use the nonlocal potentials (RGM-ε or RGM-$\not\varepsilon$ for $\alpha\alpha$ and SB for $\alpha\Lambda$). Note that in the semi-microscopic models, the Pauli forbidden states of the $\alpha\alpha$ RGM potentials are to be eliminated too.

We consider the $1/2^+$ ($L=0$) ground state and the (here degenerate) $3/2^+$ and $5/2^+$ ($L=2$) excited state of ${}^{9}_{\Lambda}$Be.

We first make a comparison with published Faddeev $\alpha\alpha\Lambda$ calculations [17] using the SB $\alpha\Lambda$ potential and the local (ABd, PBFW) and nonlocal RGM-ε $\alpha\alpha$ potentials. For the ground state, with the local[3] ABd and PBFW poten-

[3]For this comparison only, the used parameters slightly differ: $\hbar^2/2m_N = 20.893$ MeV fm^2 in both cases; $\nu = 0.27127$ fm^{-2} for the ABd potential, $\nu = 0.257$ fm^{-2} for the BFW potential. [17]

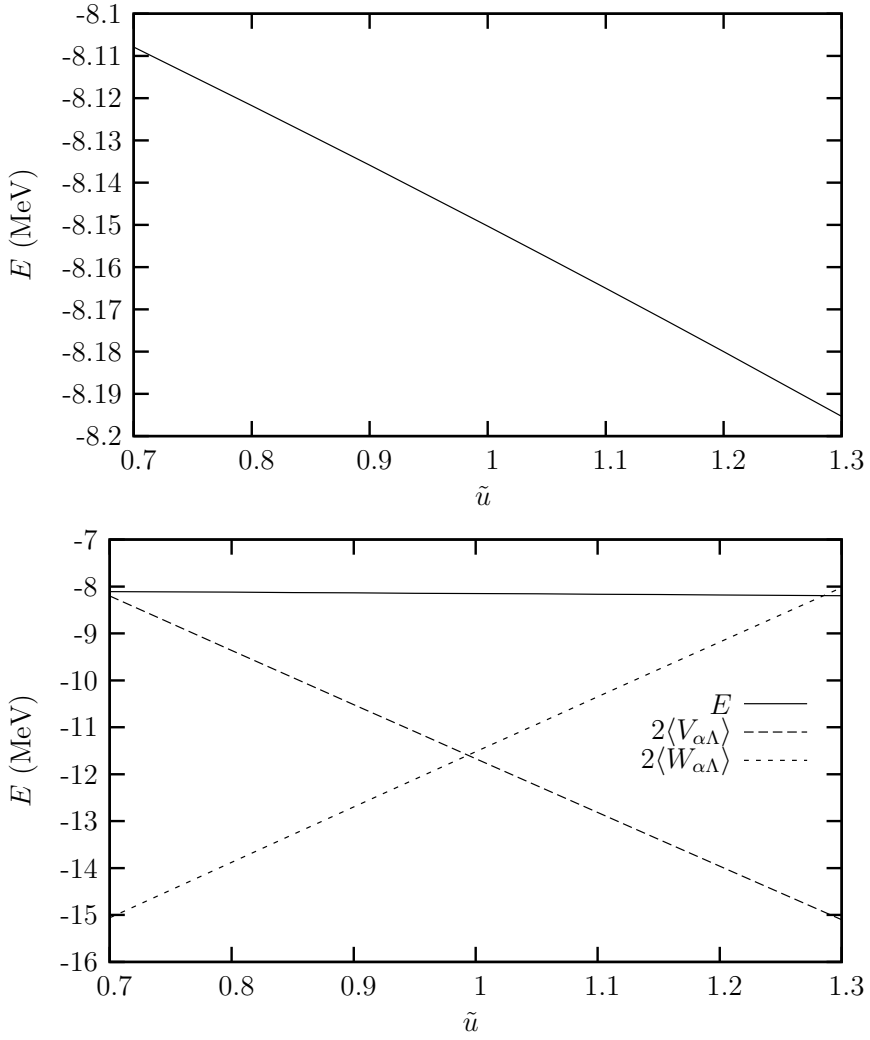

Figure 6.4: Dependence on the exchange parameter $\tilde{u}$ of the energy E (top) in the semi-microscopic model of ${}^{6}_{\Lambda\Lambda}$He, and the corresponding local and nonlocal potential energies $2\langle V_{\alpha\Lambda}\rangle$ and $2\langle W_{\alpha\Lambda}\rangle$ (bottom) for comparison

tials, we obtain [19] the binding energies $B({}^{9}_{\Lambda}\mathrm{Be}) = 7.153$ and 7.043 MeV, respectively, i.e., a perfect agreement with Table XI of Ref. [17].

For the calculation with the nonlocal RGM-ε $\alpha\alpha$ potentials, we obtain $B({}^{9}_{\Lambda}\mathrm{Be}) = 6.839$ MeV, with the self-consistent $\alpha\alpha$ energy $\varepsilon_{\alpha\alpha} = 1.18$ MeV [20]. This result agrees within 2 keV with Ref. [17]. The slight difference could be due to the fact that we treat the Coulomb interaction between the α-particles exactly, while in Ref. [17] a Coulomb cutoff approximation is made. This again validates our calculation method using the hyperspherical harmonics and the Lagrange-mesh technique, with nonlocal potentials.

Our results for the energies of the ground and excited states of ${}^{9}_{\Lambda}\mathrm{Be}$ are given in Table 6.7 for the different potentials. The conditions of calculation are identical for all the potentials (see Section 6.5.1).

The experimental Λ-separation energy of ${}^{9}_{\Lambda}\mathrm{Be}$ is 6.71 ± 0.04 MeV [74]. The corresponding experimental ground-state energy in the three-body ($\alpha\alpha\Lambda$) model is $E_{1/2^+} = -6.62 \pm 0.04$ MeV.

In Table 6.7, we first observe that the models with the phenomenological local potentials (ABd, SBFW, PBFW for $\alpha\alpha$ and Isle for $\alpha\Lambda$) give an overbinding of about 2 MeV with respect to experiment.

Using the non-local SB $\alpha\Lambda$ potential instead of the Isle potential improves the situation. The overbinding is reduced: there is only 0.5 to 0.8 MeV of difference, when the local $\alpha\alpha$ potentials are used. Note that it is the opposite of the ${}^{6}_{\Lambda\Lambda}\mathrm{He}$ case. Here the results with the nonlocal SB potential, compared to the local Isle $\alpha\Lambda$ potential, are closer to experiment.

While the local $\alpha\alpha$ potentials (ABd, SBFW, PBFW) lead to overestimates of the binding energy, the microscopically-founded RGM $\alpha\alpha$ potentials give rather excellent results. The semi-microscopic model using the nonlocal energy-dependent RGM-ε potential give a binding energy with only 0.2 MeV of difference with respect to experiment. The excellent result is that the semi-microscopic model with the energy-independent RGM-$\not{\varepsilon}$ potential give the right energy $E_{1/2^+} = -6.596$ MeV (since experimentally $E_{1/2^+} = -6.62\pm0.04$ MeV). Notice that this result is obtained without adjustable parameters: the $\alpha\alpha$ potential is configured to reproduce the $\alpha+\alpha$ scattering phase shifts and the $\alpha\Lambda$ potential is configured to reproduce the ${}^{5}_{\Lambda}\mathrm{He}$ binding energy.

Two excited states (presumably $5/2^+$ and $3/2^+$) are experimentally located at 3.029 ± 0.003 MeV and 3.060 ± 0.003 MeV [70] giving an average excitation energy of 3.045 ± 0.003 MeV. The different theoretical results in Table 6.7 all lie within 150 keV of this experimental value. In particular, the excitation energy with the RGM potentials is $E_x = 2.92$ MeV.

$V_{\alpha\Lambda}$	$V_{\alpha\alpha}$	$E_{1/2^+}$	$\sqrt{\langle r^2\rangle}$	$E_{3/2^+,5/2^+}$	$\sqrt{\langle r^2\rangle}$	E_x	$B(E2)$
Isle	ABd	-8.437	2.32	-5.575	2.30	2.862	13.06
	SBFW	-8.682	2.28	-5.677	2.27	3.005	11.76
	PBFW	-8.986	2.22	-5.842	2.23	3.144	9.51
SB	ABd	-7.101	2.37	-4.203	2.38	2.898	14.86
	SBFW	-7.429	2.31	-4.341	2.34	3.088	12.98
	PBFW	-7.292	2.27	-4.179	2.32	3.113	11.61
SB	RGM-ε	-6.839	2.34	-3.922	2.37	2.917	13.76
	RGM-$\not\varepsilon$	-6.596	2.41	-3.675	2.47	2.921	17.26

Table 6.7: Energies (in MeV) and r.m.s matter radii (in fm) of the ground state and first excited state of ${}^{9}_{\Lambda}$Be for different combinations of $\alpha\Lambda$ and $\alpha\alpha$ potentials. The excitation energy $E_x(= E_{3/2^+,5/2^+} - E_{1/2^+})$ and the $B(E2)$ (in $e^2\text{fm}^4$) for the $L = 2 \rightarrow L = 0$ transition are also given. For the RGM-ε $\alpha\alpha$ potential, the self-consistent value of the $\alpha\alpha$ energy is $\varepsilon_{\alpha\alpha} = 1.18$ MeV for $E_{1/2+}$ and $\varepsilon_{\alpha\alpha} = 4.01$ MeV for $E_{3/2+,5/2+}$.

The reduced transition probabilities, from $5/2^+$ and $3/2^+$ excited states to the $1/2^+$ ground state (i.e., the $B(E2)$ for the $L = 2$ to $L = 0$ transition) are also presented in Table 6.7. The experimental value is $5.7^{+2.1}_{-2.0}$ $e^2\text{fm}^4$ [70]. All the model values are about twice as large, except for the result with the RGM-$\not\varepsilon$ potential, which reaches a higher value $B(E2) = 17.26$ $e^2\text{fm}^4$. The magnitude of $B(E2)$ for local (ABd, SBFW, PBFW) and RGM-ε potentials is consistent with the predicted (theoretical) result 11.26 $e^2\text{fm}^4$ of Motoba et al. [81]. The $B(E2)$ obtained with the RGM-ε potential is lower ($B(E2) =$ 13.76 $e^2\text{fm}^4$) than the one obtained with the RGM-$\not\varepsilon$ potential. Practical information about the calculation of $B(E2)$ in hyperspherical coordinates can be found in Refs. [27, 82].

In Table 6.7, the r.m.s radii of the states of ${}^{9}_{\Lambda}$Be are also given. They are computed as

$$\langle r^2\rangle = \frac{1}{2A_\alpha + A_\Lambda}\left[\langle\rho^2\rangle + 2A_\alpha r_\alpha^2\right], \tag{6.11}$$

with $r_\alpha = 1.47$ fm for the radius of the α-particles. The radius of the model using the RGM-$\not\varepsilon$ potential (2.41 fm for g.s., 2.47 for excited state) is larger than the radius of the model using the RGM-ε potentials (2.34 fm for g.s. and 2.37 fm for excited state).

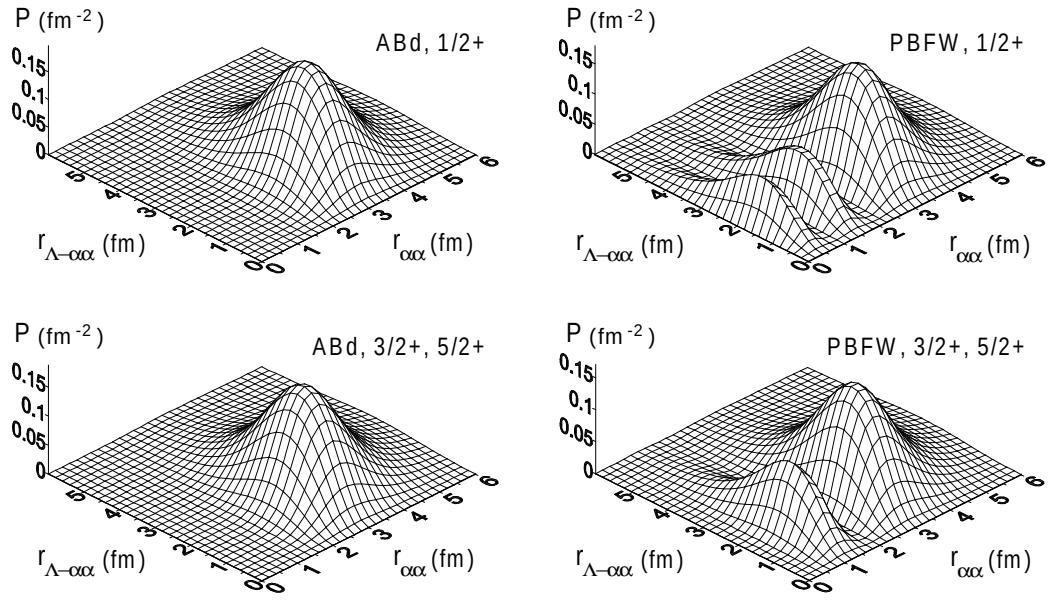

Figure 6.5: Probability densities for the $1/2^+$ (top) and $3/2^+, 5/2^+$ (bottom) states of ${}^{9}_{\Lambda}$Be as functions of the Jacobi coordinates $r_{\alpha\alpha}$ and $r_{\Lambda-\alpha\alpha}$ (in fm) for the shallow ABd potential (left) and the deep PBFW potential with projection of the forbidden states (right), the $\alpha\Lambda$ potential being the nonlocal SB potential.

Comparison of the probability densities

The probability densities, as functions of the $\alpha\alpha$ and $\Lambda-\alpha\alpha$ distances, for the ${}^{9}_{\Lambda}$Be ground and excited states are displayed in Figures 6.5 and 6.6.

The case of the models with local $\alpha\alpha$ potentials is treated in Figure 6.5. This figure clearly shows the fundamental difference between the wave functions obtained with shallow (ABd) and deep (PBFW) potentials. The probability densities are similar only for large $\alpha\alpha$ distances, above 2 fm. Otherwise, for small $\alpha\alpha$ distances (below 2 fm) the densities are qualitatively very different. This illustrates the effect of the Pauli forbidden states, the exclusion of which is, of course, not taken into account in models with shallow $\alpha\alpha$ potentials. With the deep PBFW $\alpha\alpha$ potential, the wave function is constrained to be orthogonal to the forbidden states (the unphysical bound states of the deep potential): this leads to nodes in the wave function, describing the $\alpha\alpha$ relative motion. Hence the ground-state probability density displays three bumps and the excited-state probability density displays two bumps. With the shallow ABd $\alpha\alpha$ potential, the densities do not have such bumps: the densities are flat until the $\alpha\alpha$ distance reaches 2 fm, and then have a single

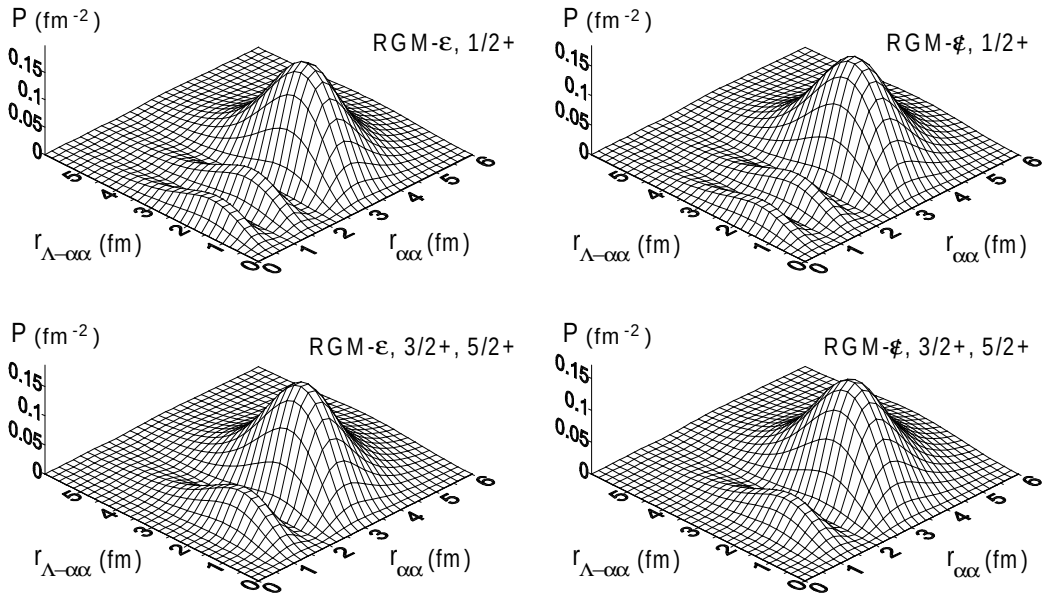

Figure 6.6: Probability densities for the $1/2^+$ (top) and $3/2^+, 5/2^+$ (bottom) states of ${}^{9}_{\Lambda}$Be as functions of the Jacobi coordinates $r_{\alpha\alpha}$ and $r_{\Lambda-\alpha\alpha}$ (in fm) for the semi-microscopic models with the RGM-ε potential (left) and the RGM-$\not\varepsilon$ potential (right).

maximum, very similar to the last bump obtained with the PBFW potential.

With the shallow SBFW $\alpha\alpha$ potential, we obtain probability densities that are quite similar to those obtained with the ABd potential, hence such densities are not displayed.

The probability densities obtained with the semi-microscopic models are displayed in Figure 6.6. In those models (with the nonlocal RGM-ε and RGM-$\not\varepsilon$ $\alpha\alpha$ potentials), the $\alpha\alpha$ Pauli forbidden states must also be eliminated from the wave function. The forbidden states are taken as harmonic-oscillator wave functions, as in the RGM. The probability densities show that the local model with the deep PBFW $\alpha\alpha$ potential (in Figure 6.5) is qualitatively correct. Because of the exclusion of the forbidden states, the densities display three bumps, for the ground state, and two bumps, for the excited states. The size of the bumps depends on the choice of the $\alpha\alpha$ interaction. The bumps are slightly less high with the RGM-$\not\varepsilon$ potential than with the RGM-ε potential; this is consistent with the fact that the r.m.s radius in Table 6.7 is larger with RGM-$\not\varepsilon$ potential than with the RGM-ε potential.

Nevertheless, the probability densities of ${}^{9}_{\Lambda}$Be are very similar between the different models. For example, for the ground state, the maximum density (0.20 fm^{-2} for RGM-ε, and 0.19 fm^{-2} for RGM-$\not\varepsilon$) is obtained for nearly

J^π	$V_{\alpha\Lambda}$	$V_{\alpha\alpha}$	$\langle T\rangle$	$\langle V_{\alpha\alpha}\rangle$	$\langle W_{\alpha\alpha}\rangle$	$2\langle V_{\alpha\Lambda}\rangle$	$2\langle W_{\alpha\Lambda}\rangle$	E
$\frac{1}{2}^+$	Isle	ABd	13.674	−3.733	0	−18.378	0	−8.437
		SBFW	13.420	−3.217	0	−18.885	0	−8.682
		PBFW	37.134	−26.958	0	−19.162	0	−8.986
	SB	ABd	12.265	−3.510	0	−8.308	−7.549	−7.101
		SBFW	12.224	−3.015	0	−8.704	−7.934	−7.429
		PBFW	34.302	−25.116	0	−9.025	−7.453	−7.292
$\frac{1}{2}^+$	SB	RGM-ε	27.350	−15.872	−2.408	−8.602	−7.307	−6.839
		RGM-$\not\varepsilon$	23.347	−13.189	−1.523	−8.180	−7.051	−6.596
$\frac{3}{2}^+$	Isle	ABd	20.000	−6.834	0	−18.741	0	−5.575
		SBFW	20.324	−6.970	0	−19.031	0	−5.677
		PBFW	38.085	−24.844	0	−19.083	0	−5.842
	SB	ABd	18.253	−6.355	0	−8.485	−7.616	−4.203
		SBFW	18.789	−6.579	0	−8.722	−7.829	−4.341
		PBFW	34.744	−22.646	0	−8.902	−7.374	−4.179
$\frac{3}{2}^+$	SB	RGM-ε	29.470	−15.532	−2.008	−8.581	−7.271	−3.922
		RGM-$\not\varepsilon$	25.300	−12.693	−1.178	−8.112	−6.992	−3.675

Table 6.8: Mean values (in MeV) of the kinetic energy $\langle T\rangle$ and of the local and nonlocal potential energies: $\langle V_{\alpha\alpha}\rangle$ and $2\langle V_{\alpha\Lambda}\rangle$ correspond to the local terms, and $\langle W_{\alpha\alpha}\rangle$ and $2\langle W_{\alpha\Lambda}\rangle$ to the nonlocal terms, of the $\alpha\alpha$ and $\alpha\Lambda$ interactions. $\langle T\rangle + \langle V_{\alpha\alpha}\rangle + \langle W_{\alpha\alpha}\rangle + 2\langle V_{\alpha\Lambda}\rangle + 2\langle W_{\alpha\Lambda}\rangle = E$.

equal $\alpha\alpha$ distances (3.2 fm for RGM-ε and 3.3 fm for RGM-$\not\varepsilon$) and for a same $\Lambda - \alpha\alpha$ distance (1.9 fm for both models).

Kinetic and potential energies

In Table 6.8, we display the detailed values of the kinetic, local- and nonlocal-potential energies of the different results of Table 6.7.

The results obtained with the ABd and SBFW $\alpha\alpha$ potentials are very similar. This is because ABd and SBFW are comparable shallow potentials [40].

Here again, we see a significant difference between deep (PBFW) and shallow (SBFW and ABd) $\alpha\alpha$ potentials. The kinetic energies $\langle T\rangle$ are indeed very different according to whether the $\alpha\alpha$ potential is PBFW or SBFW. There are more than 20 MeV of difference in the kinetic energy $\langle T\rangle$ between the models with local deep and shallow potentials. Consequently, there is also a difference in the potential energies $\langle V_{\alpha\alpha}\rangle$. However, we observe that

the sum $\langle T\rangle + \langle V_{\alpha\alpha}\rangle$ is essentially independent of the choice of the local $\alpha\alpha$ potential (e.g., $\langle T\rangle + \langle V_{\alpha\alpha}\rangle \approx 9$ MeV with the SB $\alpha\Lambda$ potential, for the ground state). Thus the difference in the kinetic energies $\langle T\rangle$ between the models is canceled out by the difference in the $\alpha\alpha$ potential energies $\langle V_{\alpha\alpha}\rangle$ (e.g., $\langle T\rangle_{\rm PBFW} - \langle T\rangle_{\rm SBFW} \approx 22$ MeV and $\langle V_{\alpha\alpha}\rangle_{\rm PBFW} - \langle V_{\alpha\alpha}\rangle_{\rm SBFW} \approx -22$ MeV for the ground state with the SB $\alpha\Lambda$ potential).

We also see that the $\alpha\Lambda$ potential energy ($2\langle V_{\alpha\Lambda}\rangle + 2\langle W_{\alpha\Lambda}\rangle$) is almost insensitive to the depth of the local $\alpha\alpha$ potential. The $\alpha\alpha\Lambda$ binding is weaker with the SB $\alpha\Lambda$ potential than with the Isle potential.

The kinetic energy $\langle T\rangle$ obtained with the semi-microscopic models is located between the SBFW and PBFW results (for the ground state, $\langle T\rangle$ is about 23 MeV with the RGM-$\not\varepsilon$ potential). In the RGM $\alpha\alpha$ interactions, the local term is significantly predominant with respect to the nonlocal term ($\langle V_{\alpha\alpha}\rangle / \langle W_{\alpha\alpha}\rangle \sim 7$). For the $\alpha\Lambda$ SB interactions, the local and nonlocal terms are comparable in magnitude ($\langle V_{\alpha\Lambda}\rangle / \langle W_{\alpha\Lambda}\rangle \sim 1.2$). The model with the RGM-ε $\alpha\alpha$ potential leads to different kinetic and potential energies compared to the RGM-$\not\varepsilon$ $\alpha\alpha$ potential.

For the excited state, the most significant changes with respect to the ground-state values are in the kinetic energy (except for the PBFW case). In the semi-microscopic models, the change in kinetic energy $\langle T\rangle$ is about 2 MeV, out of the 3 MeV of excitation energy.

6.6 Conclusion

In this chapter, we have successfully tested our hyperspherical harmonics method with the Lagrange-mesh technique for the three-body models with nonlocal potentials [19, 20]. As first applications, we have studied two hypernuclei, ${}^{\ 6}_{\Lambda\Lambda}$He and ${}^{\ 9}_{\Lambda}$Be. The practical test has been carried out by comparing some results with published results, independently obtained, under the same conditions, with the momentum-space Faddeev method [17, 18]. An advantage of our method is that the Coulomb terms do not need any special treatment. Also, working directly in the configuration space allows us to easily obtain new information, such as probability densities, radii or reduced transition probabilities.

In addition, we have also compared the nonlocal semi-microscopic models with simple, phenomenological, models using local potentials. The nonlocal potentials take into account the internal structure of the α clusters. The nonlocality arises (i) because of the exchange forces in the baryon-baryon interactions, as in the $\alpha\Lambda$ interaction, and (ii) because of the Pauli antisymmetrisation between the nucleons, as in the $\alpha\alpha$ interactions. Also, because

of the Pauli principle and the internal structure of the clusters, there exist forbidden states in the $\alpha\alpha$ relative motion. The effects of the Pauli forbidden states are particularly visible in the probability densities.

Considering the $\alpha\Lambda$ interaction, in the case of ${}^{6}_{\Lambda\Lambda}$He, the local and nonlocal models give rather similar results, with some differences: the local $\alpha\Lambda$ potential gives a smaller binding energy (and a larger radius) than the nonlocal $\alpha\Lambda$ potential. However this is not a general rule. It is the exact opposite in the case of ${}^{9}_{\Lambda}$Be: the local $\alpha\Lambda$ potential gives larger binding energies (and smaller radii) than the nonlocal $\alpha\Lambda$ potential. The models with simple local potentials overestimate the binding energy of ${}^{9}_{\Lambda}$Be. In comparison, the nonlocal semi-microscopic models, especially with the energy-independent RGM potential, successfully give the correct binding energy, without adjustable parameter. This encourages the development and application of the semi-microscopic three-body model, using pairwise RGM potentials. However, we notice that if the results are correct in terms of binding energy, there is a difference between the three-body model and experiment for the reduced transition probability $B(E2)$ for the excited ${}^{9}_{\Lambda}$Be.

Chapter 7

Three-body models of ^{6}He, ^{9}Be and ^{12}C using the energy-dependent RGM potentials

7.1 Three-body models

In this chapter, we will apply the three-cluster models to three typical examples of atomic nuclei: ^{6}He, ^{9}Be, and ^{12}C. In particular, we will study the validity of the semi-microscopic model that uses the energy-dependent RGM-ε inter-cluster potentials [20]. To this end, we will compare the results of that semi-microscopic approximation with the exact results of the corresponding fully microscopic model.

The advantage of the semi-microscopic model is that it allows us to approximate the three-cluster problem by a simple three-body model (where the clusters are considered as pointlike particles). Also, it is interesting to compare this model with the simplified macroscopic three-body models with local potentials. Thus, before applying the semi-microscopic model, we will first see the results of the three-body local models [20, 27], for ^{6}He, ^{9}Be, and ^{12}C. This will motivate the use of the semi-microscopic approximation.

Here we start by giving the three-body models of ^{6}He, ^{9}Be, and ^{12}C. Next, in Section 7.2, we will give the numerical parameters of the models. In Section 7.3, the results of the local models will be discussed. In Section 7.4, the semi-microscopic model will be analysed, and compared with the microscopic model. Conclusions will be drawn in Section 7.5.

The first example of nucleus that presents a pronounced three-body structure is ^{6}He. The ^{6}He is a halo nucleus [6, 7], which can be represented by an αnn system (i.e., a core which is an α-particle, and two loosely bound valence neutrons). The binding energy of this three-body ($\alpha + n + n$) structure is given by the two-neutron separation energy $S_{2n} = 0.973 \pm 0.001$ MeV [15]. The experimental studies of ^{6}He also reveal the matter radius of the nucleus ($R_{rms}(^6\text{He}) \sim 2.5$ fm [7,83]), which is large in comparison with the one of ^{4}He ($R_{rms}(\alpha) \sim 1.5$ fm). This large radius is interpreted as a result of the halo structure. The ground state of ^{6}He is a 0^+ state. The neutron-rich isotope ^{6}He is unstable and decays, by β-emission ($^6\text{He} \xrightarrow{\beta} {}^6\text{Li}$), with a half-life of 806.7 ± 1.5 ms[15].

The ^{9}Be and ^{12}C stable nuclei can also be represented by simplified three-body models [20–22]. The ^{9}Be is represented by an $\alpha\alpha n$ system. The three clusters (α+α+n) are bound, inside ^{9}Be, with a binding energy of 1.573±0.01 MeV[16]. The ground state of ^{9}Be is a $3/2^-$ state. The ^{12}C is represented by a 3α system. In this cluster model, in the 0^+ ground state of ^{12}C, the three α-particles are bound with a binding energy of 7.275 ± 0.01 MeV [14]. Also, more specifically, this 3α cluster structure of ^{12}C is expected to be an excellent approximation in an excited state (the 0_2^+ resonance) of ^{12}C, because this state is situated at 7.65 MeV (that is, slightly above the threshold for breackup into three free α-particles). This resonance (known as the Hoyle state) plays a decisive role in nuclear astrophysics [10, 11] because it enables the stellar triple-α process, where three α-particles combine to form ^{12}C.

Thus, we will describe ^{6}He, ^{9}Be and ^{12}C in αnn, $\alpha\alpha n$ and 3α models, respectively. These models need effective $\alpha\alpha$ and αn potentials. In the semi-microscopic model, these potentials are represented by the nonlocal RGM-ε $\alpha\alpha$ and αn potentials. The parameters of the potentials are given in the next section.

7.2 Parameters and numerical conditions

Before discussing the results, we specify the numerical parameters [21]. We adopt the same parameters in every model (local, semi-microscopic, and microscopic cluster models). The mass unit is given by the value $\hbar^2/2m_N = 20.736$ MeV fm^2, where m_N is the effective nucleon mass. The mass of an α-cluster is thus $m_\alpha = 4m_N$.

In the semi-microscopic model, we use the αn and $\alpha\alpha$ RGM-ε potentials, given in Appendix C. The potentials are calculated by using MN (5.8) or

V2 (5.10), as effective nucleon-nucleon interactions. For the αn potential, we add a spin-orbit force (5.13) (with $\kappa \to 0$). The internal wave functions of the α-clusters (2.6) are taken with the parameter $b = 1.36$ fm [53] to fit the radius of the α-particle: $r_\alpha = 1.44$ fm, according to (5.5).

The experimental data about the αn and $\alpha\alpha$ potentials are essentially the scattering data. We adjust the MN and V2 forces in order to reproduce the $\alpha+n$ and $\alpha+\alpha$ elastic scattering phase shifts. For MN we set $u = 0.9474$ and $S_0 = 37$ MeV fm^5, for the spin-orbit force. For V2 we set $m = 0.605$ and $S_0 = 49$ MeV fm^5. With these values the $\alpha + n$ and $\alpha + \alpha$ phase shifts are simultaneously reproduced, in agreement with experiment. However, in the case of ^{12}C (in the 3α model), the spin-orbit force is not necessary, since the spin of the α-cluster is zero; hence we consider a slight variant by using a more accurate value $u = 0.94687$ for MN.

When we compare the semi-microscopic model with the microscopic three-cluster model, of course, we use the same parameters in both models.

In the semi-microscopic model, the Pauli forbidden states of the αn and $\alpha\alpha$ subsystems (according to the two-cluster RGM) must necessarily be projected out from the wave function, in the three-body Schrödinger equation. The techniques that can be used to eliminate the Pauli forbidden state are described in Section 5.5.

Let us now specify the conditions of the numerical calculations. The number of Lagrange-mesh points (3.109) is $N = 30$ with the scale parameter $h = 0.3$ fm. For the local potentials, integrals (B.4) are performed with a Gauss-Legendre quadrature with 64 points. For the nonlocal RGM-ε potentials, the parameters of the Gaussian quadrature in equation (B.24) are $N_2 = 30$ and $h_2 = 0.08$ fm. The integration over y in this equation is performed with a constant step 0.06 fm and extends up to 48 fm.

In Table 7.1, we give a typical example of convergence of the calculations, with respect to the K_M parameter [20] (in the semi-microscopic and microscopic models). In the semi-microscopic model, for each value of K, all possible values of (l_x, l_y) are considered (without restriction). However, in the microscopic model, in order to simplify the calculations, the l_x values are limited by the condition $l_x \leq 4$ [53]. As a test, if we apply the same restriction $l_x \leq 4$ in the semi-microscopic model, then the energy becomes $E_{3/2-} = -3.83$ MeV, instead of -3.86 MeV, for $K_M = 19$. The restriction on l_x thus plays most probably a marginal role, in the microscopic model.

The physical relevance of the results in Table 7.1 will be discussed below in Section 7.4.

	Semi-microscopic			Microscopic		
K_M	$E_{3/2^-}$	$E_{5/2^-}$	ΔE	$E_{3/2^-}$	$E_{5/2^-}$	ΔE
5	−1.64	0.87	2.50	−1.27	1.51	2.28
7	−2.39	0.17	2.55	−1.89	0.57	2.46
9	−3.41	−0.84	2.57	−2.23	0.22	2.46
11	−3.68	−1.11	2.57	−2.49	0.02	2.51
13	−3.79	−1.23	2.56	−2.55	−0.04	2.52
15	−3.83	−1.29	2.55	−2.60	−0.08	2.52
17	−3.85	−1.30	2.55	−2.61	−0.09	2.52
19	−3.86					

Table 7.1: Convergence of the $3/2^-$ and $5/2^-$ energies (in MeV) and of their difference ($\Delta E = E_{5/2^-} - E_{3/2^-}$) with respect to K_M, in the semi-microscopic and microscopic three-cluster models of ^{9}Be, using the MN potential. The semi-microscopic results are obtained with the RGM-ε $\alpha\alpha$ and αn potentials; the values of the energies, in the nonlocal kernel, are $\varepsilon_{\alpha\alpha} = 3.61$ MeV and $\varepsilon_{\alpha n} = 6.28$ MeV for the $3/2^-$ state, and $\varepsilon_{\alpha\alpha} = 5.57$ MeV and $\varepsilon_{\alpha n} = 6.39$ MeV for the $5/2^-$ state.

Hereafter, we use $K_M = 28$, $K_M = 19$ and $K_M = 30$ in the models of ^{6}He, ^{9}Be and ^{12}C, respectively.

7.3 Failure of local three-body models

Three-body models with local potentials are discussed in detail with the Lagrange-mesh technique and the hyperspherical harmonics in Ref. [27]. Here, we shall just give the energies and the root mean-square radii of ^{6}He, ^{9}Be and ^{12}C (described as αnn, $\alpha\alpha n$ and 3α systems, respectively) calculated with various αn and $\alpha\alpha$ local potentials. The aim of this section is simply to illustrate the well-known fact [7, 27, 45] that three-body models with strict two-body local potentials, without readjustement, commonly give unsatisfactory results in disagreement with experiment.

We consider the following local potentials (see Section 5.4.3): as αn potential, we take the deep KKNN potential (5.14), and as $\alpha\alpha$ potential, we use two variants: the deep potential BFW (5.15) and the shallow potential ABd (5.16). These αn and $\alpha\alpha$ local potentials fit the $\alpha + n$ and $\alpha + \alpha$ elastic scattering phase shifts, respectively.

However, the deep potentials contain unphysical bound states, which must be eliminated (see Sections 5.5 and 5.4.3). To exclude these states, we test two techniques: either we use supersymmetric transformations (2.80) (which convert the deep potentials into shallow potentials) or we use the projection technique (5.22) (projecting out the forbidden bound states from the wave function). When we use the projection technique, the KKNN and the BFW potentials are then denoted PKKNN and PBFW, respectively. Otherwise, when we use the supersymmetric transformations, the potentials are denoted SKKNN and SBFW, respectively.

The treatment of the Pauli forbidden states is shown in Refs. [60, 84] to be a sensitive question: the accuracy of the projection technique plays a critical role. Here, we eliminate rigorously the forbidden bound states of the deep αn and $\alpha\alpha$ potentials. Other theoretical variants, e.g. defining the Pauli forbidden states by harmonic-oscillator wave functions (like in the αn and $\alpha\alpha$ RGM), in the local models, are discussed in Refs. [20, 60, 84]. Anyway, all three-body models with deep potentials are rather unsatisfactory, because they lead to inaccurate binding energies.

We first consider the three-body model of ^{6}He. The ground state of ^{6}He is a 0^+ state with an experimental energy $E = -0.973$ MeV, with respect to the αnn threshold.

The nn potential is chosen as the Minnesota potential (5.8) (with the parameter $u = 1$). The results for the energy E and the root mean-square radius are given in Table 7.2. The radius is obtained according to equation (5.1) by assuming that the radius of the α-particle is 1.44 fm. We see that the energy disagrees with the experimental value. Indeed the shallow (SKKNN)

$V_{\alpha n}$	E	$\sqrt{\langle r^2 \rangle}$
SKKNN	-0.01	3.07
PKKNN	-0.42	2.63

Table 7.2: Ground-state energy (in MeV) and r.m.s. radius (in fm) of ^{6}He in the three-body local models, with shallow (SKKNN) or deep (PKKNN) αn potentials. The experimental energy is $E = -0.973$ MeV.

and deep (PKKNN) potentials, which fit the $\alpha + n$ phase shifts, yield poor results for ^{6}He. This fact is actually well-known [7, 27, 45]: in three-body local models of ^{6}He, if you want to reproduce the experimental ground-state energy, then you must somehow phenomenologically modify the interaction potentials.

We also consider the case of ^{9}Be described as an $\alpha\alpha n$ system, with local αn and $\alpha\alpha$ potentials. The ground state is a $3/2^-$ state with an experimental energy $E = -1.57$ MeV, with respect to the $\alpha\alpha n$ threshold. We study this ground state, but also the first $5/2^-$ excited state, which corresponds to the experimental energy $E = 0.86$ MeV.

The results for ^{9}Be are listed in Table 7.3. Here again, we see that the local models cannot reproduce the experimental energy of the three-body system. Such local $\alpha\alpha n$ models are unrealistic for ^{9}Be. For example, with the PKKNN αn and PBFW $\alpha\alpha$ potentials, the calculated $3/2^-$ state (which should be the ground state) is not bound, while the $5/2^-$ excited state is slightly bound. There is no $3/2^-$ bound state in this model, because of the exclusion of the forbidden αn and $\alpha\alpha$ states of the deep potentials [20].

We also consider the ^{12}C nucleus, described as a 3α cluster system. The results for the 0^+ ground state with the $\alpha\alpha$ potentials are given in Table 7.4. The experimental energy is $E = -7.27$ MeV. The local models strongly underestimate the binding energy. Again, the three-body local model, without modifying the $\alpha\alpha$ potentials cannot reproduce the experimental value.

Thus, in the cases of ^{6}He, ^{9}Be, and ^{12}C, we observe that in general, the simple local αn and $\alpha\alpha$ potentials, which reproduce the αn and $\alpha\alpha$ phase shifts, give incorrect results in three-body models. Typically, if one wants to use local potentials in three-body models, then one needs somehow (phenomenologically) to rectify the cluster-cluster potentials [27].

J^π	$V_{\alpha n}$	$V_{\alpha\alpha}$	E	$\sqrt{\langle r^2 \rangle}$
$\frac{3}{2}^-$	SKKNN	ABd	-2.77	2.38
	SKKNN	SBFW	-3.12	2.32
	PKKNN	PBFW	Unbound	
$\frac{5}{2}^-$	SKKNN	ABd	-0.65	2.38
	SKKNN	SBFW	-0.87	2.34
	PKKNN	PBFW	-0.19	2.35

Table 7.3: Energies (in MeV) and r.m.s radii (in fm) of ^{9}Be in the local three-body model, for different αn and $\alpha\alpha$ potentials. The experimental energies are $E = -1.57$ MeV for the $3/2^-$ ground state, and $E = 0.86$ MeV for the $5/2^-$ excited state.

$V_{\alpha\alpha}$	E	$\sqrt{\langle r^2 \rangle}$
ABd	-1.60	2.74
SBFW	-1.40	2.73
PBFW	-0.73	2.76

Table 7.4: Energy (in MeV) and r.m.s radius (in fm) of the 0^+ ground state of ^{12}C in the local 3α model, for different $\alpha\alpha$ potentials. The experimental energy is $E = -7.27$ MeV.

This motivates the development of more realistic models, such as the semi-microscopic approximations, which use the nonlocal αn and $\alpha\alpha$ RGM potentials as effective interactions.

7.4 Semi-microscopic versus microscopic models

Since the local models give poor results, we now investigate the semi-microscopic models [20–22]. These are three-body models with the nonlocal αn and $\alpha\alpha$ potentials provided by the two-cluster RGM (see Appendices C and E). It is interesting to compare such three-body models with a fully microscopic three-cluster model. Indeed, the ingredients (i.e., the nucleon-nucleon force and the α-cluster densities) of the nonlocal RGM potentials are exactly the ones of a microscopic cluster model. Therefore the semi-microscopic models may be considered as a plausible approximation of the microscopic model. The only difference between the models is the treatment of the Pauli principle (which is fully respected in the microscopic model, but which is only (partially) simulated, via the RGM potentials and the exclusion of the Pauli forbidden states, in the semi-microscopic models).

Thus, comparing the models, we shall see whether the nonlocal RGM potentials, which are valid for two-cluster systems, may be reasonably valid in three-cluster systems.

In the present chapter, we consider the semi-microscopic model that uses the energy-dependent RGM-ε potentials [20] (see Appendix C). In this model, the potentials depend explicitly on two-body energies ε_{ij}. These energies are treated as parameters of the RGM-ε potentials. Their values, for each potential, are first calculated by the (self-consistent) condition (5.27), i.e., ε_{ij} is interpreted as the mean energy of the corresponding two-body subsystem. These energy parameters, corresponding to the αn and $\alpha\alpha$ potentials, will be denoted $\varepsilon_{\alpha n}$ and $\varepsilon_{\alpha\alpha}$, respectively.

However, when the self-consistent prescription (5.27) will not give satisfactory results, we will look for other values of parameters $\varepsilon_{\alpha n}$ and $\varepsilon_{\alpha\alpha}$, which can improve the semi-microscopic approximation.

7.4.1 ^{6}He

The ^{6}He nucleus is described as an αnn system. In Table 7.5, we compare results of the microscopic and semi-microscopic models for the 0^+ ground

state, considering the same nucleon-nucleon forces (MN or V2). However, some approximations are made in order to simplify the calculations. For computing time reasons, the hyperspherical harmonic basis in the microscopic model is limited to $K_M = 18$ with $l_x \leq 4$ (like in Ref. [53]). Such a l_x restriction is not applied in the semi-microscopic model (where all the possible l_x values are considered). Moreover, the zero-range spin-orbit potential (which is added to MN and V2) is taken into account in the microscopic model and in the nonlocal αn RGM-ε potential, but is neglected in the nn interaction (between the halo neutrons) in the semi-microscopic model[1]. We have checked that these approximations play a marginal role (they may slightly modify the results but do not affect the comparison between the models).

In Table 7.5, different cases (with MN and V2 forces) are considered: in case (a), the parameter (u or m) fits the αn scattering phase shifts; and in case (b), it fits the experimental energy of ^{6}He in the microscopic model. The self-consistent values $\varepsilon_{\alpha n}$, used as a parameter in the αn RGM-ε potential, are given in the table. These energies $\varepsilon_{\alpha n}$ are calculated for $K_M = 28$ in the semi-microscopic model.

In case (a) with MN, we obtain a very weak binding energy: the microscopic model yields an energy of -0.07 MeV. Thus, here again, we see that a potential which fits the $\alpha + n$ scattering phase shifts cannot simultaneously fit the correct energy of ^{6}He in an αnn model. In the semi-microscopic model with MN, the energy is -0.08 MeV for $K_M = 28$ (and the self-consistent value $\varepsilon_{\alpha n} = 1.65$ MeV). If we apply a truncation at $K_M = 18$, then this energy becomes -0.03 MeV, in close agreement with the microscopic model. The agreement between the models, with MN, is also verified in case (b), when the nucleon-nucleon force is modified to fit the right ^{6}He energy. Thus, with MN, the semi-microscopic model yields very close results to the microscopic model. There is only about 0.05 MeV of difference in the energy between the models.

With V2, the results are different. In case (a), ^{6}He is strongly overbound with V2 (while the nucleus is hardly bound with MN). The semi-microscopic approximation turns out to be less good. The semi-microcopic model with V2 underestimates the binding energy by about 0.32 MeV. In case (b), we also see that the r.m.s. radius is unrealistically very large with V2.

[1]We have checked that this approximation in the semi-microscopic model plays a negligible role, by making tests with $\kappa = 0.01$ fm (instead of pure $\kappa = 0$ fm) in a spin-orbit potential in the nn potential.

	J^π	Potential		Microscopic		Semi-micro RGM-ε		
				E	$\sqrt{\langle r^2\rangle}$	E	$\sqrt{\langle r^2\rangle}$	$\varepsilon_{\alpha n}$
(a)	0^+	MN	$u = 0.9474$	-0.07	2.57	-0.08	3.08	1.65
		V2	$m = 0.605$	-2.43	2.46	-2.04	2.64	2.21
(b)	0^+	MN	$u = 1.0045$	-0.98	2.38	-1.03	2.55	1.50
		V2	$m = 0.6573$	-0.98	2.90	-0.66	4.14	2.37

Table 7.5: Comparison of the ^{6}He energy (in MeV), defined from the $\alpha + 2n$ threshold, and r.m.s matter radius (in fm) in the microscopic model and in the semi-microscopic model using the RGM-ε αn potential; $\varepsilon_{\alpha n}$ is the self-consistent value of the αn energy, used as a constant parameter in the RGM-ε potential. In case (a), the exchange parameter (u or m) fits the αn scattering, while in case (b), it fits the experimental ground-state energy (-0.973 MeV) of ^{6}He in the microscopic model.

7.4.2 ^{9}Be

While the semi-microscopic model seems a fair approximation of the microscopic model for ^{6}He with MN, we see an important discrepancy between the models in Table 7.6 with the results for ^{9}Be, described as an $\alpha\alpha n$ system. Here, the semi-microscopic model strongly overestimates the energy, especially with MN, where we see more than 1.2 MeV of difference with respect to microscopic results. Note that the convergence of the results with respect to K_M is given above in Table 7.1, for the examples of case (a) with MN.

Thus, for ^{9}Be, we see that such a semi-microscopic model is unfortunately a poor approximation of the microscopic model. In case (a), we also notice that the models disagree with experiment. Nevertheless, in Tables 7.1 and 7.6, the excitation energy of the $5/2^-$ state (i.e., the gap between the $3/2^-$ and $5/2^-$ states) is very close between the models, but also relatively close to the experimental value (which is $\Delta E = 2.43$ MeV [16]).

With V2 in case (a), the $5/2^-$ excited state is unbound ($E > 0$); hence in Table 7.6 we give the positive energies approximately, because the calculated energies ($E > 0$) are not converged. Note that this $5/2^-$ energy level is also positive experimentally (with respect to the $\alpha + \alpha + n$ threshold).

We now focus on the example of case (a) with MN, in order to understand the reason for the disagreement between the models in Table 7.6. The strong overbinding ($E = -3.86$ MeV) in the semi-microscopic model leads us to reconsider the values of $\varepsilon_{\alpha n}$ and $\varepsilon_{\alpha\alpha}$, i.e., the role of prescription (5.27) for the αn and $\alpha\alpha$ RGM-ε potentials [20]. According to this prescription,

	J^π	Potential		Microscopic		Semi-microscopic: RGM-ε			
				E	$\sqrt{\langle r^2\rangle}$	E	$\sqrt{\langle r^2\rangle}$	$\varepsilon_{\alpha\alpha}$	$\varepsilon_{\alpha n}$
(a)	$\frac{3}{2}^-$	MN	$u = 0.9474$	-2.61	2.36	-3.86	2.30	3.61	6.28
		V2	$m = 0.605$	-1.36	2.60	-2.19	2.56	2.91	4.64
	$\frac{5}{2}^-$	MN	$u = 0.9474$	-0.09	2.39	-1.30	2.33	5.57	6.39
		V2	$m = 0.605$	≈ 1		≈ 0.1		4.51	4.68
(b)	$\frac{3}{2}^-$	MN	$u = 0.9250$	-1.57	2.43	-2.71	2.37	3.75	6.03
		V2	$m = 0.6024$	-1.57	2.58	-2.45	2.54	2.87	4.69

Table 7.6: Comparison of ^{9}Be energies (in MeV) defined with respect to the $\alpha+\alpha+n$ threshold, and r.m.s matter radii (in fm) in the microscopic model and in the semi-microscopic model with the RGM-ε $\alpha\alpha$ and αn potentials; $\varepsilon_{\alpha\alpha}$ and $\varepsilon_{\alpha n}$ are the self-consistent values of the $\alpha\alpha$ and αn energies, respectively, used as parameters in the RGM-ε potentials. In case (a), the exchange parameter (u or m) simultaneously fits the $\alpha\alpha$ and αn scatterings, while in case (b), it fits the experimental ground-state energy (-1.57 MeV) of ^{9}Be in the microscopic model.

in the αn potential, the self-consistent value $\varepsilon_{\alpha n}$ for the ground state of ^{9}Be is $\varepsilon_{\alpha n} = 6.28$ MeV. This value is used as a constant parameter in the αn RGM-ε potential. The corresponding effective αn interaction is analysed in Figure 7.1, which shows $\alpha + n$ elastic phase shifts. The curves $\varepsilon_{\alpha n} = \varepsilon$ correspond to the exact phase shifts within the RGM. They fit the experimental phase shifts, since they are calculated with MN in case (a). The dash-dotted curves are obtained from the RGM-ε potential with the energy ε replaced by a constant parameter $\varepsilon_{\alpha n} = 6.28$ MeV in the nonlocal kernel. They show the quality of the effective αn interaction that is actually used in the three-body model with the RGM-ε potentials. Such an approximation is exact for the relative energy $\varepsilon = \varepsilon_{\alpha n}$ (and thus most accurate around this energy). Within this fixed $\varepsilon_{\alpha n}$ approximation, the s-wave phase shift is good. However, the p-wave phase shifts and especially the $p3/2$ resonance are not well reproduced with the self-consistent value of $\varepsilon_{\alpha n}$: the energy of the resonance is shifted down by about 0.8 MeV. The strong overbinding of ^{9}Be in the semi-microscopic model is most probably related to this drastic shift of the αn resonance. Rather than using prescription (5.27), it may be more efficient to use an $\varepsilon_{\alpha n}$ value which reproduces the p-wave phase shifts as well as possible, such as $\varepsilon_{\alpha n} = 1.5$ MeV (dashed lines in Figure 7.1).

The situation is more satisfactory for the $\alpha\alpha$ RGM-ε potential. Figure 7.2 presents the $l = 0$ to 4 phase shifts for the $\alpha + \alpha$ elastic scattering.

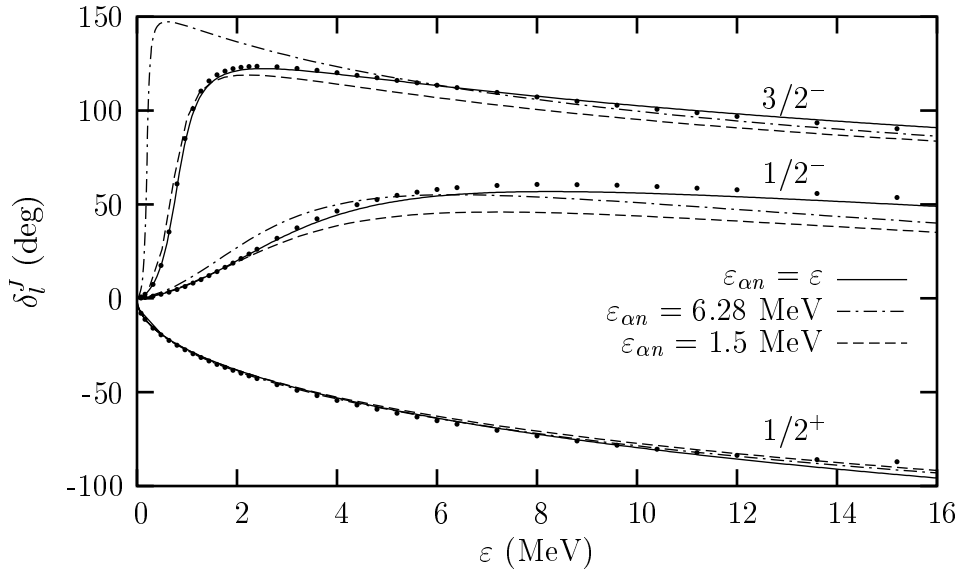

Figure 7.1: $\alpha + n$ elastic scattering phase shifts obtained with MN for $u = 0.9474$: RGM results (full lines), and results with $\varepsilon_{\alpha n}$ fixed to its self-consistent value 6.28 MeV for ^{9}Be (dash-dotted lines) and the value 1.5 MeV reproducing the $p3/2$ resonance (dashed line). Dots represent the empirical phase shifts of Ref. [85].

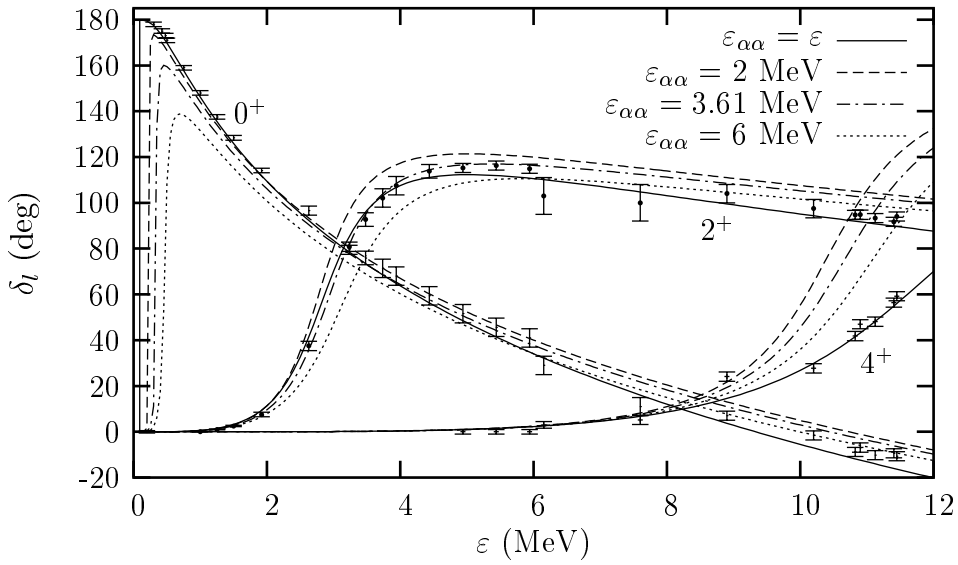

Figure 7.2: $\alpha + \alpha$ elastic scattering phase shifts obtained with MN for $u = 0.9474$: RGM results (full lines), and results with $\varepsilon_{\alpha\alpha}$ fixed to its self-consistent value 3.61 MeV for ^{9}Be (dash-dotted lines) and two other values (dashed and dotted lines). Dots represent the experimental phase shifts of Ref. [86].

The effective $\alpha\alpha$ interaction in the three-body model of ^{9}Be corresponds to $\varepsilon_{\alpha\alpha} = 3.61$ MeV. This value gives results rather close to the experimental phase shifts analysis [86], except above an energy of 9 MeV for the $l = 4$ wave. It also affects the $l = 0$ resonance which is shifted to 0.5 MeV. The agreement is quite good around the $l = 2$ resonance. Other values of $\varepsilon_{\alpha\alpha}$ such as 2 or 6 MeV do not provide better results.

Thus, using constant values for $\varepsilon_{\alpha n}$ and $\varepsilon_{\alpha\alpha}$ in the RGM-ε potentials modifies the αn and $\alpha\alpha$ interactions in terms of phase shifts. In particular, the value $\varepsilon_{\alpha n} = 6.28$ MeV does not seem physically reasonable (it alters the $p3/2$ resonance in the $\alpha+n$ phase shifts; and it gives an overbinding of ^{9}Be in the semi-microscopic model in Table 7.6). This means that the self-consistent prescription (5.27) (i.e., setting $\varepsilon_{\alpha n}$ and $\varepsilon_{\alpha\alpha}$ equal to the expectation value of the two-body energies) is rather inadequate for the case of the ^{9}Be nucleus [20].

This leads us to change the value of $\varepsilon_{\alpha n}$, i.e., now we regard $\varepsilon_{\alpha n}$ and $\varepsilon_{\alpha\alpha}$ as free parameters of the RGM-ε potentials. We therefore study the dependence of the energy E on $\varepsilon_{\alpha n}$ and $\varepsilon_{\alpha\alpha}$ in the semi-microscopic $\alpha\alpha n$

model. As shown in Figure 7.3, this dependence is essentially linear with respect to both parameters $\varepsilon_{\alpha n}$ and $\varepsilon_{\alpha\alpha}$. The curves in Figure 7.3 can be fitted by

$$E \approx -2.64 + 0.16\varepsilon_{\alpha\alpha} - 0.28\varepsilon_{\alpha n} \tag{7.1}$$

in MeV. Some $\alpha + \alpha$ and $\alpha + n$ phase shifts for various values of $\varepsilon_{\alpha\alpha}$ or $\varepsilon_{\alpha n}$ are presented in Figures 7.1 and 7.2. We suggest a new prescription for the RGM-ε potentials [20]: the idea is to take a value of $\varepsilon_{\alpha n}$ that leads to a better description of the $\alpha + n$ phase shifts, especially near the $p3/2$ resonance. For example, with $\varepsilon_{\alpha n} = 1.5$ MeV and $\varepsilon_{\alpha\alpha} = 3.61$ MeV, in case (a) with MN, the semi-microscopic model with the RGM-ε potentials then gives the energy $E = -2.48$ MeV. This really improves the semi-microscopic model: this energy $E = -2.48$ MeV (with $\varepsilon_{\alpha n} = 1.5$ MeV, $\varepsilon_{\alpha\alpha} = 3.61$ MeV) is now comparable to the microscopic result, which is $E = -2.61$ MeV (see Table 7.6 in case (a) with MN).

Of course, we can make the same test for the other cases presented in Table 7.6. Considering the $5/2^-$ excited state of ^{9}Be, in case (a) with MN, we find in the semi-microscopic model a dependence on $\varepsilon_{\alpha n}$ and $\varepsilon_{\alpha\alpha}$ which can be fitted by

$$E \approx -0.42 + 0.16\varepsilon_{\alpha\alpha} - 0.28\varepsilon_{\alpha n} \tag{7.2}$$

in MeV [20]. Comparing with equation (7.1), we see that the linear dependence is the same as for the ground state. Thus, the gap between the $5/2^-$ and $3/2^-$ levels for a given pair $(\varepsilon_{\alpha\alpha}, \varepsilon_{\alpha n})$ does not depend much on the value of this pair. This constant gap is about 2.22 MeV – i.e., somewhat smaller than in the microscopic model (see Table 7.1). (Notice that this gap is better in Tables 7.1 and 7.6 because the parameters $\varepsilon_{\alpha\alpha}$ and $\varepsilon_{\alpha n}$ are different for each state.)

Let us see the other cases in Table 7.6. Figure 7.4 shows the $\alpha + n$ and $\alpha+\alpha$ elastic phase shifts calculated using the potentials of Table 7.6 (case (b) with MN, and cases (a), (b) with V2). The full curves represent the phase shifts given by an exact RGM calculation. The dotted curves are obtained from the actual RGM-ε potentials with the energy ε replaced by a constant parameter (i.e., $\varepsilon_{\alpha n}$ and $\varepsilon_{\alpha\alpha}$ given in Table 7.6) in the nonlocal kernel. The RGM phase shifts (full curves) correspond to the microscopic model; they are nothing but the direct result of the nucleon-nucleon potentials. The dotted curves correspond to the αn and $\alpha\alpha$ potentials (with the prescription (5.27)) used in the semi-microscopic model of ^{9}Be.

We can make the same observations as before: the semi-microscopic model yields phase shifts which are different from those of the original RGM

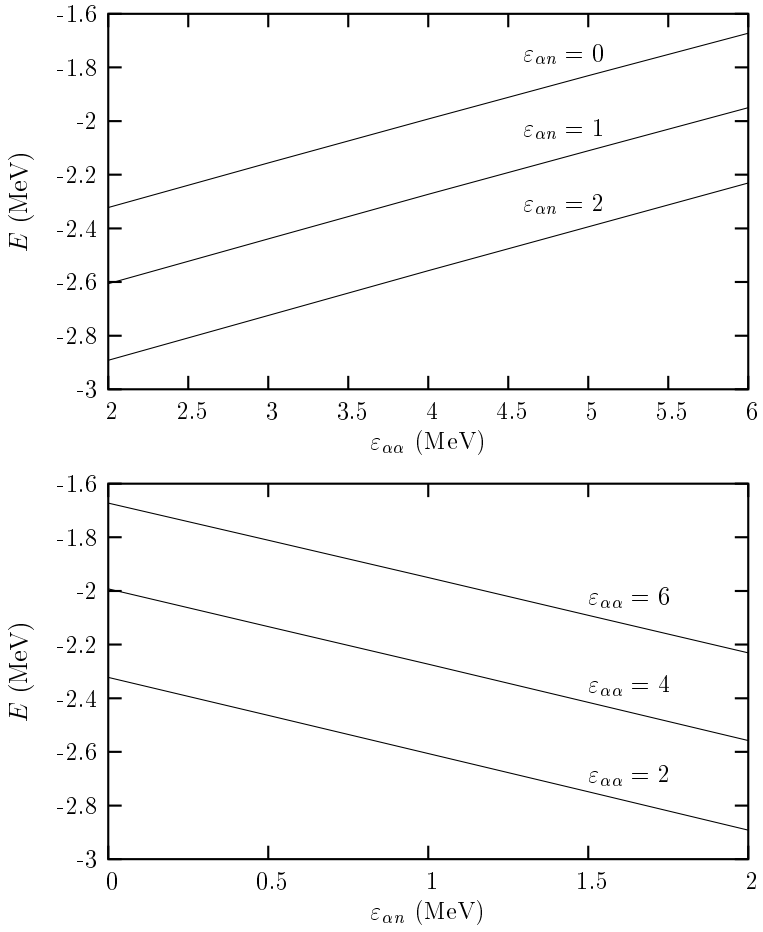

Figure 7.3: Dependence on $\varepsilon_{\alpha\alpha}$ and $\varepsilon_{\alpha n}$ of the ground-state energy of ^{9}Be in the semi-microscopic model with the RGM-ε potentials (in case (a) with MN).

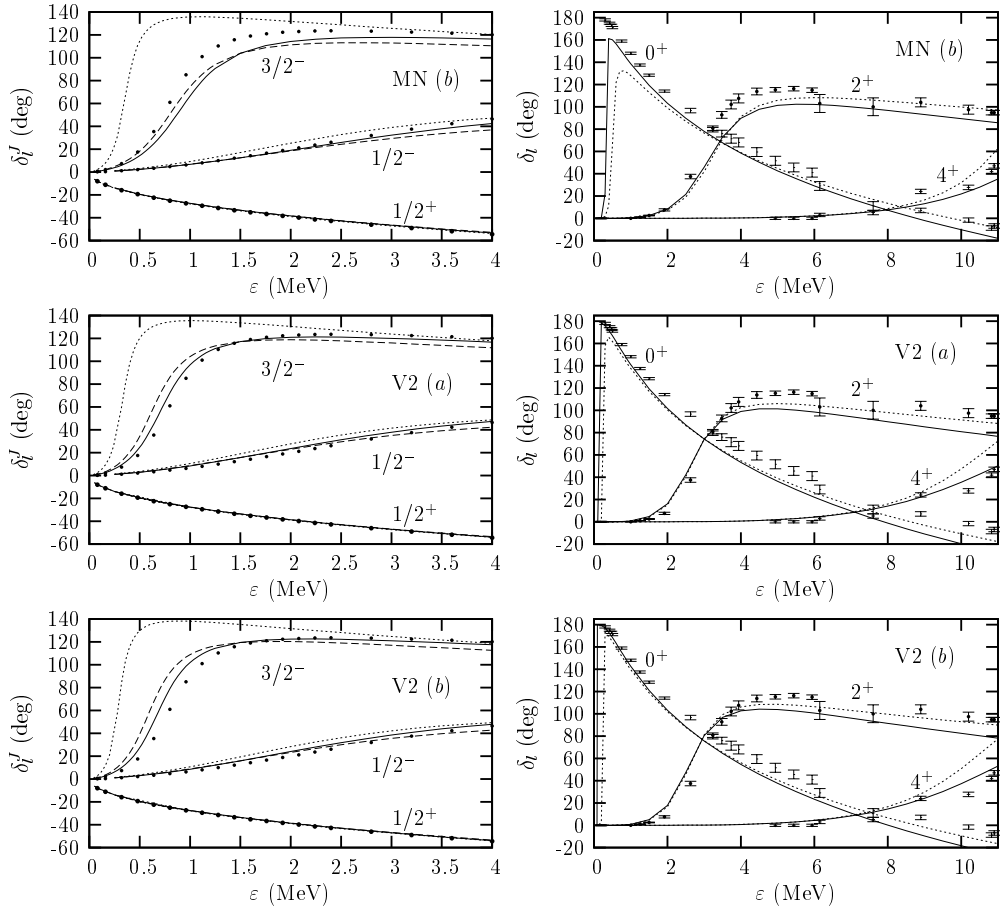

Figure 7.4: $\alpha + n$ (left) and $\alpha + \alpha$ (right) scattering phase shifts calculated for MN (case (b)) and V2 (cases (a) and (b)) of Table 7.6: exact RGM results (full lines), and semi-microscopic results obtained for the fixed values of $\varepsilon_{\alpha n}$ and $\varepsilon_{\alpha\alpha}$ given in Table 7.6 for ^{9}Be, used as constant parameters in the nonlocal RGM-ε potentials (dotted lines) – these parameters ($\varepsilon_{\alpha n}$, $\varepsilon_{\alpha\alpha}$) being those for the ground state of ^{9}Be. Also shown are the $\alpha + n$ phase shifts for $\varepsilon_{\alpha n} = 1.5$ MeV (dashed line) as constant parameter, in order to have a more reasonable description of the $p3/2$ resonance in the semi-microscopic model. Dots represent the experimental phase shifts of Refs. [85, 86].

	J^π	Potential		Microscopic		Semi-microscopic: RGM-ε			
				E	$\sqrt{\langle r^2\rangle}$	E	$\sqrt{\langle r^2\rangle}$	$\varepsilon_{\alpha\alpha}$	$\varepsilon_{\alpha n}$
(a)	$\frac{3}{2}^-$	MN	$u = 0.9474$	-2.61	2.36	-2.48	2.34	3.6	1.5
		V2	$m = 0.605$	-1.36	2.60	-1.33	2.62	3.6	1.5
(b)	$\frac{3}{2}^-$	MN	$u = 0.9250$	-1.57	2.43	-1.47	2.42	3.6	1.5
		V2	$m = 0.6024$	-1.57	2.58	-1.56	2.60	3.6	1.5

Table 7.7: Comparison of the ground-state ^{9}Be energy (in MeV) and r.m.s matter radius (in fm) in the microscopic model and in the semi-microscopic model with the RGM-ε $\alpha\alpha$ and αn potentials for $\varepsilon_{\alpha\alpha} = 3.6$ MeV and $\varepsilon_{\alpha n} = 1.5$ MeV.

(microscopic model). In particular, in the $\alpha + n$ phase shifts, the $p3/2$ resonance is not well reproduced with the semi-microscopic (RGM-ε with constant $\varepsilon_{\alpha n}$) potentials: it is drastically shifted down. Thus, the self-consistent prescription (5.27) seems physically inadequate for the ^{9}Be case: it significantly alters the $\alpha+n$ phase shifts. Nevertheless, the $\alpha+\alpha$ semi-microscopic phase shifts are reasonable. Notice in Figure 7.4 that there may be a slight discrepancy in case (b) between the RGM phase shifts (full curves) and the experimental data [85, 86] (compare with Figure 7.1, showing case (a) for $\alpha + n$ with MN), because in case (b), the nucleon-nucleon force is modified in order to get the right energy in the microscopic model of ^{9}Be. This shows how modifying the potentials may affect the phase shifts.

Because the prescription (5.27) is inadequate for ^{9}Be, we now test our new prescription, i.e., we drop this condition (5.27) and instead, we choose two constant values of $\varepsilon_{\alpha n}$ and $\varepsilon_{\alpha\alpha}$, which yield phase shifts in better agreement with the microscopic RGM phase shifts. For example, we set $\varepsilon_{\alpha\alpha} = 3.6$ MeV and $\varepsilon_{\alpha n} = 1.5$ MeV. As seen in Figures 7.4 and 7.1, the value $\varepsilon_{\alpha n} = 1.5$ MeV (dashed line) yields reasonable αn phase shifts, especially near the $p3/2$ resonance. Table 7.7 presents the results of the semi-microscopic model of ^{9}Be for these arbitrary values of $\varepsilon_{\alpha n}$ and $\varepsilon_{\alpha\alpha}$. We see that this new prescription significantly improves the semi-microscopic model. Now, in contrast with the previous results of Table 7.6, the semi-microscopic model becomes a nice approximation of the microscopic model. Indeed, in Table 7.7, in case (b) there is only some 0.01 MeV or 0.1 MeV of difference, for V2 and MN respectively, between the semi-microcopic and microscopic models of ^{9}Be. Thus, now the semi-microcopic and microscopic models essentially agree.

	J^π	Potential		Microscopic		Semi-micro RGM-ε		
				E	$\sqrt{\langle r^2\rangle}$	E	$\sqrt{\langle r^2\rangle}$	$\varepsilon_{\alpha\alpha}$
(a)	0_1^+	MN	$u = 0.94687$	-11.61	2.18	-9.78	2.04	13.60
		V2	$m = 0.605$	-4.53	2.50	-3.19	2.33	9.03
	2^+	MN	$u = 0.94687$	-9.22	2.16	-7.49	2.03	14.61
		V2	$m = 0.605$	-1.88	2.46	-0.55	2.30	10.62
	0_2^+	MN	$u = 0.94687$	0.7		≈ 0.5		5.34
		V2	$m = 0.605$	1.6		≈ 0.8		3.01
(b)	0_1^+	MN	$u = 0.9122$	-7.27	2.25	-5.49	2.09	13.62
		V2	$m = 0.5929$	-7.27	2.41	-5.68	2.25	9.53

Table 7.8: Comparison of ^{12}C energies (in MeV) defined with respect to the 3α threshold, and r.m.s matter radii (in fm) in the microscopic model and in the semi-microscopic model with the RGM-ε $\alpha\alpha$ potential; $\varepsilon_{\alpha\alpha}$ is the self-consistent value of the $\alpha\alpha$ energy, used as a parameter in the RGM-ε potential. In case (a), the exchange parameter (u or m) fits the $\alpha\alpha$ scattering, while in case (b), it fits the experimental ground-state energy (-7.27 MeV) of ^{12}C in the microscopic model.

7.4.3 ^{12}C

We now consider the case of ^{12}C, described as a 3α cluster system[2]. The results comparing the semi-microscopic model (with the RGM-ε $\alpha\alpha$ potential using the prescription (5.27) for $\varepsilon_{\alpha\alpha}$) with the fully microscopic model are given in Table 7.8. Here again, we see a discrepancy between the models.

However, we have learned from the ^{9}Be case that a departure from the self-consistent prescription (5.27) may improve the semi-microscopic approximation, with respect to the microscopic results. Thus let us check the dependence of the 3α energy E on $\varepsilon_{\alpha\alpha}$, when $\varepsilon_{\alpha\alpha}$ is considered as a free parameter of the RGM-ε $\alpha\alpha$ potential. This dependence is shown on Figure 7.5, for the 0_1^+ ground state. Here, unfortunately, the value $\varepsilon_{\alpha\alpha} = 3.6$ MeV (which seems reasonable for ^{9}Be, as seen in Table 7.7) is unsatisfactory: it would lead us to energies E which are quite unrealistic, in disagreement with the microscopic model.

[2]Note that calculations of the 3α model with the RGM-ε $\alpha\alpha$ potential are available in Ref. [17] (for slightly different parameters) but they are performed in a Faddeev formalism, considering only the self-consistent value for $\varepsilon_{\alpha\alpha}$. Of course, we have tested that we can reproduce the results of Ref. [17] with our hyperspherical formalism [20]. Here we will revisit this case, with our own parameters in order to explore the validity of the model with the self-consistent value $\varepsilon_{\alpha\alpha}$.

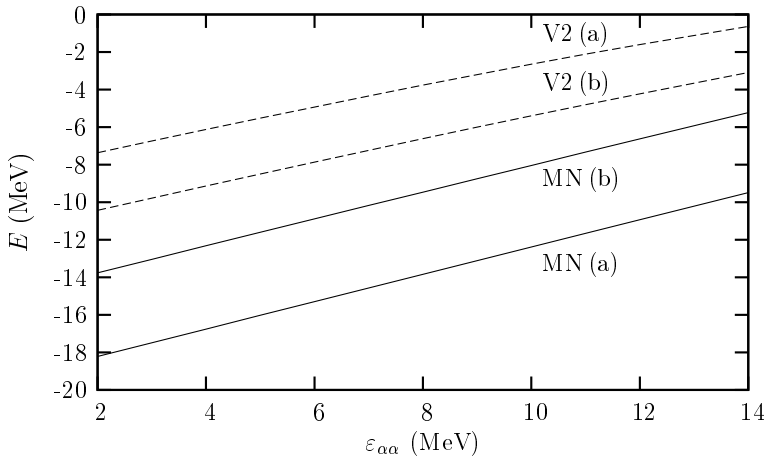

Figure 7.5: Dependence on $\varepsilon_{\alpha\alpha}$ of the 0^+ ground-state energy of ^{12}C in the semi-microscopic 3α model with the RGM-ε $\alpha\alpha$ potentials, for the various (MN or V2) forces of Table 7.8.

Let us also look at the $\alpha+\alpha$ phase shifts, in order to analyse the quality of the potentials of Table 7.8. The phase shifts (for the potentials used for ^{12}C, in the 0_1^+ state) are represented in Figure 7.6. We see that the prescription (5.27) for $\varepsilon_{\alpha\alpha}$ (in the RGM-ε $\alpha\alpha$ potential) here gives $\alpha + \alpha$ phase shifts which are quite different (especially with MN) from those obtained with the exact microscopic RGM calculation.

According to Figure 7.5, if we want to get semi-microscopic results closer to the microscopic results by taking an arbitrary $\varepsilon_{\alpha\alpha}$ value, then we must set for example, $\varepsilon_{\alpha\alpha} = 11$ MeV for MN and $\varepsilon_{\alpha\alpha} = 7$ MeV for V2. This yields the energies presented in Table 7.9 (where the semi-microscopic energies essentially agree with the microscopic energies for the 0_1^+ state). However, the corresponding $\alpha + \alpha$ scattering phase shifts, shown in Figure 7.7, are similar to those given by the self-consistent $\varepsilon_{\alpha\alpha}$. Therefore they are still in disagreement with the original (microscopic) RGM phase shifts (full lines), especially in MN cases. Nevertheless, with $V2$ the results seem more satisfactory: the semi-microscopic model then gives $\alpha + \alpha$ phase shifts (dashed lines) which are rather close to the microscopic RGM data (full lines), and also rather close to the experimental data.

From all these examples, we can now draw some conclusions about the semi-microscopic approximation (which uses the RGM-ε potentials) and its practical validity.

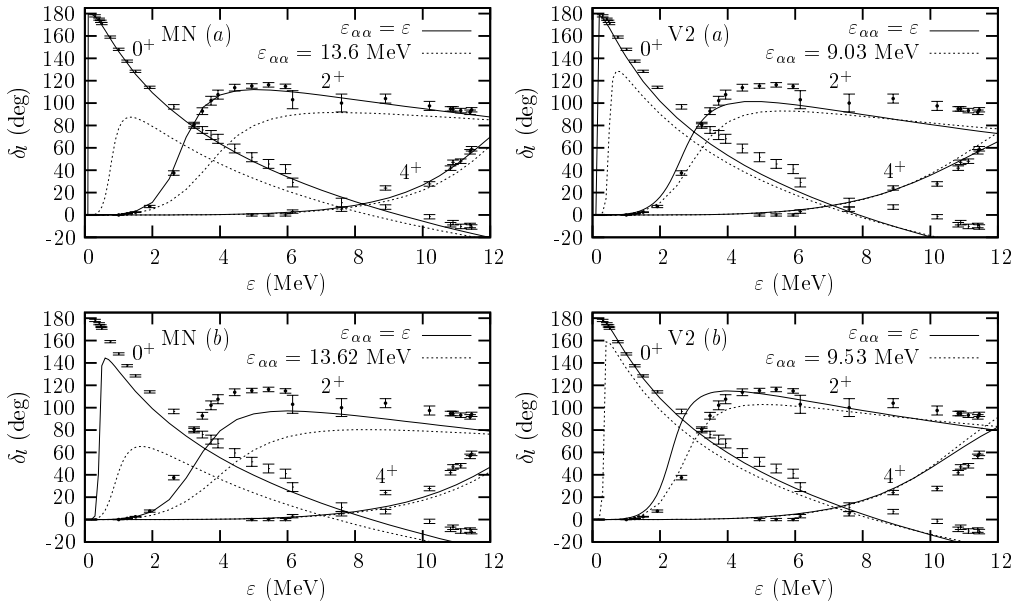

Figure 7.6: $\alpha + \alpha$ scattering phase shifts calculated for MN (right) and V2 (left), for the cases (a) and (b) given in Table 7.8: exact RGM results (full lines) and results with self-consistent values of $\varepsilon_{\alpha\alpha}$ (dotted lines) for ^{12}C, used as constant parameters in the nonlocal RGM-ε $\alpha\alpha$ potentials. Dots represent the empirical phase shifts of Ref.[86].

	J^π	Potential		Microscopic		Semi-micro RGM-ε		
				E	$\sqrt{\langle r^2 \rangle}$	E	$\sqrt{\langle r^2 \rangle}$	$\varepsilon_{\alpha\alpha}$
(a)	0_1^+	MN	$u = 0.94687$	-11.61	2.18	-11.66	2.03	11
		V2	$m = 0.605$	-4.53	2.50	-4.34	2.28	7
	2^+	MN	$u = 0.94687$	-9.22	2.16	-10.12	2.03	11
		V2	$m = 0.605$	-1.88	2.46	-2.69	2.23	7
(b)	0_1^+	MN	$u = 0.9122$	-7.27	2.25	-7.33	2.07	11
		V2	$m = 0.5929$	-7.27	2.41	-7.24	2.21	7

Table 7.9: Comparison of ^{12}C energies (in MeV) and r.m.s radii (in fm) in the microscopic model and in the semi-microscopic model with arbitrary values of $\varepsilon_{\alpha\alpha}$, as a constant parameter in the RGM-ε $\alpha\alpha$ potential.

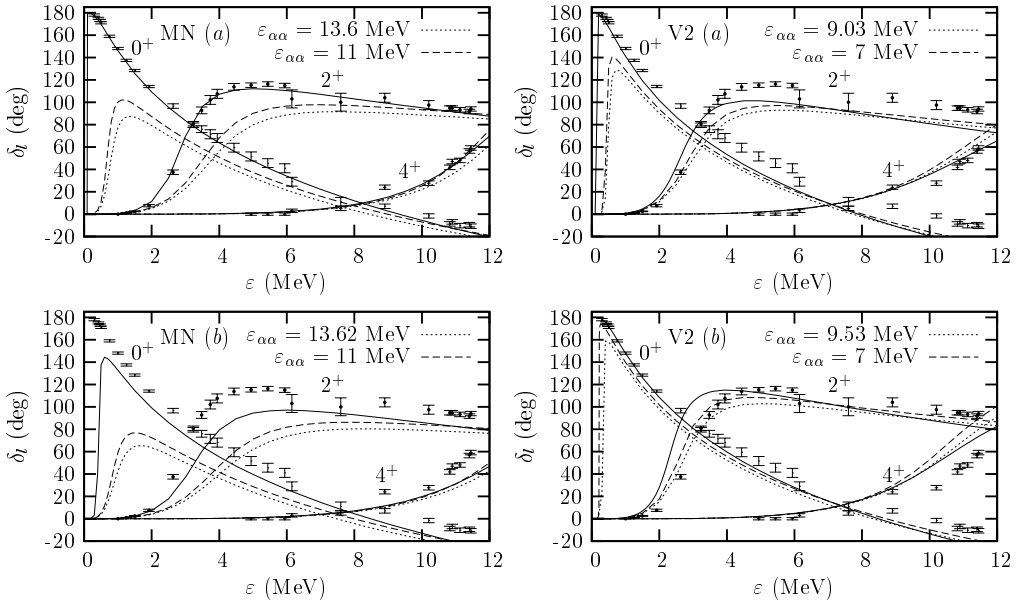

Figure 7.7: $\alpha + \alpha$ phase shifts for some arbitrary values of $\varepsilon_{\alpha\alpha}$ (dotted and dashed lines) as constant parameter in the RGM-ε $\alpha\alpha$ potential, in various cases (corresponding to Tables 7.8 and 7.9) used for the 3α model. The full lines are given by the exact (fully microscopic) RGM calculation.

7.5 Conclusions

As a preliminary remark, we can confirm the following well-known observation. In general, in the models (in cases (a) and also in the local models), the potentials that fit the two-cluster ($\alpha + n$ and $\alpha + \alpha$) elastic scattering phase shifts fail to reproduce the right energies in three-cluster systems (αnn, $\alpha\alpha n$ and 3α). Therefore, in the microscopic model (cases (b)), to obtain the three-cluster energies in agreement with experiment, one must change a tuning parameter of the effective nucleon-nucleon forces (and thus modify the original $\alpha + n$ and $\alpha + \alpha$ phase shifts).

Because the local models are unsatisfactory, and because the fully microscopic models require heavy calculations, the semi-microscopic model seems especially interesting: it is a simple three-body model (i.e., assuming point-like clusters) where the effective cluster-cluster potentials are represented by the non-local RGM-ε potentials.

However, the RGM-ε potentials are *energy-dependent*. This is a real drawback of the model, because the values of the energies (i.e., $\varepsilon_{\alpha\alpha}$ or $\varepsilon_{\alpha n}$) to be used in the potentials are not well defined in a three-body model. However, a plausible prescription for these $\varepsilon_{\alpha\alpha}$ or $\varepsilon_{\alpha n}$ parameters is proposed by Ref. [17]: these energies are taken as their mean values (calculated from the two-body Hamiltonian) given by the three-body wave function. This self-consistent prescription seems to be reasonable in some given examples, such as the ^{6}He nucleus (and also the hypernuclei, as seen in Chapter 6 and in Ref.[17]).

But this prescription becomes problematic when applied to the ^{9}Be case [20]. It yields three-body energies in disagreement with the microscopic model (and thus with experiment). It is also problematic when we look at the $\alpha + n$ and $\alpha + \alpha$ scattering phase shifts. Indeed, the semi-microscopic model, by using constant $\varepsilon_{\alpha n}$ and $\varepsilon_{\alpha\alpha}$ values in the RGM-ε potentials, inevitably modifies the $\alpha + n$ and $\alpha + \alpha$ phase shifts. (This modification is drastic for the $\alpha + n$ and $\alpha + \alpha$ phase shifts, in the examples of ^{9}Be and ^{12}C, respectively).

This naturally leads us to drop this prescription. So $\varepsilon_{\alpha n}$ and $\varepsilon_{\alpha\alpha}$ become free parameters of the model [20]. Choosing their values is not easy. However, in the case of ^{9}Be, we have found some $(\varepsilon_{\alpha n}, \varepsilon_{\alpha\alpha})$ values that judiciously give a fair agreement between the semi-microscopic and microscopic models, for the three-body ($\alpha\alpha n$) energy and the ($\alpha + n$ and $\alpha + \alpha$) phase shifts simultaneously. But unfortunately, in the case of ^{12}C, it is not easy (and not possible with MN) to find such an $\varepsilon_{\alpha\alpha}$ value able to reconcile the models for both three-body (3α) energies and ($\alpha + \alpha$) phase shifts simultaneously. From this, we may conclude that there is no obvious criteria for $\varepsilon_{\alpha\alpha}$ and $\varepsilon_{\alpha n}$. The

values of $\varepsilon_{\alpha\alpha}$ and $\varepsilon_{\alpha n}$ become quite arbitrary parameters. This is clearly a drawback of the semi-microscopic model.

This strongly encourages us to use other cluster-cluster potentials in three-body models. In particular, this leads us to develop and investigate the semi-microscopic approximation that uses the *energy-independent* RGM-$\not{\varepsilon}$ potentials, which will be discussed in the next chapter.

Chapter 8

Three-body models of ^{6}He, ^{9}Be and ^{12}C using the energy-independent RGM potentials

8.1 Energy-independent potentials

In this chapter, we investigate the semi-microscopic model using the energy-independent RGM-$\not\varepsilon$ cluster-cluster potentials [22, 23]. The nonlocal RGM-$\not\varepsilon$ $\alpha\alpha$ and αn potentials have the following advantages: they take into account the Pauli principle, they give exactly the same $\alpha + \alpha$ and $\alpha + n$ phase shifts as the original RGM, and they are energy-independent. In other words, these potentials seem to be more appropriate for a semi-microscopic model than the RGM-ε potentials, in the sense that they will not create the problems of the energy dependence, met in the previous chapter.

That three-body models should be developed with these nonlocal RGM-$\not\varepsilon$ potentials has been suggested several times [2, 36] but it has never been thoroughly investigated in view of the technical difficulties involved. Indeed, not only the complicated RGM-$\not\varepsilon$ potentials must be evaluated but their use requires simultaneously mastering accurate calculations of three-body models with nonlocal potentials and of the microscopic three-cluster model for comparison. This know-how has been successfully developed in the present work [21, 22].

We compare this semi-microscopic model with the corresponding microscopic model. To this end, we apply the three-body models to the ^{6}He, ^{9}Be and ^{12}C nuclei, with the same parameter as in the previous chapter. In

Section 8.2, we briefly summarise the models, and then discuss the results. Conclusions are given in Section 8.3.

8.2 Semi-microscopic versus microscopic models

The models are applied to ^{6}He, ^{9}Be and ^{12}C (described as αnn, $\alpha\alpha n$ and 3α systems, respectively) [21]. We consider the same calculations as in the previous chapter, but using the nonlocal RGM-$\not\varepsilon$ $\alpha\alpha$ and αn potentials instead of the RGM-ε potentials in the semi-microscopic model. We therefore take the same parameters as previously (see Section 7.2).

The nonlocal RGM-$\not\varepsilon$ $\alpha\alpha$ and αn potentials are calculated from the energy-dependent RGM-ε potentials (see Appendices C and E). The semi-microscopic model, in the present chapter, using the RGM-$\not\varepsilon$ potentials, does not contain any free parameter: it just needs the same parameters as the microscopic model (i.e., MN or V2, and b the oscillator parameter for the α clusters). In particular, it does not need any $\varepsilon_{\alpha\alpha}$, or $\varepsilon_{\alpha n}$, parameter, since the RGM-$\not\varepsilon$ potentials (unlike the RGM-ε variant) are energy-independent.

Also, the RGM-$\not\varepsilon$ $\alpha\alpha$ and αn potentials reproduce exactly the same $\alpha+\alpha$ and $\alpha+n$ phase shifts as in the original (two-cluster) RGM. This means in particular that here both semi-microscopic and microscopic models provide strictly the same phase shifts.

The models only differs in the treatment of the Pauli principle. The semi-microscopic model approximate the Pauli principle, via the nonlocal RGM-$\not\varepsilon$ cluster-cluster potentials and the exclusion of the Pauli forbidden states in each two-cluster subsystem. Hence we may consider that the two-cluster aspects of the Pauli antisymmetrisation are essentially simulated in the semi-microscopic model. (That is indeed the two-cluster Pauli antisymmetrisation that is responsible for the nonlocality of the RGM-$\not\varepsilon$ inter-cluster potential.) Thus, the only effects that are missing in the semi-microscopic approximation should be the purely three-body antisymmetrisation effects, which involve all three clusters simultaneously. Therefore, comparing this approximation with the fully microscopic model, we can determine whether or not these effects are significant.

We compare the models via the binding energies and the r.m.s radii of the nuclei. We also consider the monopole neutron or proton densities (see Appendix F), calculated from the wave functions, in order to compare the

	J^π	Potential		Microscopic		Semi-microscopic	
				E	$\sqrt{\langle r^2\rangle}$	E	$\sqrt{\langle r^2\rangle}$
(a)	0^+	MN	$u = 0.9474$	-0.07	2.57	-0.08	2.93
		V2	$m = 0.605$	-2.43	2.46	-1.96	2.56
(b)	0^+	MN	$u = 1.0045$	-0.98	2.38	-0.95	2.46
		V2	$m = 0.6573$	-0.98	2.90	-0.65	4.11
(c)	0^+	MN	$u = 1.0055$	-1.02	2.37	-0.97	2.46
		V2	$m = 0.640$	-1.43	2.74	-0.98	3.23

Table 8.1: Comparison of the ^{6}He energy (in MeV), defined from the $\alpha + 2n$ threshold, and r.m.s matter radii (in fm) in the microscopic model and in the semi-microscopic model using the RGM-$\not\varepsilon$ αn potential. In case (a), the parameter (u or m) fits the αn scattering, while in cases (b)/(c), it fits the experimental ground-state energy (-0.973 MeV) of ^{6}He in the microscopic/semi-microscopic models.

models. These densities, denoted by $\rho(r)$, are normalised as

$$\int_0^\infty \rho(r) r^2 dr = \frac{Z}{\sqrt{4\pi}}, \tag{8.1}$$

for a proton density, or similarly

$$\int_0^\infty \rho(r) r^2 dr = \frac{N}{\sqrt{4\pi}}, \tag{8.2}$$

for a neutron density, where Z and N are the proton and neutron numbers, respectively (e.g., $N = 4$ for ^{6}He, $N = 5$ for ^{9}Be and $Z = 6$ for ^{12}C).

8.2.1 ^{6}He

The results of the models for ^{6}He are presented in Table 8.1 [21]. The energies given by the RGM-$\not\varepsilon$ αn potential turn out to be similar to those given by the RGM-ε potential (see Table 7.5, previous chapter). Nevertheless, of course, here (with the RGM-$\not\varepsilon$ potential) the semi-microscopic and microscopic models have rigorously the same parameters (whereas with the RGM-ε potential, there were an extra $\varepsilon_{\alpha n}$ parameter).

In case (a), with MN and V2 fitting the $\alpha + n$ phase shifts, the αnn model does not reproduce the right energy of ^{6}He. This must be due to the fact

that MN and V2 are simplified effective nucleon-nucleon potentials [1]. Hence the u or m parameter of these potentials is modified in cases (b) and (c), in order to reproduce the ^{6}He energy, in the microcopic and semi-microscopic models, respectively. Of course, with these modifications, MN and V2 do not fit the $\alpha + n$ phase shifts.

There is a very nice agreement between the models with MN, i.e., the semi-microscopic and microscopic models provide virtually the same binding energy with MN. This agreement is not confirmed with V2, where there is a discrepancy between the models. The discrepancy clearly depends on the nucleon-nucleon force (e.g., with V2, there is about 0.33 MeV in case (b) between the semi-microscopic and microscopic calculations). Notice that the semi-microscopic model provides smaller binding energies than the microscopic approach, hence the three-body antisymmetrisation effects, which are missing in the semi-microscopic model, should be attractive (but these effects seem to be negligible with MN). The semi-microscopic model also provides larger matter radii. With V2, it gives an unrealistic (very large) radius for ^{6}He.

In Figure 8.1, the neutron densities of ^{6}He are shown. They are calculated for the models when the experimental binding energy of ^{6}He is reproduced (case (b) for the microscopic model, and case (c) for the semi-microscopic model). With MN, the neutron densities of the microscopic and semi-microscopic models are close to each other. This confirms that the semi-microscopic approximation is better with MN for ^{6}He. Also, in the microscopic model, V2 and MN give a similar density. This is different with V2 in the semi-microscopic model: since the density is lower at short distance, the neutron radius must be larger. This is consistent with the extremely large radius with V2.

8.2.2 ^{9}Be

The results for ^{9}Be (in the $\alpha\alpha n$ model) are displayed in Table 8.2 [21]. First, notice the progress in comparison with the previous results of Table 7.6: here, the semi-microscopic model yields comparable energies to the microscopic model. This is clearly due to the quality of the potentials: the nonlocal RGM-$\not{\epsilon}$ potentials, which are energy-independent, give exactly the same α+α and α+n phase shifts as in the original RGM (microscopic model).

[1] However, inasmuch as ^{6}He is hardly bound with MN, and strongly overbound with V2, most probably, it would be possible, in principle, to find somehow another new effective nucleon-nucleon potential fitting simultaneously the right ^{6}He energy (which is between the MN and V2 results) and the $\alpha + n$ phase shifts (in case (a)).

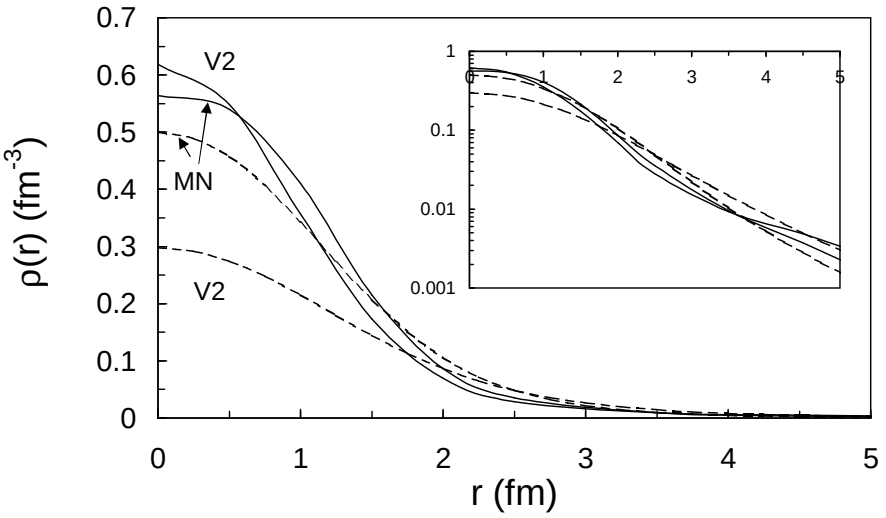

Figure 8.1: Neutron densities of ^{6}He with the MN and V2 potentials in the microscopic (solid lines) and semi-microscopic (dashed lines) models. The insert represents these densities in logarithmic scale.

	J^π	Potential		Microscopic E	Microscopic $\sqrt{\langle r^2\rangle}$	Semi-microscopic E	Semi-microscopic $\sqrt{\langle r^2\rangle}$
(a)	$\frac{3}{2}^-$	MN	$u = 0.9474$	-2.61	2.36	-2.16	2.41
		V2	$m = 0.605$	-1.36	2.60	-1.12	2.68
	$\frac{5}{2}^-$	MN	$u = 0.9474$	-0.09	2.39	≈ 0.2	
		V2	$m = 0.605$	≈ 1		≈ 1	
(b)	$\frac{3}{2}^-$	MN	$u = 0.9250$	-1.57	2.43	-1.18	2.49
		V2	$m = 0.6024$	-1.57	2.58	-1.32	2.66
(c)	$\frac{3}{2}^-$	MN	$u = 0.9340$	-1.97	2.40	-1.57	2.46
		V2	$m = 0.5997$	-1.81	2.56	-1.57	2.63

Table 8.2: Comparison of ^{9}Be energies (in MeV), defined with respect to the $\alpha+\alpha+n$ threshold, and r.m.s matter radii (in fm) in the microscopic model and in the semi-microscopic model with the RGM-$\not\in$ $\alpha\alpha$ and αn potentials. In case (a), the parameter (u or m) fits the $\alpha\alpha$ and αn scatterings, while in case (b)/(c), it fits the experimental ground-state energy (-1.57 MeV) of ^{9}Be in the microscopic/semi-microscopic models.

However, in Table 8.2, there is a discrepancy between the semi-microscopic and microscopic models.

The semi-microscopic model gives smaller binding energies than the microscopic model (with about 0.40 MeV for MN and 0.25 MeV for V2, between the models). This again means that the three-body antisymmetrisation effects, missing in the semi-microscopic approach, are probably attractive.

In case (a), with MN and V2 fitting the $\alpha+\alpha$ and $\alpha+n$ phase shifts, the models do not give the right binding energy for ^{9}Be (in the microscopic model, the nucleus is overbound by about 1 MeV with MN, while it is underbound by about 0.2 MeV with V2). The $5/2^-$ first excited state is also calculated, and when this gives a positive energy, such an energy (representing an unbound system) is only approximate. The excitation energy, i.e., the gap between $5/2^-$ and $3/2^-$ states, is in rather close agreement with experiment. The experimental value of the excitation energy is 2.43 MeV [16].

When the potentials are fitted to the experimental energy of ^{9}Be, the radii become close to each other. The corresponding neutron densities are shown in Figure 8.2, when the models reproduce the experimental ground-state energy (in case (b) for the microscopic model, and in case (c) for semi-microscopic model). Below 2 fm, the semi-microscopic model provides a rather uniform density, while the microscopic density is more peaked near the origin. This shows a qualitative difference between the models.

8.2.3 ^{12}C

We also consider the case of ^{12}C described as a 3α system. The results are given in Table 8.3 [21]. They confirm what has been said about the models for ^{6}He and ^{9}Be. The binding energies are smaller in the semi-microsocopic calculation (by, e.g., about 2.4 MeV with MN and 2.5 MeV with V2, in case (b)). Hence, in the treatment of the Pauli principle, the three-body (antisymmetrisation) effects, which are missing in the semi-microscopic model, are attractive.

In case (a), the experimental energies of ^{12}C are not reproduced: the system is overbound with MN, and underbound with V2. This is because MN and V2 are approximate nucleon-nucleon forces[2]. Also, the excitation energy of the 2^+ state does not agree with experiment (but is rather comparable between the models).

In cases (b) and (c), both models provide quite similar radii. In Figure 8.3, the proton density of ^{12}C (in its ground state) is shown, for the mod-

[2]Inasmuch as MN underbinds and V2 overbinds, in principle, it would seem possible to find an effective potential giving both the right energy of ^{12}C and the $\alpha+\alpha$ phase shifts.

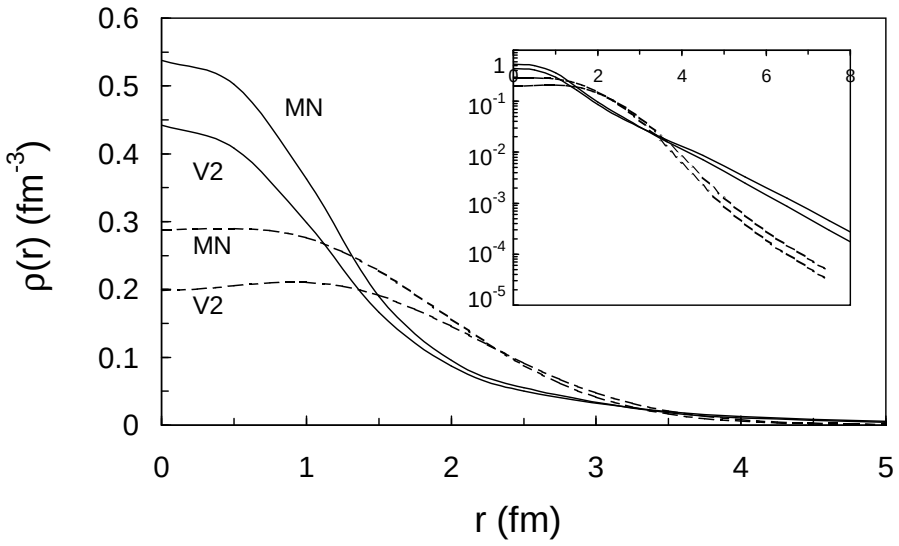

Figure 8.2: Neutron densities of ^{9}Be with the MN and V2 potentials in the microscopic (solid lines) and semi-microscopic (dashed lines) models. The insert represents these densities in logarithmic scale.

	J^π	Potential		Microscopic		Semi-microscopic	
				E	$\sqrt{\langle r^2\rangle}$	E	$\sqrt{\langle r^2\rangle}$
(a)	0_1^+	MN	$u = 0.94687$	-11.61	2.18	-9.42	2.17
		V2	$m = 0.605$	-4.53	2.50	-2.33	2.68
	2^+	MN	$u = 0.94687$	-9.22	2.16	-7.12	2.15
		V2	$m = 0.605$	-1.88	2.46	≈ 0.38	
	0_2^+	MN	$u = 0.94687$	≈ 0.7		≈ 0.5	
		V2	$m = 0.605$	≈ 1.6		≈ 1.2	
(b)	0_1^+	MN	$u = 0.9122$	-7.27	2.25	-4.90	2.27
		V2	$m = 0.5929$	-7.27	2.41	-4.73	2.52
(c)	0_1^+	MN	$u = 0.93105$	-9.57	2.21	-7.27	2.21
		V2	$m = 0.582$	-9.99	2.35	-7.27	2.42

Table 8.3: Comparison of ^{12}C energies (in MeV), with respect to the 3α threshold, and r.m.s matter radii (in fm) in the microscopic model and in the semi-microscopic model with the RGM-$\not\in$ $\alpha\alpha$ potential. Experimental energies are -7.27, -2.83 and 0.38 MeV for the 0_1^+, 2^+ and 0_2^+ states, respectively. In case (a), the parameter (u or m) fits the $\alpha\alpha$ scattering; in case (b)/(c), it fits the experimental ground-state energy of ^{12}C in the microscopic/semi-microscopic models.

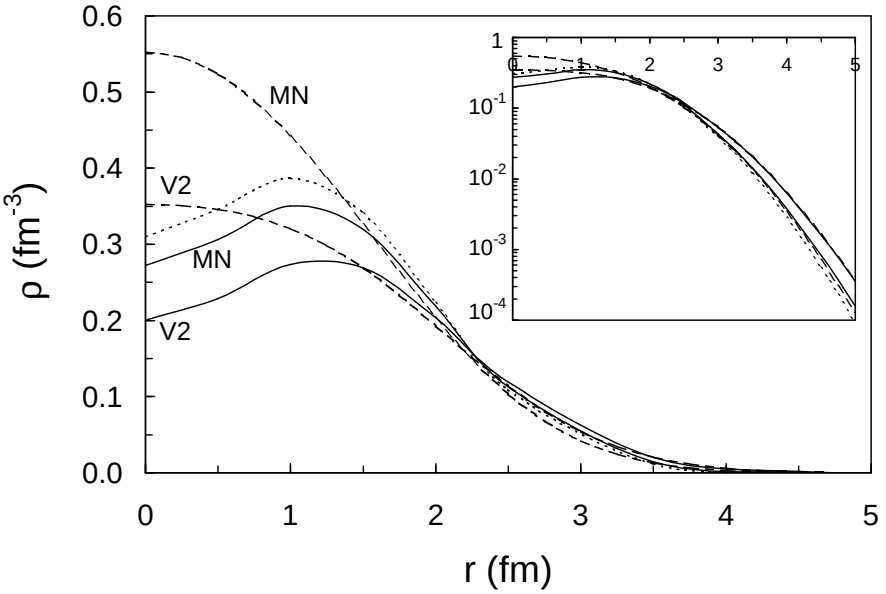

Figure 8.3: Neutron densities of ^{12}C with the MN and V2 potentials in the microscopic (solid lines) and semi-microscopic (dashed lines) models. The dotted line corresponds to the case (a) with MN, in the microscopic model. The insert represents the densities in logarithmic scale.

els reproducing the experimental energy (i.e., case (b) for the microscopic model and case (c) for the semi-microscopic model). The density for MN in case (a) in the microscopic model (when $E = -11.61$ MeV) is also displayed (dotted line), in order to illustrate the sensitivity with respect to the binding energy. The densities are lower with V2 than with MN, hence the radius of ^{12}C is larger with V2 than with MN. Beyond 2 fm, the semi-microscopic model seems to be a fair approximation. However, the short-distance behaviour is qualitatively very different: whereas the microscopic approach provides a maximum near 1 fm and then decreases, the semi-microscopic density steadily increases when r tends to zero. This is probably due to the three-body antisymmetrisation effects, not included in the semi-microscopic approximation.

8.3 Conclusions

The nonlocal RGM-$\not\varepsilon$ $\alpha\alpha$ and αn potentials are more appropriate for a semi-microscopic model than the RGM-ε potentials. They allow us to avoid the problems of the energy-dependence, which occur in three-body systems (with the RGM-ε cluster-cluster potentials).

The semi-microscopic model is a non-microscopic approximation of the microscopic cluster model. This is a simple three-body model with nonlocal potentials. The nonlocal potentials RGM-$\not\varepsilon$ simulate the Pauli principle, and give the same cluster-cluster phase shifts as the original full RGM. With these potentials, the semi-microscopic model yields comparable binding energies, with respect to the ones given by the fully microscopic model. The model has been successfully applied to ^{6}He, ^{9}Be and ^{12}C [21]. The differences in energy between the microscopic and semi-microscopic models are small, and decrease with the nucleon number (about 2.5 MeV for ^{12}C, and 0.5 MeV for ^{9}Be and ^{6}He). The discrepancy between the models depends on the choice of the nucleon-nucleon force (MN or V2). The semi-microscopic model turns out to be a very good approximation for ^{6}He with MN.

Also, because we use simple effective nucleon-nucleon forces (MN or V2) in the present work, it is not always possible to precisely reproduce the $\alpha + n$ and $\alpha + \alpha$ phase shifts and the experimental three-cluster binding energies simultaneously. Therefore, in the microscopic model, for each physical system, a tuning parameter in MN and V2 must be slightly modified in order to fit the binding energies of ^{6}He, ^{9}Be and ^{12}C.

We have also compared the neutron or proton densities given by the microscopic and semi-microscopic models. In general, differences between the microscopic and semi-microscopic densities occur at short distances. The

semi-microscopic approximation gives larger r.m.s matter radii than the microscopic model. In the simplest nucleus ^{6}He with the MN interaction, the densities given by the microscopic and semi-microscopic models are very similar to each other.

In all cases the binding energy are slightly *underestimated* by the semi-microscopic approach. This means that three-body antisymmetrisation effects, missing in this approximation should be *attractive*. The development of a reliable three-body force, which could simulate these effects, is a challenge for future works.

Chapter 9

Conclusion

In the present work, we have investigated the effects of the Pauli principle in three-cluster models. In particular, we have developed and analysed simple three-body models, which can approximate the dynamics of the three-cluster systems, such as the ^{6}He, ^{9}Be and ^{12}C nuclei. In these three-body models, the clusters are treated as structureless pointlike particles. This is a very useful simplification, but it requires to choose microscopically founded effective cluster-cluster potentials.

The consequences of the Pauli principle are rather well known in the case of the two-cluster systems. Indeed the RGM, which is a microscopic cluster model, shows that the general antisymmetrisation principle between nucleons leads to exchanges of nucleons between the clusters. As a result of the nucleon exchanges, the effective interaction between two clusters can be represented by a nonlocal potential. Furthermore, because of the antisymmetrisation, there are Pauli forbidden states for the relative motion between the clusters.

Therefore, it is not very suprising that three-body nuclear models with local effective potentials, which fit the two-cluster elastic phase shifts, yield rather poor results, in disagreement with experiment. This must be due to the fact that local potentials cannot properly simulate the subtle effects of the Pauli principle between the clusters. Hence, following a work of Fujiwara *et al.* [17, 28], we have considered the use of the effective nonlocal RGM cluster-cluster potentials. There are however two distinct variants of RGM potentials: the original *energy-dependent* potentials, and the more complicated *energy-independent* potentials. We have tested both variants. We call the three-body models using the nonlocal potentials the *semi-microscopic models*, since those potentials are extracted from the two-cluster RGM. We have analysed the semi-microscopic models, and we have compared their results with those of the fully microscopic three-cluster model.

The microscopic model and the nonlocal RGM potentials are based on

exactly the same parameters, i.e., an effective nucleon-nucleon force and an effective internal wave function for each cluster. Nevertheless, the semi-microscopic models are approximations that simulate the Pauli principle between each pair of clusters via the nonlocal potentials, but neglect the effects of the Pauli principle involving all three clusters simultaneoulsy. Furthermore, because they treat the clusters as pointlike particles, the semi-microscopic models are much simpler and faster than the microscopic model. In other words, they avoid the very long and laborious calculations of the microscopic theories.

In this context, we have studied the ^{6}He, ^{9}Be and ^{12}C nuclei [20–23], and the ${}^{\;\;6}_{\Lambda\Lambda}$He and ${}^{\;\;9}_{\Lambda}$Be hypernuclei [19]. These physical systems display three-cluster structures: they have been studied as αnn, $\alpha\alpha n$, 3α, $\alpha\Lambda\Lambda$, and $\alpha\alpha\Lambda$ systems, respectively. These examples require in particular $\alpha\alpha$ and αn effective potentials. The nonlocal RGM $\alpha\alpha$ and αn potentials have been used in the semi-microscopic models. They allow us to simulate the Pauli principle between two clusters. Also, the Pauli forbidden states in the $\alpha\alpha$ and αn relative motions must be properly eliminated from the wave functions in the semi-microscopic models. In addition, for ${}^{\;\;6}_{\Lambda\Lambda}$He and ${}^{\;\;9}_{\Lambda}$Be some effective $\alpha\Lambda$ and $\Lambda\Lambda$ potentials are also required. The $\alpha\Lambda$ potential can be nonlocal, because of the exchange forces in the baryon-baryon potentials.

We solve the three-body Schrödinger equations in configuration space by the hyperspherical harmonics method with the Lagrange-mesh technique. We have extended this method to the general case of nonlocal potentials [19]. We have developed a numerical code which implements the method. We have successfully validated our techniques [19, 20], by reproducing the results of Ref. [17, 18], for ${}^{\;\;6}_{\Lambda\Lambda}$He and ${}^{\;\;9}_{\Lambda}$Be.

With these techniques, we can calculate the binding energies of the systems, as well as other physical observables, such as matter radii, probability densities and reduced transition probabilities.

The cases of ^{6}He, ^{9}Be and ^{12}C have been analysed in detail, by comparing the results of the semi-microscopic models with the corresponding results of the fully microscopic model. All calculations have been performed from effective nucleon-nucleon forces (namely MN and V2).

We have first considered the *energy-dependent* RGM potentials in the semi-microscopic model. The energy-dependence of the potentials is rather problematic: we have discovered that the self-consistent prescription, proposed by Ref. [17], to calculate the energy parameters of the potentials is not always satisfactory. In particular, we have found that this prescription is not realistic when applied to the case of ^{9}Be. Indeed the binding energy for ^{9}Be with this prescription is in disagreement with both experiment and the microscopic model. The analysis of the $\alpha + \alpha$ and $\alpha + n$ elastic scattering

phase shifts reveals the reason behind this disagreement. We have shown that the semi-microscopic model, by using constant energy values in the energy-dependent RGM potentials, inevitably deteriorates the $\alpha+\alpha$ and $\alpha+n$ phase shifts. In particular, the low-energy resonances in the phase shifts may not be well reproduced. Hence the $\alpha\alpha$ and αn interactions, with such constant energy parameters, are physically questionable in the semi-microscopic model. Indeed, the two-body energies are not well defined in three-body models. Thus each two-body energy becomes a free parameter in the models. Therefore, the semi-microscopic model with the energy-dependent RGM potentials raises a difficulty. There is no obvious criteria to set the two-body energies.

The best solution is to use the *energy-independent* RGM potentials in the semi-microscopic model. We have thus analysed the semi-microscopic model with the energy-independent nonlocal $\alpha\alpha$ and αn potentials. The results are conclusive: this semi-microscopic model then becomes a rather fair approximation of the microscopic model. These nonlocal potentials reproduce exactly the RGM $\alpha+\alpha$ and $\alpha+n$ phase shifts. The binding energies of ${}^{9}_{\Lambda}$Be, ^{6}He, ^{9}Be and ^{12}C are well reproduced. The differences in energy between this semi-microscopic model and the microscopic model are small, and decrease with the nucleon number (about 2.5 MeV for ^{12}C, 0.5 MeV for ^{9}Be and ^{6}He). The discrepancy between the models depends on the choice of the nucleon-nucleon force (MN or V2). The semi-microscopic model turns out to be a very good approximation for ^{6}He with MN.

We have also compared the proton or neutron densities given by the microscopic and semi-microscopic models. In general, differences between the microscopic and semi-microscopic densities occur at short distances. The semi-microscopic approximation gives larger matter radii than the microscopic model. In the case of ^{6}He, the densities given by microscopic and semi-microscopic models are very similar to each other.

In all cases the binding energies are slightly *underestimated* by the semi-microscopic model. This suggests that the three-body antisymmetrisation effects of the Pauli principle, missing in this approximation should be *attractive*. The development of an effective three-cluster force, in order to improve the semi-microscopic model, is a challenge for future works.

In addition, we have observed that, with the simple effective (MN and V2) forces, the microscopic model is not able to reproduce simultaneously (with the same parameters) the two-cluster ($\alpha+\alpha$ and $\alpha+n$) elastic phase shifts and the three-cluster binding energies (in the αnn, $\alpha\alpha n$ and 3α models). Hence these effective forces contain a parameter to be tuned, for each physical system. Such effective forces are useful to simplify the calculations. In particular, they provide tractable wave functions that can be used in reaction models.

The present work thus provides a way of calculating the energies and wave functions of the three-body bound states, for any system with effective nonlocal potentials. The wave functions of the semi-microscopic model are now ready to be applied in all applications requiring three-body bound-state dynamics.

However, it would be also desirable to extend this model to the calculation of continuum states. This would require further developments to apply the formalism of the R-matrix [87] to the three-body Schrödinger equation with nonlocal potentials.

Another interesting perspective would be to explore, with the same formalism, the cases of four-cluster systems, which remain difficult with the microscopic models, but which seem more feasible in the semi-microscopic approximation.

Appendix A

Raynal-Revai coefficients

The Raynal-Revai coefficients (3.50) are used to change from one set of Jacobi coordinates to another in the hyperspherical harmonic basis (see Section 3.4.4). They are calculated from the explicit formula [42]:

$$\begin{aligned}
&\langle i, l'_x l'_y | k, l_x l_y \rangle_{KL} = \frac{\pi}{4} \left[C^{n'}_{l'_x l'_y} C^{n}_{l_x l_y} \right]^{-1/2} \\
&\times \sum_{\lambda_1 \lambda_2 \lambda_3 \lambda_4} (\mathrm{i})^{\lambda_3+\lambda_4+l'_y-l_y} (-1)^{\lambda_1+\lambda_2} f(\lambda_1, \lambda_3; l_x) f(\lambda_4, \lambda_2; l_y) f(\lambda_1, \lambda_4; l'_x) f(\lambda_3, \lambda_2; l'_y) \\
&\times \left\{ \begin{array}{ccc} \lambda_1 & \lambda_3 & l_x \\ \lambda_4 & \lambda_2 & l_y \\ l'_x & l'_y & L \end{array} \right\} \sum_{\mu\nu} (-1)^{\mu} C^{\mu}_{\lambda_3 \lambda_4} C^{\nu}_{\lambda_1 \lambda_2} (\cos\varphi_{ki})^{2\nu+\lambda_1+\lambda_2} (\sin\varphi_{ki})^{2\mu+\lambda_3+\lambda_4},
\end{aligned} \tag{A.1}$$

using the following notations:

$$C^{\alpha}_{\beta\gamma} = \frac{\Gamma(2\alpha+\beta+\gamma+2)}{\Gamma(\alpha+\beta+\frac{3}{2})\Gamma(\alpha+\gamma+\frac{3}{2})\Gamma(\alpha+1)\Gamma(\alpha+\beta+\gamma+2)}, \tag{A.2}$$

$$\begin{aligned}
f(a,b;c) &= \sqrt{(2a+1)(2b+1)}(ab00|c0) \\
&= \sqrt{(2a+1)(2b+1)(2c+1)}(-1)^{(a+b)} \begin{pmatrix} a & b & c \\ 0 & 0 & 0 \end{pmatrix},
\end{aligned} \tag{A.3}$$

i represents the complex number whose square is -1, φ_{ki} is defined by equation (3.8), and n and n' are defined by $K = 2n + l_x + l_y = 2n' + l'_x + l'_y$. The summation runs over all integers values λ_1, λ_2, λ_3, λ_4, μ and ν that satisfy

the conditions:

$$
\begin{aligned}
K &= 2\mu + 2\nu + \lambda_1 + \lambda_2 + \lambda_3 + \lambda_4, \\
|\lambda_1 - \lambda_3| &\leq l_x \leq \lambda_1 + \lambda_3, \\
|\lambda_4 - \lambda_2| &\leq l_y \leq \lambda_4 + \lambda_2, \\
|\lambda_1 - \lambda_4| &\leq l'_x \leq \lambda_1 + \lambda_4, \\
|\lambda_3 - \lambda_2| &\leq l'_y \leq \lambda_3 + \lambda_2, \\
\lambda_1 + \lambda_3 + l_x &\text{ even}, \\
\lambda_4 + \lambda_2 + l_y &\text{ even}, \\
\lambda_1 + \lambda_4 + l'_x &\text{ even}, \\
\lambda_3 + \lambda_2 + l'_y &\text{ even}.
\end{aligned}
\tag{A.4}
$$

Appendix B

Calculation of the potential matrix elements

In this appendix, we specify the practical calculations of the local and nonlocal potential matrices in the hyperspherical formalism of Chapter 3.

B.1 Local potentials

The treatment of the local potentials in the hyperspherical harmonics method is introduced in Section 3.5.3. Using the Raynal-Revai coefficients, these terms reduce to the calculations of integrals (3.67).

In the models, the potentials can depend on the relative orbital angular momentum l_x. They can also include a spin-orbit dependence, in which case the hyperspherical harmonics are expanded in a basis of eigenfunctions of the spin-orbit operator, following the procedure explained in Section B.2.

To calculate the integrals defined in equation (3.67), we apply the othogonality relations between the angular momentum eigenstates. The integrals then reduce to

$$V^{J\pi\,(ij-k)}_{\gamma' K',\gamma K}(\rho) = \int \mathcal{Y}^{JM\dagger}_{\gamma' K'}(\Omega_{5k})\, V_{ij}\left(\frac{\rho\cos\alpha_k}{\sqrt{\mu_{ij}}}\right) \mathcal{Y}^{JM}_{\gamma K}(\Omega_{5k})\, d\Omega_{5k} \tag{B.1}$$

$$= \delta_{\gamma\gamma'} \int_0^{\frac{\pi}{2}} \phi^{l_x l_y}_{K'}(\alpha_k)\, V_{ij}\left(\frac{\rho\cos\alpha_k}{\sqrt{\mu_{ij}}}\right) \phi^{l_x l_y}_{K}(\alpha_k)\, \sin^2\alpha_k\, \cos^2\alpha_k\, d\alpha_k,$$

where the functions $\phi^{l_x l_y}_K(\alpha_k)$ are defined by equations (3.37) and (3.38) and l_x is the relative-motion orbital angular momentum between particles i and j. For the sake of simplicity, the above relation assumes that the potential does not contain any spin-dependent term. The case of a spin-orbit potential is

however treated similarly, except that it requires to first modify the angular momentum coupling scheme of the hypersperical harmonics. The case of a spin-orbit operator is discussed in Section B.2. Thus, for the local potential matrix, we need to calculate integrals of the the form

$$I = \int_0^{\frac{\pi}{2}} \phi_{K'}^{l_x l_y}(\alpha)\, V_{ij}\left(\frac{\rho\cos\alpha}{\sqrt{\mu_{ij}}}\right) \phi_K^{l_x l_y}(\alpha)\, \sin^2\alpha\, \cos^2\alpha\, d\alpha, \tag{B.2}$$

With definition (3.38) of $\phi_K^{l_x l_y}(\alpha)$, the integral (B.2) can be written

$$I = N_K^{l_x l_y} N_{K'}^{l_x l_y} \int_0^{\frac{\pi}{2}} (\sin\alpha)^{2l_y+2}\, (\cos\alpha)^{2l_x+2}\, V_{ij}\left(\frac{\rho\cos\alpha}{\sqrt{\mu_{ij}}}\right) P_{n'}^{l_y+\frac{1}{2},l_x+\frac{1}{2}}(\cos 2\alpha)\, P_n^{l_y+\frac{1}{2},l_x+\frac{1}{2}}(\cos 2\alpha)\, d\alpha, \tag{B.3}$$

where $n = (K - l_x - l_y)/2$ and $n' = (K' - l_x - l_y)/2$.

We make a change of integration variable: let $v = \tan(\alpha/2)$,

$$I = N_K^{l_x l_y} N_{K'}^{l_x l_y} \int_0^1 \left(\frac{2v}{1+v^2}\right)^{2l_y+2} \left(\frac{1-v^2}{1+v^2}\right)^{2l_x+2} V_{ij}\left(\frac{\rho}{\sqrt{\mu_{ij}}}\frac{1-v^2}{1+v^2}\right) P_{n'}^{l_y+\frac{1}{2},l_x+\frac{1}{2}}\left(2\left(\frac{1-v^2}{1+v^2}\right)^2 - 1\right) P_n^{l_y+\frac{1}{2},l_x+\frac{1}{2}}\left(2\left(\frac{1-v^2}{1+v^2}\right)^2 - 1\right) \frac{2}{1+v^2}\, dv, \tag{B.4}$$

The integral over v is evaluated numerically by using a Gauss-Legendre quadrature [44]. Typically, we use a Gauss-Legendre approximation with 64 points, which gives a good accuracy.

In practice, $\rho = hu_i$, according the Lagrange-mesh method (3.102). From integrals (B.4), the matrix elements $V^{J\pi}_{\gamma K,\gamma' K'}(hu_i)$ (3.69) which represent the local forces are calculated.

B.2 Spin-orbit terms

For the spin-orbit potentials, the calculations are performed by applying angular momentum recoupling techniques to the hyperspherical harmonics.

Let us consider a spin-orbit potential

$$V_{ij} = 2\, V^{so} \boldsymbol{L_x} \cdot \boldsymbol{S_x}, \tag{B.5}$$

where $\boldsymbol{L_x}$ is the orbital angular momentum of the relative motion between particles i and j, and $\boldsymbol{S_x} = \boldsymbol{s}_i + \boldsymbol{s}_j$, with $\boldsymbol{s}_i$ denoting the spin operator of particle i. The coefficient V^{so} is assumed to be independent of $\boldsymbol{L_x}$ and $\boldsymbol{S}_x$.

In order to calculate the matrix elements of the spin-orbit potential, we expand the hyperspherical harmonics $\mathcal{Y}^{JM}_{\gamma K}(\Omega_{5k})$ into linear combinations of eigenstates of the spin-orbit operator $\boldsymbol{L_x}\cdot\boldsymbol{S_x}$. This is carried out by using the Wigner $6j$ and $9j$ coefficients [47].

The angular momenta of $\mathcal{Y}^{JM}_{\gamma K}(\Omega_{5k})$ are $\gamma=\{l_x l_y LS\}$ and J. The total spin S has been introduced in the hyperspherical harmonics through spinors χ^{SM_S} (3.43). This spin S is however the result of the individual spins s_1, s_2 and s_3 of the three particles. We need here to specify how these spins s_1, s_2 and s_3 are coupled to give total spin S.

Let us first assume that the spin S, in the spinors χ^{SM_S}, results from the coupling of s_i with s_j to give s_x, and from the coupling of s_x with s_k. Under this assumption, the short-hand symbol γ of $\mathcal{Y}^{JM}_{\gamma K}(\Omega_{5k})$ could be rewritten by mentionning the spin coupling as $\gamma=\{l_x l_y L\,((s_i s_j)s_x\,s_k)\,S\}$, and the spinors could also be rewritten with explicit labels as

$$\chi^{SM_S}=\chi^{SM_S}_{((s_i s_j)s_x\,s_k)}. \tag{B.6}$$

Of course, the spins satisfy

$$|s_i-s_j|\le s_x\le s_i+s_j, \tag{B.7}$$

$$|s_x-s_k|\le S\le s_x+s_k. \tag{B.8}$$

In order to apply the spin-orbit interaction (B.5) to the hyperspherical harmonic $\mathcal{Y}^{JM}_{\gamma K}(\Omega_{5k})$, l_x must be coupled with s_x. We make use of the Wigner $9j$ coefficients: $\mathcal{Y}^{JM}_{\gamma K}(\Omega_{5k})$ is expanded as

$$\mathcal{Y}^{JM}_{\gamma K}(\Omega_{5k})=$$
$$\sum_{j_x\,j_y}[(2j_x+1)(2j_y+1)(2L+1)(2S+1)]^{1/2}\begin{Bmatrix} l_x & s_x & j_x\\ l_y & s_k & j_y\\ L & S & J\end{Bmatrix}\mathcal{Y}^{JM}_{\substack{l_x s_x j_x\\ l_y s_k j_y}K}(\Omega_{5k}), \tag{B.9}$$

where

$$|l_x-s_x|\le j_x\le l_x+s_x, \tag{B.10}$$

$$|l_y-s_k|\le j_y\le l_y+s_k, \tag{B.11}$$

and $\mathcal{Y}^{JM}_{\substack{l_x s_x j_x\\ l_y s_k j_y}K}(\Omega_{5k})$ are thus eigenfunctions of the spin-orbit operator,

$$(2\boldsymbol{L_x}\cdot\boldsymbol{S_x})\,\mathcal{Y}^{JM}_{\substack{l_x s_x j_x\\ l_y s_k j_y}K}(\Omega_{5k})=\eta_{l_x s_x j_x}\,\mathcal{Y}^{JM}_{\substack{l_x s_x j_x\\ l_y s_k j_y}K}(\Omega_{5k}), \tag{B.12}$$

with

$$\eta_{l_x s_x j_x}=j_x(j_x+1)-l_x(l_x+1)-s_x(s_x+1). \tag{B.13}$$

Let us now consider the other case where, e.g, the spinors χ^{SM_S} are defined by first coupling s_j with s_k, to give s_{jk}, and then coupling s_i with s_{jk}, to give S. The notation γ could thus be written more explicitly, with the detail of the spins, as $\gamma = \{l_x l_y L\,(s_i\,(s_j s_k)\,s_{jk})\,S\}$, and the spinors χ^{SM_S} could be written

$$\chi^{SM_S} = \chi^{SM_S}_{\left(s_i(s_j s_k)s_{jk}\right)}. \tag{B.14}$$

The spins satisfy

$$|s_j - s_k| \leq s_{jk} \leq s_j + s_k, \tag{B.15}$$

$$|s_i - s_{jk}| \leq S \leq s_i + s_{jk}. \tag{B.16}$$

We make use of the Wigner $6j$ and $9j$ coefficients. The $6j$ coefficients are used in order to change the spin coupling:

$$\chi^{SM_S}_{(s_i(s_j s_k)s_{jk})} = \sum_{s_x} \left\langle (s_i s_j)s_x\, s_k S \middle| s_i(s_j s_k)s_{jk} S \right\rangle \chi^{SM_S}_{((s_i s_j)s_x\, s_k)}, \tag{B.17}$$

with coefficients

$$\left\langle (s_i s_j)s_x\, s_k S \middle| s_i(s_j s_k)s_{jk} S \right\rangle = (-1)^{s_i+s_j+s_k+S}\left[(2s_x+1)(2s_{jk}+1)\right]^{1/2} \left\{ \begin{array}{ccc} s_i & s_j & s_x \\ s_k & S & s_{jk} \end{array} \right\}. \tag{B.18}$$

The hyperspherical harmonics $\mathcal{Y}^{JM}_{\gamma K}(\Omega_{5k})$ can therefore be written

$$\mathcal{Y}^{JM}_{\gamma K}(\Omega_{5k}) = \sum_{s_x\, j_x\, j_y} \left[(2s_x+1)(2s_{jk}+1)(2j_x+1)(2j_y+1)(2L+1)(2S+1)\right]^{1/2} (-1)^{s_i+s_j+s_k+S} \left\{ \begin{array}{ccc} s_i & s_j & s_x \\ s_k & S & s_{jk} \end{array} \right\} \left\{ \begin{array}{ccc} l_x & s_x & j_x \\ l_y & s_k & j_y \\ L & S & J \end{array} \right\} \mathcal{Y}^{JM}_{\substack{l_x s_x j_x \\ l_y s_k j_y} K}(\Omega_{5k}), \tag{B.19}$$

Expansions (B.9) and (B.19), with the eigenvalue property (B.12), enable us to calculate the spin-orbit potential terms.

Note that the functions $\mathcal{Y}^{JM}_{\substack{l_x s_x j_x \\ l_y s_k j_y} K}(\Omega_{5k})$ satisfy the orthogonality relation

$$\int \mathcal{Y}^{JM\dagger}_{\substack{l'_x s'_x j'_x \\ l'_y s_k j'_y} K'}(\Omega_{5k})\, \mathcal{Y}^{JM}_{\substack{l_x s_x j_x \\ l_y s_k j_y} K}(\Omega_{5k})\, d\Omega_{5k} = \delta_{KK'}\delta_{l_x l'_x}\delta_{s_x s'_x}\delta_{j_x j'_x}\delta_{l_y l'_y}\delta_{s_y s'_y}\delta_{j_y j'_y}, \tag{B.20}$$

and

$$\int \mathcal{Y}^{JM\dagger}_{\substack{l'_x s'_x j'_x \\ l'_y s_k j'_y} K'}(\Omega_{5k})\, \mathcal{Y}^{JM}_{\substack{l_x s_x j_x \\ l_y s_k j_y} K}(\Omega_{5k})\, d\Omega_{x_k} d\Omega_{y_k} = \phi^{l_x l_y}_{K'}(\alpha_k)\phi^{l_x l_y}_{K}(\alpha_k)\, \delta_{l_x l'_x}\delta_{l_y l'_y}\delta_{s_x s'_x}\delta_{j_x j'_x}\delta_{s_y s'_y}\delta_{j_y j'_y}, \quad \text{(B.21)}$$

The matrix elements $V^{J\pi\,(ij-k)}_{\gamma' K',\gamma K}(\rho)$ of a spin-orbit potential therefore reduce to linear combinations of integrals of type (B.2).

B.3 Nonlocal potentials

The matrix elements $W^{J\pi}_{\gamma K i,\gamma' K' i'}$ of the nonlocal potentials are defined by equation (3.115). The hyperradial kernels $W_{\gamma K,\gamma' K'}(\rho,\rho')$ is defined in Section 3.5.4.

The kernels can be reduced to the case (3.84). Therefore, to evaluate $W^{J\pi}_{\gamma K i,\gamma' K' i'}$, we need to calculate integrals of the form

$$J = \int_0^\infty d\rho \int_0^\infty d\rho'\ \hat{f}_i(\rho/h)\ \hat{f}_{i'}(\rho'/h) \frac{1}{(\rho\rho')^{3/2}} \int_0^{\min(\rho,\rho')} W^{l_x}_{ij}\left(\frac{x}{\sqrt{\mu_{ij}}}, \frac{x'}{\sqrt{\mu_{ij}}}\right) \phi^{l_x l_y}_{K}(\alpha)\, \phi^{l_x l_y}_{K'}(\alpha')\, x\, x'\, y^2\, dy, \quad \text{(B.22)}$$

with $x = \sqrt{\rho^2 - y^2}$, $x' = \sqrt{\rho'^2 - y^2}$, $\alpha = \arctan(y/x)$, $\alpha' = \arctan(y/x')$.

The function $\min(\rho,\rho')$ has its first partial derivatives that are discontinuous for $\rho = \rho'$. Therefore we choose to change the variables: instead of using ρ, ρ' we prefer to use x, x', because their integration domains are $[0,+\infty[$. The integrals then become [19]

$$J = \int_0^\infty dy \int_0^\infty dx \int_0^\infty dx'\ \phi^{l_x l_y}_{K}\left(\arctan\frac{y}{x}\right) \phi^{l_x l_y}_{K'}\left(\arctan\frac{y}{x'}\right) \hat{f}_i\left(\frac{1}{h}\sqrt{x^2+y^2}\right) \hat{f}_{i'}\left(\frac{1}{h}\sqrt{x'^2+y^2}\right) \frac{W^{l_x}_{ij}\left({\mu_{ij}}^{-1/2}x, {\mu_{ij}}^{-1/2}x'\right) x^2 x'^2 y^2}{[(x^2+y^2)(x'^2+y^2)]^{5/4}}. \quad \text{(B.23)}$$

They are evaluated numerically. The integrals over x and x' are performed using a Gauss-Laguerre quadrature (3.93) with N_2 points and a scale param-

eter h_2,

$$J \approx (h_2)^2 \sum_{j=1}^{N_2} \sum_{j'=1}^{N_2} \lambda_j \, \lambda_{j'} \, W_{ij}^{l_x} \left(\frac{h_2 u_j}{\sqrt{\mu_{ij}}}, \frac{h_2 u_{j'}}{\sqrt{\mu_{ij}}} \right) \int_0^\infty \varphi_{Ki}^{l_x l_y}(h_2 u_j, y) \, \varphi_{K'i'}^{l_x l_y}(h_2 u_{j'}, y) \, dy, \quad \text{(B.24)}$$

where λ_j and u_j are the weights (3.99) and nodes (3.98) associated with the Gauss-Laguerre quadrature, and

$$\varphi_{Ki}^{l_x l_y}(x, y) = \phi_K^{l_x l_y} \left(\arctan \frac{y}{x} \right) \hat{f}_i \left(\frac{1}{h} \sqrt{x^2 + y^2} \right) \frac{x^2 y^2}{(x^2 + y^2)^{5/4}}. \quad \text{(B.25)}$$

The function $\phi_K^{l_x l_y}$ reads

$$\phi_K^{l_x l_y} \left(\arctan \frac{y}{x} \right) = N_K^{l_x l_y} \frac{x^{l_x} y^{l_y}}{(x^2 + y^2)^{(l_x + l_y)/2}} \; P_n^{l_y + \frac{1}{2}, l_x + \frac{1}{2}} \left(\frac{x^2 - y^2}{x^2 + y^2} \right), \quad \text{(B.26)}$$

with $n = (K - l_x - l_y)/2$ and $N_K^{l_x l_y}$ given by equation (3.33).

The final step consists in evaluating the integrals over y in (B.24). They are calculated numerically using a Gauss-Fourier quadrature [48] (or trapezoidal rule [44]):

$$\int_0^\infty \varphi_{Ki}^{l_x l_y}(h_2 u_j, y) \varphi_{K'i'}^{l_x l_y}(h_2 u_{j'}, y) \, dy \approx \sum_{n=1}^{N_y} \varphi_{Ki}^{l_x l_y}(h_2 u_j, n h_y) \, \varphi_{K'i'}^{l_x l_y}(h_2 u_{j'}, n h_y) h_y, \quad \text{(B.27)}$$

discretising the variable y with N_y points, and a constant step h_y.

Appendix C

αn and $\alpha\alpha$ RGM-ε potentials

The energy-dependent αn and $\alpha\alpha$ RGM-ε potentials are given in this appendix [20]. Their expressions are taken from Refs. [1, 88, 89]. The general form of the RGM-ε potentials is presented by equation (2.77): they contain a local part $V_D(\boldsymbol{r})$ and a nonlocal kernel $K(\varepsilon, \boldsymbol{r}, \boldsymbol{r}')$ that depends on the relative-motion energy ε of the two interacting clusters. In Section C.1 the nucleon-nucleon interactions from which the potentials are calculated are specified. The αn and the $\alpha\alpha$ potentials are given in Sections C.2 and C.3, respectively. In Section C.4, formulae to apply the nonlocal kernel to a given angular-momentum partial wave are provided.

C.1 Effective nucleon-nucleon potential

The RGM potentials are calculated from an effective nucleon-nucleon potential. In general, the nucleon-nucleon potential is chosen as $v_{ij} = V_{ij}^{NN} + V_{ij}^{SO} + V_{ij}^{C}$, where V_{ij}^{NN}, V_{ij}^{SO} and V_{ij}^{C} are nuclear central, spin-orbit and Coulomb components, respectively.

The nucleon-nucleon central interaction is assumed to be a sum of Gaussian terms of the form:

$$V_{ij}^{NN} = \sum_{n=1}^{N} V_{0n}(W_n + M_n P_{ij}^{r} + B_n P_{ij}^{\sigma} + H_n P_{ij}^{r} P_{ij}^{\sigma}) \exp(-r^2/a_n^2), \qquad \text{(C.1)}$$

where P_{ij}^{r} and P_{ij}^{σ} are the space- and spin-exchange operators, respectively, and V_{0n}, W_n, M_n, B_n, H_n and a_n are constant parameters. The effective spin-orbit force between nucleons (5.13) reads

$$V_{ij}^{SO} = -\frac{2S_0}{\hbar^2\kappa^5} \exp(-r^2/\kappa^2)\, \boldsymbol{l}_{ij} \cdot \boldsymbol{s}_{ij}, \qquad \text{(C.2)}$$

V_{ij}^{NN}	n	a_n	V_{0n}	W_n	M_n	B_n	H_n
V2	1	1.01	61.14	$1-m$	m	0	0
[57]	2	1.8	-60.65	$1-m$	m	0	0
MN	1	$(\sqrt{1.487})^{-1}$	200	$u/2$	$1-u/2$	0	0
[26]	2	$(\sqrt{0.639})^{-1}$	-178	$u/4$	$(2-u)/4$	$u/4$	$(2-u)/4$
	3	$(\sqrt{0.465})^{-1}$	-91.85	$u/4$	$(2-u)/4$	$-u/4$	$(u-2)/4$

Table C.1: Parameters of the nucleon-nucleon potentials V2 (5.10) and MN (5.8) expressed as an interaction (C.1) with $N = 2$ and $N = 3$ Gaussians, respectively. The value of parameters u and m depends on the applications. Units are MeV for energy and fm for length.

where $\boldsymbol{l}_{ij}$ is the relative orbital angular momentum and $\boldsymbol{s}_{ij}$ the total spin of the two interacting nucleons, and S_0 and κ are constants. With this notation, a limit exists as κ approaches zero, when considering the αn interaction. There is also the Coulomb potential between protons:

$$V_{ij}^{C} = \frac{e^2}{r}\left(\frac{1}{2} - t_{iz}\right)\left(\frac{1}{2} - t_{jz}\right), \tag{C.3}$$

where t_{iz} is the isospin component of nucleon i, with $t_{iz} = -1/2$ for a proton and and $t_{iz} = +1/2$ for a neutron.

The energy-dependent αn and $\alpha\alpha$ RGM potentials will be written in their general form for the interactions (C.1), (C.2) and (C.3). This allows us to calculate these potentials for MN (5.8) and V2 (5.10), which are just particular cases of interaction (C.1). The parameters of V_{ij}^{NN} (C.1) for MN and V2 are given in Table C.1.

C.2 αn potential

We give here the energy-dependent αn RGM potential [1, 23, 88, 89]. It is calculated from the interactions (C.1) and (C.2) by assuming that the α-particle is described by an oscillator internal wave function ϕ_1 (2.6). Its expression is given by

$$(V_{\alpha-n}\Psi)(\boldsymbol{r}) = V_D(r)\Psi(\boldsymbol{r}) + V_D^{SO}(r)\Psi(\boldsymbol{r}) + \int K(\varepsilon, \boldsymbol{r}, \boldsymbol{r'})\Psi(\boldsymbol{r'})\, d\boldsymbol{r'}, \tag{C.4}$$

where $\Psi(\boldsymbol{r})$ represents the wave function describing the αn relative-motion, $V_D(r)$, $V_D^{SO}(r)$ and $K(\varepsilon, \boldsymbol{r}, \boldsymbol{r'})$ are as follows. The potential depends on the energy ε of the αn relative motion.

The central local term generated by the nuclear potential (C.1) reads

$$V_D(r) = \sum_{n=1}^{N} \frac{1}{2} V_{0n} X_n^d \left(\frac{4a_n^2}{4a_n^2 + 3b^2} \right)^{3/2} \exp\left(-\frac{4r^2}{4a_n^2 + 3b^2} \right), \tag{C.5}$$

where $X_n^d = 8W_n + 4B_n - 4H_n - 2M_n$ and b is the oscillator parameter of the α-particle (2.6).

The local part generated by the spin-orbit potential (C.2) is given by

$$V_D^{SO}(r) = -\eta_{lj} \frac{5}{2} S_0 \left(\frac{4}{4\kappa^2 + 3b^2} \right)^{5/2} \exp\left(-\frac{4r^2}{4\kappa^2 + 3b^2} \right) \tag{C.6}$$

with

$$\eta_{lj} = j(j+1) - l(l+1) - s(s+1), \tag{C.7}$$

where l denotes the orbital angular momentum of the αn relative motion, $s = 1/2$, and $j = |l \pm 1/2|$ is the total angular momentum of the $\alpha + n$ system.

The nonlocal kernel $K(\varepsilon, \boldsymbol{r}, \boldsymbol{r}')$ reads

$$K(\varepsilon, \boldsymbol{r}, \boldsymbol{r}') = K_H(\boldsymbol{r}, \boldsymbol{r}') + \varepsilon K_N(\boldsymbol{r}, \boldsymbol{r}'), \tag{C.8}$$

according to equation (2.33). It arises from the nucleon exchanges and depends on the energy ε, because of the Pauli principle. The kernel $K_N(\boldsymbol{r}, \boldsymbol{r}')$ is given by

$$K_N(\boldsymbol{r}, \boldsymbol{r}') = \left(\frac{4}{5} \right)^3 \left(\frac{4}{3\pi b^2} \right)^{3/2} \exp\left[-\frac{2}{75b^2} (17r^2 + 17r'^2 + 16\boldsymbol{r} \cdot \boldsymbol{r}') \right]. \tag{C.9}$$

The kernel $K_H(\boldsymbol{r}, \boldsymbol{r}')$ can be separated into several terms,

$$K_H(\boldsymbol{r}, \boldsymbol{r}') = K_T(\boldsymbol{r}, \boldsymbol{r}') + K_V(\boldsymbol{r}, \boldsymbol{r}') + K_{SO}(\boldsymbol{r}, \boldsymbol{r}'). \tag{C.10}$$

The kinetic energy of the nucleons leads to the kernel

$$K_T(\boldsymbol{r}, \boldsymbol{r}') = -\frac{1}{4} \hbar\omega \left[\frac{49}{5} - \frac{64}{1125b^2} (38r^2 + 38r'^2 + 49\,\boldsymbol{r} \cdot \boldsymbol{r}') \right] K_N(\boldsymbol{r}, \boldsymbol{r}'), \tag{C.11}$$

where $\omega = \hbar/(m_N b^2)$, m_N being the nucleon mass unit. The nuclear potential (C.1) leads to

$$\begin{aligned} K_V(\boldsymbol{r}, \boldsymbol{r}') \;=\; & \sum_{n=1}^{N} \frac{1}{2} V_{0n} \left\{ (X_n^d + X_n^e) \left(\frac{a_n^2}{a_n^2 + 2b^2} \right)^{3/2} + X_n^e \exp\left(-\frac{16(\boldsymbol{r} - \boldsymbol{r}')^2}{25a_n^2} \right) \right. \\ - \;& (X_n^d + X_n^e) SO \left(\frac{3a_n^2}{3a_n^2 + 2b^2} \right)^{3/2} \left[\exp\left(-\frac{16(4\boldsymbol{r} + \boldsymbol{r}')^2}{75(3a_n^2 + 2b^2)} \right) \right. \\ & \left. \left. + \exp\left(-\frac{16(\boldsymbol{r} + 4\boldsymbol{r}')^2}{75(3a_n^2 + 2b^2)} \right) \right] \right\} K_N(\boldsymbol{r}, \boldsymbol{r}'), \end{aligned} \tag{C.12}$$

where $X_n^e = 8M_n + 4H_n - 4B_n - 2W_n$. The spin-orbit potential (C.2) gives the kernel

$$K_{SO}(\boldsymbol{r},\boldsymbol{r}') = -\eta_{lj} S_0 \kappa^{-3} \frac{5}{3b^2-\kappa^2} \exp\left[-\frac{16(\boldsymbol{r}-\boldsymbol{r}')^2}{25\kappa^2}\right] K_N(\boldsymbol{r},\boldsymbol{r}'). \quad \text{(C.13)}$$

In order to simplify the calculations, as suggested in Refs. [26, 58], we will assume the limit case where the range parameter κ approaches zero. In this case, the spin-orbit contribution becomes local. Let $V_{D(0)}^{SO}(r)$ be the value of the term (C.6) for $\kappa = 0$, i.e.,

$$V_{D(0)}^{SO}(r) = -\eta_{lj} \frac{5}{2} S_0 \left(\frac{4}{3b^2}\right)^{5/2} \exp\left(-\frac{4r^2}{3b^2}\right). \quad \text{(C.14)}$$

The limit of the kernel (C.13) as $\kappa \to 0$ is

$$\lim_{\kappa\to 0} K_{SO}(\boldsymbol{r},\boldsymbol{r}') = -\eta_{lj} \frac{5}{4} S_0 \left(\frac{4}{3b^2}\right)^{5/2} \exp\left(-\frac{4r^2}{3b^2}\right) \delta(\boldsymbol{r}-\boldsymbol{r}') \quad \text{(C.15)}$$

$$= \frac{1}{2} V_{D(0)}^{SO}(r)\, \delta(\boldsymbol{r}-\boldsymbol{r}'). \quad \text{(C.16)}$$

To obtain (C.15), we have used the identity

$$\delta(\boldsymbol{r}) = \lim_{\kappa\to 0} \pi^{-3/2} \kappa^{-3} \exp(-r^2/\kappa^2), \quad \text{(C.17)}$$

which leads to

$$\lim_{\kappa\to 0} \pi^{-3/2} \kappa^{-3} \exp\left(-\frac{16(\boldsymbol{r}-\boldsymbol{r}')^2}{25\kappa^2}\right) = \delta\left(\frac{4}{5}(\boldsymbol{r}-\boldsymbol{r}')\right)$$

$$= \left(\frac{5}{4}\right)^3 \delta(\boldsymbol{r}-\boldsymbol{r}'). \quad \text{(C.18)}$$

It follows from (C.16) that

$$\lim_{\kappa\to 0} \int K_{SO}(\boldsymbol{r},\boldsymbol{r}')\Psi(\boldsymbol{r}')\, d\boldsymbol{r}' = \frac{1}{2} V_{D(0)}^{SO}(r)\Psi(\boldsymbol{r}). \quad \text{(C.19)}$$

Thus, as $\kappa \to 0$, the total spin-orbit contribution is

$$\lim_{\kappa\to 0} \left[V_D^{SO}(r)\Psi(\boldsymbol{r}) + \int K_{SO}(\boldsymbol{r},\boldsymbol{r}')\Psi(\boldsymbol{r}')\, d\boldsymbol{r}'\right] = \frac{3}{2} V_{D(0)}^{SO}(r)\Psi(\boldsymbol{r}), \quad \text{(C.20)}$$

i.e., a purely local term in the αn potential. This simplifies the RGM calculations. We will then adopt this case where $\kappa \to 0$. Such a local effective

spin-orbit interaction (C.20) in the αn potential is able to reproduce in good agreement with experiment the $\alpha + n$ scattering phase shifts, by adjusting the parameter S_0.

Equations from (C.4) to (C.13) give the αn RGM potential. The expression of the corresponding α-proton potential would be quite similar, except that it would include additional terms because of the Coulomb interaction (C.3). Expressions of the α-proton RGM potential can be found, e.g., in Refs [20, 88, 89].

In Section C.4, we will give the formulae which are used to apply the nonlocal terms to any given partial wave.

C.3 $\alpha\alpha$ potential

Here we give the expression of the energy-dependent $\alpha\alpha$ RGM potential [23, 88]. It is calculated from the nucleon-nucleon interactions (C.1) and (C.3), assuming oscillator wave functions ϕ_1 (2.6) for the α-particles. The spin-orbit interaction (C.2) does not play any role in the $\alpha+\alpha$ relative motion. The expression of the $\alpha\alpha$ RGM-ε potential is

$$(V_{\alpha-\alpha}\Psi)(\boldsymbol{r}) = V_D(r)\Psi(\boldsymbol{r}) + V_D^C(r)\Psi(\boldsymbol{r}) + \int K(\varepsilon, \boldsymbol{r}, \boldsymbol{r'})\Psi(\boldsymbol{r'})\, d\boldsymbol{r'}, \quad \text{(C.21)}$$

where $V_D(r)$, $V_D^C(r)$ and $K(\varepsilon, \boldsymbol{r}, \boldsymbol{r'})$ are as follows, and $\Psi(\boldsymbol{r})$ here describes the relative motion between the α-particles. Note that $\Psi(-\boldsymbol{r}) = \Psi(\boldsymbol{r})$ by virtue of the Pauli principle, the α-particles being bosons. In other words, odd partial waves are forbidden. The potential depends on the energy ε of the relative motion of the $\alpha + \alpha$ system.

The local term generated by the nuclear potential (C.1) reads

$$V_D(r) = \sum_{n=1}^{N} 2V_{0n}X_n^d \left(\frac{2a_n^2}{2a_n^2 + 3b^2}\right)^{3/2} \exp\left(-\frac{2r^2}{2a_n^2 + 3b^2}\right), \quad \text{(C.22)}$$

where $X_n^d = 8W_n + 4B_n - 4H_n - 2M_n$. The local term given by the Coulomb potential (C.3) reads

$$V_D^C(r) = \frac{4e^2}{r}\mathrm{erf}\left(\sqrt{\frac{2}{3}}\frac{r}{b}\right). \quad \text{(C.23)}$$

The function erf is defined as

$$\mathrm{erf}(x) = \frac{2}{\sqrt{\pi}}\int_0^x \exp(-u^2)\, du \quad \text{(C.24)}$$

The kernel $K(\varepsilon, \boldsymbol{r}, \boldsymbol{r}')$ is symmetrical with respect to $\boldsymbol{r}' \to -\boldsymbol{r}'$, i.e.,

$$K(\varepsilon, \boldsymbol{r}, -\boldsymbol{r}') = K(\varepsilon, \boldsymbol{r}, \boldsymbol{r}'). \tag{C.25}$$

Hence this kernel can be written as

$$K(\varepsilon, \boldsymbol{r}, \boldsymbol{r}') = \frac{1}{2}\left[K^{(u)}(\varepsilon, \boldsymbol{r}, \boldsymbol{r}') + K^{(u)}(\varepsilon, \boldsymbol{r}, -\boldsymbol{r}')\right], \tag{C.26}$$

where $K^{(u)}(\varepsilon, \boldsymbol{r}, \boldsymbol{r}')$ is an effective unsymmetrized function, whose expression is as follows. Note that $K^{(u)}(\varepsilon, \boldsymbol{r}, \boldsymbol{r}')$ will directly lead to correct projected kernels provided only even l values are kept. The nonlocal kernel $K^{(u)}(\varepsilon, \boldsymbol{r}, \boldsymbol{r}')$ can be separated into several terms,

$$K^{(u)}(\varepsilon, \boldsymbol{r}, \boldsymbol{r}') = K_H^{(u)}(\boldsymbol{r}, \boldsymbol{r}') + \varepsilon K_N^{(u)}(\boldsymbol{r}, \boldsymbol{r}'), \tag{C.27}$$

where

$$K_H^{(u)}(\boldsymbol{r}, \boldsymbol{r}') = K_T^{(u)}(\boldsymbol{r}, \boldsymbol{r}') + K_V^{(u)}(\boldsymbol{r}, \boldsymbol{r}') + K_C^{(u)}(\boldsymbol{r}, \boldsymbol{r}'). \tag{C.28}$$

The kernel $K_N^{(u)}(\boldsymbol{r}, \boldsymbol{r}')$ reads

$$\begin{aligned} K_N^{(u)}(\boldsymbol{r}, \boldsymbol{r}') &= 4\left(\frac{8}{3\pi b^2}\right)^{3/2} \exp\left(-\frac{5r^2 + 5r'^2 - 8\boldsymbol{r}\cdot\boldsymbol{r}'}{3b^2}\right) \\ &\quad -3\left(\frac{2}{\pi b^2}\right)^{3/2} \exp\left(-\frac{r^2 + r'^2}{b^2}\right). \end{aligned} \tag{C.29}$$

The kinetic-energy kernel is given by

$$\begin{aligned} K_T^{(u)}(\boldsymbol{r}, \boldsymbol{r}') = -\hbar\omega \Bigg\{ &\left(\frac{8}{3\pi b^2}\right)^{3/2} \left(13 - \frac{112(r^2 + r'^2) - 208\boldsymbol{r}\cdot\boldsymbol{r}'}{9b^2}\right) \\ &\times \exp\left(-\frac{5r^2 + 5r'^2 - 8\boldsymbol{r}\cdot\boldsymbol{r}'}{3b^2}\right) \\ &- \left(\frac{2}{\pi b^2}\right)^{3/2} \left(\frac{27}{4} - 3\frac{r^2 + r'^2}{b^2}\right) \exp\left(-\frac{r^2 + r'^2}{b^2}\right) \Bigg\}, \end{aligned} \tag{C.30}$$

where $\omega = \hbar/(m_N b^2)$. The Coulomb interaction leads to the following kernel:

$$\begin{aligned} K_C^{(u)}(\boldsymbol{r},\boldsymbol{r}') &= e^2\left(\frac{8}{3\pi b^2}\right)^{3/2}\exp\left(-\frac{r^2+r'^2}{3b^2}\right)\exp\left(-\frac{4(\boldsymbol{r}-\boldsymbol{r}')^2}{3b^2}\right) \\ &\quad\times\left[4\left(\frac{2}{\pi b^2}\right)^{1/2}-\frac{1}{|\boldsymbol{r}-\boldsymbol{r}'|}-15\frac{\mathrm{erf}(\frac{1}{\sqrt{3}b}|\boldsymbol{r}+\boldsymbol{r}'|)}{|\boldsymbol{r}+\boldsymbol{r}'|}\right. \\ &\quad\left.-6\frac{\mathrm{erf}(\frac{1}{\sqrt{3}b}|2\boldsymbol{r}-\boldsymbol{r}'|)}{|2\boldsymbol{r}-\boldsymbol{r}'|}-6\frac{\mathrm{erf}(\frac{1}{\sqrt{3}b}|\boldsymbol{r}-2\boldsymbol{r}'|)}{|\boldsymbol{r}-2\boldsymbol{r}'|}\right] \\ &\quad+4e^2\left(\frac{2}{\pi b^2}\right)^{3/2}\exp\left(-\frac{r^2+r'^2}{b^2}\right)\left[2\frac{\mathrm{erf}(\frac{1}{b}|\boldsymbol{r}-\boldsymbol{r}'|)}{|\boldsymbol{r}-\boldsymbol{r}'|}\right. \\ &\quad\left.-\left(\frac{2}{\pi b^2}\right)^{1/2}+\frac{\mathrm{erf}(\frac{\sqrt{2}r}{\sqrt{3}b})}{r}+\frac{\mathrm{erf}(\frac{\sqrt{2}r'}{\sqrt{3}b})}{r'}\right]. \end{aligned} \tag{C.31}$$

The nuclear potential (C.1) leads to

$$\begin{aligned} K_V^{(u)}(\boldsymbol{r},\boldsymbol{r}') &= \sum_{n=1}^{N}V_{0n}\left(\frac{8}{3\pi b^2}\right)^{3/2}\exp\left(-\frac{5r^2+5r'^2-8\boldsymbol{r}\cdot\boldsymbol{r}'}{3b^2}\right) \\ &\quad\times\left\{4(X_n^d+X_n^e)\left(\frac{a_n^2}{a_n^2+2b^2}\right)^{3/2}+2X_n^e\exp\left(-\frac{4(\boldsymbol{r}-\boldsymbol{r}')^2}{a_n^2}\right)\right. \\ &\quad-2(2X_n^d-X_n^e)\left(\frac{3a_n^2}{3a_n^2+4b^2}\right)^{3/2}\exp\left(-\frac{4(\boldsymbol{r}+\boldsymbol{r}')^2}{3(3a_n^2+4b^2)}\right) \\ &\quad-4(X^d+X_n^e)\left(\frac{3a_n^2}{3a_n^2+4b^2}\right)^{3/2} \\ &\quad\left.\times\left[\exp\left(-\frac{4(2\boldsymbol{r}-\boldsymbol{r}')^2}{3(3a_n^2+4b^2)}\right)+\exp\left(-\frac{4(\boldsymbol{r}-2\boldsymbol{r}')^2}{3(3a_n^2+4b^2)}\right)\right]\right\} \\ &+ \sum_{n=1}^{N}V_{0n}\left(\frac{2}{\pi b^2}\right)^{3/2}\exp\left(-\frac{r^2+r'^2}{b^2}\right) \\ &\quad\times\left\{2(X_n^d-2X_n^e)\left(\frac{a_n^2}{a_n^2+b^2}\right)^{3/2}\exp\left(-\frac{(\boldsymbol{r}-\boldsymbol{r}')^2}{a_n^2+b^2}\right)\right. \\ &\quad-4(X_n^d+X_n^e)\left(\frac{a_n^2}{a_n^2+2b^2}\right)^{3/2}+4(X_n^d+X_n^e)\left(\frac{2a_n^2}{2a_n^2+3b^2}\right)^{3/2} \\ &\quad\left.\times\left[\exp\left(-\frac{2r^2}{2a_n^2+3b^2}\right)+\exp\left(-\frac{2r'^2}{2a_n^2+3b^2}\right)\right]\right\}, \end{aligned} \tag{C.32}$$

where $X_n^e = 8M_n + 4H_n - 4B_n - 2W_n$.

C.4 Projection on angular momentum

In order to apply the nonlocal potentials to a given orbital angular momentum (see, e.g., equation (3.83)), the nonlocal kernels are expanded in terms of spherical harmonics as

$$K(\boldsymbol{r},\boldsymbol{r}') = \sum_{l=0}^{\infty}\sum_{m=-l}^{l} Y_l^{m*}(\Omega_{r'})\, Y_l^m(\Omega_r)\, k_l(r,r'), \tag{C.33}$$

where $\Omega_{r'}$ and Ω_r represent the directions of $\boldsymbol{r}'$ and $\boldsymbol{r}$, respectively. It follows from the addition theorem of the spherical harmonics:

$$\sum_{m=-l}^{l} Y_l^{m*}(\Omega_{r'})\, Y_l^m(\Omega_r) = \frac{2l+1}{4\pi} P_l(\cos\theta), \tag{C.34}$$

and the orthogonality property of the Legendre polynomials:

$$\int_{-1}^{+1} P_l(u) P_{l'}(u)\, du = \frac{2}{2l+1}\delta_{ll'}, \tag{C.35}$$

that the kernels $k_l(r,r')$ are given by

$$k_l(r,r') = 2\pi \int_{-1}^{+1} K(\boldsymbol{r},\boldsymbol{r}') P_l(u) du, \tag{C.36}$$

with $u = \cos\theta$, where θ is the angle between $\boldsymbol{r}$ and $\boldsymbol{r}'$. The kernels $k_l(r,r')$ are calculated from the integral (C.36).

The calculations involving exponential terms in the nonlocal kernels are carried out by using the following expansions:

$$\exp(\alpha \boldsymbol{r}\cdot\boldsymbol{r}') = \sum_{l=0}^{\infty}(2l+1) P_l(\cos\theta) i_l(\alpha r r'), \tag{C.37}$$

$$\exp(-\alpha \boldsymbol{r}\cdot\boldsymbol{r}') = \sum_{l=0}^{\infty}(-1)^l(2l+1) P_l(\cos\theta) i_l(\alpha r r'), \tag{C.38}$$

where α is any number and $i_l(x)$ is a modified spherical Bessel function (or spherical Hankel function) [44]. This gives

$$\int_{-1}^{+1} \exp(\pm|\alpha|\boldsymbol{r}\cdot\boldsymbol{r}') P_l(u) du = 2(\pm 1)^l i_l(|\alpha| r r'). \tag{C.39}$$

Thus applying relation (C.36), each exponential term leads to a modified spherical Bessel function.

For the kinetic-energy terms, we also use the following property:

$$\boldsymbol{r}\cdot\boldsymbol{r}'\exp(-\alpha\boldsymbol{r}\cdot\boldsymbol{r}') = -\frac{d}{d\alpha}\big(\exp(-\alpha\boldsymbol{r}\cdot\boldsymbol{r}')\big), \tag{C.40}$$

which leads to

$$\begin{aligned}\int_{-1}^{+1} &\boldsymbol{r}\cdot\boldsymbol{r}'\exp(-\alpha\boldsymbol{r}\cdot\boldsymbol{r}')P_l(u)du \\ &= \int_{-1}^{+1} -\frac{d}{d\alpha}\big(\exp(-\alpha\boldsymbol{r}\cdot\boldsymbol{r}')\big)P_l(u)du \\ &= 2(-1)^{l+1}\frac{di_l(\alpha rr')}{d\alpha} \qquad (C.41)\\ &= 2(-1)^{l+1}\left(rr'\,i_{l+1}(\alpha rr') + \frac{l}{\alpha}\,i_l(\alpha rr')\right), \qquad (C.42)\end{aligned}$$

where (C.41) is derived from equation (C.39), while (C.42) is an application of the recurrence relation between the modified spherical Bessel functions [44]:

$$\frac{di_l(x)}{dx} = i_{l+1}(x) + \frac{l}{x}\,i_l(x). \tag{C.43}$$

Similarly, we have

$$\int_{-1}^{+1}\boldsymbol{r}\cdot\boldsymbol{r}'\exp(\alpha\boldsymbol{r}\cdot\boldsymbol{r}')P_l(u)du = 2\left(rr'i_{l+1}(\alpha rr') + \frac{l}{\alpha}\,i_l(\alpha rr')\right). \tag{C.44}$$

The kinetic-energy kernels for the partial waves are thus calculated as linear combinations of modified spherical Bessel functions.

For the Coulomb potential terms, we use the following formula:

$$\int_{-1}^{+1}\frac{1}{|\boldsymbol{r}\pm\boldsymbol{r}'|}P_l(u)du = (\mp1)^l\frac{2}{2l+1}\,\frac{r_<^l}{r_>^{l+1}}, \tag{C.45}$$

where $r_< = \min(r,r')$ and $r_> = \max(r,r')$. This relation corresponds to the generating function of the Legendre polynomials [44].

Screened Coulomb terms are more complicated. They are calculated numerically as

$$\int_{-1}^{+1}\frac{f(|\boldsymbol{r}\pm\boldsymbol{r}'|)}{|\boldsymbol{r}\pm\boldsymbol{r}'|}P_l(u)du = \frac{(\pm1)^l}{r_>}\int_{-1}^{+1}f(r_>+vr_<)P_l\left(v-(1-v^2)\frac{r_<}{2r_>}\right)dv, \tag{C.46}$$

where v is defined by

$$\begin{aligned} r_> + v r_< &= |\boldsymbol{r} \pm \boldsymbol{r}'| = \sqrt{r^2 + r'^2 \pm 2rr'u} \\ &= \sqrt{r_>^2 + r_<^2 \pm 2r_> r_< u}, \end{aligned} \tag{C.47}$$

so that the relationship between u and v is

$$u = \pm \left(v^2 \frac{r_<}{2r_>} + v - \frac{r_<}{2r_>} \right) = \pm \left(v - (1 - v^2) \frac{r_<}{2r_>} \right), \tag{C.48}$$

and

$$\frac{du}{|\boldsymbol{r} \pm \boldsymbol{r}'|} = \frac{\pm dv}{r_>}. \tag{C.49}$$

The numerical integration over v in (C.46) is performed a Gauss-Legendre quadrature. Formulae (C.39), (C.42), (C.44), (C.45) and (C.46) allow us to calculate the nonlocal kernels for the partial waves.

Appendix D

Calculation of the mean two-body energy

Each RGM-ε potential depends on the energy of the subsystem formed by the two interacting clusters. In this appendix, we specify how the self-consistent prescription (5.27) is applied in the semi-microscopic model with the energy-dependent potentials, in the hyperspherical harmonics method. This prescription reads

$$\varepsilon_{ij} = \langle \Psi^{JM\pi} |\, T_k + V_{ij}(\varepsilon_{ij}) \,| \Psi^{JM\pi} \rangle \,, \tag{D.1}$$

where $V_{ij}(\varepsilon_{ij})$ is a RGM-ε potential and T_k is the kinetic energy of the relative motion between clusters i and j. The nonlocal kernel of the potential V_{ij} is thus $K(\varepsilon_{ij}, \boldsymbol{r}, \boldsymbol{r'})$, with ε_{ij} satisfying condition (D.1).

The value of ε_{ij} is determined iteratively as follows (see Figure D.1). We start from a guess value of ε_{ij}. We put this value in the kernel $K(\varepsilon_{ij}, \boldsymbol{r}, \boldsymbol{r'})$ of the potential. We solve the three-body Schrödinger equation (3.60) with this potential. This gives a wave function $\Psi^{JM\pi}$. With the wave function, we calculate the value of the right-hand side of equation (D.1). This provides a new value for ε_{ij}. We start again the process for this new value. In practice, a few iterations must be performed to satisfy (D.1).

Now let us specify the calculation of the mean two-body energy in the hyperspherical harmonics method [20]. Here we use the basis $\mathcal{Y}^{JM}_{\gamma K}(\Omega_{5k})$, corresponding to the Jacobi coordinate $\boldsymbol{x}_k$, because the kinetic-energy operator is

$$T_k = -\frac{\hbar^2}{2m_N} \Delta_{\boldsymbol{x}_k}. \tag{D.2}$$

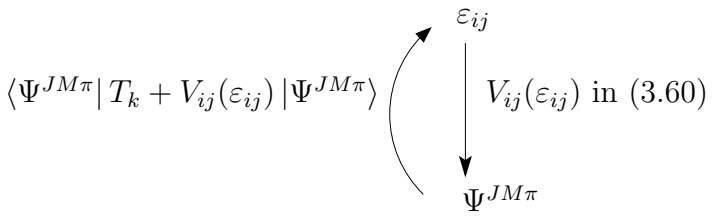

Figure D.1: Schematic representation of the iterative solution of (D.1): (i) from a given value of ε_{ij}, we calculate a wave function $\Psi^{JM\pi}$ by solving (3.60) with $V_{ij}(\varepsilon_{ij})$; (ii) from this function $\Psi^{JM\pi}$, we compute the right-hand side of (D.1), which gives us a new value for ε_{ij}; (iii) we iterate the process, until equation (D.1) is satisfied with ε_{ij}.

The wave function is expanded as

$$\Psi^{JM\pi} = \frac{1}{\rho^{5/2}} \sum_{\gamma K} \chi^{J\pi}_{\gamma K}(\rho)\, \mathcal{Y}^{JM}_{\gamma K}(\Omega_{5k}) \tag{D.3}$$

$$= \frac{1}{\sqrt{h}} \frac{1}{\rho^{5/2}} \sum_{\gamma K i} C^{JM\pi}_{\gamma K i} \hat{f}_i(\rho/h)\, \mathcal{Y}^{JM\pi}_{\gamma K}(\Omega_{5k}). \tag{D.4}$$

The calculation of the mean kinetic energy is performed from

$$\begin{aligned}
&\langle\Psi^{JM\pi}|\, T_k\,|\Psi^{JM\pi}\rangle \\
&= \frac{\hbar^2}{2m_N} \sum_{\gamma K K'} \left(\int_0^\infty y^2 dy \int_0^\infty \frac{\partial}{\partial x} \left(\frac{x\phi^{l_x l_y}_K \chi^{J\pi}_{\gamma K}}{\rho^{5/2}} \right) \frac{\partial}{\partial x} \left(\frac{x\phi^{l_x l_y}_{K'} \chi^{J\pi}_{\gamma K'}}{\rho^{5/2}} \right) dx \right. \\
&\left. + l_x(l_x+1) \int_0^{\frac{\pi}{2}} \sin^2\alpha\, \phi^{l_x l_y}_K \phi^{l_x l_y}_{K'}\, d\alpha \int_0^\infty \frac{\chi^{J\pi}_{\gamma K} \chi^{J\pi}_{\gamma K'}}{\rho^2}\, d\rho \right),
\end{aligned} \tag{D.5}$$

where $\phi^{l_x l_y}_K$ is defined by equation (3.38).

Using the expansion (D.4) of functions $\chi^{J\pi}_{\gamma K}$ in the Lagrange basis, we obtain

$$\begin{aligned}
&\langle\Psi^{JM\pi}|\, T_k\,|\Psi^{JM\pi}\rangle \\
&= \frac{\hbar^2}{2m_N h^2} \sum_{\gamma K K' i i'} \left[\frac{1}{u_i^2} \left(\frac{15}{2}\delta_{KK'} - \frac{45}{4} B_{\gamma KK'} + E_{\gamma KK'} + l_x(l_x+1) A_{\gamma KK'} \right) \delta_{ii'} \right. \\
&\left. + \hat{T}_{ii'}\, B_{\gamma KK'} - 2U_{ii'}\, D_{\gamma KK'} \right] C^{J\pi}_{\gamma K i} C^{J\pi}_{\gamma K' i'},
\end{aligned} \tag{D.6}$$

where

$$A_{\gamma KK'} = \int_0^{\frac{\pi}{2}} \sin^2\alpha\, \phi_K^{l_x l_y} \phi_{K'}^{l_x l_y} d\alpha, \tag{D.7}$$

$$B_{\gamma KK'} = \int_0^{\frac{\pi}{2}} \sin^2\alpha\, \cos^4\alpha\, \phi_K^{l_x l_y} \phi_{K'}^{l_x l_y} d\alpha, \tag{D.8}$$

$$D_{\gamma KK'} = \int_0^{\frac{\pi}{2}} \sin^3\alpha\, \cos^3\alpha\, \frac{d\phi_K^{l_x l_y}}{d\alpha}\, \phi_{K'}^{l_x l_y}\, d\alpha, \tag{D.9}$$

$$E_{\gamma KK'} = \int_0^{\frac{\pi}{2}} \sin^4\alpha\, \cos^2\alpha\, \frac{d\phi_K^{l_x l_y}}{d\alpha} \frac{d\phi_{K'}^{l_x l_y}}{d\alpha}\, d\alpha, \tag{D.10}$$

and

$$\hat{T}_{ii'} = -\int_0^{\infty} \hat{f}_i(u)\, \frac{d^2 \hat{f}_{i'}(u)}{du^2}\, du, \tag{D.11}$$

$$U_{ii'} = \int_0^{\infty} \hat{f}_i(u)\, \frac{1}{u}\, \frac{d\hat{f}_{i'}(u)}{du}\, du. \tag{D.12}$$

The matrix elements $\hat{T}_{ii'}$ and $U_{ii'}$ are evaluated with the Gauss-Laguerre quadrature. The expressions for $\hat{T}_{ii'}$ are given by equations (3.105) and (3.106). The other matrix elements read

$$U_{ii'} \approx \frac{\lambda_i^{1/2} \hat{f}'_{i'}(u_i)}{u_i} = \begin{cases} \frac{1}{2u_i^2} & \text{if } i = i', \\ \frac{(-1)^{i+i'}}{2u_{i'}(u_i - u'_i)} & \text{if } i \neq i. \end{cases} \tag{D.13}$$

The integrals $B_{\gamma KK'}$ and $D_{\gamma KK'}$ are evaluated with the help of properties of the Jacobi polynomials [90] as

$$B_{\gamma KK'} = \begin{cases} \frac{1}{2(K+2)} \sqrt{\frac{n(n+l_x+l_y+1)(2n+2l_x+1)(2n+2l_y+1)}{K(K+2)}} & \text{if } n' = n-1 \\ \frac{1}{2}\left(1 + \frac{(l_x+l_y+1)(l_x-l_y)}{(K+1)(K+3)}\right) & \text{if } n' = n \\ \frac{1}{2(K+3)} \sqrt{\frac{(n+1)(n+l_x+l_y+2)(2n+2l_x+3)(2n+2l_y+3)}{(K+2)(K+4)}} & \text{if } n' = n+1 \\ 0 & \text{otherwise} \end{cases} \tag{D.14}$$

$$D_{\gamma KK'} = \begin{cases} -\frac{K+4}{2(K+1)} \sqrt{\frac{n(n+l_x+l_y+1)(2n+2l_x+1)(2n+2l_y+1)}{K(K+2)}} & \text{if } n' = n-1 \\ \frac{3(l_x+l_y+1)(l_y-l_x)}{2(K+1)(K+3)} & \text{if } n' = n \\ \frac{K}{2(K+3)} \sqrt{\frac{(n+1)(n+l_x+l_y+2)(2n+2l_x+3)(2n+2l_y+3)}{(K+2)(K+4)}} & \text{if } n' = n+1 \\ 0 & \text{otherwise.} \end{cases} \tag{D.15}$$

where $n = (K - l_x - l_y)/2$ and $n' = (K' - l_x - l_y)/2$. The integration over α in $A_{\gamma KK'}$ and $E_{\gamma KK'}$ is performed numerically.

The expectation value of the potential energy V_{ij} is directly calculated from

$$\left\langle \Psi^{JM\pi} \right| V_{ij} \left| \Psi^{JM\pi} \right\rangle = \sum_{\gamma K i\, \gamma' K' i'} \left(V^{J\pi\,(ij-k)}_{\gamma K, \gamma' K'}(hu_i)\, \delta_{ii'} + W^{J\pi\,(ij-k)}_{\gamma K i, \gamma' K' i'} \right) C^{J\pi}_{\gamma K i}\, C^{J\pi}_{\gamma' K' i'}, \tag{D.16}$$

where $V^{J\pi(ij-k)}_{\gamma K, \gamma' K'}(hu_i)$ and $W^{J\pi(ij-k)}_{\gamma K i, \gamma' K' i'}$ are the matrix elements of the local part and nonlocal kernel of the RGM-ε potential V_{ij}, respectively, in the basis $\hat{f}_i(\rho/h)\mathcal{Y}^{JM\pi}_{\gamma K}(\Omega_{5k})$.

Appendix E

Calculation of the αn and $\alpha\alpha$ RGM-$\not{\varepsilon}$ potentials

The calculation of the energy-independent RGM potentials is presented in this appendix [22, 23, 91].

E.1 Energy-independent effective potentials

The energy-dependent nonlocal RGM potentials, which represent the αn and $\alpha\alpha$ interactions, are given in Appendix C. They have the following form:

$$(V\Psi)(\boldsymbol{r}) = V_D(r)\Psi(\boldsymbol{r}) + \int K(\varepsilon, \boldsymbol{r}, \boldsymbol{r}')\Psi(\boldsymbol{r}')\, d\boldsymbol{r}', \tag{E.1}$$

with

$$K(\varepsilon, \boldsymbol{r}, \boldsymbol{r}') = K_H(\boldsymbol{r}, \boldsymbol{r}') + \varepsilon K_N(\boldsymbol{r}, \boldsymbol{r}'). \tag{E.2}$$

Their merit is that they are directly obtained from an effective nucleon-nucleon potential by taking into account the Pauli principle between all nucleons. Nevertheless, they depend on the inter-cluster relative motion energy ε, according to equation (E.2). As shown in Chapter 7, this energy dependence can become questionable in a three-body model.

An interesting solution is then to replace the potential V by the corresponding *energy-independent* potential $\widetilde{V}$ (2.78), which reads

$$(\widetilde{V}\Psi)(\boldsymbol{r}) = V_D(r)\Psi(\boldsymbol{r}) + \int \widetilde{K}(\boldsymbol{r}, \boldsymbol{r}')\Psi(\boldsymbol{r}')\, d\boldsymbol{r}', \tag{E.3}$$

and which can be constructed from the RGM potential V [2, 29, 31, 35] by renormalising the wave function (see Equation (2.60)), as explained in Section 2.2.7. This potential $\widetilde{V}$ yields exactly the same cluster-cluster elastic

scattering phase shifts as the RGM potential V. It has also other advantages (see Sections 2.2.7 and 2.3.1) which directly result from the renormalisation (2.60) of the RGM relative-motion function.

The transformation of V into $\widetilde{V}$ requires calculations. Such calculations can be carried out [21, 22] and are given in this appendix, for the αn and $\alpha\alpha$ potentials.

Also, in the present work, comparing the semi-microscopic models, the energy-dependent potential V is referred to as the "RGM-ε potential"; the energy-independent potential $\widetilde{V}$ is then called the "RGM-$\not\varepsilon$ potential".

To determine the RGM-$\not\varepsilon$ potential $\widetilde{V}$, we must calculate the effective Hamiltonian (2.61):

$$\widetilde{\mathcal{H}} = \mathcal{N}^{-1/2}\mathcal{H}\mathcal{N}^{-1/2}, \tag{E.4}$$

where $\mathcal{H}$ and $\mathcal{N}$ are defined as

$$\mathcal{H}\Psi = -\frac{\hbar^2}{2\mu}\Delta\Psi(\boldsymbol{r}) + V_D(r)\Psi(\boldsymbol{r}) + \int K_H(\boldsymbol{r},\boldsymbol{r}')\Psi(\boldsymbol{r}')d\boldsymbol{r}', \tag{E.5}$$

$$\mathcal{N}\Psi = \Psi(\boldsymbol{r}) - \int K_N(\boldsymbol{r},\boldsymbol{r}')\Psi(\boldsymbol{r}')d\boldsymbol{r}'. \tag{E.6}$$

Such operators $\mathcal{H}$ and $\mathcal{N}$, being those of the RGM equation (2.27) [or (2.34)], contain the potential V (E.1). The Hamiltonian $\widetilde{\mathcal{H}}$ (E.4) has the following form:

$$\widetilde{\mathcal{H}}\Psi = -\frac{\hbar^2}{2\mu}\Delta\Psi(\boldsymbol{r}) + V_D(r)\Psi(\boldsymbol{r}) + \int \widetilde{K}(\boldsymbol{r},\boldsymbol{r}')\Psi(\boldsymbol{r}')d\boldsymbol{r}', \tag{E.7}$$

i.e., it is equal to the potential $\widetilde{V}$ plus the kinetic energy.

Consider the eigenvalues μ_{nl} and eigenfunctions φ_{nlm} of $\mathcal{N}$ (2.53). The operator $\mathcal{N}$ can be written as

$$\mathcal{N} = \sum_{nlm} \mu_{nl} \left|\varphi_{nlm}\right\rangle \left\langle\varphi_{nlm}\right|, \tag{E.8}$$

and the operator $\mathcal{N}^{-1/2}$ is defined as

$$\mathcal{N}^{-1/2} = \sum_{\substack{nlm \\ \mu_{nl}\neq 0}} \frac{1}{\sqrt{\mu_{nl}}} \left|\varphi_{nlm}\right\rangle \left\langle\varphi_{nlm}\right|, \tag{E.9}$$

where the sum runs over all eigenfunctions for which $\mu_{nl} \neq 0$. The eigenfunctions with $\mu_{nl} = 0$, being the Pauli forbidden states, are excluded from the sum.

The eigenfunctions and eigenvalues of $\mathcal{N}$ for the $\alpha+n$ and $\alpha+\alpha$ systems will be given below. Using equations (E.4) and (E.9), we have

$$\widetilde{\mathcal{H}} = \sum_{\substack{nlm \\ \mu_{nl}\neq 0}} \sum_{\substack{n'l'm' \\ \mu_{n'l'}\neq 0}} \frac{1}{\sqrt{\mu_{nl}\mu_{n'l'}}} \left|\varphi_{nlm}\right\rangle \left\langle\varphi_{nlm}\right| \mathcal{H} \left|\varphi_{n'l'm'}\right\rangle \left\langle\varphi_{n'l'm'}\right|. \tag{E.10}$$

This expression allows us to calculate the Hamiltonian $\widetilde{\mathcal{H}}$ (E.7), and thus to obtain the kernel $\widetilde{K}(\boldsymbol{r},\boldsymbol{r}')$. This kernel $\widetilde{K}(\boldsymbol{r},\boldsymbol{r}')$ can be written as

$$\widetilde{K}(\boldsymbol{r},\boldsymbol{r}') = K_H(\boldsymbol{r},\boldsymbol{r}') + \widetilde{K}_W(\boldsymbol{r},\boldsymbol{r}'), \tag{E.11}$$

where $\widetilde{K}_W(\boldsymbol{r},\boldsymbol{r}')$ is the only unknown function, $K_H(\boldsymbol{r},\boldsymbol{r}')$ being given in (E.2). Let $\widetilde{\mathcal{W}}$ be the difference between $\widetilde{\mathcal{H}}$ and $\mathcal{H}$,

$$\widetilde{\mathcal{W}} = \widetilde{\mathcal{H}} - \mathcal{H} = \mathcal{N}^{-1/2}\mathcal{H}\mathcal{N}^{-1/2} - \mathcal{H}. \tag{E.12}$$

We soon find that

$$\widetilde{\mathcal{W}}\Psi = \widetilde{\mathcal{H}}\Psi - \mathcal{H}\Psi = \int \widetilde{K}_W(\boldsymbol{r},\boldsymbol{r}')\Psi(\boldsymbol{r}')d\boldsymbol{r}', \tag{E.13}$$

i.e., the operator $\widetilde{\mathcal{W}}$ provides the kernel $\widetilde{K}_W(\boldsymbol{r},\boldsymbol{r}')$. Using (E.10), we have

$$\widetilde{\mathcal{W}} = \sum_{\substack{nlm \\ \mu_{nl}\neq 0}} \sum_{\substack{n'l'm' \\ \mu_{n'l'}\neq 0}} \left(\frac{1}{\sqrt{\mu_{nl}\mu_{n'l'}}} - 1\right) \left|\varphi_{nlm}\right\rangle \left\langle\varphi_{nlm}\right| \mathcal{H} \left|\varphi_{n'l'm'}\right\rangle \left\langle\varphi_{n'l'm'}\right|. \tag{E.14}$$

Therefore [21, 22]

$$\widetilde{K}_W(\boldsymbol{r},\boldsymbol{r}') = \sum_{\substack{nlm \\ \mu_{nl}\neq 0}} \sum_{\substack{n'l'm' \\ \mu_{n'l'}\neq 0}} \left(\frac{1}{\sqrt{\mu_{nl}\mu_{n'l'}}} - 1\right) \left\langle\varphi_{nlm}\right| \mathcal{H} \left|\varphi_{n'l'm'}\right\rangle \varphi_{nlm}(\boldsymbol{r})\varphi^*_{n'l'm'}(\boldsymbol{r}'). \tag{E.15}$$

The sums in equations (E.14) and (E.15) run over all eigenstates which are not Pauli forbidden states. Thus, the kernel $\widetilde{K}_W(\boldsymbol{r},\boldsymbol{r}')$ can be calculated provided that (i) the eigenvalues μ_{nl} and eigenfunctions $\varphi_{nlm}(\boldsymbol{r})$ are known and (ii) the matrix elements $\left\langle\varphi_{nlm}\right| \mathcal{H} \left|\varphi_{n'l'm'}\right\rangle$ are calculated. The potential $\widetilde{V}$ (E.3) then becomes entirely determined, using equations (E.11) and (E.15).

The eigenvalues μ_{nl} and eigenfunctions $\varphi_{nlm}(\boldsymbol{r})$ are given for the $\alpha+n$ and $\alpha+\alpha$ systems in the next section. Formulae [21, 92] to calculate the matrix elements $\left\langle\varphi_{nlm}\right| \mathcal{H} \left|\varphi_{n'l'm'}\right\rangle$ from the RGM potential V (E.1) will be given in Section E.3.

The potential $\widetilde{V}$ is simply calculated by evaluating numerically the expansion (E.15). In practice, a finite number of eigenstates $\varphi_{nlm}(\boldsymbol{r})$ is used in our calculations. For each value of l, the kernel $\widetilde{K}_W(\boldsymbol{r},\boldsymbol{r}')$ is computed for n and n' varying from 0 to 20 typically.

The shapes of the kernels $\widetilde{K}_W(\boldsymbol{r},\boldsymbol{r}')$ and $K_H(\boldsymbol{r},\boldsymbol{r}')$ are in fact very different from each other, as graphically shown in Ref. [22] for the $\alpha+\alpha$ case with the MN force (5.8), for the partial waves $l=0,2$ and 4. In particular, $\widetilde{K}_W(\boldsymbol{r},\boldsymbol{r}')$ is found to be smaller by about one order of magnitude than $K_H(\boldsymbol{r},\boldsymbol{r}')$, on average, but is not negligible at all.

E.2 Eigenvalues and eigenstates for the $\alpha+n$ and $\alpha+\alpha$ systems

In order to calculate the kernel $\widetilde{K}_W(\boldsymbol{r},\boldsymbol{r}')$ (E.15), the eigenvalues and eigenfunctions of $\mathcal{N}$ (E.8) must be determined. They are well known [2,29,34] for the $\alpha+n$ and $\alpha+\alpha$ systems. They coincide with harmonic oscillator states owing to the Gaussian α-cluster internal wave functions (2.6) in the RGM. The eigenvalues are

$$\mu_{nl}=1-\left(-\frac{1}{4}\right)^{2n+l}, \tag{E.16}$$

for $\alpha+n$, and

$$\mu_{nl}=1-4\left(\frac{1}{2}\right)^{2n+l}+3\delta_{2n+l,0}\quad\text{with } l \text{ even}, \tag{E.17}$$

for $\alpha+\alpha$. Otherwise, $\mu_{nl}=0$ for l odd for $\alpha+\alpha$. In other words, all odd waves are Pauli forbidden states for the $\alpha+\alpha$ relative motion. In both $\alpha+n$ and $\alpha+\alpha$ systems, the eigenstates $\varphi_{nlm}(\boldsymbol{r})$ are given by three-dimensional harmonic-oscillator wave functions [2,29,34], i.e.,

$$\varphi_{nlm}(\boldsymbol{r})=(-1)^n\left[\frac{n!2\left(\frac{\mu}{b^2}\right)^{l+3/2}}{\Gamma(n+l+3/2)}\right]^{1/2} r^l L_n^{(l+1/2)}\left(\frac{\mu r^2}{b^2}\right)\exp\left(-\frac{\mu r^2}{2b^2}\right)Y_l^m(\Omega_r), \tag{E.18}$$

where $L_n^{(\alpha)}(x)$ is a generalised Laguerre polynomial, μ is the reduced mass (2.32) of the two clusters (in nucleon mass unit m_N), and b is the oscillator parameter of the α-clusters (2.6). Here the reduced masses are $\mu=4/5$ for $\alpha+n$ and $\mu=2$ for $\alpha+\alpha$.

The Pauli forbidden states correspond to $\mu_{nl}=0$. Therefore, for $\alpha+n$, there is only one Pauli forbidden state, which is φ_{000}. For $\alpha+\alpha$, the quantum number l must be even, and the Pauli forbiden states are the waves φ_{000}, φ_{100} and φ_{02m}, plus all odd waves.

E.3 Calculation of the matrix elements

Here we will provide formulae to calculate the matrix elements $\langle\varphi_{nlm}|\,\mathcal{H}\,|\varphi_{n'l'm'}\rangle$, where φ_{nlm} are harmonic-oscillator eigenfunctions (E.18) and $\mathcal{H}$, represented by equation (E.5), contains local and nonlocal terms. We can split this Hamiltonian $\mathcal{H}$ into three distinct operators:

$$\mathcal{H} = \widehat{T} + \widehat{V}_D + \widehat{K}_H, \tag{E.19}$$

where $\widehat{T}$ stands for the inter-cluster relative motion kinetic energy, $\widehat{V}_D$ and $\widehat{K}_H$ stand for the local and nonlocal potential terms, respectively. We have thus

$$\langle\varphi_{nlm}|\,\mathcal{H}\,|\varphi_{n'l'm'}\rangle = \langle\varphi_{nlm}|\,\widehat{T} + \widehat{V}_D + \widehat{K}_H\,|\varphi_{n'l'm'}\rangle \tag{E.20}$$

where

$$\langle\varphi_{nlm}|\,\widehat{T}\,|\varphi_{n'l'm'}\rangle = \frac{\hbar^2}{2\mu}\int \varphi^*_{nlm}(\boldsymbol{r})\Delta\varphi_{n'l'm'}(\boldsymbol{r})\,d\boldsymbol{r} \tag{E.21}$$

$$\langle\varphi_{nlm}|\,\widehat{V}_D\,|\varphi_{n'l'm'}\rangle = \int \varphi^*_{nlm}(\boldsymbol{r})V_D(r)\varphi_{n'l'm'}(\boldsymbol{r})\,d\boldsymbol{r} \tag{E.22}$$

$$\langle\varphi_{nlm}|\,\widehat{K}_H\,|\varphi_{n'l'm'}\rangle = \iint \varphi^*_{nlm}(\boldsymbol{r})K_H(\boldsymbol{r},\boldsymbol{r}')\varphi_{n'l'm'}(\boldsymbol{r}')\,d\boldsymbol{r}'d\boldsymbol{r}. \tag{E.23}$$

The expressions of the local and nonlocal functions V_D and K_H for the $\alpha+n$ and $\alpha+\alpha$ systems can be found in Appendix C.

We will first give the matrix elements of the kinetic-energy operator. Then we will give formulae to calculate the matrix elements of the potentials. Such formulae will be derived using the generating function of the harmonic-oscillator functions [92].

E.3.1 Kinetic energy terms

The matrix elements of the kinetic-energy operator are

$$\langle\varphi_{nlm}|\,\widehat{T}\,|\varphi_{n'l'm'}\rangle = \langle\varphi_{nlm}|\,\widehat{T}\,|\varphi_{n'lm}\rangle\,\delta_{ll'}\delta_{mm'}, \tag{E.24}$$

with

$$\langle\varphi_{nlm}|\,\widehat{T}\,|\varphi_{n'lm}\rangle = \frac{\hbar\omega}{2}\times\begin{cases}\left(2n+l+\frac{3}{2}\right) & \text{if } n=n'\\ -\sqrt{(n+1)\left(n+l+\frac{3}{2}\right)} & \text{if } n=n'-1\\ -\sqrt{n\left(n+l+\frac{1}{2}\right)} & \text{if } n=n'+1\\ 0 & \text{otherwise,}\end{cases} \tag{E.25}$$

where $\omega = \hbar/(m_N b^2)$ is the pulsation associated with the harmonic-oscillator basis (E.18). This formula can be obtained as follows. Let ν be defined as

$$\nu = \mu/b^2, \tag{E.26}$$

μ being either 4/5 or 2 for $\alpha + n$ and $\alpha + \alpha$, respectively. According to their definition (E.18) and to the recurrence relations of the Laguerre polynomials [44], the wave functions φ_{nlm} satisfy

$$\begin{aligned}\nu r^2 \varphi_{nlm}(\boldsymbol{r}) = \left(2n + l + \tfrac{3}{2}\right) \varphi_{nlm}(\boldsymbol{r}) + \sqrt{n\left(n + l + \tfrac{1}{2}\right)}\varphi_{n-1lm}(\boldsymbol{r}) \\ + \sqrt{(n+1)\left(n + l + \tfrac{3}{2}\right)}\varphi_{n+1lm}(\boldsymbol{r}).\end{aligned} \tag{E.27}$$

Moreover, since they are oscillator eigenfunctions, they are known to satisfy

$$\langle \varphi_{nlm} | \, \widehat{T} + V_{HO} \, | \varphi_{n'l'm'} \rangle = \left(2n + l + \frac{3}{2}\right) \hbar\omega \, \delta_{nn'} \delta_{ll'} \delta_{mm'}, \tag{E.28}$$

where

$$V_{HO} = \frac{1}{2}\mu m_N \omega^2 r^2 = \frac{\hbar\omega}{2}\left(\frac{\mu r^2}{b^2}\right) = \frac{\hbar\omega}{2}\nu r^2 \tag{E.29}$$

is the corresponding harmonic-oscillator potential. The formula (E.25) is simply obtained by inserting (E.29) and (E.27) in the property (E.28).

E.3.2 Local potential terms

The matrix elements of the potentials are obtained by making use of the generating function of the harmonic-oscillator wave functions. The generating function [92, 93] is

$$F(\boldsymbol{k}, \boldsymbol{r}) = \left(\frac{\nu}{\pi}\right)^{3/4} \exp\left(-\frac{1}{2}k^2 + \sqrt{2\nu}\boldsymbol{k}\cdot\boldsymbol{r} - \frac{1}{2}\nu r^2\right) \tag{E.30}$$

$$= \sum_{nlm} \varphi^*_{nlm}(\boldsymbol{r}) P_{nlm}(\boldsymbol{k}), \tag{E.31}$$

where ν is the oscillator constant (E.26) and $P_{nlm}(\boldsymbol{k})$ is defined as

$$P_{nlm}(\boldsymbol{k}) = \sqrt{a_{nl}}\, k^{2n+l}\, Y_l^m(\Omega_k), \tag{E.32}$$

with the coefficient

$$a_{nl} = \frac{4\pi}{2^n n!(2n+2l+1)!!}. \tag{E.33}$$

The matrix elements (E.22) of the local potentials are determined by calculating the integral

$$\mathcal{I} = \int F(\boldsymbol{k}, \boldsymbol{r}) V_D(r) F(\boldsymbol{k}', \boldsymbol{r})\, d\boldsymbol{r}, \tag{E.34}$$

involving the generating functions (E.30). Substituting the expansion (E.31) for the generating functions in equation (E.34) yields

$$\mathcal{I} = \sum_{nlm} \sum_{n'l'm'} \langle \varphi_{nlm} | \, \widehat{V}_D \, | \varphi_{n'l'm'} \rangle \, P_{nlm}(\boldsymbol{k}) P^*_{n'l'm'}(\boldsymbol{k}'). \tag{E.35}$$

Thus, first the integral (E.34) is calculated. Then the result is simply expanded in power series of $\boldsymbol{k}$ and $\boldsymbol{k}'$ (using spherical harmonics for the directions of the vectors). By comparing the expansion with (E.35), the values of the matrix elements $\langle \varphi_{nlm} | \, \widehat{V}_D \, | \varphi_{n'l'm'} \rangle$ are found.

The local terms $V_D(r)$, in the $\alpha{+}n$ and $\alpha{+}\alpha$ potentials (see Appendix C), are linear combinations of Gaussian functions, plus the Coulomb interaction for $\alpha + \alpha$. Considering thus $V_D(r) = Ce^{-\eta r^2}$ in the integral (E.34), after calculations, we have

$$\mathcal{I} = C \left(\frac{\nu}{\nu + \eta} \right)^{3/2} e^{pk^2 + p'k'^2 + q\boldsymbol{k}\cdot\boldsymbol{k}'} \tag{E.36}$$

with

$$p = p' = -\frac{1}{2} + \frac{\nu}{2(\nu + \eta)}, \tag{E.37}$$

$$q = \frac{\nu}{\nu + \eta}. \tag{E.38}$$

Expanding this result (E.36) in series of k and k', with the help of the identities (C.37), (C.34) and

$$i_l(x) = \sum_{n=0}^{\infty} \frac{x^{2n+l}}{2^n n! (2n + 2l + 1)!!}, \tag{E.39}$$

we soon find the following matrix element:

$$\langle \varphi_{nlm} | \, Ce^{-\eta r^2} \, | \varphi_{n'l'm'} \rangle = \delta_{ll'} \, \delta_{mm'} \, C \left(\frac{\nu}{\nu + \eta} \right)^{3/2} \frac{1}{\sqrt{a_{nl} a_{n'l}}} \times \sum_{\sigma=0}^{\min(n,n')} a_{\sigma l} \frac{p^{n-\sigma} p'^{n'-\sigma} q^{2\sigma+l}}{(n-\sigma)!(n'-\sigma)!}. \tag{E.40}$$

This formula enables us to calculate the matrix elements of the Gaussian terms of the local potentials.

Now, consider the Coulomb term $\mathrm{erf}(\gamma r)/r$, occuring in the $\alpha+\alpha$ interaction. The corresponding integral (E.34) to be calculated is

$$\mathcal{I} = \int F(\boldsymbol{k},\boldsymbol{r})\frac{\mathrm{erf}(\gamma r)}{r}F(\boldsymbol{k}',\boldsymbol{r})\,d\boldsymbol{r} \tag{E.41}$$

Let $M(z)$ be a function defined as

$$M(z) = \int_0^1 e^{-z^2t^2}dt = \frac{\sqrt{\pi}}{2}\frac{1}{z}\mathrm{erf}(z). \tag{E.42}$$

The identity (E.42) can be used in equation (E.41) to replace $\mathrm{erf}(\gamma r)/r$ by an integral of a Gaussian function in the interval $[0,1]$. The integral over $\boldsymbol{r}$ of a Gaussian function between two generating functions can be calculated exactly as in the previous case. The integral over $\boldsymbol{r}$ is thus carried out. Then the following mathematical identity

$$\int_0^1 \frac{1}{(t^2+c)^{3/2}}\exp\left(\frac{d}{t^2+c}\right)dt = \frac{1}{c\sqrt{c+1}}\exp\left(\frac{d}{c}\right)M\left(\sqrt{\frac{d}{c(c+1)}}\right), \tag{E.43}$$

where c and d are constants, can be used. To prove formula (E.43) one just makes a change of integration variable $t \to u$ with

$$t = \frac{\sqrt{c}\,u}{\sqrt{\frac{d}{c}-u^2}}.$$

Using equations (E.42) and (E.43), the integral (E.41), after calculations, is found to be

$$\mathcal{I} = 2\left(\frac{2\nu\zeta}{\pi}\right)^{1/2} e^{\boldsymbol{k}\cdot\boldsymbol{k}'}M\left(\sqrt{\zeta}\,|\boldsymbol{k}+\boldsymbol{k}'|\right) \tag{E.44}$$

with

$$\zeta = \frac{\gamma^2}{2(\nu+\gamma^2)}. \tag{E.45}$$

Noting that the function M is an integral of a Gaussian function, one deduces from the expansion (E.40) that

$$\begin{aligned}\langle\varphi_{nlm}|\,\frac{\mathrm{erf}(\gamma r)}{r}\,|\varphi_{n'l'm'}\rangle = \delta_{ll'}\,\delta_{mm'}\,2\left(\frac{2\nu\zeta}{\pi}\right)^{1/2}\frac{1}{\sqrt{a_{nl}a_{n'l}}}\\ \times\sum_{\sigma=0}^{\min(n,n')}a_{\sigma l}\frac{1}{(n-\sigma)!(n'-\sigma)!}\int_0^1 p^{n-\sigma}p^{n'-\sigma}q^{2\sigma+l}dt,\end{aligned} \tag{E.46}$$

where

$$p = -\zeta t^2 \tag{E.47}$$
$$q = 1 - 2\zeta t^2. \tag{E.48}$$

The formula (E.46) gives the value of the matrix element of the local Coulomb term (C.23) in the $\alpha + \alpha$ potential.

E.3.3 Nonlocal potential terms

The matrix elements (E.23) of the nonlocal potentials are calculated by using the same method [21, 92] as above for the local potentials.

The expression of the kernel $K_H(\boldsymbol{r}, \boldsymbol{r}')$, for the $\alpha+n$ and $\alpha+\alpha$ potentials, being rather long (see Appendix C), here we will use a matrix notation (see Ref. [92]) in order to simplify the formulae and the calculations.

We define a 2×1 matrix $\boldsymbol{v}$ whose elements are $\boldsymbol{r}$ and $\boldsymbol{r}'$ and $\bar{\boldsymbol{v}}$ its transpose,

$$\boldsymbol{v} = \begin{pmatrix} \boldsymbol{r} \\ \boldsymbol{r}' \end{pmatrix}, \qquad \bar{\boldsymbol{v}} = \begin{pmatrix} \boldsymbol{r} & \boldsymbol{r}' \end{pmatrix}. \tag{E.49}$$

All linear combinations and quadratic forms involving $\boldsymbol{r}$ and $\boldsymbol{r}'$ can be written as matrix products.

In particular, the kernel $K_H(\boldsymbol{r}, \boldsymbol{r}')$ can be expressed as a sum of several simple terms:

$$K_H(\boldsymbol{r}, \boldsymbol{r}') = \sum_i \mathcal{O}_i(\boldsymbol{r}, \boldsymbol{r}'). \tag{E.50}$$

The relevant expressions of $\mathcal{O}_i(\boldsymbol{r}, \boldsymbol{r}')$ (see Appendix C) are as follows. They are typically of the form

$$\mathcal{O}_i(\boldsymbol{r}, \boldsymbol{r}') = \exp\left(-\frac{1}{2}\bar{\boldsymbol{v}} A \boldsymbol{v}\right), \tag{E.51}$$

$$\mathcal{O}_i(\boldsymbol{r}, \boldsymbol{r}') = \bar{\boldsymbol{v}} Q \boldsymbol{v} \exp\left(-\frac{1}{2}\bar{\boldsymbol{v}} A \boldsymbol{v}\right), \tag{E.52}$$

or, for Coulomb terms,

$$\mathcal{O}_i(\boldsymbol{r}, \boldsymbol{r}') = f(|\bar{\omega}\boldsymbol{v}|) \exp\left(-\frac{1}{2}\bar{\boldsymbol{v}} A \boldsymbol{v}\right), \tag{E.53}$$

where $f(s)$ is either $1/s$ or $\mathrm{erf}(\gamma s)/s$. Here, use is made of the matrix notation: A and Q are 2×2 symmetric matrices, which represent quadratic forms in $\boldsymbol{r}$ and $\boldsymbol{r}'$, and $\bar{\omega} = \begin{pmatrix}\omega_1 & \omega_2\end{pmatrix}$ is a 1×2 matrix, representing a linear combination. In other words, the above formal expressions must be interpreted as

$$\exp\left(-\frac{1}{2}\bar{\boldsymbol{v}}A\boldsymbol{v}\right) = \exp\left(-\frac{1}{2}\left(a_{11}r^2 + a_{22}r'^2 + 2a_{12}\boldsymbol{r}\cdot\boldsymbol{r}'\right)\right), \quad \text{(E.54)}$$

$$\bar{\boldsymbol{v}}Q\boldsymbol{v} = q_{11}r^2 + q_{22}r'^2 + 2q_{12}\boldsymbol{r}\cdot\boldsymbol{r}', \quad \text{(E.55)}$$

$$\bar{\omega}\boldsymbol{v} = \omega_1\boldsymbol{r} + \omega_2\boldsymbol{r}', \quad \text{(E.56)}$$

where the coefficients a_{ij} and q_{ij} are the elements of matrices A and Q, respectively. The matrix $\bar{\omega}$ contains the coefficients ω_1 and ω_2 of a linear combination. The symbol ω will represent the transpose of the matrix $\bar{\omega}$ (i.e., ω will mean a one-column 2×1 matrix whose elements are ω_1 and ω_2).

Because of equation (E.50), we have

$$\langle\varphi_{nlm}|\,\widehat{K}_H\,|\varphi_{n'l'm'}\rangle = \sum_i \langle\varphi_{nlm}|\,\widehat{\mathcal{O}}_i\,|\varphi_{n'l'm'}\rangle\,, \quad \text{(E.57)}$$

with

$$\langle\varphi_{nlm}|\,\widehat{\mathcal{O}}_i\,|\varphi_{n'l'm'}\rangle = \iint \varphi^*_{nlm}(\boldsymbol{r})\mathcal{O}_i(\boldsymbol{r},\boldsymbol{r}')\varphi_{n'l'm'}(\boldsymbol{r}')\,d\boldsymbol{r}'d\boldsymbol{r}. \quad \text{(E.58)}$$

The exact values of $\langle\varphi_{nlm}|\,\widehat{\mathcal{O}}_i\,|\varphi_{n'l'm'}\rangle$ are obtained by determining the integral

$$\mathcal{I} = \iint F(\boldsymbol{k},\boldsymbol{r})\mathcal{O}_i(\boldsymbol{r},\boldsymbol{r}')F(\boldsymbol{k}',\boldsymbol{r}')d\boldsymbol{r}d\boldsymbol{r}', \quad \text{(E.59)}$$

which is equal to the expansion

$$\mathcal{I} = \sum_{nlm}\sum_{n'l'm'} \langle\varphi_{nlm}|\,\widehat{\mathcal{O}}_i\,|\varphi_{n'lm}\rangle\,P_{nlm}(\boldsymbol{k})P^*_{n'l'm'}(\boldsymbol{k}'), \quad \text{(E.60)}$$

according to equation (E.31).

All needed formulae to calculate (E.59) for the operators (E.51) (E.52) and (E.53), are tabulated in Ref. [92].

First, for $\mathcal{O}_i(\boldsymbol{r},\boldsymbol{r}') = \exp\left(-\frac{1}{2}\bar{\boldsymbol{v}}A\boldsymbol{v}\right)$, then

$$\mathcal{I} = \left(\frac{4\pi\nu}{\det(A+C)}\right)^{3/2} e^{pk^2+p'k'^2+q\boldsymbol{k}\cdot\boldsymbol{k}'}, \quad \text{(E.61)}$$

where C is a 2×2 diagonal matrix with $C_{ij} = \nu\delta_{ij}$ and

$$p = -\frac{1}{2} + \nu\{(A+C)^{-1}\}_{11} \tag{E.62}$$
$$p' = -\frac{1}{2} + \nu\{(A+C)^{-1}\}_{22} \tag{E.63}$$
$$q = 2\nu\{(A+C)^{-1}\}_{12}. \tag{E.64}$$

The expression of $\mathcal{I}$ being strictly similar to (E.36), we have the matrix element

$$\langle\varphi_{nlm}|\, e^{-\frac{1}{2}\bar{\boldsymbol{v}}A\boldsymbol{v}}\,|\varphi_{n'l'm'}\rangle = \delta_{ll'}\,\delta_{mm'}\left(\frac{4\pi\nu}{\det(A+C)}\right)^{3/2}\frac{1}{\sqrt{a_{nl}a_{n'l}}} \times \sum_{\sigma=0}^{\min(n,n')} a_{\sigma l}\frac{p^{n-\sigma}p'^{n'-\sigma}q^{2\sigma+l}}{(n-\sigma)!(n'-\sigma)!}, \tag{E.65}$$

for each term (E.54) in the kernel $K_H(\boldsymbol{r},\boldsymbol{r})$.

For $\mathcal{O}_i(\boldsymbol{r},\boldsymbol{r}') = \bar{\boldsymbol{v}}Q\boldsymbol{v}\exp\left(-\frac{1}{2}\bar{\boldsymbol{v}}A\boldsymbol{v}\right)$, the result is

$$\mathcal{I} = \left(\frac{4\pi\nu}{\det(A+C)}\right)^{3/2} e^{pk^2+p'k'^2+q\boldsymbol{k}\cdot\boldsymbol{k}'}(s + tk^2 + t'k'^2 + u\boldsymbol{k}\cdot\boldsymbol{k}') \tag{E.66}$$

where

$$s = 3\mathrm{Tr}\{(A+C)^{-1}Q\} \tag{E.67}$$
$$t' = 2\nu\{(A+C)^{-1}Q(A+C)^{-1}\}_{11} \tag{E.68}$$
$$t' = 2\nu\{(A+C)^{-1}Q(A+C)^{-1}\}_{22} \tag{E.69}$$
$$u' = 4\nu\{(A+C)^{-1}Q(A+C)^{-1}\}_{12}, \tag{E.70}$$

p, p' and q being the same as in the previous case (E.61). Therefore we have

$$\langle\varphi_{nlm}|\,\bar{\boldsymbol{v}}Q\boldsymbol{v}e^{-\frac{1}{2}\bar{\boldsymbol{v}}A\boldsymbol{v}}\,|\varphi_{n'l'm'}\rangle = \delta_{ll'}\,\delta_{mm'}\left(\frac{4\pi\nu}{\det(A+C)}\right)^{3/2}\frac{1}{\sqrt{a_{nl}a_{n'l}}} \times \sum_{\sigma=0}^{\min(n,n')} (spp'q + (n-\sigma)tp'q + (n'-\sigma)t'pq + (2\sigma+l)upp') \times a_{\sigma l}\frac{p^{n-\sigma-1}p'^{n'-\sigma-1}q^{2\sigma+l-1}}{(n-\sigma)!(n'-\sigma)!}. \tag{E.71}$$

The Coulomb terms $\mathcal{O}_i(\boldsymbol{r},\boldsymbol{r}') = f(|\bar{\omega}\boldsymbol{v}|)\exp\left(-\frac{1}{2}\bar{\boldsymbol{v}}A\boldsymbol{v}\right)$ are calculated as follows. With the help of Ref. [92],

$$\mathcal{I} = \iint F(\boldsymbol{k},\boldsymbol{r}) f(|\bar{\omega}\boldsymbol{v}|)\exp\left(-\frac{1}{2}\bar{\boldsymbol{v}}A\boldsymbol{v}\right) F(\boldsymbol{k}',\boldsymbol{r}')d\boldsymbol{r}d\boldsymbol{r}', \tag{E.72}$$

is found to be

$$\begin{aligned}\mathcal{I} = &\left(\frac{4\pi\nu}{\det(A+C)}\right)^{3/2} e^{pk^2+p'k'^2+q\boldsymbol{k}\cdot\boldsymbol{k}'} \times \left(\frac{\tau}{2\pi}\right)^{3/2} e^{-\tau\nu(\rho_1\boldsymbol{k}+\rho_2\boldsymbol{k}')^2} \\ &\times \int f(s)\exp\left[-\frac{1}{2}\tau s^2 + \sqrt{2\nu}\tau(\rho_1\boldsymbol{k}+\rho_2\boldsymbol{k}')\cdot\boldsymbol{s}\right] d\boldsymbol{s},\end{aligned} \tag{E.73}$$

where p, p' and q are the same as previously and

$$\rho_1 = \omega_1\{(A+C)^{-1}\}_{11} + \omega_2\{(A+C)^{-1}\}_{21} \tag{E.74}$$

$$\rho_2 = \omega_1\{(A+C)^{-1}\}_{12} + \omega_2\{(A+C)^{-1}\}_{22} \tag{E.75}$$

$$\tau = (\rho_1\omega_1 + \rho_2\omega_2)^{-1} = \left(\bar{\omega}(A+C)^{-1}\omega\right)^{-1}. \tag{E.76}$$

Considering the case $f(s) = 1/s$, we have

$$\begin{aligned}&\int \frac{1}{s}\exp\left[-\frac{1}{2}\tau s^2 + \sqrt{2\nu}\tau(\rho_1\boldsymbol{k}+\rho_2\boldsymbol{k}')\cdot\boldsymbol{s}\right] d\boldsymbol{s} \\ &= \frac{4\pi}{\tau} e^{\tau\nu(\rho_1\boldsymbol{k}+\rho_2\boldsymbol{k}')^2} M(\sqrt{\nu\tau}|\rho_1\boldsymbol{k}+\rho_2\boldsymbol{k}'|),\end{aligned} \tag{E.77}$$

where the function M is defined by equation (E.42). Thus

$$\mathcal{I} = \left(\frac{4\pi\nu}{\det(A+C)}\right)^{3/2} e^{pk^2+p'k'^2+q\boldsymbol{k}\cdot\boldsymbol{k}'}\sqrt{\frac{2\tau}{\pi}} M(\sqrt{\nu\tau}|\rho_1\boldsymbol{k}+\rho_2\boldsymbol{k}'|), \tag{E.78}$$

which is similar to case (E.44). Using equation (E.42), we can write the function M as an integral of a Gaussian funtion in the interval $[0,1]$ and then employ the previous results for (E.61). Therefore we get the formula

$$\begin{aligned}\langle\varphi_{nlm}|\frac{1}{|\bar{\omega}\boldsymbol{v}|}e^{-\frac{1}{2}\bar{\boldsymbol{v}}A\boldsymbol{v}}|\varphi_{n'l'm'}\rangle = \delta_{ll'}\,\delta_{mm'}&\left(\frac{4\pi\nu}{\det(A+C)}\right)^{3/2}\sqrt{\frac{2\tau}{\pi}}\frac{1}{\sqrt{a_{nl}a_{n'l}}} \\ &\times \sum_{\sigma=0}^{\min(n,n')} a_{\sigma l}\frac{1}{(n-\sigma)!(n'-\sigma)!}\int_0^1 p_1^{n-\sigma}p_2^{n'-\sigma}p_{12}^{2\sigma+l}dt.\end{aligned} \tag{E.79}$$

where

$$p_1 = p - \tau\nu\rho_1^2t^2, \tag{E.80}$$

$$p_2 = p' - \tau\nu\rho_2^2t^2, \tag{E.81}$$

$$p_{12} = q - 2\tau\nu\rho_1\rho_2t^2. \tag{E.82}$$

The last case to consider is $f(s) = \mathrm{erf}(\gamma s)/s$ in equation (E.73). The integral is calculated as

$$\int \mathrm{erf}(\gamma s)\frac{1}{s}\exp\left[-\frac{1}{2}\tau s^2 + \sqrt{2\nu}\tau(\rho_1\boldsymbol{k} + \rho_2\boldsymbol{k}')\cdot\boldsymbol{s}\right] d\boldsymbol{s}$$

$$= \frac{2\pi}{\gamma^2}\int_0^1 \frac{1}{(t^2+c)^{3/2}}\exp\left(\frac{d}{t^2+c}\right) dt \tag{E.83}$$

$$= \frac{2\pi}{\gamma^2}\frac{1}{c\sqrt{c+1}}\exp\left(\frac{d}{c}\right) M\left(\sqrt{\frac{d}{c(c+1)}}\right), \tag{E.84}$$

with

$$c = \frac{\tau}{2\gamma^2}, \qquad d = \frac{\nu\tau^2}{2\gamma^2}(\rho_1\boldsymbol{k} + \rho_2\boldsymbol{k}')^2. \tag{E.85}$$

The integral (E.83) over t can be obtained by first expressing $\mathrm{erf}(\gamma s)/s$ as an integral using (E.42), and then calculating the integral over $\boldsymbol{s}$. The identity (E.43) yields the result (E.84). Therefore, substituting this result into equation (E.61), we have

$$\mathcal{I} = \left(\frac{4\pi\nu}{\det(A+C)}\right)^{3/2} e^{pk^2 + p'k'^2 + q\boldsymbol{k}\cdot\boldsymbol{k}'}\sqrt{\frac{2\tau\xi}{\pi}} M(\sqrt{\nu\tau\xi}|\rho_1\boldsymbol{k} + \rho_2\boldsymbol{k}'|), \tag{E.86}$$

where

$$\xi = \frac{2\gamma^2}{2\gamma^2 + \tau}. \tag{E.87}$$

Note that the result (E.86) is actually similar to the previous case (E.78). To obtain (E.86) from (E.78), we can simply replace τ in (E.78) by $\tau\xi$. Replacing τ by $\tau\xi$ in equation (E.79), we have

$$\langle\varphi_{nlm}|\frac{\mathrm{erf}(\gamma|\bar{\omega}\boldsymbol{v}|)}{|\bar{\omega}\boldsymbol{v}|}e^{-\frac{1}{2}\bar{\boldsymbol{v}}A\boldsymbol{v}}|\varphi_{n'l'm'}\rangle$$

$$= \delta_{ll'}\,\delta_{mm'}\left(\frac{4\pi\nu}{\det(A+C)}\right)^{3/2}\sqrt{\frac{2\tau\xi}{\pi}}\frac{1}{\sqrt{a_{nl}a_{n'l}}}$$

$$\times \sum_{\sigma=0}^{\min(n,n')} a_{\sigma l}\frac{1}{(n-\sigma)!(n'-\sigma)!}\int_0^1 p_1^{n-\sigma}p_2^{n'-\sigma}p_{12}^{2\sigma+l}dt \tag{E.88}$$

with here

$$p_1 = p - \tau\xi\nu\rho_1^2t^2, \tag{E.89}$$

$$p_2 = p' - \tau\xi\nu\rho_2^2t^2, \tag{E.90}$$

$$p_{12} = q - 2\tau\xi\nu\rho_1\rho_2t^2. \tag{E.91}$$

All the formulae given in this appendix allow us to calculate the matrix elements (E.20). These matrix elements are used to evaluate the expansion (E.15), which determines the energy-independent potentials (E.3) [21, 22].

Appendix F

Form factors and densities

In this Appendix [21], the calculation of the monopole proton (neutron) density is explained, first for the microscopic model and then for the non-microscopic three-body model.

In a microscopic model, the charge density and form factor operators are defined as

$$\begin{aligned} \hat{\rho}(\boldsymbol{r}) &= \sum_i^A (\frac{1}{2} - t_{iz}) \delta(\boldsymbol{r}_i - \boldsymbol{R}_{\text{c.m.}} - \boldsymbol{r}), \\ \hat{F}(\boldsymbol{q}) &= \frac{1}{Z} \sum_i^A (\frac{1}{2} - t_{iz}) \exp[i\boldsymbol{q} \cdot (\boldsymbol{r}_i - \boldsymbol{R}_{\text{c.m.}})], \end{aligned} \tag{F.1}$$

where $t_{iz}, \boldsymbol{r}_i$ and $\boldsymbol{R}_{\text{c.m.}}$ are the isospin z-component and coordinate of nucleon i, and the c.m. coordinate of the system, respectively. The neutron density and form factor operators are obtained in a similar way. The matter density is just the sum of the proton and neutron densities. Here and in the following, we use the notation $\hat{O}$ for an operator, and O for its matrix elements. The charge density and the form factor are related to each other through

$$\rho(\boldsymbol{r}) = \frac{Z}{(2\pi)^3} \int \exp(i\boldsymbol{q} \cdot \boldsymbol{r}) F(\boldsymbol{q}) d\boldsymbol{q}. \tag{F.2}$$

They are determined as explained in Ref. [94]. Owing to the Gaussian orbitals used in the Generator Coordinate Method, the densities can be easily computed, and the Fourier transform (F.2) is not necessary.

The density and the form factor are usually expanded in multipoles as

$$\begin{aligned} \rho(\boldsymbol{r}) &= \sum_{\lambda} \rho_\lambda(r) Y_{\lambda 0}(\Omega_r) \\ F(\boldsymbol{q}) &= \sum_{\lambda} F_\lambda(q) Y_{\lambda 0}(\Omega_q), \end{aligned} \tag{F.3}$$

where $\rho_\lambda(r)$ and $F_\lambda(r)$ are the multipolar densities and form factors, respectively. For zero spin nuclei, such as ^{6}He or ^{12}C, the density is spherically symmetric ($\lambda = 0$ only). The relationship between $\rho_\lambda(r)$ and $F_\lambda(r)$ is obtained with Eq. (F.2) as

$$\rho_\lambda(r) = \frac{Z}{2\pi^2} i^\lambda \int j_\lambda(qr) F_\lambda(q) q^2 dq. \tag{F.4}$$

In a non microscopic cluster model, the form factor operator is defined as

$$\hat{F}(\boldsymbol{q}) = \frac{1}{Z} \sum_{j=1}^{N} Z_j F_j(\boldsymbol{q}) \exp[i\boldsymbol{q} \cdot (\boldsymbol{r}_j - \boldsymbol{R}_{c.m.})], \tag{F.5}$$

where N is the number of clusters, and Z_j and $F_j(\boldsymbol{q})$ are the charge and form factors of cluster j. Equation (F.2) is still valid to determine the associated density. In order to be consistent with the microscopic approach, the internal form factors are defined in the HO shell model. For s-shell nuclei, the form factor is given by

$$F_j(\boldsymbol{q}) = \exp\left[-q^2 b^2 \frac{(A_j - 1)}{4A_j}\right], \tag{F.6}$$

where A_j is the nucleon number of cluster j.

In the three-cluster model the form factor operator (F.3) is written as

$$\begin{aligned} \hat{F}(\boldsymbol{q}) = \frac{1}{Z} \Bigg[& Z_1 F_1(\boldsymbol{q}) \exp\big(i\boldsymbol{q} \cdot (\frac{A_3}{A}\boldsymbol{R} + \frac{A_2}{A_{12}}\boldsymbol{r})\big) \\ & + Z_2 F_2(\boldsymbol{q}) \exp\big(i\boldsymbol{q} \cdot (\frac{A_3}{A}\boldsymbol{R} - \frac{A_1}{A_{12}}\boldsymbol{r})\big) \\ & + Z_3 F_3(\boldsymbol{q}) \exp\big(-i\frac{A_{12}}{A}\boldsymbol{q} \cdot \boldsymbol{R}\big) \Bigg], \end{aligned} \tag{F.7}$$

where we have used the coordinate system of Fig. F.1 ($A_{12} = A_1 + A_2$). Each

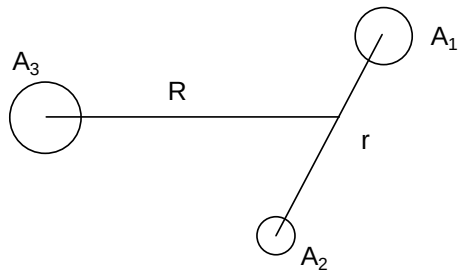

Figure F.1: Coordinate system in the three-cluster model.

term is expanded in multipoles with the help of

$$\begin{aligned}
&\exp(i\boldsymbol{q}\cdot\boldsymbol{r}) = 4\pi\sum_{\lambda\mu} i^{\lambda} j_{\lambda}(qr) Y^{\star}_{\lambda\mu}(\Omega_q) Y_{\lambda\mu}(\Omega_r),\\
&j_{\lambda}(|\alpha\boldsymbol{R}+\beta\boldsymbol{r}|) Y_{\lambda\mu}(\Omega_{\alpha\boldsymbol{R}+\beta\boldsymbol{r}}) = \sum_{\ell_1,\ell_2} i^{\ell_1+\ell_2-\lambda}\\
&\times\left[4\pi(2\ell_1+1)(2\ell_2+1)/(2\lambda+1)\right]^{1/2} \langle \ell_1\ell_2 00|\lambda 0\rangle\\
&\times j_{\ell_1}(\alpha R) j_{\ell_2}(\beta r)\left[Y_{\ell_1}(\Omega_R)\otimes Y_{\ell_2}(\Omega_r)\right]_{\lambda\mu}.
\end{aligned} \tag{F.8}$$

This provides us with the multipolar form factor. In particular, the monopole term reads

$$\begin{aligned}
&\frac{Z}{\sqrt{4\pi}}\hat{F}_0(q) = Z_3 F_3(\boldsymbol{q}) j_0\big(\frac{A_{12}}{A}qR\big)\\
&+4\pi\sum_{L}(2L+1)^{1/2}\left[Y_L(\Omega_R)\otimes Y_L(\Omega_r)\right]_{00} j_L\big(\frac{A_3}{A}qR\big)\\
&\times\left[Z_1 F_1(\boldsymbol{q}) j_L\big(\frac{A_2}{A_{12}}qr\big) + (-1)^L Z_2 F_2(\boldsymbol{q}) j_L\big(\frac{A_1}{A_{12}}qr\big)\right].
\end{aligned} \tag{F.9}$$

Finally, we have to determine the matrix elements of this operator between basis functions

First, coordinates R and r are expressed as a function of ρ and α. The integration over (Ω_R, Ω_r) is performed analytically; for the hyperangle α, we use a Fourier quadrature. Owing to the use of Lagrange functions combined with the Gauss approximation, the integration over the hyperradius reduces to a simple evaluation of Bessel functions at the mesh points. The multipolar

densities are determined from (F.4) through a numerical integration over momentum q. In practice, values up to $q \sim 10$ fm^{-1} are involved to get a good precision on the densities at short distances. The summation over L in (F.9) is carried out up to $L \sim 6 - 8$.

Bibliography

[1] K. Wildermuth and Y.C. Tang, *A unified theory of the nucleus*, Vieweg, Braunschweig, 1977.

[2] Y. Suzuki, R. G. Lovas, K. Yabana, and K. Varga, *Structure and reactions of light exotic nuclei*, Taylor & Francis, London, 2003.

[3] W. von Oertzen, M. Freer, and Y. Kanada-En'yo, *Nuclear clusters and nuclear molecules*, Phys. Rep. **432** (2006), 43.

[4] M. Freer, *The clustered nucleus — cluster structures in stable and unstable nuclei*, Rep. Prog. Phys. **70** (2007), 2149.

[5] D. M. Brink, *History of cluster structure in nuclei*, J. Phys.: Conf. Ser. **111** (2008), 012001.

[6] A. S. Jensen, K. Riisager, D. V. Fedorov, and E. Garrido, *Structure and reactions of quantum halos*, Rev. Mod. Phys. **76** (2004), 215.

[7] M. V. Zhukov, B. V. Danilin, D. V. Fedorov, J. M. Bang, I. J. Thompson, and J. S. Vaagen, *Bound state properties of Borromean halo nuclei:* ^{6}He *and* ^{11}Li, Phys. Rep. **231** (1993), 151.

[8] I. Tanihata, D. Hirata, T. Kobayashi, S. Shimoura, K. Sugimoto, and H. Toki, *Revelation of thick neutron skins in nuclei*, Phys. Lett. B **289** (1992), 261.

[9] A. Ozawa, T. Suzuki, and I. Tanihata, *Nuclear size and related topics*, Nucl. Phys. A **693** (2001), 32.

[10] H. O. U. Fynbo, C. A. Diget, U. C. Bergmann, M. J. G. Borge, J. Cederkäll, P Dendooven, L. M. Fraile, S. Franchoo, V.N. Fedosseev, B. R. Fulton, W. Huang, J. Huikari, H. B. Jeppesen, A. S. Jokinen, P. Jones, B. Jonson, U. Köster, K. Langanke, M. Meister, T. Nilsson, G. Nyman, Y. Prezado, K. Riisager, S. Rinta-Antila, O. Tengblad, M. Turrion, Y. Wang, L. Weissman, K. Wilhelmsen, J. Äystö, and The ISOLDE Collaboration, *Revised rates for the stellar triple-alpha process from measurement of* ^{12}C *nuclear resonances*, Nature **433** (2005), 136.

[11] G. Wallerstein, I. Iben, P. Parker, A. M. Boesgaard, G. M. Hale, A. E. Champagne, C. A. Barnes, F. Käppeler, V. V. Smith, R. D. Hoffman, F. X. Timmes, C. Sneden, R. N. Boyd, B. S. Meyer, and D.L. Lambert, *Synthesis of the elements in stars: forty years of progress*, Rev. Mod. Phys. **69** (1997), 995.

[12] F. Hoyle, D. N. F Dunbar, W. A. Wenzel, and W. Whaling, *A state in* ^{12}C *predicted from astrophysical evidence*, Phys. Rev **92** (1953), Contributed paper N6, p 1095.

[13] F. Hoyle, *On nuclear reactions occurring in very hot stars.I. The synthesis of elements from carbon to nickel.*, Astrophys. J. Suppl. **1** (1954), 121.

[14] F. Ajzenberg-Selove, *Energy levels of light nuclei A = 11-12*, Nucl. Phys. A **506** (1990), 1.

[15] D. R. Tilley, C. M. Cheves, J. L. Godwin, G. M. Hale, H. M. Hofmann, J. H. Kelley, C. G. Sheu, and H. R. Weller, *Energy levels of light nuclei A=5, 6, 7*, Nucl. Phys. A **708** (2002), 3.

[16] D.R. Tilley, J.H. Kelley, J.L. Godwin, D.J. Millener, J.E. Purcell, C.G. Sheu, and H.R. Weller, *Energy levels of light nuclei A=8, 9, 10*, Nucl. Phys. A **745** (2004), no. 3-4, 155.

[17] Y. Fujiwara, K. Miyagawa, M. Kohno, Y. Suzuki, D. Baye, and J.-M. Sparenberg, *Faddeev calculation of* 3α *and* $\alpha\alpha\Lambda$ *systems using* $\alpha\alpha$ *resonating-group method kernels*, Phys. Rev. C **70** (2004), 024002.

[18] Y. Fujiwara, M. Kohno, K. Miyagawa, Y. Suzuki, and J.-M. Sparenberg, *Faddeev calculation of* ${}^{6}_{\Lambda\Lambda}He$ *using* SU_6 *quark-model baryon-baryon interactions*, Phys. Rev. C **70** (2004), 037001.

[19] M. Theeten, D. Baye, and P. Descouvemont, *Three-body models of the* ${}^{6}_{\Lambda\Lambda}He$ *and* ${}^{9}_{\Lambda}Be$ *hypernuclei with non-local interactions*, Nucl. Phys. A **753** (2005), 233.

[20] M. Theeten, D. Baye, and P. Descouvemont, *Comparison of local, semi-microscopic, and microscopic three-cluster models*, Phys. Rev. C **74** (2006), 044304.

[21] M. Theeten, H. Matsumura, M. Orabi, D. Baye, P. Descouvemont, Y. Fujiwara, and Y. Suzuki, *Three-body model of light nuclei with microscopic nonlocal interactions*, Phys. Rev. C **76** (2007), 054003.

[22] Y. Suzuki, H. Matsumura, M. Orabi, Y. Fujiwara, P. Descouvemont, M. Theeten, and D. Baye, *Local versus nonlocal* $\alpha\alpha$ *interactions in a* 3α *description of* ${}^{12}C$, Phys. Lett. B **659** (2008), 160.

[23] M. Theeten, D. Baye, P. Descouvemont, Y. Fujiwara, H. Matsumura, M. Orabi, and Y. Suzuki, *Three-cluster models for light nuclei*, J. Phys.: Conf. Ser. **111** (2008), 012046.

[24] S. Ali and A. R. Bodmer, *Phenomenological* $\alpha-\alpha$ *potentials*, Nucl. Phys. A **80** (1966), 99.

[25] B. Buck, H. Friedrich, and C. Wheatley, *Local potential models for the scattering of complex nuclei*, Nucl. Phys. A **275** (1977), 246.

[26] D. R. Thompson, M. Lemere, and Y. C. Tang, *Systematic investigation of scattering problems with the resonating-group method*, Nucl. Phys. A **286** (1977), 53.

[27] P. Descouvemont, C. Daniel, and D. Baye, *Three-body systems with Lagrange-mesh techniques in hyperspherical coordinates*, Phys. Rev. C **67** (2003), 044309.

[28] Y. Fujiwara, Y. Suzuki, K. Miyagawa, M. Kohno, and H. Nemura, *Redundant components in the* 3α *Faddeev equation using the* 3α *RGM kernel*, Prog. Theor. Phys. **107** (2002), 993.

[29] S. Saito, *Theory of the Resonating Group Method and Generator Coordinate Method, and Orthogonality Condition Model*, Suppl. Prog. Theor. Phys. **62** (1977), 11.

[30] H. Horiuchi, *Kernels of GCM, RGM and OCM and Their Calculational Methods*, Suppl. Prog. Theor. Phys. **62** (1977), 90.

[31] D. Baye, *Description microscopique des collisions entre ions lourds par le modèle des coordonnées génératrices*, thèse d'agrégation, Université Libre de Bruxelles, 1983.

[32] J. A. Wheeler, *Molecular viewpoints in nuclear structure*, Phys. Rev. **52** (1937).

[33] S. Saito, *Interaction between clusters and Pauli principle*, Prog. Theor. Phys. **41** (1969), 705.

[34] D. A. Zaikin, *Pauli principle for reactions with light nuclei*, Nucl. Phys. A **170** (1971), 584.

[35] W. Timm, H. R. Fiebig, and H Friedrich, *Degree of nonlocality of various exchange contributions to the nucleus-nucleus potential*, Phys. Rev. C **25** (1982), 79.

[36] E.W. Schmid, *Theoretical description of few-cluster systems*, Nucl. Phys. A **416** (1984), 347.

[37] G. R. Satchler and W. G. Love, *Folding model potentials from realistic interactions for heavy-ion scattering*, Phys. Rep. **55** (1979), 183.

[38] A. Tohsaki-Suzuki, M. Kamimura, and K. Ikeda, *Microscopic study of the interaction between complex nuclei*, Suppl. Prog. Theor. Phys. **68** (1980), 359.

[39] H. Friedrich, *Microscopic nucleus-nucleus potentials*, Phys. Rep. **74** (1981), 209.

[40] D. Baye, *Supersymmetry between deep and shallow nucleus-nucleus potentials*, Phys. Rev. Lett. **58** (1987), 2738.

[41] D. Baye, *Phase-equivalent potentials from supersymmetry*, J. Phys. A: Math. Gen. **20** (1987), 5529.

[42] J. Raynal and J. Revai, *Transformation coefficients in the hyperspherical approach to the three-body problem*, Nuovo Cimento A **39** (1970), 612.

[43] P. M. Morse and H. Feshbach, *Methods of theoretical physics, part II*, McGraw-Hill, New York, 1953.

[44] M. Abramowitz and I. A Stegun, *Handbook of mathematical functions with formulas, graphs, and mathematical tables*, Dover, New York, 1970.

[45] I. J. Thompson, B. V. Danilin, V. D. Efros, J. S. Vaagen, J. M. Bang, and M. V. Zhukov, *Pauli blocking in three-body models of halo nuclei*, Phys. Rev. C **61** (2000), 024318.

[46] C. Cohen-Tannoudji, B. Diu, and F. Laloë, *Mécanique quantique, volume 1*, Hermann, Paris, 1973.

[47] A. Messiah, *Mecanique quantique, tome 2*, Dunod, Paris, 1964.

[48] D. Baye and P.-H. Heneen, *Generalised meshes for quantum mechanical problems*, J. Phys. A: Math. Gen. **19** (1986), 2041.

[49] M. Vincke, L. Malegat, and D. Baye, *Regularization of singularities in Lagrange-mesh calculations*, J. Phys. B: At. Mol. Opt. Phys. **26** (1993), 811.

[50] D. Baye, *Constant-step Lagrange meshes for central potentials*, J. Phys. B: At. Mol. Opt. Phys. **28** (1995), 4399.

[51] D. Baye, M. Hesse, and M. Vincke, *The unexplained accuracy of the Lagrange-mesh method*, Phys. Rev. E **65** (2002), 026701.

[52] M. Hesse, J. Roland, and D. Baye, *Solving the resonating-group equation on a Lagrange mesh*, Nucl. Phys. A **709** (2002), 184.

[53] S. Korennov and P. Descouvemont, *A microscopic three-cluster model in the hyperspherical formalism*, Nucl. Phys. A **740** (2004), 249.

[54] D. Baye and P. Descouvemont, *A microcopic cluster description of nuclear reactions*, Proc. 5th int. Conf. Clustering aspects in Nucl. and Subnucl System, Kyoto 1988, J. Phys. Soc. Jpn. Suppl. **58** (1989), 103.

[55] D. Brink, *The α-particle model of light nuclei*, Proceedings of the International School of Physics, "Enrico Fermi", course 36, Varenna, 1965, Academic Press, New York, 1966, p 247.

[56] K. Alder and R.M. Steffen, *Emission and absortion of electromagnetic radiation*, The electromagnetic interaction in nuclear spectroscopy, North-Holland, Amsterdam, 1975.

[57] A. B. Volkov, *Equilibrium deformation calculations of the ground state energies of 1p shell nuclei*, Nucl. Phys. A **74** (65), 33.

[58] D. Baye and N. Pecher, *Generator-coordinate description of heavy-ion collisions with a spin-orbit force*, Bull. Cl. Sc. Acad. Roy. Belg. **67** (1981), 835.

[59] H. Kanada, T. Kaneko, S. Nagata, and M. Nomoto, *Microscopic study of nucleon-^{4}He scattering and effective nuclear potentials*, Prog. Theor. Phys. **61** (1979), 1327.

[60] H. Matsumura, M. Orabi, Y. Suzuki, and Y. Fujiwara, *Removal of forbidden states in a three-α system*, Nucl. Phys. A **776** (2006), 1.

[61] V. I. Kukulin and V. N. Pomerantsev, *The orthogonal projection method in scattering theory*, Ann. Phys. (NY) **111** (1978), 330.

[62] K. S. Krane, *Introductory nuclear physics*, Wiley & Sons, New York, 1988.

[63] D.H. Perkins, *Introduction to high energy physics, (3rd edition)*, Addison-Wesley, New York, 1987.

[64] W.-M. Yao *et al.* (Particle Data Group), *Review of Particle Physics*, J. Phys. G **33** (2006), 1.

[65] B. F. Gibson and E. V. Hungerford, *A survey of hypernuclear physics*, Phys. Rep. **257** (1995), 349.

[66] B. F. Gibson, *Hypernuclear physics, a brief past and bright future*, Nucl. Phys. A **689** (2001), 57.

[67] R. H. Dalitz, *Hypernuclear physics as we enter the third millenium*, Nucl. Phys. A **691** (2001), 1.

[68] E. Hiyama, M. Kamimura, T. Motoba, T. Yamada, and Y. Yamamoto, *Few-body aspects of light hypernuclei*, Nucl. Phys. A **737** (2004), 138.

[69] E. Hiyama, M. Kamimura, T. Motoba, T. Yamada, and Y. Yamamoto, *Clustering aspects of light hypernuclei*, Nucl. Phys. A **738** (2004), 175.

[70] H. Akikawa, S. Ajimura, R. E. Chrien, P. M. Eugenio, G. B. Franklin, J. Franz, L. Gang, K. Imai, P. Khaustov, M. May, P. H. Pile, B. Quinn, A. Rusek, J. Sasao, R. I. Sawafta, H. Schmitt, H. Tamura, L. Tang, K. Tanida, L. Yuan, S. H. Zhou, L. H. Zhu, and X. F. Zhu, *Hypernuclear fine structure in* ${}^{9}_{\Lambda}Be$, Phys. Rev. Lett. **88** (2002), 082501.

[71] H. Takahashi, J. K. Ahn, H. Akikawa, S. Aoki, K. Arai, S. Y. Bahk, K. M. Baik, B. Bassalleck, J. H. Chung, M. S. Chung, D. H. Davis, T. Fukuda, K. Hoshino, A. Ichikawa, M. Ieiri, K. Imai, Y. H. Iwata, Y. S. Iwata, H. Kanda, M. Kaneko, T. Kawai, M. Kawasaki, C. O. Kim, J. Y. Kim, S. J. Kim, S. H. Kim, and Y. Kondo, *Observation of a* ${}^{6}_{\Lambda\Lambda}He$ *double hypernucleus*, Phys. Rev. Lett. **87** (2001), 212502.

[72] I. Filikhin, A. Gal, and V.M. Suslov, *Cluster models of* ${}^{6}_{\Lambda\Lambda}He$ *and* ${}^{9}_{\Lambda}Be$ *hypernuclei*, Nucl. Phys. A **743** (2004), 194.

[73] D. J. Prowse, ${}^{6}_{\Lambda\Lambda}He$ *double hyperfragment*, Phys. Rev. Lett. **17** (1966), 782.

[74] M. Jurič, G. Bohm, J. Klabuhn, U. Krecker, F. Wysotzki, G. Coremans-Bertrand, J. Sacton G. Wilquet, T. Cantwell, F. Esmael, A. Montwill, D. H. Davis, D. Kiełczewska, T. Pniewski, T. Tymieniecka, and J. Zakrzewski, *A new determination of the binding-energy values of the light hypernuclei* ($A \leq 15$), Nucl. Phys. B **52** (73), 1.

[75] Y. Fujiwara, M. Kohno, C. Nakamoto, and Y. Suzuki, *Interactions between octet baryons in the* SU_6 *quark model*, Phys. Rev. C **64** (2001), 054001.

[76] J.-M. Sparenberg and D. Baye, *Inverse scattering with singular potentials: A supersymmetric approach*, Phys. Rev. C **55** (1997), 2175.

[77] Y. Kurihara, Y. Akaishi, and H. Tanaka, *Central repulsion of* $\Lambda - \alpha$ *interaction with hard-core* $\Lambda - N$ *potential*, Prog. Theor. Phys. **71** (1984), 561.

[78] Y. Kurihara, Y. Akaishi, and H. Tanaka, *Effect of* $\Lambda - N$ *repulsive core on pionic decay of* ${}^{5}_{\Lambda}He$, Phys. Rev. C **31** (1985), 971.

[79] K. S. Myint, S. Shinmura, and Y. Akaishi, ΛΛ-ΞN *coupling effects in light hypernuclei*, Eur. Phys. J. A **16** (2003), 21.

[80] T. Yamada, ΛΛ-ΞN-ΣΣ *coupling in* ${}^{6}_{\Lambda\Lambda}He$ *with the Nijmegen soft-core potentials*, Phys. Rev. C **69** (2004), 044301.

[81] T. Motoba, H. Bandō, and K. Ikeda, *Light p-shell* Λ*-hypernuclei by the microscopic three-cluster model*, Prog. Theor. Phys. **70** (1983), 189.

[82] B. Fuks, *Etudes d'hypernoyaux par la méthode des coordonnées hypersphériques*, Mémoire de fin d'étude, Faculté des sciences appliquées, Université Libre de Bruxelles, 2004.

[83] B. V. Danilin, N. Ershov, and J. S. Vaagen, *Charge and matter radii of Borromean halo nuclei: The* ${}^{6}He$ *nucleus*, Phys. Rev. C **71** (2005), 057301.

[84] Y. Fujiwara, Y. Suzuki, and M. Kohno, *Case of almost redundant components in* 3α *Faddeev equations*, Phys. Rev. C **69** (2004), 037002.

[85] G. L. Morgan and R. L. Walter, *Neutron-helium interaction. II. Angular distributions and phase shifts from 0.2 to 7.0 MeV*, Phys. Rev. **168** (1968), 1114.

[86] S. A. Afzal, A. A. Z. Ahmad, and S. Ali, *Systematic survey of the $\alpha - \alpha$ interaction*, Rev. Mod. Phys. **41** (1969), 247.

[87] P. Descouvemont, E. Tursunov, and D. Baye, *Three-body continuum states on a Lagrange mesh*, Nucl. Phys. A **765** (2006), 370.

[88] D. R. Thompson, I. Reichstein, W. McClure, and Y. C. Tang, *Effective $\alpha + \alpha$ and $\alpha + N$ potentials from resonating-group calculations*, Phys. Rev. **185** (1969), 1351.

[89] I. Reichstein and Y.C. Tang, *Study of $N+\alpha$ system with the resonating-group method*, Nucl. Phys. A **158** (1970), 529.

[90] I.S. Gradshteyn and I.M. Ryzhik, *Table of Integrals, Series and Products*, Academic Press, New York, 1980.

[91] Y. Suzuki, *private communication.*

[92] Y. Suzuki and K. Varga, *Stochastic variational approach to quantum-mechanical few-body problems*, Lecture notes in physics, vol. m54, Springer, Berlin, 1998.

[93] K. T. Hecht and Y. Suzuki, *Some special $SU(3) \supseteq R(3)$ Wigner coefficients and their application*, J. Math. Phys. **24** (1983), 785.

[94] P. Descouvemont D. Baye and N. K. Timofeyuk, *Matter densities of ^8B and ^8Li in a microscopic cluster model and the proton-halo problem of ^8B*, Nucl. Phys. A **577** (1994), 624.